

Excitation of pulsation in hot pre-white dwarf stars from an observational point of view

Author:

Paulina SOWICKA

Supervisor:

Prof. Gerald HANDLER

Co-supervisor:

Dr. David JONES

A thesis submitted in fulfillment
of the requirements for the degree of
Doctor of Philosophy
in Astronomy



Nicolaus Copernicus Astronomical Center of the Polish Academy of Sciences
Warsaw, Poland

2023

Excitation of pulsation in hot pre-white dwarf stars from an observational point of view, © 2023

Author:

Paulina SOWICKA

Supervisor:

Prof. Gerald HANDLER

Co-supervisor:

Dr. David JONES

Institute:

Nicolaus Copernicus Astronomical Center of the Polish Academy of Sciences, Warsaw,
Poland

CONTENTS

List of Figures	v
List of Listings	vi
Abstract	vii
Streszczenie	ix
Acknowledgments	xi
Publications	xiii
Abbreviations	xix
1 INTRODUCTION	1
1.1 Final stages of the single star evolution of low- to intermediate-mass stars	1
1.1.1 Introduction	1
1.1.2 Evolution of low- to intermediate-mass stars	2
1.2 PG 1159 spectra	6
1.3 Stellar pulsations	8
1.4 GW Vir pulsations	12
1.4.1 Excitation mechanism(s)	13
1.4.2 Pulsational properties	15
1.4.3 Pulsators and non-pulsators	18
1.5 Planetary nebulae	19
1.6 Binarity	20
1.7 Ground-based data used in this thesis	21
1.7.1 Awarded observing time	21
1.7.2 Equipment	21
1.8 Thesis Outline	23
2 DATA REDUCTION AND ANALYSIS	25
2.1 Introduction	25
2.2 Standard steps in data reduction	26
2.2.1 Bias Frames	26
2.2.2 Dark Frames	26
2.2.3 Flat field images	29
2.2.4 Science frames	30
2.2.5 Possible additional steps	31

2.3	Photometry	32
2.3.1	Aperture photometry	32
2.3.2	Adaptive photometry pipeline	34
2.3.3	Differential photometry	39
2.3.4	Extinction correction	40
2.3.5	Differential magnitude vs. seeing	41
2.4	Time-Series Analysis	41
2.5	Summary	46
3	ON ϵ MECHANISM-DRIVEN PULSATIONS IN VV 47	47
4	IS NITROGEN THE KEY TO UNDERSTANDING WHETHER PG 1159 STARS PULSATE?	55
5	THE GW VIR INSTABILITY STRIP IN THE LIGHT OF NEW OBSERVATIONS OF PG 1159 STARS	63
6	CONCLUSIONS AND FUTURE WORK	95
	BIBLIOGRAPHY	99

LIST OF FIGURES

Figure 1.1	Evolution and final fate of single stars depending on their initial masses.	2
Figure 1.2	Evolutionary tracks on the HR diagram	3
Figure 1.3	Post-AGB evolutionary tracks for VLTP, LTP, and AFTP scenarios . .	6
Figure 1.4	PG 1159 absorption trough	7
Figure 1.5	Elemental abundances of five PG 1159 stars	8
Figure 1.6	Hertzsprung-Russell diagram for pulsating stars	9
Figure 1.7	Spherical harmonics	11
Figure 1.8	Instability strip for $\kappa - \gamma$ and ϵ -driven modes in PG 1159 stars	14
Figure 1.9	Light curves of compact pulsators	15
Figure 1.10	Period spectra of two GW Vir stars	16
Figure 1.11	Asteroseismic mass determination	17
Figure 1.12	Planetary nebulae associated with PG 1159 stars	19
Figure 2.1	An illustration of the basic data reduction process	27
Figure 2.2	A master dark from ProEM	29
Figure 2.3	Signal-to-noise ratio as a function of aperture size	33
Figure 2.4	Labelled PG 1144+005 FOV	38
Figure 2.5	Extinction correction	41
Figure 2.6	A plot of seeing against differential magnitude	42
Figure 2.7	Differential magnitudes for different scaling factors and corresponding Fourier amplitude spectra	45

LIST OF LISTINGS

Listing 1	Bash script for AUTOPHOTOM run in optimal extraction mode . . .	35
Listing 2	Terminal output for AUTOPHOTOM run in optimal extraction mode	35
Listing 3	Terminal output for AUTOPHOTOM run in aperture extraction mode	37

ABSTRACT

Stars of PG 1159 spectral type are hot pre-white dwarf stars with atmospheres rich in helium, carbon, and oxygen, that are considered the main progenitors of hydrogen-deficient white dwarfs. Those stars lay in GW Virginis instability strip and some of them show short-period oscillations in photometric observations. In this thesis, we present new ground-based time-series photometric observations of 31 pre-white dwarf stars of PG 1159 spectral type. These observations provide a substantial step towards obtaining the first statistically significant sample of well-studied PG 1159 stars with information about their evolutionary history and excitation of pulsations.

Stellar pulsations driven by the ϵ mechanism were theoretically predicted almost 100 years ago. Theoretical calculations showed that the ϵ mechanism can operate in pre-white dwarf stars with helium-burning shells, giving rise to short-period g modes. One of the candidates to show such pulsations was the central star of planetary nebula VV 47. Observations by various groups did not detect any pulsations in this star, until the detection of pulsations in VV 47 was claimed in 2006. The presence of some high-frequency peaks was attributed to the ϵ mechanism, even though the detection was marginal. We conducted new observations, reaching an improved detection threshold, of VV 47 to test those claims and did not detect any variability. Therefore, we re-analyzed the discovery data set using the same methods as for our new observations, and did not detect the alleged pulsations. We attributed the detection by other authors to a relaxed detection criterion.

Previous observations revealed two groups within the PG 1159 stars: Nitrogen-rich pulsators and N-poor non-pulsators, with one counterexample being PG 1144+005, the only N-rich PG 1159 star with no detection of pulsations. We observed the star and preliminarily detected two pulsation modes consistent with GW Vir pulsations, and confirmed those findings with follow-up observations with a longer time base, characterizing the star as a multiperiodic pulsator. With this study, we confirmed the existence of N dichotomy in PG 1159 stars, with an important conclusion that the pulsating and non-pulsating PG 1159 stars have different evolutionary histories while N is a tracer of these histories, and it seems necessary that a star undergoes a Very Late Thermal Pulse to develop pulsations.

In the years 2014–2022 we carried out an ambitious survey for variability among PG 1159 stars using telescopes of 1 to 10.4-m aperture size located in both Hemispheres. Thanks to newly obtained photometric time-series observations for 29 stars, we discovered pulsations in the central star of planetary nebula Abell 72, variability in RX J0122.9–7529 that can be attributed to pulsations, binarity, or other sources, and put significant limits for non-variability for the rest of the sample. We obtained the most robust fraction of pulsating PG 1159 stars (36%) to date, conclusively proving that the impurity of the GW Vir instability strip is unlikely due to observational bias. We compiled literature data on atmospheric parameters, variability, and nitrogen content of all known PG 1159 stars with

available measurements from *Gaia* DR3, which allowed us to calculate the luminosities and for the first time place all PG 1159 stars in the theoretical Hertzsprung-Russell diagram. Finally, we analyzed the pulsators as a group and questioned currently used nomenclature.

This thesis presents the most complete picture of GW Vir stars that puts us in place to study the whole PG 1159 group. We conclude with a discussion of possible improvements to the work presented here, future prospects for the study of GW Vir stars, and our plans for future work. In particular, in order to fully study the PG 1159 stars as a group, we need to complement the photometric observations with spectroscopy, a project that we have already started.

STRESZCZENIE

Gwiazdy typu widmowego PG 1159 to gorące gwiazdy przed etapem białego karła, których atmosfery są bogate w hel, węgiel i tlen. Uważane są za głównych protoplaszów białych karłów ubogich w wodór. Gwiazdy te leżą w pasie niestabilności GW Virginis i niektóre z nich wykazują krótkookresowe oscylacje w obserwacjach fotometrycznych. W tej pracy prezentujemy nowe szeregi czasowe naziemnych obserwacji fotometrycznych 31 gwiazd typu PG 1159. Obserwacje te stanowią znaczący krok w kierunku otrzymania pierwszej statystycznie istotnej próbki dobrze zbadanych gwiazd typu PG 1159 z informacją na temat ich historii ewolucji i mechanizmu wzbudzenia pulsacji.

Pulsacje gwiazd wzbudzone mechanizmem ϵ przewidywano teoretycznie prawie 100 lat temu. Obliczenia teoretyczne wykazały, że mechanizm ϵ może działać w gwiazdach przed etapem białego karła, w których zachodzi synteza helu w powłoce, powodując wzbudzenie krótkookresowych modów grawitacyjnych. Centralna gwiazda mgławicy planetarnej VV 47 została zaproponowana jako najbardziej obiecująca kandydatka mogąca pulsować w wyniku mechanizmu ϵ . Pulsacje w VV 47 doczekały się obserwacyjnego potwierdzenia dopiero w 2006 roku, chociaż próby weryfikacji podejmowane były przez różne grupy na przestrzeni lat. Obecność modów o wysokich częstotliwościach przypisano mechanizmowi ϵ , ale detekcja była marginalna. Przeprowadziliśmy nowe obserwacje VV 47, osiągając lepszy próg wykrywalności, aby zweryfikować tę detekcję i nie wykryliśmy żadnej zmienności. Dlatego ponownie przeanalizowaliśmy oryginalne dane, stosując te same metody, co w przypadku naszych nowych obserwacji i nie wykryliśmy rzekomych pulsacji. Wykrycie modów przez innych autorów przypisaliśmy szczególnie dobranemu przez nich kryterium detekcji.

Poprzednie obserwacje ujawniły podział gwiazd typu PG 1159 na dwie grupy: gwiazdy pulsujące bogate w azot (N) i niepulsujące ubogie w N, przy czym jednym z kontrprzykładów jest PG 1144+005, jedyna bogata w N gwiazda typu PG 1159, w której nie wykryto pulsacji. Ten obiekt obraliśmy za drugi przedmiot badań. Przeprowadziliśmy obserwacje tej gwiazdy, a wykonana przez nas fotometria wstępnie wykazała istnienie dwóch modów pulsacji charakterystycznych dla obiektów typu GW Vir. Kolejne wykonane przez nas obserwacje potwierdziły te ustalenia oraz pozwoliły scharakteryzować pulsacje jako wielookresowe. W tym badaniu potwierdziliśmy istnienie dychotomii N w gwiazdach typu PG 1159, wyciągając ważny wniosek, że gwiazdy pulsujące i niepulsujące typu PG 1159 mają różne historie ewolucji, podczas gdy N jest wyznacznikiem tych historii i wydaje się konieczne, aby gwiazda doświadczyła bardzo późnego pulsu termicznego (VLTP), aby pulsacje mogły zostać wzbudzone.

W latach 2014–2022 przeprowadziliśmy ambitny przegląd w kierunku wykrycia zmienności w gwiazdach typu PG 1159 przy użyciu teleskopów o średnicy apertury od 1 do 10.4 metra, zlokalizowanych na obu półkulach. Dzięki nowo uzyskanym obserwacjom

fotometrycznym w postaci szeregów czasowych dla 29 gwiazd odkryliśmy pulsacje w centralnej gwiazdzie mgławicy planetarnej Abell 72, zmienność w RX J0122.9–7529, której podłożem mogą być pulsacje, układ podwójny lub inne źródła, i wyznaczyć istotne ograniczenia na brak zmienności fotometrycznej dla pozostałych gwiazd. Uzyskaliśmy jak dotąd najsolidniejszą frakcję pulsujących gwiazd typu PG 1159 (36%), co niezbicie dowodzi, że występowanie niepulsujących gwiazd typu PG 1159 w pasie niestabilności GW Vir nie jest wynikiem biasu obserwacyjnego. Zestawiliśmy dane z literatury na temat parametrów atmosferycznych, zmienności i zawartości azotu wszystkich znanych gwiazd PG 1159 z dostępnymi pomiarami z misji *Gaia*, co pozwoliło nam obliczyć jasności i po raz pierwszy umieścić wszystkie gwiazdy typu PG 1159 na teoretycznym diagramie Hertzsprunga-Russella. Na koniec dokonaliśmy analizy gwiazd pulsujących jako grupy i zakwestionowaliśmy obecnie stosowaną nomenklaturę.

Niniejsza praca przedstawia najpełniejszy obraz gwiazd typu GW Vir, który pozwoli nam zbadać całą grupę gwiazd typu PG 1159. Praca ta domknięta jest dyskusją na temat możliwych ulepszeń zaprezentowanych wyników, perspektyw badań gwiazd typu GW Vir oraz omówieniem naszych przyszłych planów badawczych. W szczególności, aby w pełni zbadać gwiazdy typu PG 1159 jako grupę, musimy uzupełnić obserwacje fotometryczne obserwacjami spektroskopowymi, w projekcie, który już rozpoczęliśmy.

ACKNOWLEDGMENTS

First and foremost, I am extremely grateful to my supervisor, Prof. Gerald Handler, for sharing his knowledge and experience, his patience, understanding and continuous support in every situation, for giving me the opportunity to learn and grow, and freedom in choosing my projects. Thank you for taking me to the IAU Symposium 301 (Precision Asteroseismology) when I was an undergraduate student, as this conference planted the seed (thanks to Prof. Don Kurtz) that made me interested in stellar pulsations, and for my first observing trip during my PhD to the South African Astronomical Observatory to fulfill my dream of seeing the southern night sky.

I am also grateful to my co-supervisor, Dr. David Jones, for his invaluable advice, guidance, friendship, help with my Python-related issues, always being supportive and motivating. Thank you for teaching me about binary central stars of planetary nebulae as well as spectroscopy, and for all the fun data I could work with. I am also very grateful to you for lifting my spirits by taking me for observing trips in La Silla. Starting a collaboration with you during my ING Studentship was one of the highlights of my stay on La Palma.

I would like to acknowledge the ING Support and Research Studentship that allowed me to work as a support astronomer for the Isaac Newton Telescope, which I wholeheartedly enjoyed, and provided the opportunity to obtain a large part of data without which this thesis would not be possible.

I am grateful to all the observers and support astronomers who helped with obtaining the observations included in this thesis – it would not be possible without you.

Magda and Tuğça – thank you for everything. Many thanks to my friends for always being there for me, both in good and bad times. Thank you for your friendship, company, all the fun, excellent food, concerts, trips, and board games. Special thanks to Tuğça and Bartek for proofreading, and my figure skating friends for all the fun we had on the ice as my perfect getaway.

I thank colleagues from white dwarf and asteroseismic communities for fun at conferences (and at the KITP), cheering on (during my talks), and interest in my work.

I also thank Teka, Kiciula, and Gırgır for dog/cat therapy and a helping paw along the way.

Dziękuję mojej rodzinie za wsparcie podczas mojej edukacji.

Serdecznie dziękuję dyrekcji i pracownikom CAMKu za okazane wsparcie. Dziękuję również Grzegorzowi i Młodziejowemu Obserwatorium Astronomicznemu w Niepołomicach za pomoc i zainteresowanie moją pracą.

This research was supported in part by the Polish National Science Center (NCN) through grant 2015/18/A/ST9/00578, CAMK grant for young researchers 2016/2017, and the National Science Foundation under Grant No. NSF PHY-1748958.

PUBLICATIONS

This thesis includes work by the author that has been published or accepted for publication. These publications contain the own work of the author of this thesis, and the author has the permission of the publishers to reproduce the contents of these publications for academic purposes.

In particular, some data, ideas, opinions, and figures presented in this thesis have previously appeared or may appear shortly after the submission of this thesis as follows:

- Sowicka, P., Handler, G., Jones, D., “**On ϵ -mechanism-driven pulsations in VV 47**”, published in the *Monthly Notices of the Royal Astronomical Society*, 2018, MNRAS, 479, 2476, DOI: [10.1093/mnras/sty1660](https://doi.org/10.1093/mnras/sty1660)
- Sowicka, P., Handler, G., Jones, D., van Wyk, F., “**The Missing Link? Discovery of Pulsations in the Nitrogen-rich PG 1159 Star PG 1144+005**”, published in the *Astrophysical Journal Letters*, 2021, ApJ, 918, L1, DOI: [10.3847/2041-8213/ac1c08](https://doi.org/10.3847/2041-8213/ac1c08)
- Sowicka, P., Handler, G., Jones, D., Caldwell, J. A. R., van Wyk, F., Paunzen, E., Bałowska, K., Peralta de Arriba, L., Suárez-Andrés, L., Werner, K., Karjalainen, M., Holdsworth, D. L., “**The GW Vir instability strip in the light of new observations of PG 1159 stars. Discovery of pulsations in the central star of Abell 72 and variability of RX J0122.9–7521**”, accepted for publication in the *Astrophysical Journal Supplement Series* on September 19, 2023, arXiv: [2309.16537](https://arxiv.org/abs/2309.16537)

No other person’s work has been used without due acknowledgment in the main text of the thesis.

FULL LIST OF PUBLICATIONS

I. *Refereed publications*

1. “The GW Vir instability strip in the light of new observations of PG 1159 stars. Discovery of pulsations in the central star of Abell 72 and variability of RX J0122.9–7521”
Sowicka, P., Handler, G., Jones, D., Caldwell, J. A. R., van Wyk, F., Paunzen, E., Bałowska, K., Peralta de Arriba, L., Suárez-Andrés, L., Werner, K., Karjalainen, M., Holdsworth, D. L., 2023, accepted in ApJS, arXiv: [2309.16537](https://arxiv.org/abs/2309.16537)
2. “Everything that glitters is not gold: V1315 Cas is not a dormant black hole”
Zak, J., Jones, D., Boffin, H. M. J., Beck, P. G., Klencki, J., Bodensteiner, J., Shenar, T., Van Winckel, H., Skarka, M., Arellano-Córdova, K., Viuhio, J., **Sowicka, P.**, Guenther, E. W., Hatzes, A., 2023, MNRAS, 524, 5749, DOI: [10.1093/mnras/stad2137](https://doi.org/10.1093/mnras/stad2137)

3. "HD 42477: coupled r modes, g modes, and a p mode in an A0Vne star"
Kurtz, D. W., Jayaraman, R., **Sowicka, P.**, Handler, G., Saio, H., Labadie-Bartz, J., Lee, U., 2023, MNRAS, 521, 4765, DOI: [10.1093/mnras/stad858](https://doi.org/10.1093/mnras/stad858)
4. "The post-common-envelope binary central star of the planetary nebula Ou 5: a doubly eclipsing post-red-giant-branch system"
Jones, D., Munday, J., Corradi, R. L. M., Rodríguez-Gil, P., Boffin, H. M. J., Zak, J., **Sowicka, P.**, Parsons, S. G., Dhillon, V. S., Littlefair, S. P., Marsh, T. R., Reindl, N., García-Rojas, J., 2022, MNRAS, 510, 3102, DOI: [10.1093/mnras/stab3736](https://doi.org/10.1093/mnras/stab3736)
5. "The Missing Link? Discovery of Pulsations in the Nitrogen-rich PG 1159 Star PG 1144+005"
Sowicka, P., Handler, G., Jones, D., van Wyk, F., 2021, ApJL, 918, L1, DOI: [10.3847/2041-8213/ac1c08](https://doi.org/10.3847/2041-8213/ac1c08)
6. "The post-common-envelope binary central star of the planetary nebula ETHOS 1"
Munday, J., Jones, D., García-Rojas, J., Boffin, H. M. J., Miszalski, B., Corradi, R. L. M., Rodríguez-Gil, P., Rubio-Díez, M. del Mar, Santander-García, M., **Sowicka, P.**, 2020, MNRAS, 498, 6005, DOI: [10.1093/mnras/staa2753](https://doi.org/10.1093/mnras/staa2753)
7. "The post-common-envelope binary central star of the planetary nebula PN G283.7-05.1. A possible post-red-giant-branch planetary nebula central star"
Jones, D., Boffin, H. M. J., Hibbert, J., Steinmetz, T., Wesson, R., Hillwig, T. C., **Sowicka, P.**, Corradi, R. L. M., García-Rojas, J., Rodríguez-Gil, P., Munday, J., 2020, A&A, 642, A108, DOI: [10.1051/0004-6361/202038778](https://doi.org/10.1051/0004-6361/202038778)
8. "Physics of Eclipsing Binaries. IV. The Impact of Interstellar Extinction on the Light Curves of Eclipsing Binaries"
Jones, D., Conroy, K. E., Horvat, M., Giammarco, J., Kochoska, A., Pablo, H., Brown, A. J., **Sowicka, P.**, Prša, A., 2020, ApJS, 247, 63, DOI: [10.3847/1538-4365/ab7927](https://doi.org/10.3847/1538-4365/ab7927)
9. "Tidally trapped pulsations in a close binary star system discovered by TESS"
Handler, G., Kurtz, D. W., Rappaport, S. A., Saio, H., Fuller, J., Jones, D., Guo, Z., Chowdhury, S., **Sowicka, P.**, Kahraman Alicavus, F., Streamer, M., Murphy, S. J., Gagliano, R., Jacobs, T. L., Vanderburg, A., 2020, NatAs, 4, 684, DOI: [10.1038/s41550-020-1035-1](https://doi.org/10.1038/s41550-020-1035-1)
10. "The first view of δ Scuti, γ Doradus stars with the TESS mission"
Antoci, V., Cunha, M. S., Bowman, D. M., Murphy, S. J., Kurtz, D. W.; Bedding, T. R., Borre, C. C., Christophe, S., Daszyńska-Daszkiewicz, J., Fox-Machado, L., García Hernández, A., Ghasemi, H., Handberg, R., Hansen, H., Hasanzadeh, A., Houdek, G., Johnston, C., Justesen, A. B., Kahraman Alicavus, F., Kotysz, K., Latham, D., Matthews, J. M., Mønster, J., Niemczura, E., Paunzen, E., Sánchez Arias, J. P., Pigulski, A., Pepper, J., Richey-Yowell, T., Safari, H., Seager, S., Smalley, B., Shutt, T., Sódor, A., Suárez, J. -C., Tkachenko, A., Wu, T., Zwintz, K., Barceló Forteza, S., Brunsten, E., Bognár, Z., Buzasi, D. L., Chowdhury, S., De

- Cat, P., Evans, J. A., Guo, Z., Guzik, J. A., Jevtic, N., Lampens, P., Lares Martiz, M., Lovekin, C., Li, G., Mirouh, G. M., Mkrtychian, D., Monteiro, M. J. P. F. G., Nemeč, J. M., Ouazzani, R.-M., Pascual-Granado, J., Reese, D. R., Rieutord, M., Rodon, J. R., Skarka, M., **Sowicka, P.**, Stateva, I., Szabó, R., Weiss, W. W., 2019, MNRAS, 490, 4040, DOI: [10.1093/mnras/stz2787](https://doi.org/10.1093/mnras/stz2787)
11. “The short orbital period binary star at the heart of the planetary nebula M 3-1”
Jones, D., Boffin, H. M. J., **Sowicka, P.**, Miszalski, B., Rodríguez-Gil, P., Santander-García, M., Corradi, R. L. M., 2019, MNRAS, 482, L75, DOI: [10.1093/mnrasl/sly142](https://doi.org/10.1093/mnrasl/sly142)
 12. “On ϵ -mechanism-driven pulsations in VV 47”
Sowicka, P., Handler, G., Jones, D., 2018, MNRAS, 479, 2476, DOI: [10.1093/mnras/sty1660](https://doi.org/10.1093/mnras/sty1660)
 13. “Towards an improvement in the spectral description of central stars of planetary nebulae”
Weidmann, W., Gamen, R., Mast, D., Fariña, C., Gimeno, G., Schmidt, E. O., Ashley, R. P., Peralta de Arriba, L., **Sowicka, P.**, Ordonez-Etxeberria, I., 2018, A&A, 614, A135, DOI: [10.1051/0004-6361/201731805](https://doi.org/10.1051/0004-6361/201731805)
 14. “280 one-opposition near-Earth asteroids recovered by the EURONEAR with the Isaac Newton Telescope”
Vaduvescu, O., Hudin, L., Mocnik, T., Char, F., Sonka, A., Tudor, V., Ordonez-Etxeberria, I., Díaz Alfaro, M., Ashley, R., Errmann, R., Short, P., Moloceniuc, A., Cornea, R., Inceu, V., Zavoianu, D., Popescu, M., Curelaru, L., Mihalea, S., Stoian, A. -M., Boldea, A., Toma, R., Fields, L., Grigore, V., Stoev, H., Lopez-Martinez, F., Humphries, N., **Sowicka, P.**, et al., 2018, A&A, 609, A105, DOI: [10.1051/0004-6361/201731844](https://doi.org/10.1051/0004-6361/201731844)
 15. “The planetary nebula IC 4776, its post-common-envelope binary central star”
Sowicka, P., Jones, D., Corradi, R. L. M., Wesson, R., García-Rojas, J., Santander-García, M., Boffin, H. M. J., Rodríguez-Gil, P., 2017, MNRAS, 471, 3529, DOI: [10.1093/mnras/stx1697](https://doi.org/10.1093/mnras/stx1697)
 16. “Search for exoplanets around pulsating stars of A-F type in Kepler short-cadence data, the case of KIC 8197761”
Sowicka, P., Handler, G., Dębski, B., Jones, D., Van de Sande, M., Pápics, P. I., 2017, MNRAS, 467, 4663, DOI: [10.1093/mnras/stx413](https://doi.org/10.1093/mnras/stx413)
 17. “Survey of period variations of superhumps in SU UMa-type dwarf novae. VI. The sixth year (2013-2014)”
Kato, T., Dubovsky, P. A., Kudzej, I., Hamsch, F.-J., Miller, I., Ohshima, T., Nakata, Ch., Kawabata, M., Nishino, H., Masumoto, K., Mizoguchi, S., Yamanaka, M., Matsumoto, K., Sakai, D., Fukushima, D., Matsuura, M., Bouno, G., Takenaka, M., Nakagawa, Sh., Noguchi, R., Iino, E., Pickard, R. D., Maeda, Y., Henden, A., Kasai, K., Kiyota, S., Akazawa, H., Imamura, K., de Miguel, E., Maehara, H., Monard, B., Pavlenko, E. P., Antonyuk, K., Pit, N., Antonyuk, O. I.,

Baklanov, A. V., Ruiz, J., Richmond, M., Oksanen, A., Harlinton, C., Shugarov, S. Yu., Chochol, D., Masi, G., Nocentini, F., Schmeer, P., Bolt, G., Nelson, P., Ulowetz, J., Sabo, R., Goff, W. N., Stein, W., Michel, R., Dvorak, S., Voloshina, I. B., Metlov, V., Katysheva, N., Neustroev, V. V., Sjoberg, G., Littlefield, C., Dębski, B., **Sowicka, P.**, et al., 2014, PASJ, 66, 90, DOI: [10.1093/pasj/psu072](https://doi.org/10.1093/pasj/psu072)

II. *Other publications*

1. “GW Vir instability strip in the light of new observations of PG 1159 stars”
Sowicka, P., 2022, hypa.conf, 39., DOI: [10.5281/zenodo.7104586](https://doi.org/10.5281/zenodo.7104586)
2. “Discovery of Five Probable Novae in M81”
Hornoch, K., Errmann, R., **Sowicka, P.**, Humphries, N., Vaduvescu, O., 2015, ATel, 8180, [URL](#)
3. “A search for pulsating blue stars in the vicinity of NGC 6791 using Kepler LC data”
Sowicka, P., Bachulski, S., Baran, A., 2015, EPJWC, 101, 06061, [10.1051/epj-conf/201510106061](https://doi.org/10.1051/epj-conf/201510106061)
4. “Spectroscopic classification of CSS150213:100134+453359 in SDSS J100134.51+453339.9”
Elias-Rosa, N., Benetti, S., Dennefeld, M., De Cicco, D., **Sowicka, P.**, Ordovas-Pascual, I., Lam, M. C.-Y., 2015, ATel, 7120, [URL](#)
5. “Variable stars in the field of the young open cluster Roslund 2”
Sowicka, P., Handler, G., Taubner, R., Brunner, M., Passegger, V.-M., Bauer, F., Paunzen, E., 2014, IAUS, 301, 495, [10.1017/S1743921313015226](https://doi.org/10.1017/S1743921313015226)

Against all odds.

ABBREVIATIONS

(2/3)-D	(Two/Three)-Dimensional
(E/TP)-AGB	Early/Thermally Pulsing AGB
[WC]	Central Star of Planetary Nebula with C-rich Wolf-Rayet spectrum
ACAM	Auxiliary-port CAMera
ADC	Analogue-to-Digital Converter
ADU	Analog Digital Unit
AFTP	AGB Final Thermal Pulse
AGB	Asymptotic Giant Branch
BJD	Barycentric Julian Date
CCD	Charge-Coupled Device
DAV	Pulsating WD of DA spectral type
DBV	Pulsating WD of DB spectral type
DFOSC	Danish Faint Object Spectrograph and Camera
DK	1.54-m Danish Telescope at ESO
FDU	First Dredge-Up
FOV	Field of View
FTP	Final Thermal Pulse
FWHM	Full Width at Half Maximum
g mode	gravity mode
GTC	10.4-m Gran Telescopio Canarias
GW Vir	GW Virginis
HB	Horizontal Branch
HR	Hertzsprung-Russell
INT	2.54-m Isaac Newton Telescope
ISCZ	Intershell Convection Zone
LTE	Local Thermodynamic Equilibrium
LTP	Late Thermal Pulse
MS	Main Sequence
NLTE	Non-Local Thermodynamic Equilibrium
OCZ	Outer Surface Convection Zone

OSIRIS	Optical System for Imaging and low-Intermediate-Resolution Integrated Spectroscopy
p mode	pressure mode
PN	Planetary Nebula
PSF	Point Spread Function
RGB	Red Giant Branch
s-process	slow neutron capture process
S/N	Signal-to-Noise ratio
SAAO	South African Astronomical Observatory
SDU	Second Dredge-Up
SGB	Sub-Giant Branch
SHOC	Sutherland High Speed Optical Camera
TDB	Barycentric Dynamical Time
TDU	Third Dredge-Up
TP	Thermal Pulse
UHE	Ultra-High-Excitation lines
UV	Ultraviolet
VLTP	Very Late Thermal Pulse
WD	White Dwarf
WFC	Wide Field Camera
WHT	4.2-m William Herschel Telescope
ZAMS	Zero-Age Main Sequence

INTRODUCTION

This thesis describes observational efforts to solve some of the most important puzzles regarding the excitation of pulsations in hot pre-white dwarf stars, with a special focus on pre-white dwarfs of PG 1159 spectral type. Our aim is to improve our understanding of this stage of stellar evolution, which is of particular importance as these stars are supposed to be the principal progenitors of hydrogen-deficient white dwarfs (WDs).

Parts of this Chapter were written based on the following resources: **Stellar Structure and Evolution** (Kippenhahn et al., 2013), **Asteroseismology** (Aerts et al., 2010), and **The Importance of Binaries in the Formation and Evolution of Planetary Nebulae** (Boffin & Jones, 2019) textbooks, and review papers by Werner & Herwig (2006), Fontaine & Brassard (2008), Winget & Kepler (2008), Althaus et al. (2010), Handler (2013), and Córscico et al. (2019).

1.1 FINAL STAGES OF THE SINGLE STAR EVOLUTION OF LOW- TO INTERMEDIATE-MASS STARS

1.1.1 Introduction

According to canonical stellar evolution, over 97% of all stars in the Galaxy will end their lives as WDs (Fontaine et al. 2001). The evolution and fate of a star is mainly determined by its mass, and to a lesser extent by its chemical composition (metallicity) and rotation (Maeder & Meynet, 2000). The initial masses for stars following different evolutionary paths and their final fate are shown in Figure 1.1. The evolution of stars after the Main Sequence (MS) can be divided into three groups based on the initial mass: low mass stars (between about $0.8 - 2 M_{\odot}$, they develop a degenerate helium core and ignite helium in a helium flash), intermediate mass stars (between about $2 - 8 M_{\odot}$, they develop a non-degenerate helium core and helium burning ignition is stable), and massive stars (over about $8 M_{\odot}$ they ignite carbon burning, and over about $11 M_{\odot}$ they also ignite nuclear burning of heavier elements, up to the development of an iron core). Most of the stars that are formed with an initial mass between about 0.08^1 and $8 M_{\odot}$ (low to intermediate mass) will eventually end as WD stars. The evolution of massive stars ends violently, as the iron core collapses in a stellar explosion called supernova, leaving behind a neutron star or black hole remnant, embedded in an expanding nebula containing the matter expelled in

¹ The first determination of the lower limit to the mass of the main-sequence stars was done by Hayashi & Nakano (1963).

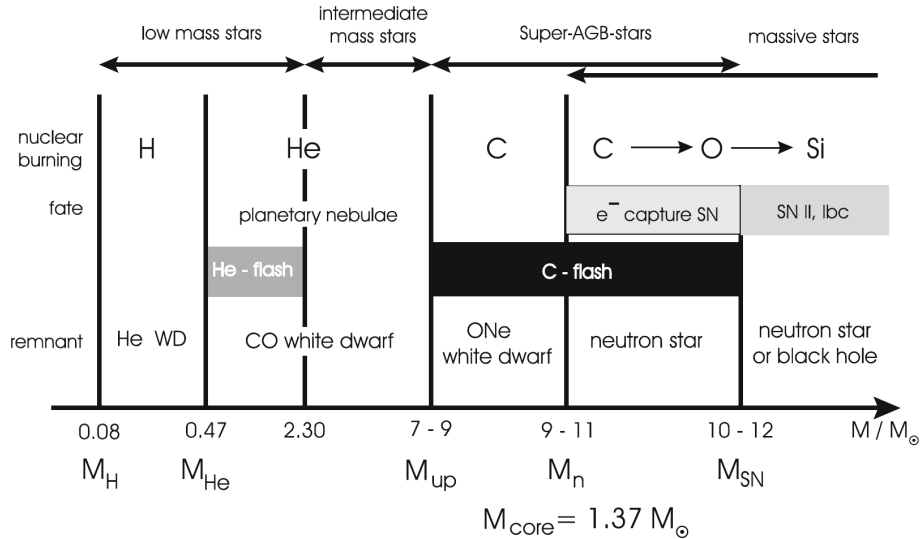


Figure 1.1: Evolution and final fate of single stars depending on their initial masses. These masses can vary with different initial composition and models used for computations. Reproduced with permission from the **Stellar Structure and Evolution** textbook (Kippenhahn et al., 2013).

the explosion. We will follow the evolution of low- to intermediate-mass stars across the Hertzsprung-Russell (HR) diagram, shown in Figure 1.2, as those stars are the focus of this thesis.

1.1.2 Evolution of low- to intermediate-mass stars

Stars are born in molecular clouds. A contracting star with mass greater than $0.08 M_{\odot}$ ignites Hydrogen (H) in the core and becomes a Zero-Age Main Sequence (ZAMS) star.

The initial stage of evolution of the low- to intermediate-mass stars involves burning H into Helium (He) in their cores while on the MS via p-p chains (dominating in low-mass stars) or the CNO cycle (dominating in intermediate-mass stars). Stars spend most of their lives on the MS (the time a star spends on the MS depends on its mass and decreases with increasing mass) at near constant effective temperature and luminosity. They evolve off the MS when the core H is exhausted, and at that point the star has a He core surrounded by a H envelope with H burning in a shell at the bottom of the envelope. The core grows in mass due to H burning ash and the H burning shell moves outwards, causing the envelope to expand and cool while maintaining similar luminosity – the star is a subgiant (its He core is in thermal equilibrium and the mass of the He core is below the Schönberg-Chandrasekhar limit, Schönberg & Chandrasekhar 1942) on the Subgiant Branch (SGB). The subsequent evolution is slightly different for low- and intermediate-mass stars.

In the case of low-mass stars, shell H burning continues until the He core increases in mass, up to the point when it becomes degenerate. Then the core contracts while its temperature increases, and the energy generation rate in the H burning shell increases as well because it is strongly dependent on the temperature – the star is at the bottom of the Red Giant Branch (RGB).

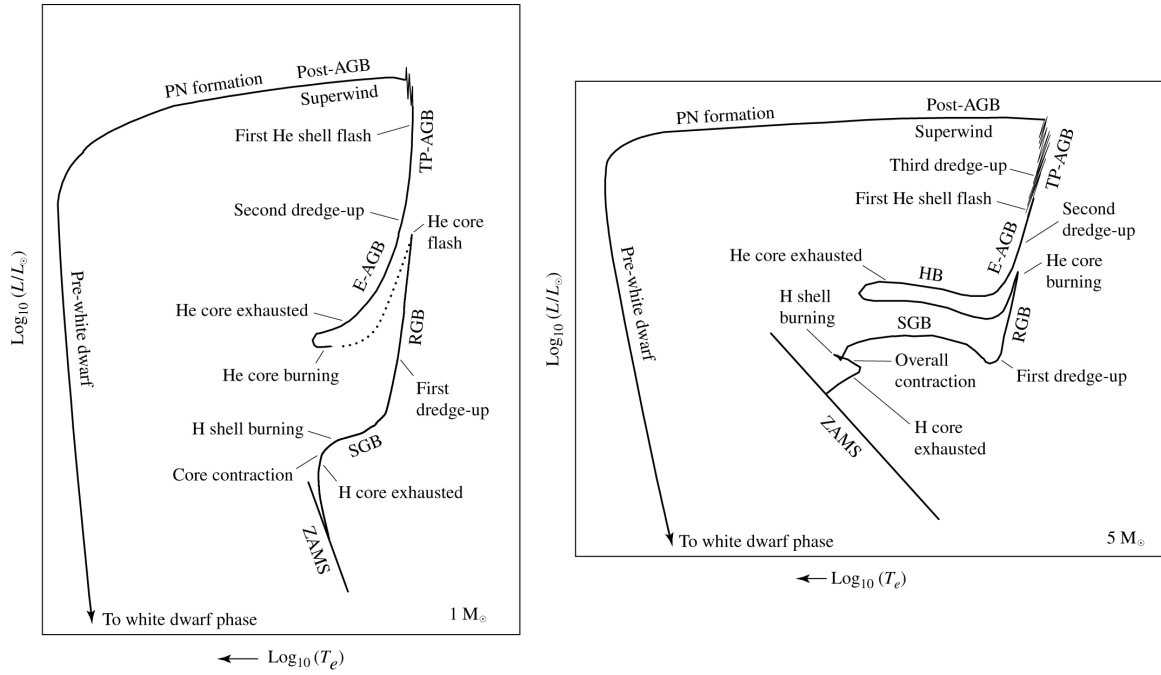


Figure 1.2: Evolutionary tracks for a $1 M_{\odot}$ star (left) and a $5 M_{\odot}$ star (right) from the Zero-Age Main Sequence (ZAMS) to the white dwarf cooling track. Figure reproduced from Carroll & Ostlie (2017).

In the case of intermediate-mass stars, the Schönberg-Chandrasekhar limit is reached before the He core becomes degenerate, meaning that it is no longer in thermal equilibrium. It begins to contract and heat up, while the stellar envelope expands and cools, and the star moves towards the RGB. Before the He core becomes degenerate, the opacity in the cooling envelope increases until it becomes convective which ends the cooling phase, while the energy generation rate in the shell increases and so does luminosity, and the star reaches the bottom of the RGB. The subgiant phase in this case is very short, and hardly any star is found in that part of the HR diagram, in a so-called Hertzsprung gap.

The evolution on the RGB is similar in both cases. Nuclear burning in the H shell continues, causing the He core to further increase in mass and temperature, causing the star to increase its luminosity, expand, and slightly cool. At this point, the star ascends on the RGB. During the ascent, the convective envelope grows and reaches deeper layers of the star, until eventually it reaches the products of H burning and brings them to the surface, in a so-called first dredge-up (FDU), which changes the surface composition. In low-mass stars, this process lasts until the star reaches the tip of the RGB, at which point the core is degenerate and cannot grow more. The core temperature is sufficient to ignite He burning via the triple- α reaction, but because the core is degenerate, the ignition results in a thermal runaway (a He-flash). The He-flash lifts the degeneracy in the core, and the star starts stable He burning in the core and continues H burning in the shell, now being on the Horizontal Branch (HB). In intermediate-mass stars, He ignition is not violent, as they do not develop a degenerate core (its mass is below the Schönberg-Chandrasekhar limit). These stars become hot enough to start the triple- α process before the core becomes degenerate and they reach the tip of the RGB, moving along a “blue-loop” (towards higher effective

temperatures, then increasing luminosity and cooling). The size of the loop depends on the stellar mass, with more massive stars performing more extended blue loops.

Stars remain on the HB until He in their cores is exhausted, both in the low- and intermediate-mass case. At this point, the core is made of C and O (He-burning ashes), He burning moves to a shell, and the star is on the Asymptotic Giant Branch (AGB). Only stars that are massive enough (initial masses between about $0.8 M_{\odot}$ and $8 M_{\odot}$) evolve through the AGB stage. The AGB stage consists of two phases, the first being the early AGB (E-AGB), where He is burned in a shell (no H-burning at that time) with a transition layer between the H-rich convective envelope and He reservoir. Convection may reach below that layer and bring ashes of H-shell burning to the surface, in a process called the second dredge-up (SDU). The SDU ends when convection has brought enough H down to reignite the outer H-burning shell. Thermal instabilities (Härm-Schwarzschild instabilities, Schwarzschild & Härm 1965) in the He-burning shell lead to unstable shell burning, resulting in a thermal runaway, in a reoccurring cycle called thermal pulses (TP) – a star is in the thermally pulsing AGB (TP-AGB) phase. A short-lived, pulse-driven intershell convection zone (ISCZ) mixes the matter between the two shells into the He-burning shell, and the outer surface convection zone (OCZ) can reach into the H-shell. The ISCZ may dredge H into the intershell region, as well as bring carbon into the outer layers. The OCZ can reach the intershell region and dredge up this material into the outer envelope, also transporting H-rich material downwards. This process is called the third dredge-up (TDU). Low-mass stars do not experience SDU at the end of the He-burning in the core – their He-burning shell moves outwards towards the outer H-burning shell and forms an intershell region, which drives thermal pulses the same way as in the case of intermediate-mass stars. In both cases, each thermal pulse drives the TDU episode which brings the nucleosynthesis products from both H- and He-shell burning to the surface, including the slow neutron capture process (s-process) elements and C (forming a Carbon star). The AGB stars of lower mass are thought to be the main source for s-process elements, where ^{13}C nuclei form the ^{13}C -pocket and provide the necessary neutron source.

During the TP-AGB phase, significant mass loss is triggered in a form of a slow and dense stellar wind, and the star expels most of the envelope material into the interstellar medium. Because of the strong mass reduction, the star departs from the AGB and enters its post-AGB evolution, when the core is contracting and heating at almost constant luminosity. The mass loss causes the deeper layers of the star to emerge, leading to an increase in effective temperature. Eventually, the temperature of the exposed C/O core is high enough to begin to ionize the expelled surrounding material (by ultraviolet (UV) radiation) which becomes visible as a planetary nebula (PN). Emission lines originating from the different ionized chemical species in the ejecta are responsible for the characteristic spectra of PNe (and false colors seen in the composite images of PNe). The post-AGB star continues to move towards its maximum effective temperature, and when the nuclear burning ceases, the star enters the WD cooling track. The post-AGB evolution described above outlines the main channel, that is responsible for the creation of H-rich stars (the majority of post-AGB stars). Those stars keep their H envelope throughout their evolution,

although it can become contaminated by processed material dredged-up during the RGB and AGB stages, and end up as WDs of DA spectral type.

Another channel creates H-deficient post-AGB stars – about a quarter of all post-AGB stars. Among those are the He-dominated O(He) stars and C-dominated PG 1159 stars (and their predecessors, the central stars of planetary nebulae with C-rich Wolf-Rayet spectra – [WC] stars, Crowther et al. 1998). Other classes of H-deficient post-AGB stars exist, but will not be discussed here. The currently accepted scenario for the formation of O(He) stars involves different types of binary mergers or common envelope scenarios (Reindl et al. 2014). The formation of PG 1159 stars is understood by the means of a “born-again” scenario (e.g., Fujimoto 1977, Schoenberner 1979, Iben et al. 1983). In some cases, the star may experience the final thermal pulse after leaving the AGB. Such a late thermal pulse causes the star to evolve back to the AGB and create an extra “loop” in its evolutionary track. This final pulse alters the evolution of the star, as can be seen in Figure 1.3. The timing of the final thermal pulse (FTP) is responsible for the surface abundance of H (see Herwig, 2001). A pulse-driven convection zone mixes the envelope with the intershell region, which results in a H-deficient surface, as H is diluted in the intershell material. The final surface composition and H abundance critically depends on the mass of the envelope in comparison to the intershell region when the FTP occurs. When those two regions are of comparable mass, the FTP happens at the descent from the AGB and therefore is called the AGB final thermal pulse (AFTP, dashed-dotted line in Fig. 1.3). The AFTP, however, does not lead to a “born-again” evolution and creates the hybrid PG 1159 stars with detectable hydrogen surface abundances of about 10-20% by mass (Löbbling et al., 2019). If the FTP happens during the post-AGB evolution at constant luminosity (nuclear burning still ongoing), where the H-rich envelope is less massive, the star expands and returns to the AGB creating a “loop”. This FTP is called the late thermal pulse (LTP, dotted line in Fig. 1.3) and it reduces the H surface abundance below the detection limit (about 1% by mass; Werner & Herwig 2006; Löbbling et al. 2019) because of dilution. Finally, when the star has already entered the WD cooling track, the envelope mass had decreased further and nuclear burning had ceased. In that case, the FTP causes the entire H-rich envelope to mix down to the He-burning shell, where all the remaining H is burned. That FTP is called the very late thermal pulse (VLTP, solid line in Fig. 1.3) and the star becomes H-free, with a detectable higher Nitrogen (N) abundance as another tracer of the evolutionary history.

[WC] stars are believed to be the progenitors of the PG 1159 stars, and two [WC]-PG 1159 transition objects are known (Abell 30 and Abell 78, Leuenhagen et al. 1993, Toalá et al. 2015). PG 1159 stars that originate from a VLTP scenario will eventually turn into WDs of DO spectral type (He II lines, no H), when gravitational settling cannot be prevented because the radiation-driven wind has weakened. In the case of PG 1159 stars having evolved according to the AFTP or LTP scenarios, the stars will turn into DA-type WDs (H lines).

The single star evolution scheme described above is not the only channel proposed to produce PG 1159 stars. Werner et al. (2022b) and Miller Bertolami et al. (2022) recently suggested that a binary WD merger scenario is a plausible explanation for the formation

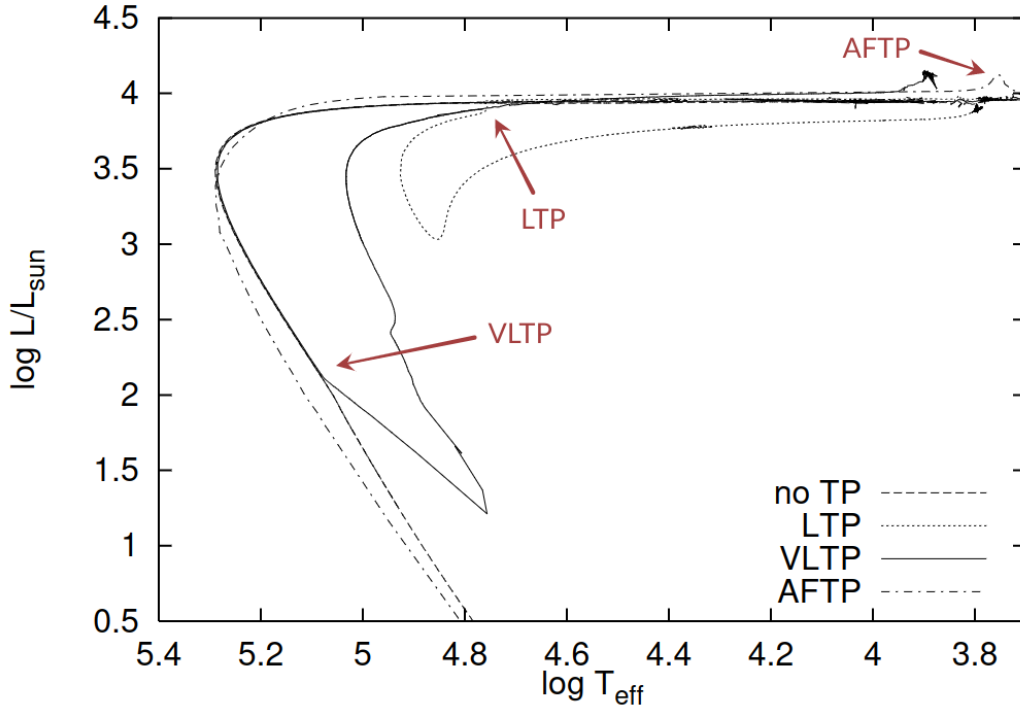


Figure 1.3: Evolutionary tracks for a $0.6 M_{\odot}$ star for different post-AGB evolution scenarios. Dashed line: no FTP (canonical evolution), dotted line: LTP, solid line: VLTP, dashed-dotted line: AFTP. Arrows indicate when the FTP starts. Adapted from Herwig (2001).

of low-luminosity PG 1159 stars, because the newly established spectroscopic class of hot H-deficient subdwarfs (CO-sdO) shows similar surface abundances to PG 1159 stars but at lower temperatures, and higher surface gravities than predicted by the “born-again” scenario.

PG 1159 stars are the main focus of this thesis, and only that group of pre-WD stars will be described further.

1.2 PG 1159 SPECTRA

Primarily, WD stars were spectroscopically classified according to the presence of hydrogen in their atmospheres into the DA WDs (hydrogen-rich, around 80% of WDs) and non-DA WDs (hydrogen-deficient, helium-rich, around 20%)². The non-DA WDs are further split into several classes: DO (dominant He II lines in the optical spectrum, McCook & Sion 1999), DB (dominant He I lines), DQ (dominant C lines), DZ (dominant metal lines), and DC (no dominant lines, continuous spectrum). The spectral evolution of non-DA WDs is not completely clear, but PG 1159 stars are thought to belong to two evolutionary channels, the post-VLTP one – [WC] → PG 1159 → DO → DB → DQ (Althaus et al., 2005b; Bédard et al., 2022), or the post-LTP/AFTP one – [WC] → PG 1159 → DA (Althaus et al., 2005a; Weidmann et al., 2020).

² Greenstein (1958) was the first to recognize these two types, while Córscico et al. (2019) provided the most recent percentage.

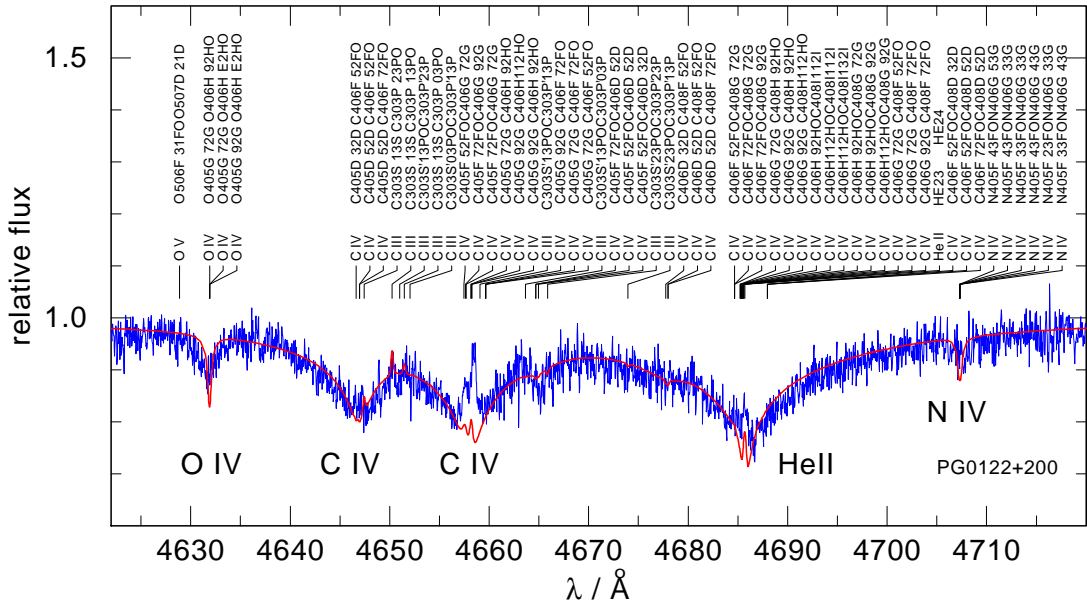


Figure 1.4: Characteristic absorption trough in the “cool” PG 1159 star PG 0122+200. Overplotted is a model with $T_{\text{eff}}=80000$ K, $\log g = 7.5$, $C/\text{He} = 0.1$, $N/\text{He} = 0.01$, and $O/\text{He} = 0.01$. Credit: Werner & Rauch (2014), reproduced with permission ©ESO.

Green & Liebert (1979) showed the first optical spectrum of PG 1159–035, revealing a broad absorption “trough” made by He II 4686Å and adjacent C IV lines (see Figure 1.4 for the identification of the individual lines in the absorption trough). PG 1159–035 became the prototype of a new spectroscopic class, and the aforementioned trough serves as the main spectral feature for distinguishing PG 1159-type stars. Years later, Schoenberner & Napiwotzki (1990) showed that several central stars of PNe are spectroscopic twins of PG 1159 stars, which were added to that class. Finally, Werner (1992) subdivided those stars based on the characteristics of the absorption trough, as sometimes central emission reversals are observed, into three classes: “A” – absorption lines, “E” – emission lines, and “lgE” – low gravity with emission lines. The elemental abundances in hydrogen-deficient, helium-, carbon-, and oxygen-rich atmospheres of PG 1159 stars are typically $X_{\text{He}} \approx 0.33$, $X_{\text{C}} \approx 0.50$, $X_{\text{O}} \approx 0.17$ by mass (this abundance pattern comes from PG 1159–035 itself and could be called “mean”, Werner & Herwig 2006). However, notable variations in He, C, and O abundances were found from star to star (Table 2 in Werner & Herwig 2006), as were traces of other, heavier elements (e.g., even zinc, a trans-iron group element, detected in PG 1707+427, Hoyer et al. 2018). Figure 1.5 shows elemental abundances determined for five PG 1159 stars, where notable differences in abundances between different stars, especially for nitrogen, oxygen, and fluorine, can be found.

The whole picture is complicated even more by peculiarities discovered in the spectra. The presence of hydrogen (visible Balmer lines) was discovered by Napiwotzki & Schoenberner (1991) in the spectrum of the central star of planetary nebula Sh 2–68, and such stars are denoted PG 1159 “hybrid” type since (five members of this subclass are currently known). The two hottest members of the PG 1159 class ($T_{\text{eff}} \geq 200000$ K),

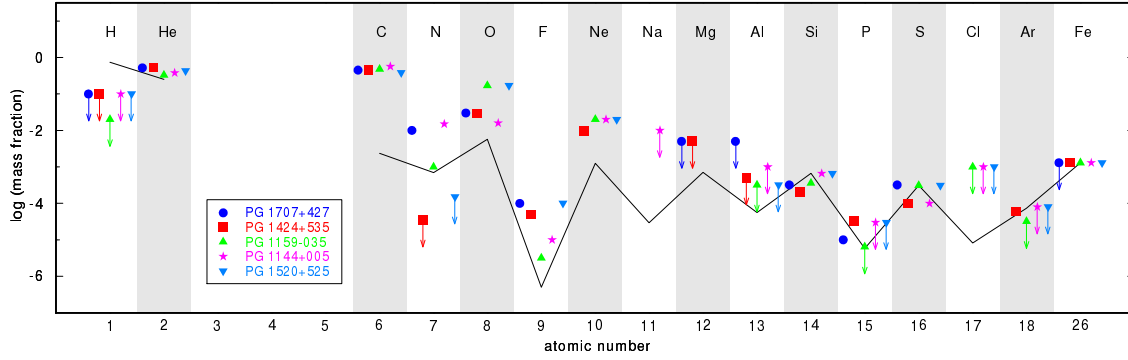


Figure 1.5: Elemental abundances of five PG 1159 stars. Black solid line indicates solar values. Credit: Werner et al. (2016), reproduced with permission ©ESO.

namely RX J0439.8–6809 and H 1504+65, show *both* H- and He-deficiency and a C/O abundance ratio of 1 (Werner & Rauch, 2015). SDSS J121523.09+120300.8 displays ultra-high-excitation (UHE) lines in absorption, still an unexplained phenomenon (Hügelmeier et al. 2006, Reindl et al. 2021). What more, there is an observed nitrogen dichotomy: the N-rich stars are characterized by the atmospheric nitrogen abundance of about 1% N/He, while the N-poor ones – below about 0.01% N/He (Dreizler & Heber 1998, the dichotomy can be seen also in Figure 1.5).

In the family of hot, He-rich pre-WDs and WDs, other groups also show HeII and CIV lines. O(He) stars are He-rich pre-WDs with significantly less carbon than PG 1159 stars (up to 3% of C in their atmospheres, Reindl et al. 2014). The progeny of PG 1159 stars, hot He-rich (DO) WDs, present a reduction of the C abundance as a star evolves. In a “transition” phase, the stellar wind weakens to the point when gravitational settling becomes more effective, leading to continuous sinking of heavier elements (Quirion et al. 2012). The limit is model-dependent, and the choice is arbitrary – Werner et al. (2014) adopted $C/He < 9\%$ (by mass) to distinguish between PG 1159 and DO stars. Besides very different chemical compositions, PG 1159 stars also cover a wide range of effective temperatures ($T_{\text{eff}} = 75000 - 250000$ K) and surface gravities ($\log g = 5.5 - 8$ cm/s²).

Spectral analysis of PG 1159 stars is especially challenging, both observationally and theoretically. For such hot stars, the assumption of local thermodynamic equilibrium (LTE) is not valid, and model calculations should be done in the non-local thermodynamic equilibrium (NLTE) case. This implies a need for reliable atomic data, and increases the computational effort. From the observational point of view, spectra in the UV are desired to better constrain the physical parameters and surface abundances, especially of metals, of those stars (see, e.g., Werner et al. 2015, Werner et al. 2016).

1.3 STELLAR PULSATIONS

The stellar interiors of most stars are unavailable to study. That, however, is not the case for one particular group of intrinsic variable stars, which change their light due to inter-

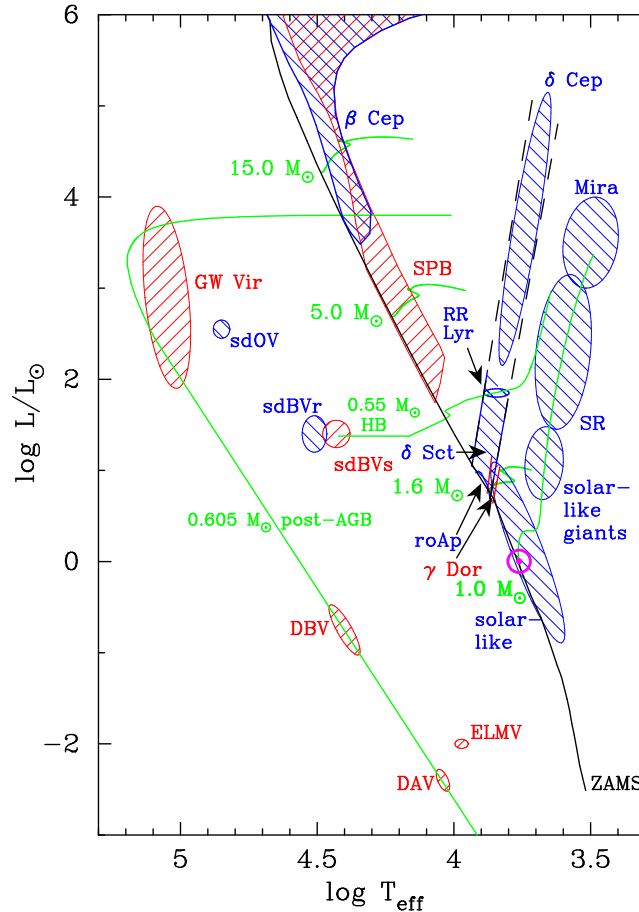


Figure 1.6: Theoretical Hertzsprung-Russell diagram showing locations of various groups of pulsating stars. The classical instability strip is indicated by black dashed straight lines. Locations of p mode pulsators are shown in blue; those of g mode pulsators in red, whereas the green lines show some example evolutionary tracks. Figure courtesy of Gerald Handler.

nal physical processes³ – pulsating stars. Pulsating stars change their sizes/shapes, which causes changes in their light output, that can be measured. In photometric observations, pulsations are manifested as periodic brightness changes in a light curve, while spectroscopic observations reveal changes in the shapes of spectral lines and radial velocity. The observations and analysis of stellar pulsations is the basis of asteroseismology. Asteroseismology is a branch of astrophysics that utilizes stellar oscillations as seismic waves to study stellar interiors, therefore allowing a “view” beneath stellar photosphere.

Stellar pulsations are common – pulsating stars populate almost the entire Hertzsprung-Russell diagram, as shown in Figure 1.6, indicating that stars at almost any evolutionary stage can be probed through the methods of asteroseismology.

A star can pass through various instability strips during its evolution across the HR diagram. When a star is destabilized, causing it to start pulsating, a driving mechanism is needed to sustain pulsations. The oscillations that a given star shows are associated with its internal conditions.

³ As opposed to extrinsic variables, that change their light due to external processes, e.g., eclipsing binary stars.

Many classes of pulsating stars oscillate in normal modes that can be separated into two groups: radial and nonradial modes. During the radial mode oscillations, the spherical symmetry is preserved. This is not the case for the nonradial oscillations, where the star changes its shape: it causes distortions on the stellar surface in a form of alternating sectors of opposite phases. Stars are three-dimensional (3-D) spheres, and the changes of their shape are best described using superposition of spherical harmonics given by

$$Y_\ell^m(\theta, \phi) = (-1)^m c_{\ell m} P_\ell^m(\cos \theta) e^{im\phi}, \quad (1.1)$$

where θ is co-latitude (measured from the polar axis), ϕ is longitude, $P_\ell^m(\cos \theta)$ are Legendre polynomials, and $c_{\ell m}$ is a normalization constant. For 3-D stars there are three quantum numbers that describe the modes: ℓ – the spherical degree, m – the azimuthal order, and k – the radial overtone, also called radial order and sometimes denoted n (ℓ and m are included in Equation 1.1). ℓ specifies the number of node lines on the surface (regions where no motion takes place that separate sectors in antiphase), and is greater or equal to 0. Modes with $\ell = 0$ are radial modes, while modes with $\ell > 0$ are nonradial modes. Modes with $\ell = 1$ are also called dipole modes, while those with $\ell = 2$ – quadruple modes. $|m|$ is the number of node lines that intersect the equator, and the values of m are in the range $\langle -\ell, \ell \rangle$, meaning there are $2\ell + 1$ modes for each ℓ . Modes with $m \neq 0$ are travelling waves, and the sign denotes the direction of motion: modes with $m > 0$ are travelling in the direction of stellar rotation and are called prograde modes, while those with $m < 0$ are travelling against the direction of rotation and are called retrograde modes. k describes the number of nodes in the stellar interior. When $k = 0$, there are no nodal lines in the interior, and such a mode is called a fundamental mode, or f mode (sometimes abbreviated as F). Consequently, a mode with one nodal line is described by $k = 1$ and called the first overtone (1O), with two lines and $k = 2$ – the second overtone (2O), and so on. In the case of nonradial modes, there is always a node line and $k \geq 1$. Figure 1.7 shows a graphical representation of spherical harmonics with different values of ℓ and m .

Pulsation modes can also be divided according to the restoring force that tries to bring the star back into equilibrium, into pressure modes (p modes) and gravity modes (g modes). For p modes (acoustic waves), pressure is the primary restoring force, while for g modes it is buoyancy. Pressure modes are associated with vertical gas motions and gravity modes with primarily horizontal gas motions. Therefore, radial modes are always pressure modes. Pressure and gravity modes differ by a number of observed properties. A general property of p modes is that their frequencies increase with the radial overtone k , while the opposite takes place for g modes. Pressure and gravity modes probe different regions of the stellar interior: p modes are the most sensitive to the conditions in the outer layers of a star, while g modes probe the deep interior – except for WD stars, where the g modes are sensitive to the outer layers. In the asymptotic regime, where $k \gg \ell$, p modes are equally spaced in frequency, whereas g modes are equally spaced in period. There are also mixed modes, meaning that p modes and g modes are simultaneously excited in a star – such modes provide information about both the stellar interior and the envelope. Mixed-mode pulsations can be found in stars laying in overlapping regions for p- and

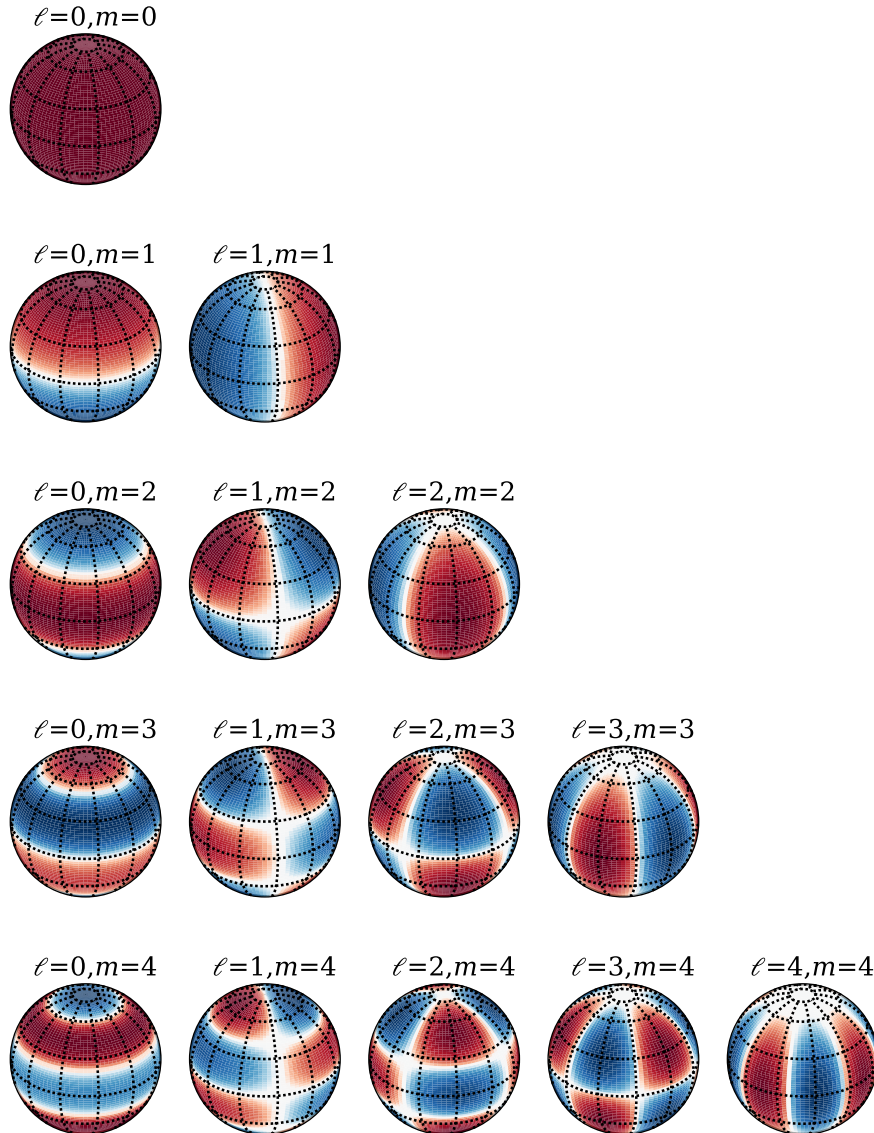


Figure 1.7: A graphical illustration of spherical harmonics. Red and blue colors denote areas that are moving in the opposite direction. Figure generated using a modified Python code originally written by Alex DeCaria.

g-mode pulsations in the HR diagram (cf. Figure 1.6), and such stars are called “hybrid” pulsators, examples being δ Scuti/ γ Doradus stars (e.g., Handler & Shobbrook, 2002) or β Cephei/SPB stars (e.g., Handler et al., 2009). Other groups of modes also exist, e.g., the r modes – global normal modes of Rossby waves in rotating stars (Papaloizou & Pringle, 1978; Saio et al., 2018).

A driving mechanism must be operating for a star to maintain pulsations. The main driving mechanisms that were proposed are the ϵ mechanism, the $\kappa - \gamma$ mechanism, stochastic driving, and convective blocking. The ϵ mechanism (Eddington, 1926) is based on a variable nuclear energy generation rate, ϵ , which strongly depends on the temperature. During compression of the nuclear burning region, pressure and temperature rise, and so does the energy production. That causes expansion, and the pressure and temperature

drop, and the energy generation drops as well. Then, the cycle continues. So far, the ϵ mechanism is only a theoretical concept, as no convincing observational evidence for pulsations driven by the ϵ mechanism exists to date. In Chapter 3, the ϵ mechanism will be discussed further. Another driving mechanism that is connected with an increase in opacity is known as the $\kappa - \gamma$ mechanism (Zhevakin, 1953; Baker & Kippenhahn, 1962). If the opacity increases in a certain layer inside a star (an ionization layer of a certain species), the radiation from the layers below is blocked, increasing pressure and causing the gas to heat up (during compression). When the star tries to reach equilibrium by expanding, the excess energy accumulated in this layer causes the star to expand beyond the equilibrium point. When the gas is ionized, the opacity reduces, the gas cools down and eventually the star contracts, while the ions recombine, and the process repeats. The $\kappa - \gamma$ mechanism is associated with regions where (partial) ionization of certain chemical species takes place. For example, pulsations excited in stars in the classical instability strip, i.e., δ Cephei, RR Lyrae, and δ Scuti stars, are connected to the He II ionization zone, whereas H I and He I ionization zones are believed to be responsible for pulsations in e.g., roAp stars. Convective blocking (Guzik et al., 2000) is a similar mechanism to the $\kappa - \gamma$ mechanism, but the layer blocking the flux is not the ionization zone of certain elements, but rather the base of a convection zone. This mechanism is thought to excite or at least contribute to pulsations of, e.g., DAV (pulsating WDs of DA spectral type) and DBV (pulsating WDs of DB spectral type) stars, as well as γ Doradus stars. Finally, pulsations in the Sun and solar-like stars are stochastically excited due to turbulent motion in the surface convection zones (Christensen-Dalsgaard & Frandsen, 1983).

As the pulsation modes excited in a star strictly depend on the internal conditions, asteroseismology is a unique tool of great importance for stellar physics. Its basic application concerns the determination of stellar parameters, like density (and eventually mass), or H content (and eventually age). Furthermore, observed frequencies of pulsation modes can be compared to the ones computed using theoretical models, to not only learn about the interiors of the stars, but also verify and refine those models. The determination of interior rotation profiles (Aerts et al., 2019) and chemical stratification are other possible applications of asteroseismology. The list is by no means exhaustive, but highlights the potential and possible applications of asteroseismology.

1.4 GW VIR PULSATIONS

Back in 1979, pulsations were discovered in the class prototype, PG 1159-035 \equiv GW Virginis (GW Vir) (McGraw et al., 1979). The GW Vir class was born a few years later with the discovery of the second variable star of PG 1159 spectral type, K 1-16 (Grauer & Bond, 1984)⁴. Currently, 30 GW Vir stars are known: 24 of PG 1159 spectral type (including PG 1159-hybrids, Sowicka et al. 2023, Table 2 in Chapter 5) and six of [WC] spectral type (including [WC]-PG 1159 transition objects, Quirion et al. 2007).

⁴ PG 1159–035 became the prototype of two classes: PG 1159 spectral class, and GW Vir variable class (GW Vir is the variable designation of PG1159–035).

1.4.1 *Excitation mechanism(s)*

The excitation mechanism operating in GW Vir stars was correctly identified for the first time in the works of the Los Alamos National Laboratory group (Starrfield et al. 1983, Starrfield et al. 1984, Starrfield et al. 1985; Stanghellini et al. 1991)⁵. Their calculations showed that the driving in PG 1159 models corresponds to the classic $\kappa - \gamma$ mechanism associated with the opacity bump due to the partial ionization of the K-shell electrons of carbon and oxygen in the envelope. Those early works were not able to explain all the observed properties of GW Vir stars, like the He-deficiency in the driving zone needed to drive the pulsations (“helium poisoning” leading to a hypothesis of composition gradients between the photosphere and the driving region), or problems with the excitation of the long-period modes. The improvement in opacity calculations allowed Saio (1996) and Gautschy (1997) to use the OPAL opacity tables to show that pulsations can be successfully driven in their simplified evolutionary models⁶ with a uniform surface composition that is observed in PG 1159-type stars (thus no need for the composition gradient reported before), and all the observed period ranges of the modes could be reproduced. The existence of a composition gradient was further tested by Bradley & Dziembowski (1996) and Cox (2003), who also used modern opacity tables and still found a need for a different chemical composition in the driving regions of their models. The following work by Quirion et al. (2004) explored the question of mode excitation in models with chemically homogenous envelopes of typical PG 1159 surface compositions, and found no need to invoke composition gradients, further supporting the idea of significant mass loss in these stars homogenizing the envelopes (see, e.g., Unglaub & Bues 2000). Moreover, Quirion et al. (2004) confirmed the results of the pioneering work from the Los Alamos group and described in detail the driving/damping process. A significant step forward was made by Gautschy et al. (2005), who used state-of-the-art models accounting for the evolutionary history: following the evolution starting from the main sequence and including the final helium flash after the thermally pulsing AGB phase. Their main results included showing (again) no need to invoke abundance gradients, and identifying a theoretical blue and red edge of the instability strip. Córscico et al. (2006) re-examined the GW Vir instability strip on the basis of newly computed PG 1159 evolutionary models of Althaus et al. (2005b) and Miller Bertolami & Althaus (2006), following the complete evolutionary history from ZAMS through the “born-again” scenarios. Aside from the confirmation of the previous results described here but based on more realistic stellar models, they identified the existence of a red edge at high luminosities (mass-dependent). These results were the basis of further asteroseismic studies of GW Vir stars by the La Plata group (e.g., Córscico et al., 2007; Córscico et al., 2009a; Córscico et al., 2011; Calcaferro et al., 2016), which provided extensive and consistent results for those stars. Subsequent stability studies by Quirion et al. (2007) also confirmed previous results regarding $\kappa - \gamma$ -driven pulsations, but more importantly found that the instability domain in the $\log g - T_{\text{eff}}$ plane is strongly dependent on the C and O content

⁵ Starrfield et al. used static envelope models, while Stanghellini et al. used simplified evolutionary models.

⁶ There were no evolutionary models with realistic histories, i.e., evolved through the thermally pulsing AGB phase, that the authors could use.

of the envelopes of GW Vir stars. With strong variations in the surface abundances of these stars, it implied that the blue edge is, in fact, “fuzzy” – as a superposition of blue edges for different compositions.

In the context of the excitation mechanisms operating in GW Vir stars, the work of Córscico et al. (2009b) is particularly relevant. The ϵ mechanism was first introduced by Sir Arthur Eddington (Eddington, 1926) and is based on the strong dependence of nuclear burning rate on temperature. The stability analysis by Córscico et al. (2009b) was an extension of the pioneering work by Kawaler et al. (1986), and already mentioned studies by Bradley & Dziembowski (1996) and Gautschy (1997). Kawaler et al. (1986) were the first to report pulsational instabilities driven by the ϵ mechanism at the position of the He-burning shell on the basis of fully nonadiabatic g mode pulsation calculations for H-deficient pulsating central stars of PNe. While stability analyses regarding the ϵ mechanism were already included in the works by the latter authors and by Gautschy et al. (2005), Córscico et al. (2009b) were the first to identify a separate, well-defined theoretical PG 1159 instability strip in the $\log T_{\text{eff}} - \log g$ plane originating from the short-period g modes excited by the ϵ mechanism (Figure 1.8). Moreover, the new instability strip partially overlapped with

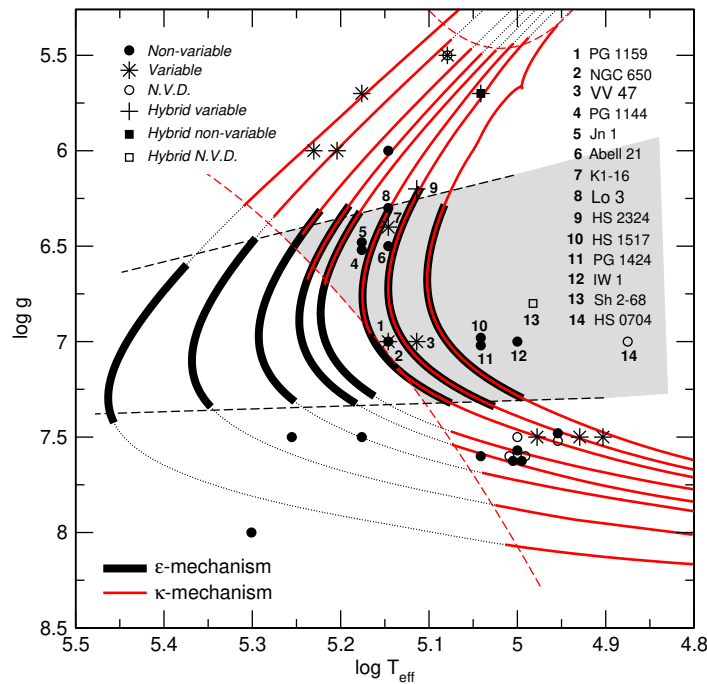


Figure 1.8: PG 1159 evolutionary tracks with stellar masses from $0.515 M_{\odot}$ (right) to $0.742 M_{\odot}$ (left). Solid red curves show the $\ell = 1$ κ -destabilized modes, while thick black curves correspond to ϵ -destabilized modes. The gray shaded area indicates the stellar models with both κ - and ϵ -destabilized modes. Relevant PG 1159 stars known at that time are overplotted. Reproduced from Córscico et al. (2009b).

the GW Vir instability strip for the $\kappa - \gamma$ -driven modes. Even though a number of known PG 1159 stars lies in the region where both mechanisms can operate, there is no convincing evidence for the ϵ mechanism to operate in any PG 1159 star to date (see, e.g., Sowicka et al. 2018). More information about the ϵ mechanism can be found in Chapter 3.

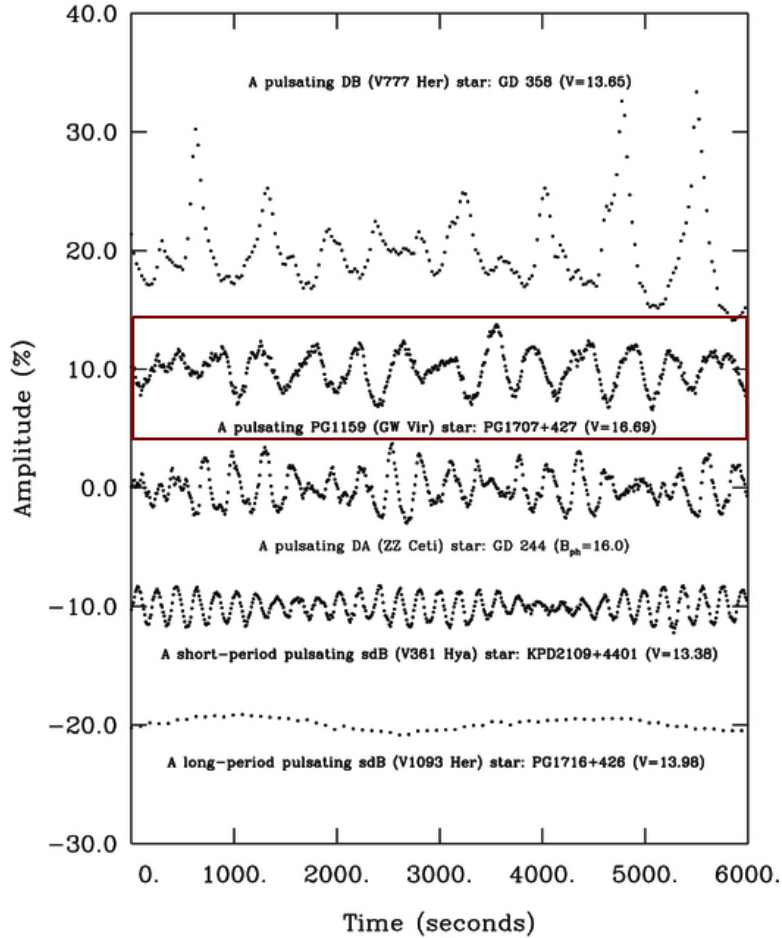


Figure 1.9: GW Vir pulsator (marked in a red box) in a family of compact pulsators. Adapted from Fontaine & Brassard (2008).

1.4.2 Pulsational properties

As briefly discussed above, pulsations provide a wealth of information about the stars and their interiors. The pulsations of pre-WDs and WDs give an additional advantage – they allow insight into the evolutionary history engraved in their interiors. Those stars show a large variety of light curve shapes, as can be seen in Figure 1.9. Pulsations exhibited by GW Vir stars, with an exemplary light curve marked in Figure 1.9, are multiperiodic and usually characterized by low amplitudes (1 mmag – 0.15 mag) and short periods (300 s – 6000 s, Córscico et al. 2019). The oscillations are due to nonradial g modes (where the restoring force is buoyancy) with low spherical degree, ℓ , and high radial order, k .

The first information that can be directly extracted from a light curve is the pulsation spectrum. The periods (Π) of detected pulsations allow the identification of the class of the mode (e.g., p or g mode) from a comparison against the periods computed from appropriate stellar models. In the asymptotic theory of nonradial stellar oscillations (Tassoul 1980), the modes of the same spherical degree ℓ with consecutive radial overtones k should be equally spaced in period. Such a common pattern (called a mean period spacing, $\Delta\Pi$) can be identified in the period spectrum of g mode pulsations (Figure 1.10), and compared against the theoretical asymptotic period spacing values computed from a grid of models

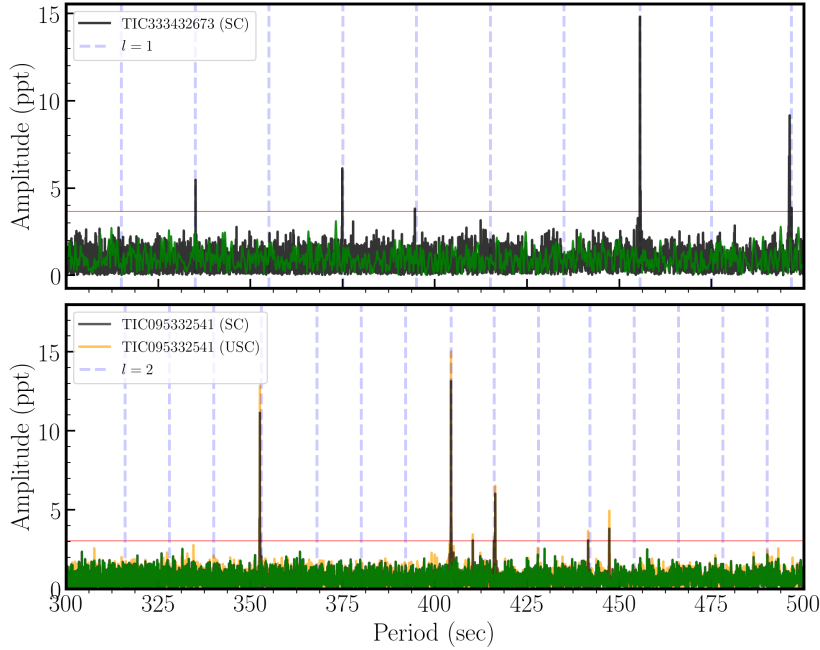


Figure 1.10: Period spectra of two GW Vir stars: TIC 333432673 (upper panel) and TIC 095332541 (lower panel). The horizontal red line in both panels indicates the detection threshold adopted by the authors. The Fourier Transform (FT) of 120-s and 20-s cadence data is shown in black and orange (only for TIC 095332541), respectively. The prewhitened FT is shown in green. The blue vertical dashed lines indicate the expected locations of $\ell = 1$ modes for TIC 333432673 and $\ell = 2$ modes for TIC 095332541. Credit: Uzundag et al. (2021), reproduced with permission ©ESO.

with different masses at a given star's effective temperature. A variation of this method is based on the comparison of the observed period spacings with the average of the computed period spacings. In the case of pulsating (pre-)white dwarf stars, in which the mean period spacing primarily depends on the mass of the star and its effective temperature (see, e.g., Kawaler & Bradley 1994), this comparison allows an estimate of the asteroseismic mass⁷. Typical values of the mean period spacing for $\ell = 1$ modes in GW Vir stars are between about 12 and 24 seconds, depending mainly on the mass (lower values for higher masses, see e.g., Oliveira da Rosa et al. 2022). It is important to note here, that the discrepancy between mass determination of PG 1159 stars using spectroscopy and asteroseismology was studied by Althaus et al. (2008) and attributed to the use of a different method in the case of the latter, with the one based on the average of the computed period spacings giving more consistent results than the one using the asymptotic period spacing. The reason is that PG 1159 stars may also pulsate in low and intermediate radial orders, and the asymptotic period spacing is valid for those pulsating in high radial orders. Figure 1.11 shows an exemplary application of the average of the computed period spacings method to derive the asteroseismic mass of PG 1159–035. The mean period spacing of high-order g modes is different for different values of ℓ and should relate as $\Delta\Pi_{\ell=1}/\Delta\Pi_{\ell=2} = \sqrt{3}$ (Unno et al., 1989). Due to geometric cancellation effects⁸, predominantly low-degree modes ($\ell = 1$ and/or 2)

⁷ The other method is based on fitting the individual observed pulsation periods to find a best-fit model that also reflects the internal composition of the star.

⁸ The observed amplitudes of modes are reduced because the effects of oscillations for modes with high spherical degree average out over the visible stellar disk.

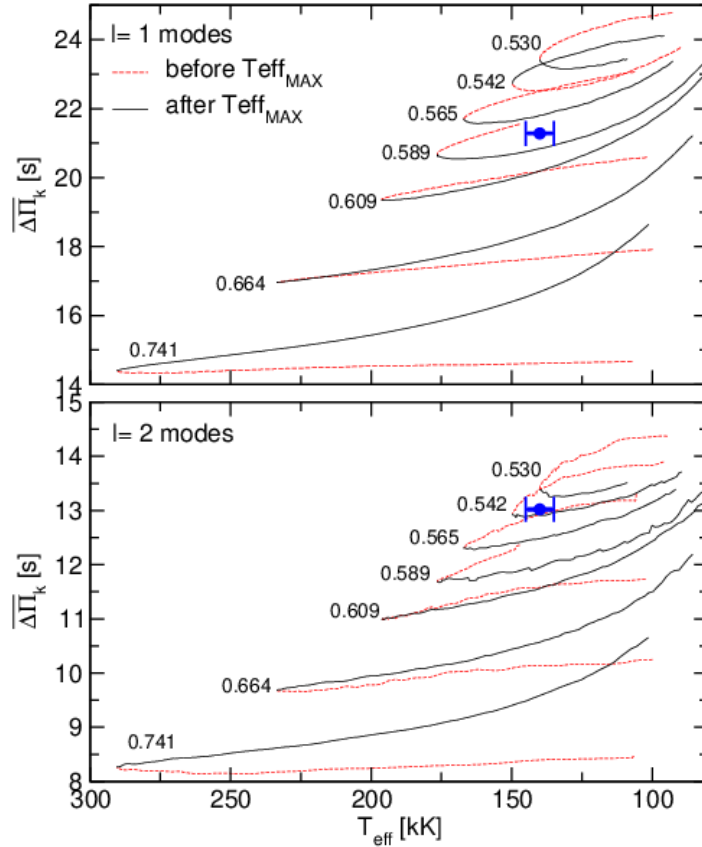


Figure 1.11: Upper panel: dipole ($\ell = 1$) average of the computed period spacings, $\overline{\Delta\Pi}_k$, computed in a range of periods observed in PG 1159–035 corresponding to PG 1159 evolutionary models of different mass. Red dashed (black solid) lines correspond to stages before (after) the model reaches the maximum effective temperature. The blue circle indicates the location of PG 1159–035 with uncertainties, for the observed period spacing of 21.28 ± 0.02 s. Lower panel: same as in upper panel, but for quadrupole ($\ell = 2$) modes with the observed period spacing of 13.02 ± 0.04 s. Reproduced from Oliveira da Rosa et al. (2022).

are expected to be observed in GW Vir stars (Dziembowski, 1977). The above example is, however, an ideal case of a homogenous star – in reality stars, including PG 1159 stars, are chemically stratified. In such cases, the observed period spacings show regular departures from a uniform pattern, as a result of resonant mode trapping by the composition gradient at the base of the He-rich surface layer (Kawaler & Bradley, 1994).

The range of observed periods in GW Vir stars is significantly larger than in other WD pulsators, but this is due to the fact that the GW Vir stars have a larger range of surface gravities ($\log g$ between 5.3 and 8.0 cm/s^2). The observed range of periods is therefore determined by the evolutionary stage of a given star – the more “compact” ones will have shorter pulsation periods (see also Figure 7 in Chapter 5).

For a spherically symmetric star, the frequencies of all nonradial modes with a given spherical degree ℓ and radial order k are indistinguishable. Departures from the spherical symmetry, caused by various effects like, e.g., rotation or magnetic fields, can lift this degeneracy. In most stars, it is the (slow) rotation that is responsible for that lifting, by splitting the modes into $2\ell + 1$ components. It is therefore expected to see three ($m =$

$+1, m = 0, m = -1$) components for $\ell = 1$ modes, five for $\ell = 2$ modes, and so on, if all are observed. That allows the identification of the ℓ and m numbers of a mode, and determination of the mean frequency splitting, from which the rotation period of the star can be inferred. Typical rotation periods measured for GW Vir stars are on the order of a few hours to over a day, indicating that those stars are very slow rotators (see, e.g., Table 10 in Córscico et al. 2019). It has to be noted that the most common issue while looking for such systematics is a broken pattern - one or more components are missing, which can be caused by e.g., a mode not being excited or resolved, or having too low amplitude for a significant detection. Another issue is a deviation from uniformity of the frequency splitting within multiplets, that can be caused by differential rotation and a number of other effects, as listed by Vauclair et al. (2002): 1) non-linearities from resonant coupling between components of multiplets, 2) mode trapping, 3) structural changes in the wave propagation cavities, 4) magnetic fields.

Finally, the changes in pulsation spectrum can be studied over the course of many years in order to determine the rate of period change (dP/dt). For GW Vir stars, which are evolving relatively fast, this is especially appealing – for K 1-16 Grauer & Bond (1984) predicted that the evolutionary contraction will lead to a rapid period decrease of 1 second in only 2 years, while Oliveira da Rosa et al. (2022) showed that the periods observed in PG 1159–035 change on shorter timescales than predicted.

1.4.3 Pulsators and non-pulsators

The striking difference between the GW Vir instability strip and the domains of other WD pulsators (DBVs and DAVs) is that the GW Vir instability strip is not pure, i.e., not all stars within its borders show pulsations, in contrast to the two others. Therefore, their interiors that can be studied using asteroseismology do not necessarily represent the interiors of all PG 1159 stars. According to previous studies, only about 50% of them pulsate (see, e.g., Quirion et al. 2004 or Uzundag et al. 2022).

The existence of both pulsating and nonpulsating stars within the GW Vir instability strip was a real challenge to the pulsation theory. The observed nitrogen dichotomy (N-rich pulsators and N-poor non-pulsators) suggested that nitrogen is essential for pulsation driving (despite its low abundance, even in N-rich stars; Dreizler & Heber, 1998). Quirion et al. (2007) argued that predominantly a high oxygen abundance is responsible for driving. The whole picture is complicated by the variety of surface abundances in PG 1159 stars, the role of metallicity, and “helium poisoning”. More recently, Werner & Rauch (2014) studied a pulsator and non-pulsator with the same carbon and oxygen abundance, but different nitrogen abundances, confirming the findings of Dreizler & Heber (1998). One star, PG 1144+005, was the counterexample for about 30 years, as the only N-rich PG 1159 star not shown to pulsate – until Sowicka et al. (2021) discovered multiperiodic GW Vir pulsations in that star. Chapter 4 provides a more detailed description of the N dichotomy, the discovery of pulsations in PG 1144+005, whereas Chapter 5 provides the updated fraction of pulsating PG 1159 stars within the GW Vir instability strip (36%).

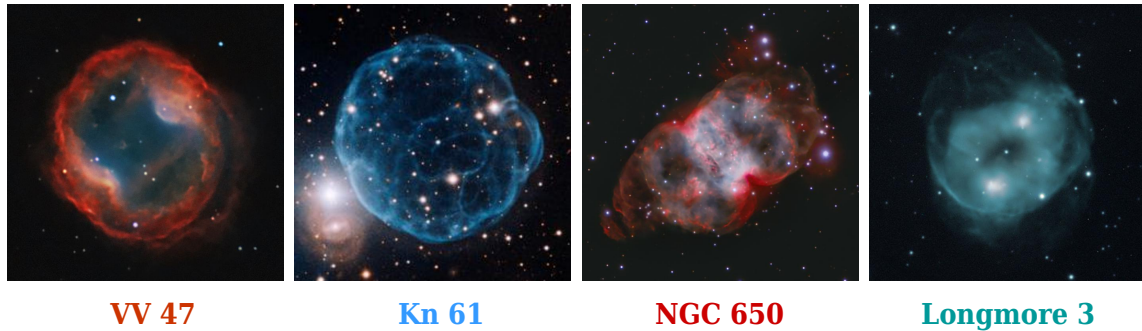


Figure 1.12: Planetary nebulae associated with PG 1159 stars. Image credits: J-P Metsävainio; International Gemini Observatory/AURA; Göran Nilsson, Wim van Berlo & Liverpool Telescope; European Southern Observatory. Sizes are not to scale.

The part played by nitrogen as a tracer of the previous evolutionary history is interesting in this context. Is a VLTP a necessity for destabilizing a star to develop pulsations? If yes, this would allow the important conclusion that the GW Vir stars have a fundamentally different evolutionary history than the non-pulsators.

1.5 PLANETARY NEBULAE

A PN is a relatively short-lived transition phase between the AGB and WD stage in the life of low- to intermediate-mass stars. PNe have been known for over two centuries, and the variety of their shapes and colors is striking. Besides the nebulae themselves, their central stars are also a group showing a great variation of properties. The central stars of PNe are found in a region of the HR diagram encompassing a wide range of hot stars. PG 1159 stars are often found at the centers of planetary nebulae. Within the GW Vir instability strip, 23 of 67 known PG 1159 stars are surrounded by a PN (Sowicka et al. 2023, Table 2 in Chapter 5), and six stars belong to the class of [WC] stars. The first pulsating PG 1159 star with a PN discovered was the central star of K 1-16 (Grauer & Bond 1984). A subsequent survey conducted by Ciardullo & Bond (1996) revealed a group of central stars of PNe with low amplitude pulsations that have variable pulsation spectra. Those stars were found to have longer pulsation periods than the GW Vir stars without nebulae, and some authors started to divide those stars into two groups of pulsators within the GW Vir family: the “PNNVs” that were surrounded by a planetary nebula, and the “DOVs” that were lacking a nebula. The current state of our knowledge of those stars does not support this division, and we discuss it in more detail in Chapter 5. Figure 1.12 shows exemplary PNe surrounding PG 1159 stars – in that sample only the central star of Kn 61 was shown to pulsate (Sowicka et al. in preparation). Because of the short-lived nature of the PNe (a few tens of thousands of years), it is highly unlikely that the PG 1159 stars found inside PNe represent a different evolutionary pathway but rather a phase in the evolution of all PG 1159 stars. Given that the nebula itself has no impact on the pulsational properties of the central star, we do not dedicate any further discussion to the nebulae or their properties.

1.6 BINARITY

Over 50% of all solar-mass stars are found to be in binaries or higher order multiples (Raghavan et al., 2010), while for more massive stars this fraction can approach 100% (Sana et al., 2012). In spite of this, only five PG 1159 stars have confirmed companions or are suspected binaries, hinting that there might be a hidden binary fraction among PG 1159 stars. The first PG 1159 star with a detection of a companion in the spectrum was PG 2131+066, a pulsating PG 1159 star (Bond et al., 1984). The companion is an early M-type main-sequence star (Wesemael et al., 1985), and was resolved in Hubble Space Telescope observations (Reed et al., 2000). The first confirmed close binary central star with a PG 1159-type star was SDSS J212531.92–010745.8 (Nagel et al., 2006), and it would be the first such system with a dynamical mass determination (Schuh et al., 2008; Beeck et al., 2009; Schuh et al., 2009; Shimansky et al., 2015). Especially that it has not been shown to pulsate, therefore asteroseismic mass cannot be determined. The only confirmed hierarchical triple system with a PG 1159 star is NGC 246 (Adam & Mugrauer, 2014) and can be resolved in ground-based observations. Interestingly, the PG 1159 star in NGC 246 is also a pulsator (Ciardullo & Bond, 1996). The list of candidate PG 1159 stars with stellar companions is also short, as there are only two such objects, SDSS J155610.40+254640.3 (Reindl et al., 2016) and Kn 61 (García-Díaz et al., 2014; De Marco et al., 2015). A significant radial velocity shift was found in the spectra of SDSS J155610.40+254640.3 but still needs to be confirmed as originating from a close companion (Reindl et al., 2016). Kn 61, on the other hand, shows odd photometric behavior in the form of reoccurring light curve maxima on time scales of several days with triangular shapes. While the origin of this variability is still unknown, possible scenarios involve binarity, variable winds, and accretion (De Marco et al., 2015). Moreover, the PG 1159 central star of Kn 61 is also a pulsator (Sowicka et al. in preparation). For the sake of completeness we add to the list Abell 30 – a [WC]-PG 1159 transition object that has recently been suggested to host a binary central star (Jacoby et al., 2020), and Abell 78 – also a [WC]-PG 1159 star – that shows radial velocity variations, but their origin is still uncertain (as wind variability could not have been ruled out; De Marco et al., 2004).

Recently, Miller Bertolami et al. (2022) and Werner et al. (2022b) proposed a new evolutionary channel creating low-luminosity PG 1159 stars that involves binary evolution. In that scenario, the CO+He WD merger is a possible explanation for the existence of low-luminosity PG 1159 stars that do not fit the “born-again” scenario. RL 104 (Werner et al., 2022a) is the best candidate that could be explained by the merger scenario.

Therefore, we cannot assume all the stars we study to either be single, or be the outcome of single star evolution. Here, it is important to stress that the photometric observations used to probe the pulsation spectra of GW Vir stars would, in most cases, also be sensitive to the detection of longer period variability associated with the presence of a companion (Jones & Boffin, 2017). In any case, further discussion of the impact of binarity on the pulsational properties of PG 1159 stars is beyond the scope of this thesis and is reserved for future work.

1.7 GROUND-BASED DATA USED IN THIS THESIS

This thesis is based entirely on ground-based data of one kind – time series photometric observations in a single band. There were no such pre-existing data sets for the work presented here. While most observations were gathered through the observing time application process, some come from collaborations that did not require applying for observing time.

1.7.1 *Awarded observing time*

Observing time for observations included in this thesis was awarded to the author (PI) or collaborators (co-I). The target selection, preparation of observing proposals and planning the observations was done by the author with the help of supervisors and collaborators. The accepted observing proposals and the amount of awarded time are listed below:

- 2014, SAAO, 1.9-m, SHOC, 7 nights, **PI**
- 2015B/SI2015b08, ORM La Palma, 2.54-m INT, WFC, 21.5 hours, **PI**
- 2016A/136-GTC80/16A, ORM La Palma, 10.4-m GTC, OSIRIS, 15 hours, **PI**
- 2016-2/2.1-5, McDonald Observatory, 2.1-m, ProEM, 7 nights, **Co-I**
- 2016-3/2.1-2, McDonald Observatory, 2.1-m, ProEM, 14 nights, **PI**
- 2016B/104-MULTIPLE-2/16B, ORM La Palma, 2.54-m INT & 4.2-m WHT, WFC & ACAM, 5 nights & 6 nights, **PI**
- 2017B/104-GTC73/17B, ORM La Palma, 10.4-m GTC, OSIRIS, 14 hours, **Co-I**
- 2021/2021-01-Lesedi-385, SAAO, 1.0-m Lesedi, SHOC, 7 nights, **PI**
- 2022/Sowicka-2022-09-1.0-m-498, SAAO, 1.0-m, SHOC, 7 nights, **PI**

1.7.2 *Equipment*

This thesis is based on an extensive collection of photometric observations obtained in several world-leading observatories. The telescope+instrument setups are introduced in this Section.

DFOSC at the 1.54-m Danish Telescope at ESO (DK)

The 1.54-m Danish Telescope located at La Silla Observatory was equipped with the Danish Faint Object Spectrograph and Camera (DFOSC; Andersen et al. 1995). DFOSC uses a 2K×2K thinned Loral CCD chip with a Field of View (FOV) of 13.7×13.7 arcmin. No filter was used.

OSIRIS at the 10.4-m Gran Telescopio Canarias (GTC)

The 10.4-m Gran Telescopio Canarias is located at the Observatorio del Roque de los Muchachos (ORM, La Palma) and was equipped with Optical System for Imaging and low-Intermediate-Resolution Integrated Spectroscopy (OSIRIS; Cepa 1998). OSIRIS consists of a mosaic of two CCDs of 2048×4096 pixels each and has an unvignetted FOV of 7.8×7.8 arcmin. Either no filter or a Sloan r' filter was used. We used 2×2 binning and a standard readout time of about 23 seconds.

WFC at the 2.54-m Isaac Newton Telescope (INT)

The 2.54-m Isaac Newton Telescope is located at the Observatorio del Roque de los Muchachos (ORM, La Palma) and was equipped with the Wide Field Camera (WFC; Walton et al. 2001), an optical mosaic camera mounted in the prime focus. WFC consists of four thinned EEV $2k \times 4k$ CCDs. Because the readout time of the whole CCD mosaic is rather long, we used it in windowing mode – for a FOV of 5×5 arcmin (910×910 pixels) the readout time was 6 seconds in the slow (less noisy) mode. No binning was used. We used a Harris V filter.

ProEM at the 2.1-m Otto Struve Telescope (MD)

The 2.1-m Otto Struve Telescope is located at McDonald Observatory, and is equipped with ProEM, which is a frame-transfer CCD detector with optional electron-multiplication with high frame-rate, optimized for high-speed time-series photometry (providing effectively zero readout time). The CCD has 1024×1024 pixels and a FOV of 1.6×1.6 arcmin. We used 4×4 binning for an effective plate scale of 0.36 arcsec pixel⁻¹. We used a BG40 filter.

Andor at the 1.3-m McGraw-Hill Telescope (MDM):

The 1.3-m McGraw-Hill Telescope is located at the MDM Observatory, on the southwest ridge of Kitt Peak in Arizona. It was equipped with Andor Ikon DU937_BV CCD camera, which was used in Frame Transfer mode and 4×4 binning, resulting in a FOV of 2.3×2.3 arcmin (128×128 pixels). We used a BG38 filter.

SHOC at the SAAO 1.9-m Telescope and 1.0-m Telescope (SA19, SA10):

The telescopes are located at the Sutherland station of the South African Astronomical Observatory (SAAO), and are equipped with one of the Sutherland High Speed Optical Cameras (SHOC; Coppejans et al. 2013). SHOC 1 and 2 are high-speed cameras operating in frame-transfer mode for visible wavelength range that have an electron-multiplying (EM) capability⁹. The imaging area of the detectors is 1024×1024 pixels, which corresponds to a FOV of 2.79×2.79 arcmin for the 1.9-m telescope with the focal reducer, and 2.85×2.85 arcmin for the 1.0-m telescope. A selection of amplifiers can be used, each resulting in a different gain setting, as well as binning and readout speed. The slowest readout speed was usually chosen, resulting in the lowest readout noise. Binning was determined by the observer to match the observing conditions and especially avoid undersampling of the Point Spread Function (PSF). Observations were done without a filter.

⁹ The EM mode has not been used for observations presented in this work.

ACAM at the 4.2-m William Herschel Telescope (WHT)

The 4.2-m William Herschel Telescope (WHT) is located at the Observatorio del Roque de los Muchachos (ORM, La Palma) and was equipped with Auxiliary-port CAMera (ACAM; Benn et al. 2008). ACAM detector (AUXCAM) is a low-fringing, deep-depletion $2k \times 4k$ EEV CCD. The FOV in imaging mode is 8.3 arcmin in diameter, and we used windowing to reduce the readout time to about 3 seconds in a slow readout mode. We used Sloan G filter and no binning.

1.8 THESIS OUTLINE

The remainder of this thesis is organized as follows.

Chapter 2 provides a detailed description of standard CCD data reduction, photometry, and frequency analysis techniques employed in this work. We describe the photometry pipeline developed by the author of this thesis to improve the signal-to-noise ratio of the results.

Chapter 3 presents our attempt to confirm a previously reported preliminary discovery of ϵ mechanism-driven modes in the central star of planetary nebula VV 47. On the basis of new data, obtained using the 4.2-m William Herschel Telescope, as well as a re-analysis of the discovery data, we do not find a convincing evidence not only for ϵ -driven modes in this star, but also for any short-period variability. We also describe differences between our significance criterion and the one adopted by the previous authors.

Chapter 4 describes our discovery of long-sought-after pulsations in PG 1144+005, at that time the only N-rich PG 1159 star not shown to pulsate that was a counterexample to the hypothesis of all N-rich PG 1159 stars being pulsators, and all N-poor ones being non-pulsators. We detected pulsations consistent with g modes excited in GW Vir stars in two independent runs, and characterized PG 1144+005 as a multiperiodic pulsator.

Chapter 5 summarizes an ambitious survey for variability among PG 1159 stars carried out in the years 2014–2022. We obtained new photometric time-series observations of 29 stars, discovered pulsations in the central star of planetary nebula Abell 72, and variability in RX J0122.9–7521. We derived the most robust pulsator fraction to date, and provided an updated list of all known PG 1159 stars and their properties. In order to place the whole sample on the theoretical Hertzsprung-Russell diagram, we calculated luminosities for all PG 1159 stars from their astrometric parallaxes for the first time. Finally, we argued against continuing to use the traditional “DOV” and “PNNV” designations based on the analysis of the pulsators.

Chapter 6 concludes this thesis. We summarize all the results, discuss future prospects in the field of pulsating hot pre-WD stars, and plans for future work.

DATA REDUCTION AND ANALYSIS

This Chapter introduces the standard data reduction techniques employed to reduce the data, and the basics of the time series analysis necessary for the science goals of presented data sets. All the data were reduced and analyzed by the author of this thesis, unless clearly stated otherwise.

Parts of this Chapter were written based on the following resources: **Handbook of CCD Astronomy**, Howell (2006); CCD Data Reduction Guide by Matthew Craig and Lauren Chambers (<https://www.astropy.org/ccd-reduction-and-photometry-guide/>); **Asteroseismology**, Aerts et al. (2010).

2.1 INTRODUCTION

The observational data presented in this thesis were obtained using different setups (telescope and instrument) with the common ground that all the detectors were Charge-Coupled Device (CCD) cameras. The invention of the CCD in 1969 by Willard S. Boyle and George E. Smith at Bell Labs (Boyle & Smith, 1970) started a new era in astronomical imaging, with the technology first used for astronomical purposes in 1976 by Jim Janesick and Brad Smith at the 61-inch telescope on Mt. Bigelow (Smith, 1976)¹. CCD cameras are now a gold-standard for many astronomical applications, like imaging, astrometry, photometry, polarimetry, and spectroscopy. Briefly, the basic CCD working principle is based on the photoelectric effect²: photons that hit the detector composed by silicon photosites (pixels in the final image) carry energy that can liberate electrons from the silicon atoms, and those electrons are then stored in photosite capacitors that hold charge (thus converting light – photons, into electrons – charge). The charge is then shifted over the detector using different voltages for different potential wells along the way to the Serial Register, in order to read out the measurements for individual pixels, and finally convert the electrical charge into electrical voltage by the camera electronics (the Analogue-to-Digital Converter, ADC). The final image consists of information about the charge accumulated in each pixel in an Analog Digital Unit (ADU), which are the “raw” data and the starting point of the data reduction.

¹ <https://aas.org/posts/news/2019/10/month-astronomical-history-50-years-ccds>

² The Nobel Prize in Physics in 1921 was awarded to Albert Einstein “for his services to Theoretical Physics, and especially for his discovery of the law of the photoelectric effect”. Source: <https://www.nobelprize.org/prizes/physics/1921/summary/>

2.2 STANDARD STEPS IN DATA REDUCTION

The main purpose of data reduction is to remove any instrumental artifacts that can influence the data. In reality, every astronomical image contains not only the light from astronomical object(s) and sky background, but also signals and features from the telescope and detector used, including dust particles on the telescope mirror, vignetting, offset introduced as bias, different sources of noise from the detector electronics.

2.2.1 *Bias Frames*

To ensure that the ADC always receives a positive value for voltage conversion, CCDs are adjusted by adding a constant offset (voltage), known as bias level, so that the output is above zero even when the detector is not exposed to light. Another unavoidable CCD characteristic is the readout noise, which is associated with the CCD electronics responsible for the CCD read out, shows up as the fluctuations around the bias level, and sets the noise floor for the camera. In order to get the data representative of the recorded pixel counts, the bias level must be subtracted in the data reduction process. This is usually done either by using bias frames or overscan regions³. Since bias frames provide more information (a two-dimensional – 2-D – map of bias level across the chip) and can always be taken when observing with a CCD camera, we chose to only use those. A bias frame is an exposure of zero seconds integration time (sometimes in practice it is the shortest possible exposure time) taken with the CCD shutter closed, which in an ideal case would show the same value for each pixel and would not be time-dependent. However, in practice the bias level varies slightly because of a different pixel-to-pixel sensitivity, its value can change with time, and it might show a fixed structure across the chip. This is usually accounted for by taking several (at least 10 or more) bias frames before and/or after each observing night and average/median combining them to reduce the readout noise variations and any other random fluctuations in a single bias frame. The combined bias is often called a “master” bias and is subtracted from all frames, both scientific raw frames and other calibration frames. For the data presented in this work, bias frames were combined into a “master bias” frame using the `ccdproc` Python package (Craig et al., 2017) and the `combine` routine with the `“method=‘median’”` option. Then, bias-corrected images were produced using `subtract_bias` routine. Exemplary bias and master bias frames are shown in Figure 2.1.

2.2.2 *Dark Frames*

Even when the CCD camera shutter is closed, meaning no exposure to light, additional charge accumulates in pixels due to the thermal effects in the CCD. As in every material at

³ The overscan region is usually a strip (a few columns and/or rows wide) at an edge of the chip generated artificially in the CCD output electronics and contains just the offset level. The overscan can be useful to determine any frame-to-frame variations in the bias level. However, not every CCD mode allows it (e.g., the windowing mode in WFC@INT), nor is it always advised to use it.

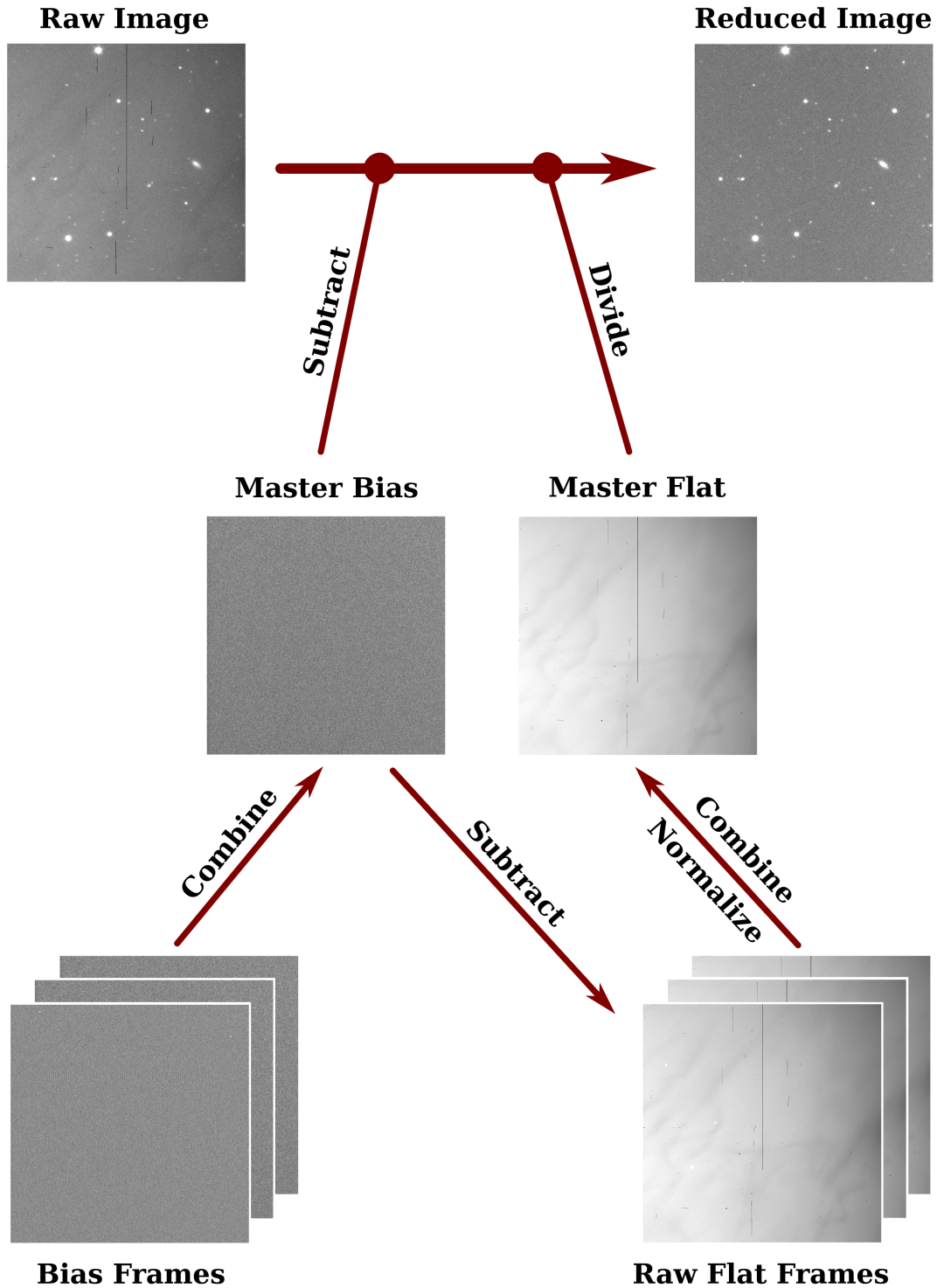


Figure 2.1: An illustration of the basic data reduction process. Exemplary data used here are observations of PG 1144+005 with OSIRIS@GTC. All frames are trimmed from the original size. In the case when dark current is not negligible, either bias frames are replaced by dark frames, or dark subtraction is performed as an additional step after bias subtraction (when dark frames need to be scaled). See Section 2.2 for details. Inspiration for this figure came from Berry & Burnell (2005).

a temperature significantly above absolute zero, due to thermal agitation⁴ some electrons' thermal energies might be sufficient for them to be freed from the silicon atoms and to fall into the potential well of a pixel. Those electrons are then read out together with the signal from astronomical sources and become indistinguishable from the ones excited by photons. Dark current refers to the number of such thermal electrons generated at a given temperature per second per pixel, and strongly depends on the temperature. Most modern CCD cameras are cooled to decrease dark current, either using thermoelectric coolers (usually cooled by a fixed amount below the ambient temperature) or liquid coolers (usually with liquid nitrogen, they keep the same operating temperature). Calibration frames from some instruments (e.g., those efficiently cooled with liquid nitrogen) do not even contain dark frames, because the cooling efficiency of the liquid nitrogen coolers is so high that the dark current is essentially not present (or very small, smaller than the readout noise) and performing a correction for dark count would only increase the background noise in the images. Despite that, some pixels may have a much higher dark current and are called "hot pixels". Sometimes there are other sources of counts which originate from non-thermal effects that scale with exposure time (e.g., cosmic ray traces). Like bias frames, dark frames are images taken with the shutter closed but with rather long exposure time that usually equals the exposure time of scientific frames and flat field frames. Dark current linearly increases with time, and dark frames can be scaled accordingly⁵. Several dark frames are usually taken and combined to reduce the noise in the final "master" dark.

For the data presented in this work, dark frames were used to reduce the data from ProEM camera. Due to a pattern present in the images taken with ProEM (Figure 2.2), sets of dark frames with the exposure time matching the exposure time of science frames and flat fields were (always) taken.

If the dark frames are not scaled, bias subtraction is not required because the bias level is already included in the dark frame. However, because we observed many objects during a single observing night with different exposure times, we applied bias subtraction to dark frames, so they can be scaled if necessary (e.g., the matching ones cannot be used for some reason). The dark frames were combined into a "master dark" frame for each exposure time and camera setting using the `combine` function from `ccdproc` with "method='median'" and median sigma clipping function "sigma_clip_func=np.ma.median" from `numpy` (Van Der Walt et al., 2011; Harris et al., 2020). As an additional step, master darks were gain corrected using `gain_correct` routine, that scales the data and uncertainty of the image with the gain value provided for the camera setup in e^-/ADU ⁶. Then, dark-corrected flat fields and science images (also gain-corrected) were produced using `subtract_dark` routine.

⁴ thermal agitation: Random movements of the free electrons in a conductor, producing noise signals that may become noticeable when they occur at the input of a high-gain amplifier. Also known as thermal effect. From McGraw-Hill Dictionary of Scientific & Technical Terms, 6E. (2003). Retrieved from <https://encyclopedia2.thefreedictionary.com/thermal+agitation>

⁵ This should be done with caution. Taking too short dark frames to scale them up may only increase noise, if they do not have enough counts over the readout noise.

⁶ Gain determines the conversion between the amount of charge collected in each pixel and a digital number from the ADC converter in the output image.

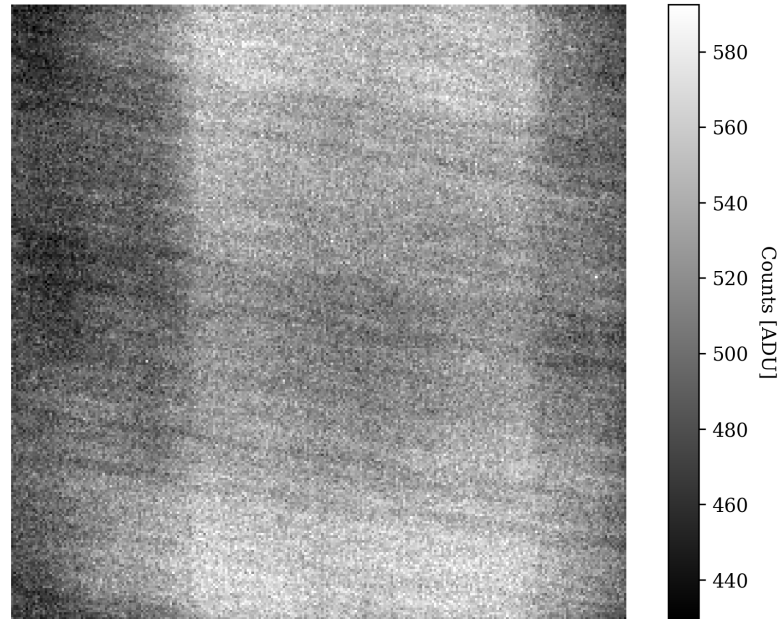


Figure 2.2: A master dark combined from 31 dark frames, each with 20 s integration time, taken with ProEM mounted on the 2.1-m Otto Struve telescope at McDonald Observatory on the 5th of May 2017. A specific pattern is present in the image, which has to be corrected for in the science frames and flat fields by subtracting such a master dark with matching exposure time.

2.2.3 Flat field images

Flat fielding is an essential step in the data reduction, and perhaps the most challenging one. The main purpose of a flat field correction is to compensate for slight differences in the response of each pixel to incoming light. The sources of this non-uniformity might be within the CCD, like variations in pixel-to-pixel sensitivity, and in the optical path, like dust grains on the filter and/or glass covering the CCD and vignetting (a reduction of image brightness in the corners of the image). In theory, an ideal flat field image would be uniformly illuminated by a source of light matching the spectral response of the object of interest. Practically, this is impossible to achieve, and even achieving uniformly illuminated flats is a difficult task.

There are a few ways flat field images can be taken: twilight flats (also called sky flats), dome flats, and night sky flats⁷ (often used in the infrared but rarely used in the optical and therefore omitted here). Twilight flats are images taken after sunset or before sunrise of a sky field near zenith, preferably without stars brighter than the sky background. They can be taken with telescope tracking turned off, leaving star traces in the image, or while it is on and in such case a dithering pattern (spatial offset) must be applied (to avoid stars exposed in the same position on the frame). Ideally, flats should be well exposed ($T_{\text{exp}} > 1$ s to minimize possible photometric effects due to the camera shutter) – usually

⁷ Those sky flats mean spatially offset images of the dark night sky.

the aim is to reach about half of the maximum counts available for the dynamic range of the used CCD⁸.

Twilight flats can only be taken when the atmospheric conditions allow observations, and since the time window allowing to take them is short, that is not always the case. When daily or weekly flat field fluctuations are small, the same flat fields can be used within a couple of days before or after the observations. If nightly flat fields must be taken and the conditions do not allow it, dome flats can be used as a backup. Many observatories have special flat field screens mounted inside each dome, which can be illuminated using, e.g., special lamps (different colors and luminosities). Dome flats, for some telescope and instrument setups, present a challenge to achieve a uniform illumination on a large scale. That is the case for GTC equipped with OSIRIS, which provides a relatively large FOV for a telescope of its size. Dome flats taken with OSIRIS, in contrast to twilight or night sky flats, provide larger fluctuations due to imperfect dome illumination⁹, and are provided as the last choice.

It is often advised in instrument user manuals which method and what settings give the best results for a given instrument. Multiple exposures per filter and instrument setup are taken, and filtering (e.g., median) while combining the flats must be applied to remove the contribution from stars. All flat field images should be inspected, and those which happen to be significantly under- or over-exposed or have saturated stars/star traces should be rejected before combining. An important step before combining flat field images is the normalization of the calibrated (bias/dark) flat frames to a mean or median¹⁰ level, scaled to unity, because the counts (especially in twilight and sky flats) vary from frame to frame.

For each flat field frame in a given filter, a scaling function that calculates the inverse of the median was given to `ccdproc.combine` together with the median sigma clipping function. The resulting master flats were gain-corrected using `gain_correct`. Then, science frames were divided by a matching master dark using `flat_correct`. Exemplary twilight flats and a master flat are shown in Figure 2.1.

2.2.4 Science frames

Science frames taken for this work contained the target of interest (a pre-WD star), all the other stars in the FOV, as well as contributions from sky background (sometimes quite high, when the target was observed in bright time, i.e., close to Full Moon), bias level, dark current, associated readout noise, and sometimes also cosmic ray traces. Each of these contributions was removed during the reduction process, together with the correction for pixel-to-pixel response to light. The basic workflow for data reduction is the following:

$$\text{Reduced image} = \frac{\text{Raw image} - \text{Master bias} (-\text{Master dark})}{\text{Master flat}}, \quad (2.1)$$

⁸ For a 16-bit ADC the full dynamic range would be 65 535 ADU, so well exposed flats would have counts around 30 000 ADU (or slightly less, depending on the linearity curve of the CCD).

⁹ http://www.gtc.iac.es/instruments/osiris/#OSIRIS_MasterFlats_BroadBand_Imaging

¹⁰ Median is usually a better choice because it is not as affected by extreme values as the mean is.

where master bias might be replaced by master dark, as described in Section 2.2.2. Figure 2.1 shows an illustration of the basic reduction process using real data: observations of PG 1144+005 with OSIRIS mounted on the 10.4-m GTC. Appropriate files must be used per filter, gain, readout, and binning settings of the used camera.

2.2.5 Possible additional steps

A reduced science image might still need additional processing. In particular, frames might be trimmed to reduce the size and computation time (especially when the FITS files are read into the computer memory). As already mentioned, some pixels in an image might be problematic due to various reasons, e.g., their response to light is different. Another example might be the presence of a bad row or column, making that section of a CCD unusable. Some observatories provide a bad pixel mask image and those pixels can be masked, if desired. In this work, masking was not necessary.

Pixels in an image may also be affected by occasional cosmic ray hits. Cosmic rays are high-energy charged particles that originate in space and produce showers of secondary particles when colliding with atoms and molecules in the Earth's atmosphere. Those secondary particles reach the Earth's surface and might hit a CCD mid-exposure, having sufficient energy to cause a dramatic increase in counts in the affected region. Often one or two pixels are affected, but sometimes they can leave longer traces. The number of cosmic ray incidents increases with the exposure time, and any image taken with a CCD can be affected. While proper combination of calibration frames is usually enough to remove those extreme outliers, scientific frames require different treatment. A widely used technique is to remove cosmic rays using the L.A.Cosmic algorithm¹¹. This algorithm is based on Laplacian edge detection – detects sharp edges of cosmic rays and distinguishes them from point sources (van Dokkum, 2001). van Dokkum originally implemented it in IRAF and different authors later expanded it to use in other programs. The implementation used in this work is the one by McCully et al. (2018) that is included in the Astro-SCRAPPY package and read by a wrapper within the ccdproc Python package. The cleaning is done with the `cosmicray_lacosmic` routine that requires selecting an appropriate value of `sigclip`, which is usually adjusted for each data set, and providing a gain value if the images were not gain-corrected. This procedure was used only for a few runs that were heavily affected by cosmic ray hits.

When the observations are carried out with the presence of a bright Moon, intensity gradients sometimes occur across the FOV due to moonlight, especially when the angular distance between the observed field and the Moon is small or the FOV is large. Frames can be corrected for this effect, and for example IRAF provides necessary tools¹².

Finally, frames might be aligned in preparation for photometry to ensure that the measured objects can be found near a given position, which is important especially when a large telescope drift is present. However, this is not always necessary, as new positions for

¹¹ <http://www.astro.yale.edu/dokkum/lacosmic/>

¹² "A User's Guide to CCD Reductions with IRAF", <https://home.ifa.hawaii.edu/users/meech/a399/handouts/ccduser3.pdf>

stars might be calculated and fed directly to the photometry program without a necessity to perform operations on the images.

2.3 PHOTOMETRY

The fundamental technique used for the work presented in this thesis is photometry. Named from the Greek “phōs” and “metro” meaning “light” and “measure”¹³, it is the basic method to measure the flux emitted by an astronomical object. This measurement can be done in different ways – the main ones are aperture photometry, PSF photometry, and difference image photometry (also called image subtraction). Aperture photometry is the simplest of these techniques, but can be successfully used only in specific circumstances – for instance, the stars of interest must be well separated. PSF photometry and image subtraction are usually used for crowded fields, where source blending is a problem. All the targets observed in this work were isolated, therefore we only used aperture photometry.

2.3.1 Aperture photometry

Aperture photometry is simply a measurement of the brightness of a star within a specified, centered aperture. The apertures essentially can have any shape, but most often they are circular or elliptical, and sometimes also square. Recently, Bowman & Holdsworth (2019) showed the advantage of using adaptive elliptical apertures over fixed circular apertures to obtain higher quality ground-based light curves of roAp stars¹⁴. Examples of a successful use of irregularly shaped (square) apertures are the *Kepler* (Koch et al., 2010) and *TESS* missions (Ricker et al., 2015). Aperture photometry does not depend on the actual shape of the star PSF but sums all the counts from pixels enclosed by the aperture. Then, using a second aperture (or sky annulus surrounding the first one), the sky background level is measured, which is then subtracted from the first aperture counts. The sky annulus has an inner and outer radius¹⁵ and the inner one should be larger than the aperture for the target with some margin, to prevent the same pixels being measured twice (the consequence of using circular apertures on square pixels) and to avoid having the wings of the stellar PSF fall into in the sky aperture.

The total formal error of aperture photometry consists of a number of noise sources: 1) shot noise from the source, 2) shot noise from the sky in aperture, 3) readout noise, 4) other sources, e.g., dark current. There are two limiting cases, one when the photometry error is dominated by the signal from a bright source, and the other when the photometry error is dominated by the signal from the sky (“sky-limited”). Therefore, the aperture size depends on the brightness of the target, and is smaller for fainter objects.

¹³ <https://www.astro4edu.org/resources/glossary/term/249/>

¹⁴ We used their program, TEA-Phot, for the data presented in Chapter 4.

¹⁵ Annulus implies circular shape, but these annuli do not necessarily need to be circular, e.g., ellipses are also used.

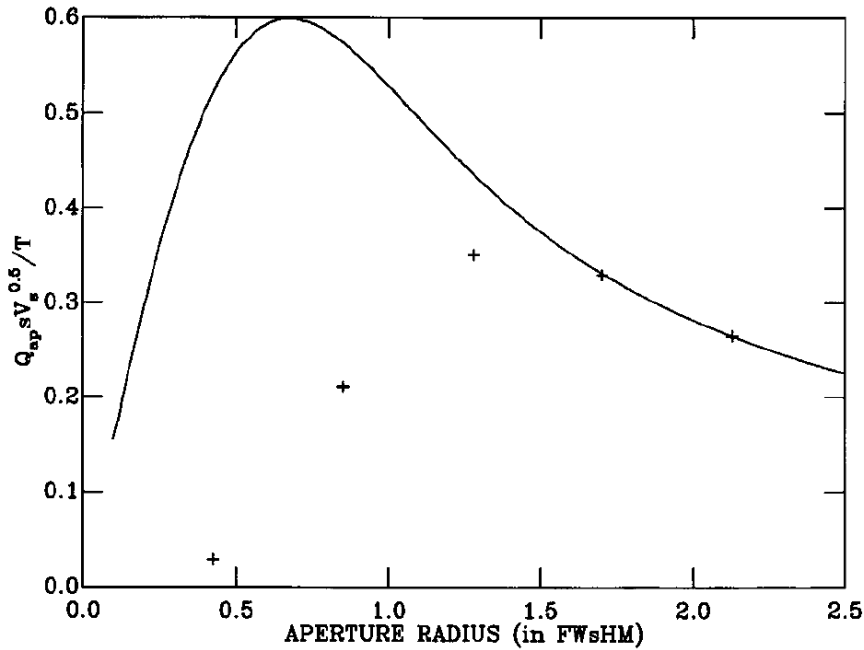


Figure 2.3: Signal-to-noise ratio as a function of aperture size. The solid line represents a theoretical model for a faint star, represented by a well sampled Gaussian PSF. Crosses represent real data obtained with the Keele 0.6-m telescope with a CCD camera, with the seeing FWHM of approximately 2 pixels. Figure reproduced from Naylor (1998).

2.3.1.1 The choice of optimal aperture

The choice of aperture shape and size is crucial for achieving satisfactory results. In the case of pulsating pre-WDs and other faint, low-amplitude and short-period pulsators, obtaining high-quality photometry is required, but due to the necessary short cadence it is a challenging task. The aperture that would contain $\sim 98\%$ of the total flux from the object would be defined by the radius $r = 3 \cdot$ Full Width at Half Maximum (FWHM, Merline & Howell, 1995). However, that does not mean it is the optimal choice. Many authors showed that there is a relation between the aperture radius and the obtained signal-to-noise ratio (S/N) (e.g., see Howell 1989, Howell 1992, Naylor 1998). The theoretical S/N curve for a point source peaks for a radius about $r \sim 1 \cdot$ FWHM, while Naylor (1998) showed that an aperture with a radius of $r \sim 1.5 \cdot$ FWHM presents the maximum S/N (Figure 2.3), and is larger than the theoretical one due to finite pixel size. Further concern in the choice of optimal aperture is the quality of an imaging system. In the absence of isoplanatism, i.e., when the PSF varies over the FOV, the optimal aperture chosen for one target, may not necessarily be the optimal one for another at some distance from the first one. The optimal aperture also depends (slightly) on the source brightness, usually being smaller for fainter ones¹⁶. The final aperture choice is therefore a matter of a compromise. The comparison stars used for differential photometry are usually brighter than the targets, therefore a good approach is to optimize the aperture choice for those faintest objects measured in the FOV. That way, their S/N is maximized, while it is only slightly degraded for the bright

¹⁶ For fainter sources, the wings in PSF have larger contribution from the sky background, hence the photometric noise from the sky background increases the error budget.

ones. Another possibility is to use a set of different aperture sizes for objects in different brightness ranges, but that procedure requires the use of aperture corrections or curve of growth.

2.3.1.2 *Atmospheric variations*

For ground-based observations, the effects of the Earth’s atmosphere might come into play. Besides clouds, sky transparency variations can occur on good photometric nights on time scales of 15 minutes and longer, and show up in the Fourier domain as a frequency-dependent noise, with the amplitude increasing towards lower frequencies (“pink” noise, Aerts et al. 2010). Another source is scintillation, which is caused by variable refraction due to the Earth’s turbulent atmosphere, causes the observed brightness of stars to fluctuate, and is usually referred to as “twinkling”. Scintillation contributes as a “white” noise, i.e., independent of frequency, and dominates at frequencies higher than those corresponding to periods shorter than about 15 minutes on photometric nights. Finally, seeing degrades the observed stellar image beyond the diffraction limit (defined by the size of telescope aperture). Seeing variations on short time scales¹⁷ would cause non-optimal results for photometry with a fixed aperture size – if the seeing becomes better, the FWHM of the seeing disk becomes smaller and that would cause more sky background within the aperture, and when it worsens, the opposite happens and some flux might be lost outside the aperture. To achieve the best results, optimal apertures can be determined for each CCD frame individually.

2.3.2 *Adaptive photometry pipeline*

With the challenges of obtaining optimal photometric results described above, we developed a procedure for obtaining such results based on the choice of an adaptive circular aperture scaled with the seeing.

Our photometry pipeline was based on AUTOPHOTOM within the PHOTOM package¹⁸ included in the STARLINK software suite. PHOTOM extracts sky corrected fluxes and magnitudes of sources with circular or elliptical apertures, using different algorithms for extraction – aperture or optimal. AUTOPHOTOM was designed to be used non-interactively, in particular within a script.

The running of the pipeline consisted of a series of scripts and Python-based programs. The first step of the procedure consisted of preparation of input files. The CCD observations were reduced as described in Section 2.2.4 and the infile for each run was prepared. The infile consisted of the description of the objects for photometry and associated sky regions (or annuli). The program was run twice over the data. In the first pass, the program was run in optimal extraction mode. The infile for this run, in comparison with the one to be used in aperture mode, needed an additional star to be defined – the PSF star. In most cases, the target was used as the PSF star, because the main reason of this pass was

¹⁷ For short exposures necessary for observations of short-period pulsating stars.

¹⁸ <https://starlink.eao.hawaii.edu/docs/sun45.htx/sun45.html>

to obtain FWHM measurements for the definition of aperture size used in the second pass. The positions of the target and up to four comparison stars were determined using GAIA within STARLINK and “Pick Object” option, with the results saved to a text file and copied into the input file for AUTOPHOTOM. The infile also required some initial parameters: SEE – seeing in pixels to estimate the FWHM of the PSF by the optimal extraction algorithm, and CLIP – the clipping radius beyond which the mask weights in the optimal extraction are set to zero. The SEE value was taken from “Pick Object” tool, and the CLIP radius was estimated as $2 \cdot \text{FWHM}$, following Naylor (1998). Then, the program was run from a bash script written by the author of this thesis, shown in Code Listing 1, which yielded the output shown in Code Listing 2.

Listing 1: Bash script for AUTOPHOTOM run in optimal extraction mode.

```
#!/usr/bin/env bash

export STARLINK_DIR=/home/paula/Software/star-2018A
source $STARLINK_DIR/etc/profile

cp first_infile_photomSDSS114635.dat infile_photom.dat
convert # calls a package allowing the usage of FITS files
photom # calls the PHOTOM package

for f in *.fits; do
    echo "File = "$f
    cp $f input.fits
    autophotom BIASLE=0 EXSOURCE=HEADER ETIME=EXPTIME OPTIMA=TRUE PADU=1.0 PHOTON=2
        POSITIVE=TRUE SKYEST=3 USEMAGS=FALSE FIXANN=FALSE CENTRO=TRUE MAXSHIFT=20 <<
        EOF
input.fits # input image file
infile_photom.dat # input file with positions
newphotom.dat # output file for photometry results
EOF

rm input.fits
cp newphotom.dat $f.newphotom.dat
mv newphotom.dat infile_photom.dat # uses objects' coords as input for the next file

done
```

Listing 2: Terminal output for AUTOPHOTOM run in optimal extraction mode. The first line contains the measurements for the PSF star while the following lines – for the target and comparison stars (in this case the target was also the PSF star).

```
$ ./skrypt_autophotom_optimalSDSS114635.sh

CONVERT commands are now available -- (Version 1.8)

Defaults for automatic NDF conversion are set.
```

```

Type conhelp for help on CONVERT commands.
Type "showme sun55" to browse the hypertext documentation.

PHOTOM applications are now available -- (Version 1.12-2)

Support is available by emailing starlink@jiscmail.ac.uk
Type photomhelp for help or consult SUN/45

File = RED0001419641-20180116_chip2_gregister.fits
IN - NDF containing input image /@input.fits/ > input.fits
INFILE - Input aperture description file /'infile_photom.dat'/ > infile_photom.dat
Exposure time = 6.00
 242.61 1024.98 5.3719 4.5727 -0.1090 OK 12.0 6.00 regions
 242.61 1024.99 0.16591E+06 1164.5 604.30 0.16591E+06 OK regions
 407.30 1041.26 60693. 721.44 606.03 60693. OK regions
 797.81 1533.66 46359. 637.44 604.46 46359. OK annulus
 104.35 1261.91 16475. 411.64 605.14 16475. OK annulus
OUTFILE - Output aperture description file /'newphotom.dat'/ > newphotom.dat

```

AUTOPHOTOM in optimal extraction mode required a number of parameters, the ones we chose were the following: BIASLE=0 – the level of any constant offset in the data; EXSOURCE=HEADER – where the program should look for the exposure time, in this case it would be the FITS header (possible options are HDS, CONSTANT, HEADER); ETIME=EXPTIME – header keyword defining the exposure time (for CONSTANT it is a floating point value); OPTIMA=TRUE – whether optimal extraction should be used; PADU=1.0 – should be set to the gain value for the data that were not gain-corrected; PHOTON=2 – selects the method for calculation of the measurement errors (2 means that “the errors are estimated from the measured variance in the sky aperture, assuming that it is due to photon statistics and estimates the error in the object aperture accordingly”); POSITIVE=TRUE – “find the object centroid for image features which are positive or negative with respect to the background”; SKYEST=3 – selects the estimator for the background level in the sky aperture (option 3 – mode; the peak of the histogram of pixel values in the sky aperture is estimated); USEMAGS=FALSE – whether the output values should be converted into magnitudes; FIXANN=FALSE – whether the annular sky regions in the infile should be interpreted as radii in pixels, and not as scale factors; CENTRO=TRUE – center the aperture around the object before the measurement; and MAXSHIFT=20 – the maximum shift that is allowed between the initial object position and the aperture centroid. This script produced an outfile with optimal photometry results for each input FITS file (the results shown in Code Listing 2).

For the next step, a photometry program written in Python by D. Jones was adapted by the author of this thesis. This program first read in the object coordinates, exposure time, and observing date and time (UTC) from the FITS headers for a given telescope location to calculate BJD(TDB)¹⁹ time stamps. Then, it read in optimal photometry results, especially the FWHM in X and Y direction, and based on that calculated the aperture size

¹⁹ Barycentric Julian Date (BJD) given in the Barycentric Dynamical Time (TDB) standard is the most accurate time stamp and is recommended to use when high accuracy of astrophysical data is required (Eastman et al., 2010).

using a given aperture scaling factor $a \cdot \text{FWHM}$. Given the fact that an aperture radius of $1.5 \cdot \text{FWHM}$ may not always give the best results, a few scaling factors were used: 0.9, 1.2, 1.5, 1.8, 2.1 (each required a separate run of bash and Python scripts). In the last step, it produced a new infile for each FITS file with the coordinates of the same objects as in the optimal extraction infile, and calculated aperture size. It also produced a single time-series file with optimal photometry results and measured FWHM.

The second pass through the data was done with a similar script as in the Code Listing 1, with the only difference in the AUTOPHOTOM parameters being OPTIMA=FALSE, meaning the use of aperture extraction. An exemplary terminal output for this run is shown in Code Listing 3. Then, a slightly modified Python program was used to read in the aperture photometry results, calculate BJD(TDB) time stamps, as well as the object's air mass at the time of observations for further extinction correction, and finally produce a file containing all the measurements. Finally, the scripts were run again for different aperture scaling factors.

Listing 3: Terminal output for AUTOPHOTOM run in aperture extraction mode.

```

$ ./skrypt_autophotom_aperSDSS114635.sh

  CONVERT commands are now available -- (Version 1.8)

  Defaults for automatic NDF conversion are set.

  Type conhelp for help on CONVERT commands.
  Type "showme sun55" to browse the hypertext documentation.

  PHOTOM applications are now available -- (Version 1.12-2)

  Support is available by emailing starlink@jiscmail.ac.uk
  Type photomhelp for help or consult SUN/45

File = RED0001419641-20180116_chip2_gregister.fits
IN - NDF containing input image /@input.fits/ > input.fits
INFILE - Input aperture description file /'infile_photom.dat'/ > RED0001419641-20180116_chip2_gregister.
fits.infile_photom_scaled15.dat
Exposure time = 6.00
  242.50  1024.99  1031.5  1.0344  604.30  0.18133E+06  OK 7.5 0.00 0. regions circle
  407.22  1041.31  375.01  0.67399  606.03  65933.  OK 7.5 0.00 0. regions circle
  797.79  1533.70  296.95  0.65132  613.14  52208.  OK 7.5 0.00 0. annulus circle
  104.30  1261.92  100.12  0.45437  605.77  17603.  OK 7.5 0.00 0. annulus circle
  362.00  1774.14  2510.8  1.8527  639.68  0.44145E+06  OK 7.5 0.00 0. annulus circle
OUTFILE - Output aperture description file /'newphotom.dat'/ > RED0001419641-20180116_chip2_gregister.fits.
newphotom_scaled_aper15.dat

```

At each step of this procedure, the results for several frames were inspected. Thanks to the compatibility of different STARLINK programs, a selected frame was displayed in GAIA, and photometry results from AUTOPHOTOM were loaded in from a corresponding file using “Image-Analysis” → “Aperture/Optimal photometry”. Figure 2.4 shows a single frame of PG 1144+005 observations with OSIRIS@GTC with the positions of stars and corresponding sky regions/annuli overlaid in GAIA.

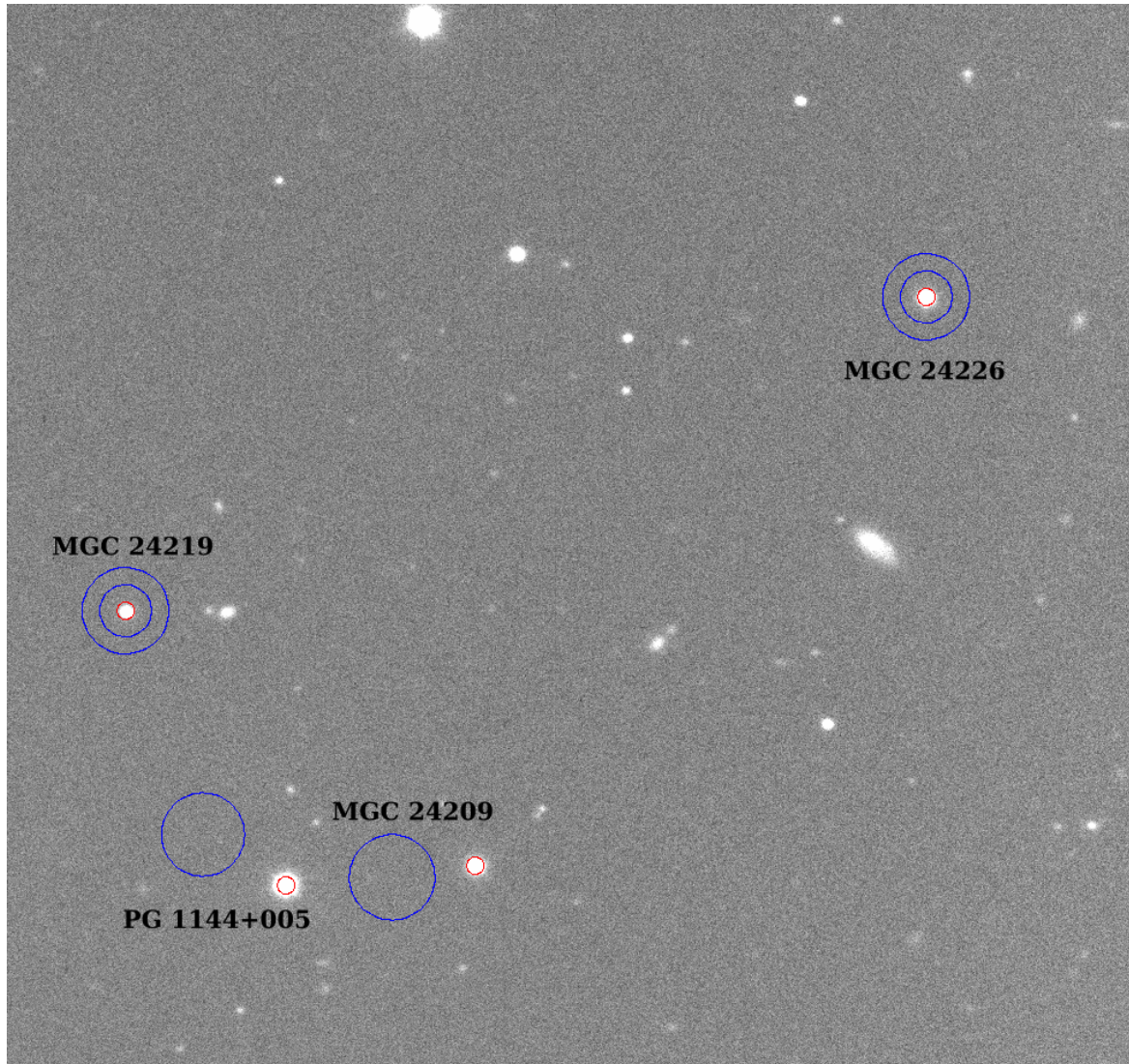


Figure 2.4: A single (trimmed) frame of PG 1144+005 observations with OSIRIS@GTC with the positions of the target and three comparison stars and corresponding sky regions/annuli overlaid in GAI A. Red circles denote circular apertures used to extract photometry, in this case with a radius of $1.5 \times \text{FWHM}$. Blue circles show sky regions or sky annuli used to measure the sky background. Sky regions were used for PG 1144+005 and MGC 24209 because of nearby bad columns in the camera. North is up and East is to the left. FOV is about $11' \times 11'$.

This allowed us to check, e.g., whether the apertures were properly centered, the sky regions have adequate dimensions (i.e., they would neither be too close to the star, nor would they contain background stars), or inspect frames that produced outlying points in the final time-series data. While this procedure might be redundant and inefficient in terms of the time needed to run it for a single observing run and the number of necessary files created, it allows a subsequent check of each of the steps and an adjustment of parameters for a single file to improve the result. The results were also checked against photometry derived with a fixed circular aperture (for a data set of a known pulsating star that is not included in this thesis).

There are at least a few possible improvements to this pipeline before a potential release on github. Firstly, the run could be optimized in terms of the necessary user interaction and time to run it, for instance the Python programs definitely could be merged into one, and the bash scripts could be called from it. That would result in a single Python program run producing a series of final photometry files with different aperture scaling factors for one observing run.

Moreover, the number of tested aperture scaling factors can be larger, and the grid finer. At present, that would however complicate and lengthen the whole process.

Another possible improvement concerns the quality of obtained photometry, that might be improved by the usage of elliptical apertures. We noticed that in the case of objects being observed at high airmass or at telescope positions where there were imperfections in telescope tracking, the obtained stellar images were elongated. When this effect is significant, using circular apertures would lead to non-optimal results – either some flux would be lost if the aperture was too small, or background noise would be introduced with too large aperture. The choice of optimal axes is not trivial – it does not only depend on the FWHM like in the circular aperture case, but also the shape of the ellipse. The complexity of this problem was not explored here, but it is a possible future improvement to the photometry pipeline developed by the author. However, the TEA-Phot program (Bowman & Holdsworth, 2019) is based on adaptive elliptical apertures, and was used to carry out data reduction and photometry of data collected using SHOC@SAAO for PG 1144+005 (see Chapter 4 for a description).

2.3.3 *Differential photometry*

The science objective of the observations obtained, reduced, and analyzed in this thesis – to search for, confirm, and characterize pulsations in pre-WD stars – did not require obtaining absolute photometric measurements. While the absolute photometry needs a transfer of observed instrumental magnitudes to a standard photometric system (which might require observing additional standard fields at the cost of observing time) in order to derive an absolute result, the differential photometry provides only a relative result, which for relative variability searches or periodicity analysis is sufficient.

Differential photometry is based on the measurement of the difference in brightness of the source compared with one or more reference sources, usually called comparison stars. CCD observations and modern photometry programs allow the measurement of even all stars in a given field of view, which helps to choose a final set of comparison stars even after the observations. In the present work, at least two comparison stars were attempted to be used (one of them served as a check star, to ensure that the comparison star is not variable). Because the FOVs of some instruments were small, the pipeline was written for up to five stars. Unfortunately, there were cases where only one comparison star was available (e.g., due to very small FOV with ProEM, see Section 1.7.2). Whenever possible, the comparison stars were chosen based on the following criteria: brighter than the target to reduce the contribution of the Poisson noise from the star (equal to the square root of the number

of counts in e^-); similar color index to reduce the effect of differential color extinction; relatively isolated to reduce the possibility of blending in poor seeing conditions; close to the target to reduce the consequences of nonisoplanatism or different background counts (e.g., if a gradient from the Moon or inhomogeneous clouds is present).

The derivation of differential magnitudes is based on the definition of instrumental magnitude. The differential magnitude of stars 1 and 2 is given by

$$\Delta m = m_1 - m_2, \quad (2.2)$$

where m_1 and m_2 are apparent magnitudes of those stars, respectively. The apparent magnitude is related to the instrumental magnitude m_{instr} (uncalibrated apparent magnitude, the one that is measured) by

$$m = m_{\text{instr}} + KX + ZP, \quad (2.3)$$

where X is the air mass at the time of observation, K is the atmospheric extinction coefficient, and ZP is the photometric zero point of the used instrumental setup. If the measured stars have similar color indices, the term $KX + ZP$ is the same for all stars on a given frame, and the equation for differential magnitude reduces to

$$\Delta m = m_{\text{instr},1} - m_{\text{instr},2}, \quad (2.4)$$

meaning that by properly reducing the data, using suitable comparison stars, and calculating differential magnitudes, it is possible to remove the influence of the observing conditions from the light curves. The instrumental magnitude, by definition, is

$$m_{\text{instr}} = -2.5 \log_{10} F + C, \quad (2.5)$$

where F is the signal from the star in counts per second, and C is an arbitrary constant²⁰. Finally, the magnitude relation is given by

$$\Delta m = m_1 - m_2 = -2.5 \log_{10} \left(\frac{F_1}{F_2} \right) \quad (2.6)$$

and this relation was used to calculate the final differential magnitudes. Formal photometry errors were propagated accordingly, and outlying points were rejected at a 3.5σ level.

2.3.4 Extinction correction

The observed pre-WD stars are usually bluer than the available comparison stars. This causes different extinction coefficients, as they are wavelength-dependent. In order to correct for this difference, in the first approximation we plotted differential magnitudes against the air mass X (a Bouguer method), and used the `stats.linregress` module from SciPy (Virtanen et al., 2020) to calculate a linear least-squares regression (Figure 2.5). The

²⁰ It is usually set to a large value, to prevent confusion between instrumental magnitudes and the corresponding calibrated magnitudes.

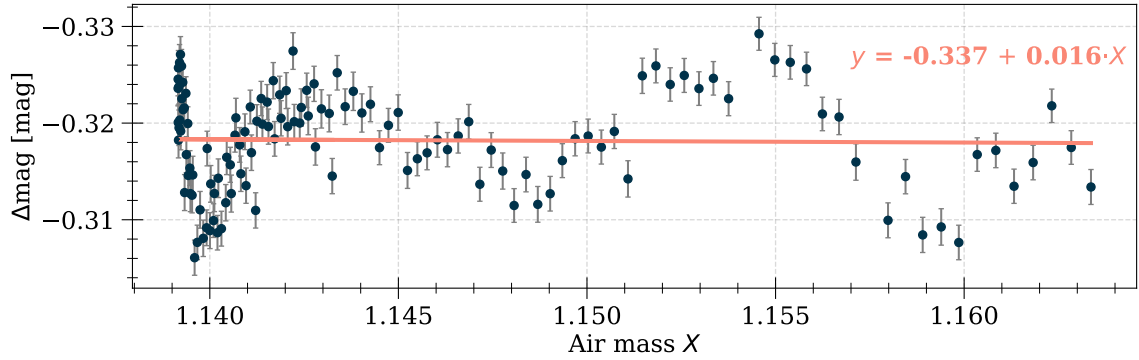


Figure 2.5: An illustration of the Bouguer method: differential magnitudes plotted against airmass X with an overplotted linear least-squares regression fit, to correct the PG 1144+005 OSIRIS@GTC time-series for residual differential color extinction. See text for details.

difference here is not significant, because we used a “master” comparison star created as a sum of flux from three stars (marked in Figure 2.4), which removes the color factor to some extent. The fit was then subtracted from the differential magnitudes to provide the final extinction-corrected light curves for time-series analysis (Figure 1 in Chapter 4). We note that for higher air mass values (greater zenith distance) the assumption of a plane-parallel atmosphere is not realistic and the prescription used here might not give accurate results, but most of the objects observed in this work were not observed at zenith distances over 60° , where this assumption can still be used.

2.3.5 Differential magnitude vs. seeing

To ensure that the procedure we used does not introduce anything spurious, we plotted differential magnitudes against seeing to check whether there is any correlation. Figure 2.6 shows the data for PG 1144+005 observed with OSIRIS@GTC. It can be seen that there is no correlation (the Pearson correlation coefficient equals 0.012), meaning that the aperture adapted to seeing does not influence the results. It should be noted that this may not be the case if a planetary nebula is present (Jones et al., 2015), but an examination of this suspicion was out of the scope of this thesis, as the targets presented here did not have visible nebulae.

2.4 TIME-SERIES ANALYSIS

Time-series analysis is a well-developed field in statistics that provides tools for the study of frequency content in time-dependent data. Asteroseismology is based on recovering the pulsation frequencies and providing mode identifications for comparison with theoretical models. Photometric time series, created from the measurements of stellar brightness (e.g., differential magnitudes) and time stamps, provide the fundamental data for recovering pulsation frequencies, as photometry is primarily sensitive to temperature variations caused by stellar pulsations (Aerts et al., 2010).

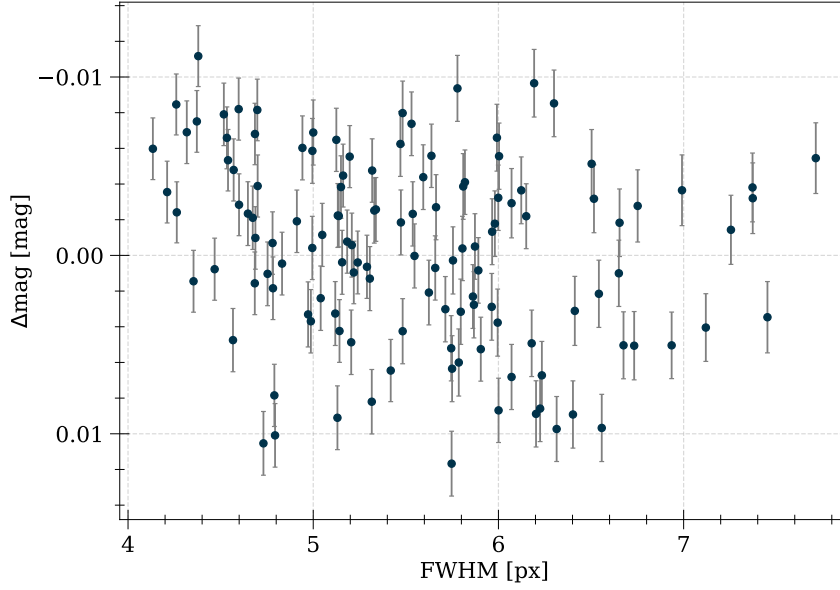


Figure 2.6: A plot of seeing against differential magnitude for PG 1144+005 observed with OSIRIS@GTC using an aperture adapted to the seeing. The plot indicates that the procedure does not introduce spurious variability. The Pearson correlation coefficient equals 0.012.

In an ideal case of an infinite, evenly sampled time series with no gaps, the continuous Fourier transform of a function $x(t)$ is given by (Aerts et al., 2010)

$$F(\nu) \equiv \int_{-\infty}^{+\infty} x(t) \exp(2\pi i \nu t) dt. \quad (2.7)$$

A function $x(t)$ can be written as a sum of harmonic functions with frequencies ν_1, \dots, ν_M and amplitudes A_1, \dots, A_M :

$$x(t) = \sum_{k=1}^M A_k \exp(2\pi i \nu_k t) \quad (2.8)$$

and the Fourier transform of this function is given by

$$F(\nu) \equiv \sum_{k=1}^M A_k \delta(\nu - \nu_k), \quad (2.9)$$

where $\delta(\nu - \nu_k)$ is the Dirac delta function. This is the foundation of frequency determination from Fourier analysis.

In practice, the time series are neither infinite, nor continuous. In the case of a real data set, the function $x(t)$ is only known for a discrete number of time points $t_i, i = 1, \dots, N$ and it is impossible to determine its $F(\nu)$. Deeming (1975) introduced the discrete Fourier transform:

$$F_N(\nu) \equiv \sum_{i=1}^N x(t_i) \exp(2\pi i \nu t_i). \quad (2.10)$$

While F_N and F are different, they can be associated by the window function:

$$w_N(t) \equiv \frac{1}{N} \sum_{i=1}^N \delta(t - t_i). \quad (2.11)$$

F_N can be transferred to an integral form using the window function and the properties of the Dirac delta function:

$$\frac{F_N}{N} = \int_{-\infty}^{+\infty} x(t) w_N(t) \exp(2\pi i \nu t) dt. \quad (2.12)$$

Then, the spectral window $W_N(\nu)$ is defined as the discrete Fourier transform of the window function:

$$W_N(\nu) = \frac{1}{N} \sum_{i=1}^N \exp(2\pi i \nu t_i). \quad (2.13)$$

Finally, the discrete Fourier transform can be written as the convolution of the spectral window and the Fourier transform:

$$F_N(\nu)/N = (F * W_N)(\nu). \quad (2.14)$$

It can also be shown that $F_N(\nu)/N$ is the sum of M spectral windows centered around different frequencies ν_k , and interference might be present because the spectral window can differ from 0 at frequencies ν_k , which may not be equal to $\nu_k, k = 1, \dots, M$. As a result, some spurious peaks might appear that do not correspond to real frequencies. These peaks are caused by gaps in photometric time series and are called alias frequencies (one of the most common are daily aliases, occurring in intervals corresponding to $\pm 1, \pm 2 \text{ d}^{-1}$, etc.). Alias frequencies can hinder the extraction of the real peaks in the data, and caution is necessary in a difficult process of deciding whether a frequency is real or not. The aliasing structure of the data occurs in the spectral window, and this property should be used by inspecting the spectral window in the process. Aliases can also be restrained, e.g., Bell et al. (2017) showed how ground-based data together with space-based data can help distinguish between the real and alias frequencies.

The number of frequencies that can be recovered depends on the quality of the time series. A higher photometric precision allows the detection of a larger set of frequencies, as stellar signals of lower amplitude can be detected. In the study of pulsating stars, the primary goal is to maximize the S/N of a peak in a Fourier transform. Therefore, proper data reduction and photometry techniques are important to achieve the lowest possible noise level in the Fourier transform of the data. Many detection criteria are based on the S/N and can be affected by imperfections in the data, leading for example to non-detection of a real peak. Often used is the amplitude criterion of $S/N \geq 4$ for ground-based data from Breger et al. (1993). However, this criterion is not universal as, e.g., Baran & Koen (2021) showed that for space-based data from the *TESS* mission, the S/N threshold should be higher and determined individually per data set. Another widely used criterion, especially for space-based data, is based on the false alarm probability, FALSE (Kepler, 1993). A given FALSE value, e.g., FALSE=1/1000, applied to $P_{\text{obs}} = \ln\left(\frac{N_i}{\text{FALSE}}\right) \cdot \langle P \rangle$ (where

N_i is the number of independent frequencies, and $\langle P \rangle$ the average power for the region of studied frequencies), gives a power criterion that a peak must fulfill to have 1 chance in 1000 to be only due to noise.

One of the most important characteristics of time series data concerns the timing. Proper planning of observations with a clear scientific goal, tailored to the expected variability, is crucial in observational asteroseismology. The time sampling, Δt (usually the exposure time + read out time), needs to be chosen in such a way that it provides the expected S/N for the target counts in a single frame, and at the same time allows proper sampling of the variability. In Fourier space, this translates to the highest frequency that can be reliably detected in a given data set, called the Nyquist frequency: $f_{\text{Nyq}} = 1/2\Delta t$. However, this is only valid in the case of evenly sampled data. For unevenly sampled data (e.g., with large gaps), Eyer & Bartholdi (1999) showed that it is better to use the greatest common divisor p of all $(t_i - t_{i-1})$ pairs, i.e., differences between consecutive observing times²¹: $f_{\text{Nyq}} = 1/2p$. Murphy et al. (2013) showed that in specific circumstances, the true frequencies can appear even above the Nyquist frequency in a so-called super-Nyquist regime.

Even though the observational goal is to reach a duty cycle (total time spent on target) of 100%, this is impossible to achieve in reality. While space-based observatories like *Kepler* or *TESS* provide almost continuous coverage, ground-based observations not only suffer from the day-night cycle, but are also prone to gaps due to telescope scheduling, weather conditions, telescope or instrument malfunctions, funding or other related factors. This makes obtaining continuous observations for extended periods of time nearly impossible. This has important consequences, because T – the total length of the time series – translates in Fourier space to the frequency resolution: $\Delta f = 1/T$ (Loumos & Deeming, 1978). This frequency resolution, also called the Rayleigh criterion, is only treated as the first estimate of the accuracy of frequency detection. The study by Loumos & Deeming (1978) showed that for two close frequencies with separation in the range $1/T < \Delta f < 1.5/T$, the maxima in the Fourier transform may be shifted from the real ones because of the interference between those frequencies. They also showed that the difference between the real frequencies and their peaks in the Fourier transform are negligible when $\Delta f > 2.5/T$. As a practical consequence, even longer observing runs are necessary to resolve closely spaced frequencies. This is important for the asteroseismic study of pre-WD stars to resolve rotationally split modes for typical rotation periods of those stars being longer than 1 d (Table 10 in Córscico et al. 2019).

For the frequency analysis of photometric time series included in this thesis, we used the *Period04* program written by Lenz & Breger (2005), which is an extended version of *Period98* by Sperl (1998). This program is especially designed for the analysis of large time series with gaps, but its capabilities are not limited to that. The basic run of *Period04* consists of the following steps. First, the data sets are loaded in and can be adjusted if necessary (that includes dividing a data set into substrings, rejecting parts of a data set, combining different data sets, and so on). The second step consists of the calculation of a Fourier spectrum of the original time series based on a discrete Fourier transform al-

²¹ There are other methods, and we refer the reader to the book by Aerts et al. (2010).

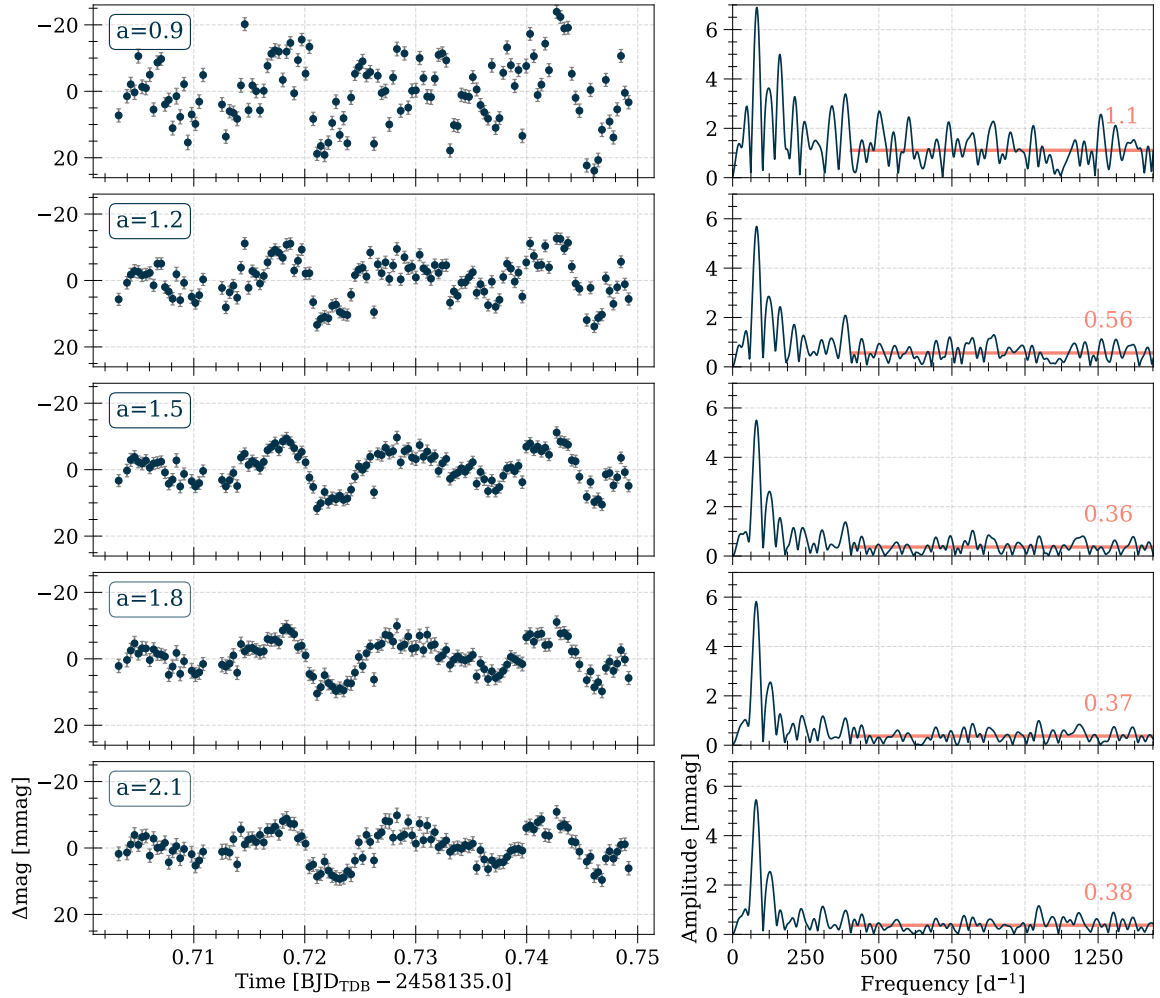


Figure 2.7: A plot showing differential magnitudes obtained for different scaling factors a for PG 1144+005 observed with OSIRIS@GTC, and corresponding Fourier amplitude spectra. Solid lines represent the median noise level calculated in the $400 - 1439 \text{ d}^{-1}$ range. Note the same scales for the light curves and Fourier spectra.

gorithm until a given Nyquist frequency, and the extraction of detected frequency/frequencies. Next, a least squares fit is performed for a number of requested frequencies and their frequencies, amplitudes, and phases are optimized. Finally, the fitted frequencies are subtracted – this procedure is called prewhitening – and a residual Fourier transform is calculated. This procedure can be repeated until all significant frequencies are prewhitened, and the decision when to stop is up to the user. The Fourier calculation panel also provides an option to calculate a spectral window of the data set. All the fitted frequencies, Fourier spectra, and multiperiodic fits to data can be saved to text files.

The full evaluation of photometric time series created using scaled circular apertures, as described in Section 2.3.2, can only be done with simultaneous inspection of the Fourier transforms of those time series. In the study of oscillating stars, the goal is not only to minimize the scatter in the light curve, but also to maximize the amplitude S/N of a peak in the corresponding Fourier transform. The average differential magnitude and standard deviation were calculated for each time series using a dedicated Python program. After that, the Fourier transforms were calculated using `Period04` for the same time series, then

all peaks were prewhitened, and the median noise level was calculated for the residual Fourier transform. In the case of objects that did not show any variability in the Fourier transform, no prewhitening was done. Then, those values were compared against the same measurements for another scaling factor, and the decision on which light curve to use was made supported by the visual inspection. Figure 2.7 shows this procedure for observations of PG 1144+005 with OSIRIS@GTC. Time series and Fourier transforms are shown for different aperture scaling factors: 0.9, 1.2, 1.5, 1.8, and 2.1. It can be seen that the aperture with a radius of $1.5 \cdot \text{FWHM}$ provides the lowest median noise level in the $400 - 1439 \text{ d}^{-1}$ range of the Fourier spectrum, while preserving the light curve shape, and giving the lowest scatter in the light curve, and lowest photometric errors per data point.

2.5 SUMMARY

In this Chapter, we have presented the data reduction and analysis techniques employed in Chapters 3, 4, and 5. Using the techniques described here, in Chapter 3 we refuted a preliminary discovery of ϵ -driven pulsations in VV 47 thanks to new data of improved quality and a re-analysis of discovery data. The same techniques were used to obtain the median noise level of the Fourier amplitude spectrum of 0.36 mmag for the GTC data presented in Chapter 4, which allowed us to discover long-sought-after pulsations in PG 1144+005. Finally, we employed these techniques in our survey for variability among PG 1159 stars to discover new pulsators and provide improved limits for non-variability, as described in Chapter 5.

ON ϵ MECHANISM-DRIVEN PULSATIONS IN VV 47

This chapter has been published in the Monthly Notices of the Royal Astronomical Society as

“On ϵ mechanism-driven pulsations in VV 47”

Sowicka, P., Handler, G., Jones, D., 2018, MNRAS, 479, 2476, DOI: [10.1093/mnras/sty1660](https://doi.org/10.1093/mnras/sty1660)

The author was responsible for the preparation of observing proposals and application for observing time, planning the observations, reducing the data, doing photometry and frequency analysis, as well as preparing figures and writing the paper.

WORK IN CONTEXT

Stellar pulsations driven by the ϵ mechanism were theoretically predicted almost 100 years ago by Sir Arthur Eddington (Eddington, 1926). Since then, all kinds of stars across the HR diagram, from M dwarfs (Baran et al., 2011) and subdwarfs (Miller Bertolami et al., 2011; Randall et al., 2015; Battich et al., 2018) to very massive stars (e.g., Blecha et al., 1992; Bratschi & Blecha, 1996), were considered when looking for convincing evidence, to no avail. Theoretical calculations showed that the ϵ mechanism can also operate in pre-WD stars with helium-burning shells, giving rise to short-period g modes. One of the candidates to show such pulsations was the central star of planetary nebula VV 47. Observations by various groups (Liebert et al., 1988; Ciardullo & Bond, 1996) did not detect any pulsations in this star, until González Pérez et al. (2006) claimed the detection of pulsations in VV 47 and attributed the presence of some high-frequency peaks to the ϵ mechanism. Those claims were followed by extensive asteroseismic modelling (Córscico et al., 2009b; Calcaferro et al., 2016), which allowed the derivation of an asteroseismic mass in agreement with other methods, but did not yield an unambiguous model characterizing the star.

The aim of this work was to test the earlier claims of pulsation modes driven by the ϵ mechanism operating in this star. We obtained new time-series photometric observations using the 4.2-m William Herschel Telescope for a total on-target time of 33 h 48 m over four

nights. We did not detect *any* variability up to a limit of 0.52 mmag ($S/N \geq 4$, Breger et al. 1993) in the Fourier amplitude spectrum. Given the null result, we re-analyzed the data of González Pérez et al. (2006) with the alleged pulsations. As in the case of the new data, we were unable to detect *any* variability, with a limit of 0.92 mmag. Those results showed that VV 47 was not pulsating in either of these observing runs, and it might not even be a variable star. We attributed the claims by González Pérez et al. (2006) to a particularly relaxed detection criterion.

The case of VV 47 is a cautionary tale for other observers to not claim potentially exciting results without solid proof, to save observing and computing time of other scientists.

On ϵ -mechanism-driven pulsations in VV 47

Paulina Sowicka,¹★ Gerald Handler¹ and David Jones^{2,3}

¹*Nicolaus Copernicus Astronomical Center, Bartycka 18, PL-00-716 Warsaw, Poland*

²*Instituto de Astrofísica de Canarias, E-38205 La Laguna, Tenerife, Spain*

³*Departamento de Astrofísica, Universidad de La Laguna, E-38206 La Laguna, Tenerife, Spain*

Accepted 2018 June 14. in original form 2018 May 25

ABSTRACT

We report new observations of the central star of the planetary nebula VV 47 carried out to verify earlier assertions that the short-period pulsation modes detected in the star are driven by the ϵ -mechanism. In our data, VV 47 was not variable up to a limit of 0.52 mmag in the Fourier amplitude spectrum up to the Nyquist frequency of 21.7 mHz. Given this null result we re-analysed the data set in which oscillations were claimed. After careful data reduction, photometry, extinction correction, and analysis with a conservative criterion of $S/N \geq 4$ in the Fourier amplitude spectrum, we found that the star was not variable during the original observations. The oscillations reported earlier were due to an over-optimistic detection criterion. We conclude that VV 47 did not pulsate during any measurements at hand; the observational detection of ϵ -driven pulsations remains arduous.

Key words: stars: individual: PN VV 47 – stars: oscillations – white dwarfs.

1 INTRODUCTION

It has been almost 100 yr since Sir Arthur Eddington, in his book ‘The Internal Constitution of the Stars’ (Eddington 1926), suggested the existence of a pulsational driving mechanism dependent on the nuclear energy generation rate, now known as *the ϵ -mechanism* (and referred to historically as ‘nuclear driving’). Briefly, the ϵ -mechanism driving is caused by the strong dependence of nuclear burning rates on temperature. The layers of a star where nuclear reactions take place are compressed by the enhancement of nuclear energy release causing a gain in thermal energy, while the opposite happens when these layers expand giving back the energy (Unno et al. 1989). The existence of such a mechanism operating in a star is somewhat obvious, although in most classes of stars it is apparently too weak to drive any pulsations at a detectable level, or at all. For a more detailed description of the ϵ -mechanism we refer the reader to, e.g. the paper by Kawaler (1988).

In the decades following Eddington’s work, there was much interest in this mechanism from the community, giving as example the work by Ledoux (1941) and Schwarzschild & Härm (1959) that suggested that this mechanism may be responsible for the pulsational instability of very massive stars. In the early 1980s –early 1990s, it was suggested that the instability caused by the ϵ -mechanism might also operate in Wolf–Rayet stars, possibly driving their strong stellar winds. In the best candidate (WR40), Blecha, Schaller & Maeder (1992) detected a 627-s periodicity, but were unable to confidently assign it to the ϵ -mechanism. A later study by Bratschi & Blecha (1996) could not confirm this detection. Mo-

tivated by theoretical calculations suggesting that M-dwarf stars can experience pulsational instability driven by nuclear burning, Baran et al. (2011) carried out a survey for variability among such stars, but failed to detect any variability consistent with this idea. Miller Bertolami, Córscico & Althaus (2011) attributed the observed variability of the hot subdwarf B star LS IV-14°116 to non-radial g-mode pulsations excited by the ϵ -mechanism, operating in He-burning shells that appear before the star settles in the He-core burning phase. Randall et al. (2015), disputed this conclusion based on their determinations of the stellar parameters being more consistent with a star on the Helium main sequence. In turn, Battich et al. (2018) argued that these parameters may be consistent with their models of pre-horizontal branch stars, and the ϵ -mechanism could still excite pulsations with periods roughly similar to those observed.

Theoretical calculations have shown that pulsations can also be driven in pre-white dwarfs via the ϵ -mechanism operating in the remnants of nuclear burning in their envelopes (Kawaler et al. 1986). The mechanism operating in such conditions is not very effective, and could possibly only be responsible for driving the lowest order g modes, which have not yet been seen in these stars.

One of the candidates to show such pulsations is the central star of the planetary nebula (PN) VV 47 (hereinafter referred to as VV 47). Observations by Liebert et al. (1988) in 1984, found the star to be variable across multiple nights, but with the source of the variability remaining elusive. They summarized by saying that any real periodicities range from tens of minutes to several hours, and concluded: ‘However, any real light variability in this object appears to be irregular in nature, and may be due to a different mechanism than the types of pulsations believed to be responsible in K 1–16, PG 1159–035, and similar stars.’ A few years later Ciardullo &

* E-mail: paula@camk.edu.pl

Bond (1996) observed VV 47 on four nights between 1987 and 1990. They did not confirm the tentative variability reported by Liebert et al. (1988), but neither could they rule out very low amplitude variations between nights.

Finally, González Pérez, Solheim & Kamben (2006) (hereinafter GP06) concluded VV 47 to be a low-amplitude pulsator with an extremely complicated power spectrum based on multiple nights of observations using the 2.56-m Nordic Optical Telescope (NOT). In addition to some low-frequency variability, the authors explained the presence of some high-frequency peaks as possibly being driven by the ϵ -mechanism, which would have been the first observational evidence for pulsational driving by this mechanism.

Following the findings of GP06, VV 47 became the subject of extensive asteroseismic modelling. Córscico et al. (2009) presented a fully non-adiabatic stability analysis based on their PG 1159 models and explored the possibility of pulsational driving by the ϵ -mechanism. The authors found strong evidence for the existence of an additional instability strip originating from the short-period g modes excited by the ϵ -mechanism, with VV 47 lying in the region where both κ - and ϵ -destabilized modes are predicted. They estimated the mass from the period spacing data, with the mean period spacing of about 24 s, to be about 0.52–0.53 M_{\odot} , in perfect agreement with the spectroscopic mass ($\approx 0.525 M_{\odot}$) also derived by Córscico et al. (2009). Although the uncertainties on $T_{\text{eff}} - \log g$ for VV 47 are so large, that the error box covers evolutionary tracks for masses between about 0.51–0.59 M_{\odot} , the two independent mass estimations being in such a good agreement narrow the possible mass range down. A stability analysis of all possible oscillations listed by GP06 suggested that if all reported modes were real, the shortest periodicities would be due to the ϵ -mechanism. When taking into account only the modes with the highest probability of being real according to GP06, the shortest period mode over the FAP of GP06 (~ 261 s) would be too long to be explained as ϵ -driven (see fig. 5 of Córscico et al. 2009).

Calcaferro, Córscico & Althaus (2016) attempted to find an asteroseismic model of the star with the main aim to derive its total mass. The authors estimated the mean period spacing based on GP06 data with three methods: the inverse variance, the Kolmogorov–Smirnov test, and the Fourier transform (FT) significance test (references in the original paper). When using the complete list of periods all of these methods were inconclusive. Instead, when rejecting one or more periods, the authors were able to find excellent agreement between the methods implying strong evidence for a constant period spacing of 24.2 s. This period spacing value together with the evolutionary models indicated a total mass of about 0.52 M_{\odot} , in perfect agreement with all previous estimations. However, even when taking different sets of periods and evolutionary stages of VV 47, the authors were unable to find an unambiguous model characterizing the star.

In this work, we return to VV 47 with new observations using the 4.2-m William Herschel Telescope (WHT) in order to re-examine the possible existence of the ϵ -driven pulsations reported by GP06.

2 NEW WHT OBSERVATIONS

VV 47 was observed using the WHT located at the Observatorio del Roque de los Muchachos (La Palma, Spain), equipped with Auxiliary-port CAMera (ACAM), on 3–8 January 2017. The log of observations is presented in Table 1. We used exposure times of about 20 s, varying it slightly from night to night to suppress aliasing at the sampling frequency. We also used windowing to reduce the readout time to about 3 s. Observations were started in

dark time (3–4 Jan) with growing influence of the Moon over the next nights, up to 84 per cent illumination at 60° from the target on the last night. The total on-target time was 33 h 48 m, comprising two complete nights, another which was frequently interrupted by passing clouds and a fourth night on which only one hour of observations could be acquired (see Fig. 1 and Table 1). The data were reduced using our own PYTHON-based routines based mostly on ASTROPY package, which consisted of standard bias subtraction, flat-fielding, and aligning the data.

2.1 Photometry

The varying conditions during our observations made optimizing the photometric measurements challenging. We found that traditional aperture photometry gave the best results when the aperture size was scaled with seeing. We used a trial and error approach to find the optimal scaling factor for the aperture size for a given night’s observations by minimizing the rms scatter (Table 1) of photometric measurements extracted using the STARLINK AUTOPHOTOM package (Eaton et al. 2014). In our windowed field of view, there were three other stars bright enough to be used as possible comparison stars. We achieved the best results in terms of signal-to-noise ratio when using an ‘artificial’ comparison star comprising the summed flux from all three available comparison stars. Because our target is much hotter than the comparison stars, it was necessary to correct the resulting light curves for differential colour extinction, which was done using the first approximation linear fit to the $\Delta\text{mag}(\sec z)$ relation. The last step consisted of rejecting outlying points with a dedicated program that runs a moving-average filter over the data and rejects the most obvious single outliers. The final light curve is shown in Fig. 1. The time-scales of the remaining, low-amplitude long-term trends are too long to be due to stellar pulsation.

2.2 Pulsations of VV 47?

We calculated the FT amplitude spectrum of all nights of VV 47 data (Fig. 2) up to the Nyquist frequency of the data set (≈ 21.7 mHz) using PERIOD04 (Lenz & Breger 2005). Aside from the manifestation of the above-mentioned long-term trend, the spectrum is flat with no significant peaks up to a limit of 0.52 mmag. This detection limit was calculated following the conservative criterion that for any peak to be reliably detected it must fulfil $S/N \geq 4$ in amplitude (Breger et al. 1993). We then calculated the amplitude FT for each night separately, again not finding any statistically significant peaks. With this null result we conclude that VV 47 did not pulsate during our observations, and hence might not be a pulsator at all – and perhaps not even a variable star.

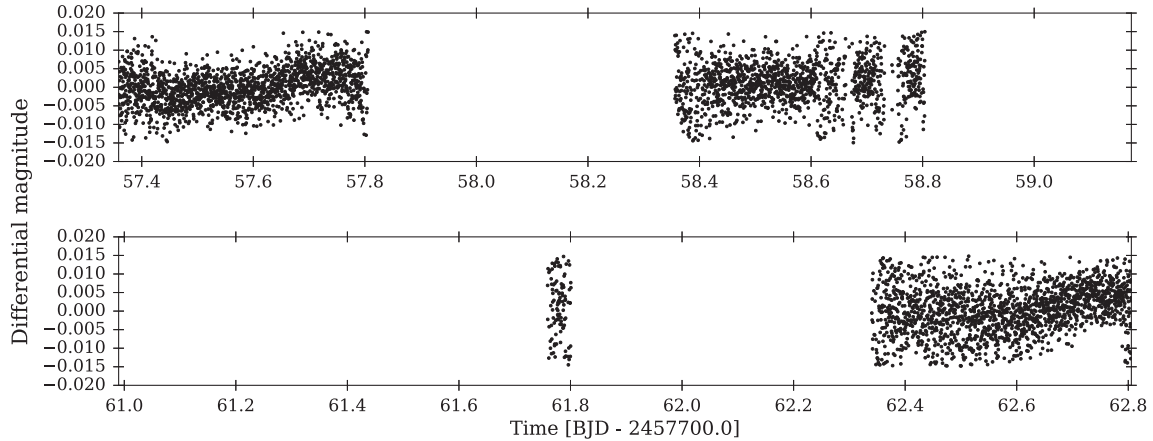
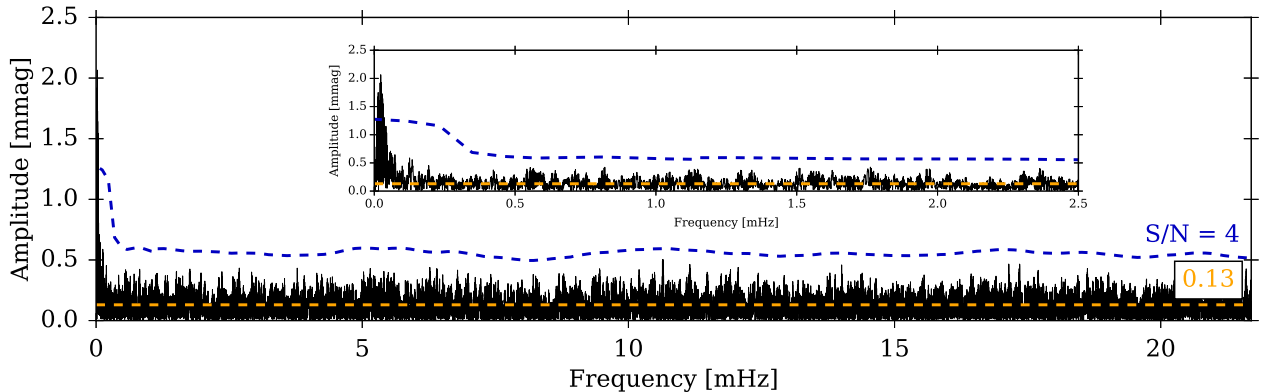
3 RE-ANALYSIS OF ARCHIVAL DATA

Intrigued by the apparent absence of not only the pulsation modes detected by previous authors, but any pulsations at all, we re-examined the data set of GP06. These authors reported the results of a survey for photometric variability among 11 hot, H-deficient PN nuclei (PNNi), carried out in years 2000–2001 with the NOT. VV 47 was observed on three nights for a total of 22.2 h using the Andalucía Faint Object Spectrograph and Camera (ALFOSC); for details of these observations see GP06.

We retrieved the data of GP06 from the NOT archive that did not include the final light curves their analysis was based upon. Therefore, we decided to reduce the original CCD frames anew. To this end, the original frames were converted to 2D images using

Table 1. The log of our new observations with the WHT.

JD-245 7700.0	Exp. time (s)	N_i	Total time	Filter	Min–median–max FWHM of the night (arcsec)	Aperture scaling factor	rms scatter (mmag)
57.356 2262–57.803 4369	20.0	1679	10 h 44 min	Sloan G	0.86–1.46–4.24	1.37	5.08
58.353 6221–58.802 5573	20.2	1671	10 h 46 min	Sloan G	1.02–1.79–4.76	1.20	10.55
61.756 9323–61.799 7911	20.3	159	1 h 2 min	Sloan G	3.55–4.97–7.41	0.85	15.86
62.334 3397–62.804 1082	19.7	1787	11 h 16 min	Sloan G	0.88–1.54–3.06	1.27	7.27

**Figure 1.** Light curve of VV 47 from our WHT observations. Note the discontinuity between the two panels.**Figure 2.** The Fourier amplitude spectrum of all four nights of VV 47 WHT data. There are no significant peaks in the spectrum, except for a low-frequency signal close to 2 cycles per sidereal day (which is about 0.023 mHz) that we consider of instrumental origin. A zoom of the low-frequency region is presented in inset.

the `RTCONV` program (Østensen 2000), which was adapted to run on modern computers (Greg Stachowski, private communication). Bias and flat-field, but no gain correction were applied. Next we performed photometry, using the same approach as described in Section 2.1. The conditions during each run varied but ultimately the best aperture scaling factor was found to be 1.3 for all runs. A differential light curve was created dividing the flux from the target by the summed flux of two comparison stars available during each run. We corrected for differential colour extinction following the methodology described in Section 2.1, with the final estimated rms scatter per data point in each run being about 4–6 mmag (Table 2). Next, we calculated amplitude FTs for each run separately up to the Nyquist frequency, i.e. runs 1–3: ≈ 720 c/d = 8333 μ Hz, run 4: 1080 c/d = 12500 μ Hz.

Before we proceed to the direct comparison of the results, we have to discuss two fundamental differences in our analyses compared

to GP06. These authors decided to use a different approach to assess the significance of an individual peak – not our conservative criterion of $S/N \geq 4$ (Breger et al. 1993), but a variant of the method described by Kepler (1993). In brief, this method assesses the probability for a given peak in the FT of being real by using the equation

$$P_{\text{obs}} = \ln \frac{N_i}{\text{FALSE}} \langle P \rangle, \quad (1)$$

where P_{obs} is the power that satisfies this criterion, N_i – the number of independent frequencies, FALSE – a false alarm probability (FAP), and $\langle P \rangle$ is the average power in the region around the frequency of interest. A FAP of 1/100 means that a peak is taken as being real only if it has less than 1 in 100 possibility to be due to noise.

There are however differences between the original paper by Kepler (1993) and the approach by GP06. N_i is defined by Kepler

Table 2. The log of observations by GP06.

Run	UT start date	Duty cycle (s)	N_i	Total time	Filter	Min–median–max FWHM of the night (arcsec)	Aperture scaling factor	rms scatter (mmag)
1	2001-01-16T00:36:53	60.0	348	5 h 47 min	B	1.09–1.33–2.18	1.3	4.377
2	2001-01-16T21:04:03	60.0	377	6 h 16 min	B	0.89–1.18–1.93	1.3	4.641
3	2001-01-17T05:04:47	60.0	106	1 h 45 min	B	1.20–1.33–1.87	1.3	5.351
4	2001-01-18T20:17:01	40.0	709	8 h 24 min	B	0.91–1.20–2.18	1.3	5.541

(1993) as the number of independent frequencies, while in GP06 as the number of points in the light curve. This is only correct in the case of equally spaced data without gaps when the periodogram is computed from zero to the sampling frequency ($= 2 f_{\text{Nyquist}}$). The first condition seems fulfilled by the authors as they do not mention an outlier removal procedure, plus the number of data points in their table corresponds to the number of frames taken. However, the second condition may not have been fulfilled – judging purely from the FTs presented in the paper – as the authors plot all FTs for VV 47 starting from 130 μHz up to about 8500 μHz except for the last run, where the curve exceeds 8500 μHz but it is unclear at which value it ends. As such, this appears to be a calculation up to the Nyquist frequency rather than to the sampling frequency (i.e. $2 f_{\text{Nyquist}}$). Also, the mean power $\langle P \rangle$ would then need to be evaluated over the whole FT, which does not appear to be the case in their analysis. If this is indeed true, then the significance criterion of GP06 was incorrectly applied. Also, their choice of the FALSE value of 1/20 is a rather relaxed criterion for this kind of star, with conservative values of $\sim 1/1000$ being more typical (e.g. Castanheira et al. 2013).

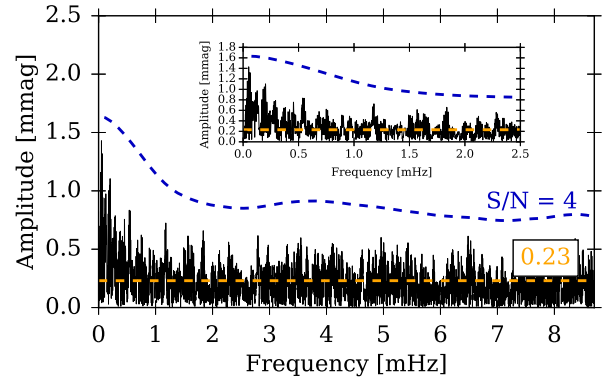
GP06 justified the need of such an alteration with the statement that ‘periods that have been observed for PNNi have quite low amplitude (a few mmag) and show temporal variability in the amplitude on different time-scales’. The peaks the authors found in the FTs of their targets in that way had low amplitudes and were variable on time-scales of days or hours. Low amplitudes are common for this type of star, but the only known mechanisms that would make signals vary in amplitude on such short time-scales would be beating of unresolved pulsation frequencies (which should become resolved and detected when analysing longer strings of data), interference with noise peaks, or those peaks indeed being due to noise themselves. We decided to not use GP06’s approach and instead remain with the classical conservative criterion of $S/N \geq 4$ in amplitude (Bregier et al. 1993).

In their first run (2001 January 15/16), GP06 estimated the average power to be 0.15 μmp , while our estimation was 0.22 μmp . The average power estimated by GP06 appears over-optimistic (their figs 8 – 9). They detected four peaks, with two of them above their FAP. We did not detect any significant peaks above our criterion (no peaks were even close to our significance curve).

For the second run (2001 January 16/17), the average power was estimated by GP06 to be 0.17 μmp , while we estimated it to be 0.23 μmp . Three peaks satisfied their criterion with two of them being strong candidates for real ones – we found no peaks satisfying our criterion.

In the third run (2001 January 16/17), GP06 estimated the average power to be 1.03 μmp , while our estimate was 1.08 μmp , close to their value. The one order of magnitude higher noise level for this run is due to its very short duration (less than 2 h). GP06 found one peak satisfying the criterion, again we found none.

For the final run, the authors estimated the average power to be 0.42 μmp , while our value was 0.17 μmp . This time the value obtained by GP06 is suspiciously high. This run was the longest


Figure 3. The Fourier amplitude spectrum of González Pérez et al. (2006) data after our reduction.

and, as such, the noise level should be the lowest. They claimed two peaks above the FAP, while we did not find any. The most interesting result of GP06 was the possible detection of the highest frequency peak attributed to the ϵ -mechanism in the first section of the run lasting 2.3 h. We scrutinized this section of the run in our data and found no evidence for the claimed oscillations.

In Fig. 3, we present our overall FT of the GP06 data. There are no significant peaks up to a 0.92 mmag level. This level is almost two times higher than that of our new observations, highlighting a significant reduction in the detection limit of the new observations. No variability found at such a low level, neither in the range where ϵ -driven oscillations, nor where κ -driven modes are expected (insets in Figs 2 and 3), suggests that VV 47 is not even a variable star within the accuracy of our measurements.

4 SUMMARY AND CONCLUSIONS

We have presented a variability study of VV 47 based on new observations as well as a re-analysis of previously published data (GP06). Our new observations, made using the 4.2-m WHT, arrive at a significantly lower detection limit than the previously published data. Adopting the classical significance criterion of $S/N \geq 4$ in the Fourier amplitude spectrum, the detection limit was 0.52 mmag for the new data, and 0.92 mmag for the archival data. Even at such a low limit, we were unable to detect significant peaks in either data set, neither in the high-frequency domain where ϵ -driven pulsations may be present, nor at lower frequencies where possible κ -driven oscillations are expected. Instead, we attribute GP06’s claims for pulsations in VV 47 to a particularly relaxed significance criterion for the detection of periodicities in their data set (especially for stars of this type). In conclusion, no pulsations or demonstrably intrinsic variability were detected during either observing campaign. Therefore, VV 47 is not only a non-pulsator, it may not even be a variable star.

In any case, the findings of GP06 were exciting enough that theoretical work on the star soon followed. Córscico et al. (2009) took

the highest frequency peaks as candidates for low- k -order g modes excited by the ϵ -mechanism and estimated the mass from the period spacing data. Interestingly, the noise peaks detected by GP06 spaced by about 20–30 s, arrived at mass estimation that was in perfect agreement with the spectroscopic mass of VV 47. Given the $T_{\text{eff}} - \log g$ uncertainties, it is not possible to find an unambiguous model without further constraints, which in this case were over-interpreted asteroseismic measurements. The true mass of VV 47 hence might be different, and what follows, the evolutionary tracks used for the model may not be appropriate since these tracks characterize, e.g. the thickness of the He-rich envelope, which is crucial for the assessment of the efficiency of the ϵ -mechanism linked to the active He-burning shell. With the evolutionary sequence of $M_* = 0.530 M_{\odot}$ and all periods reported by GP06, the authors could attribute most of the longest period modes to the κ mechanism and the shortest ones to the ϵ -mechanism. However, when taking into account only the modes described by GP06 as having the best chances of being real, the shortest period mode would not be explicable as destabilized by the ϵ -mechanism. This can be taken as an argument that the physically sound models of Córscico et al. (2009) were not in agreement with the periodicities reported by GP06.

Interestingly, the spurious periodicities of GP06 led Calcaferro et al. (2016) into finding a period spacing value for VV 47 in excellent agreement within three used methods, with a mass estimation based on this spacing agreeing with all previous determinations. Even though the estimated parameters looked correct, Calcaferro et al. (2016) were not able to find an unambiguous model for VV 47.

The example of VV 47 shows that it is possible to derive credible model fits even if based on inadequate data, in addition even being in agreement with values determined using other methods. Careful analysis and interpretation of observational data should therefore prevail over the temptation to claim potentially exciting results on a poor base.

ACKNOWLEDGEMENTS

We thank Peter Meldgaard Sorensen and Sergio Armas Perez for their help with retrieving archival NOT data, Greg Stachowski for his help with RTCONV, as well as Hiromoto Shibahashi, Alosza Pamyatnykh, and Alejandro Córscico for helpful suggestions. PS and

GH thank the Polish National Center for Science (NCN) for support through grant 2015/18/A/ST9/00578. PS also acknowledges CAMK grant for young researchers. This research has been supported by the Spanish Ministry of Economy and Competitiveness (MINECO) under the grant AYA2017-83383-P.

REFERENCES

- Baran A. S. et al., 2011, *Acta Astron.*, 61, 37
 Battich T., Miller Bertolami M. M., Córscico A. H., Althaus L. G., 2018, *A&A*, 614, A136
 Blecha A., Schaller G., Maeder A., 1992, *Nature*, 360, 320
 Bratschi P., Blecha A., 1996, *A&A*, 313, 537
 Breger M. et al., 1993, *A&A*, 271, 482
 Calcaferro L. M., Córscico A. H., Althaus L. G., 2016, *A&A*, 589, A40
 Castanheira B. G., Kepler S. O., Kleinman S. J., Nitta A., Fraga L., 2013, *MNRAS*, 430, 50
 Ciardullo R., Bond H. E., 1996, *AJ*, 111, 2332
 Córscico A. H., Althaus L. G., Miller Bertolami M. M., González Pérez J. M., Kepler S. O., 2009, *ApJ*, 701, 1008
 Eaton N., Draper P. W., Allan A., Naylor T., Mukai K., Currie M. J., McCaughrean M., 2014, *Astrophysics Source Code Library*, record ascl:1405.013
 Eddington A. S., 1926, *The Internal Constitution of the Stars*. Cambridge Univ. Press, Cambridge
 González Pérez J. M., Solheim J.-E., Kamben R., 2006, *A&A*, 454, 527 (GP06)
 Kawaler S. D., 1988, *ApJ*, 334, 220
 Kawaler S. D., Winget D. E., Hansen C. J., Iben I., Jr, 1986, *ApJ*, 306, L41
 Kepler S. O., 1993, *Balt. Astron.*, 2, 515
 Ledoux P., 1941, *ApJ*, 94, 537
 Lenz P., Breger M., 2005, *Commun. Asteroseismology*, 146, 53
 Liebert J., Fleming T. A., Green R. F., Grauer A. D., 1988, *PASP*, 100, 187
 Miller Bertolami M. M., Córscico A. H., Althaus L. G., 2011, *ApJ*, 741, L3
 Østensen R., 2000, *Time Resolved CCD Photometry*, PhD Thesis, University of Tromsø, Norway
 Randall S. K., Bagnulo S., Ziegerer E., Geier S., Fontaine G., 2015, *A&A*, 576, A65
 Schwarzschild M., Härm R., 1959, *ApJ*, 129, 637
 Unno W., Osaki Y., Ando H., Saio H., Shibahashi H., 1989, *Nonradial Oscillations of Stars*, 2nd ed. University of Tokyo Press, Tokyo

This paper has been typeset from a $\text{\TeX}/\text{\LaTeX}$ file prepared by the author.

IS NITROGEN THE KEY TO UNDERSTANDING WHETHER PG 1159 STARS PULSATE?

This chapter has been published in the *Astrophysical Journal Letters* as

**“The Missing Link? Discovery of Pulsations in the Nitrogen-rich PG 1159 Star
PG 1144+005”**

Sowicka, P., Handler, G., Jones, D., van Wyk, F., 2021, *ApJ*, 918, L1, DOI: [10.3847/2041-8213/ac1c08](https://doi.org/10.3847/2041-8213/ac1c08). ©IOP Publishing. Reproduced with permission. All rights reserved.

The author was responsible for the preparation of observing proposals and application for observing time, planning the observations, reducing the data, doing photometry and frequency analysis, as well as preparing figures and writing the paper.

WORK IN CONTEXT

PG 1159 stars are thought to be formed as a result of a “born-again” episode, where the star experiences the final thermal pulse either during the post-AGB evolution when hydrogen burning is still active (Late Thermal Pulse, LTP), or while it is already on the WD cooling track (Very Late Thermal Pulse, VLTP). The LTP leads to an atmospheric composition with residual H diluted below the detection threshold of current observations, whereas the VLTP leads to a H-free star (as H was burnt) with a detectable nitrogen abundance of about 1% N/He. N and H are therefore regarded as indicators of the evolutionary history.

The nitrogen abundance pattern in PG 1159 stars is particularly interesting. Dreizler & Heber (1998) found two distinct levels of the observed N abundance, a so-called N-dichotomy: N-rich stars (about 1% N/He) and N-poor stars (below 0.01% N/He). Interestingly, all N-rich stars were pulsators, whereas all N-poor ones were non-pulsators. However, there was one counterexample – PG 1144+005, the only nonpulsating N-rich PG 1159 star, despite a number of searches for photometric variability (Grauer et al., 1987a; Grauer et al., 1987b; Schuh et al., 2000; Steininger et al., 2003).

We discovered pulsations in PG 1144+005 based on new time-series photometric observations obtained using the 10.4-m Gran Telescopio Canarias and the 1-m Lesedi telescope, with improved detection limits compared to the previous searches. Our data show that

PG 1144+005 is a multiperiodic pulsator with pulsation periods consistent with g modes excited by the $\kappa - \gamma$ mechanism in GW Vir stars.

Our result puts the missing piece in the link between the N abundance and pulsational variability in PG 1159 stars. It suggests that the pulsating and nonpulsating PG 1159 stars have different evolutionary histories, an important conclusion in the context of the evolution of post-AGB, pre-WD, and WD stars.

We speculate that the VLTP may provide the interior structure required to make a GW Vir pulsator, and conclude that the link between the N abundance and GW Vir pulsations should be tested on a larger sample of PG 1159 stars.



The Missing Link? Discovery of Pulsations in the Nitrogen-rich PG 1159 Star PG 1144+005

Paulina Sowicka¹ , Gerald Handler¹ , David Jones^{2,3} , and Francois van Wyk⁴

¹Nicolaus Copernicus Astronomical Center, Polish Academy of Sciences, ul. Bartycka 18, PL-00-716, Warszawa, Poland; paula@camk.edu.pl, gerald@camk.edu.pl

²Instituto de Astrofísica de Canarias, E-38205 La Laguna, Tenerife, Spain

³Departamento de Astrofísica, Universidad de La Laguna, E-38206 La Laguna, Tenerife, Spain

⁴South African Astronomical Observatory, P.O. Box 9, Observatory, 7935 Cape, South Africa

Received 2021 July 30; accepted 2021 August 10; published 2021 August 25

Abstract

Up to 98% of all single stars will eventually become white dwarfs—stars that link the history and future evolution of the Galaxy, and whose previous evolution is engraved in their interiors. Those interiors can be studied using asteroseismology, utilizing stellar pulsations as seismic waves. The pulsational instability strips of DA and DB white dwarf stars are pure, allowing for the important generalization that their interior structure represents that of all DA and DB white dwarfs. This is not the case for the hottest pulsating white dwarfs, the GW Vir stars: only about 50% of white dwarfs in this domain pulsate. Several explanations for the impurity of the GW Vir instability strip have been proposed, based on different elemental abundances, metallicity, and helium content. Surprisingly, there is a dichotomy that only stars rich in nitrogen, which by itself cannot cause pulsation driving, pulsate—the only previous exception being the nitrogen-rich nonpulsator PG 1144+005. Here, we report the discovery of pulsations in PG 1144+005 based on new observations. We identified four frequency regions: 40, 55, 97, and 112 day⁻¹ with low and variable amplitudes of about 3–6 mmag and therefore confirm the nitrogen dichotomy. As nitrogen is a trace element revealing the previous occurrence of a very late thermal pulse (VLTP) in hot white dwarf stars, we speculate that it is this VLTP that provides the interior structure required to make a GW Vir pulsator.

Unified Astronomy Thesaurus concepts: PG 1159 stars (1216); Pulsating variable stars (1307); Stellar pulsations (1625); Non-radial pulsations (1117); Stellar evolution (1599)

1. Introduction

White dwarf stars are the most common end point of stellar evolution with up to 98% of all single stars eventually reaching this phase. Despite their importance, detailed knowledge of the interior structure of only a limited number of white dwarfs is available. White dwarf stars pulsate in certain zones of instability along their cooling curves that define the three classical types of white dwarf pulsators (e.g., Winget & Kepler 2008) within the growing family of (pre-)white dwarf pulsators (Córscico et al. 2019). The first pulsational instability strip entered by a post-asymptotic giant branch (AGB) star is that of the GW Vir stars, followed by the domains of the DB and DA white dwarf pulsators. White dwarfs residing in the GW Vir domain span a large range of effective temperatures (≈ 75 –250 kK) and surface gravities ($\log g \approx 5.5$ –8). Some stars show photometrically detectable pulsations with periods as short as a few minutes due to nonradial gravity modes driven by the κ mechanism associated with the partial ionization of the K-shell electrons of carbon and/or oxygen in the envelope (Starrfield et al. 1983, 1984).

GW Vir pulsators are distinguished by their spectra: most are of the PG 1159-type but there are also [WC]-types, central stars of planetary nebulae with Wolf-Rayet spectra of the carbon sequence (Crowther et al. 1998). Such stars are thought to be formed as a result of a “born-again” episode (a very late thermal pulse (VLTP) experienced by a hot white dwarf during its early cooling phase) or a late thermal pulse that occurs during the post-AGB evolution when H burning is still active (e.g., Iben et al. 2003; Blöcker 2001; Miller Bertolami & Althaus 2006). They are supposed to be the main progenitors of

H-deficient white dwarfs, which makes them important to study in the context of stellar evolution. PG 1159 stars exhibit He-, C- and O-rich surface abundances, but strong variations of the He/C/O ratio were found from star to star (Dreizler & Heber 1998; Werner 2001), as were traces of other, heavier elements. The presence of H (such stars are classified as “hybrid PG 1159”) together with a N dichotomy (N rich, about 1% in mass and N poor, below about 0.01% in mass, stars) are tracers of the evolutionary history, i.e., when the progenitor experienced the final thermal pulse (Herwig 2001; Werner et al. 2008). The variety of surface abundance patterns observed in PG 1159 stars indeed poses a challenge to the theory of stellar evolution, but its understanding may be key in revealing their evolutionary history.

The instability strips of the pulsating DA and DB white dwarfs are believed to be pure, i.e., all stars within their respective borders do pulsate. Consequently, the pulsators are otherwise normal white dwarfs and their interiors—which can be studied using the technique of asteroseismology—represent the interiors of all white dwarfs. This is not the case for the PG 1159 stars, as the GW Vir instability strip is not pure; according to the literature (e.g., Quirion et al. 2004) only about 50% of them pulsate. This raises the questions of what separates the pulsators from the nonpulsators and whether there are fundamental differences in their interior structures and thus evolutionary histories.

The observed nitrogen dichotomy, i.e., N-rich stars are pulsators, whereas N-poor stars are all nonpulsators (Dreizler & Heber 1998), suggests that N may play a role in driving pulsation, despite its rather small abundance even in N-rich stars. Quirion et al. (2007) refuted this idea finding that a high

O abundance is predominantly responsible for driving pulsation. The whole picture, however, is more complicated, involving the physical parameters and chemical compositions of PG 1159 stars, including metallicity and the role of helium “poisoning” the driving of pulsations. The part played by nitrogen as a tracer of the previous evolutionary history of GW Vir stars is therefore interesting in this context. Is a VLTP a necessity for achieving the chemical mixture required to destabilize a star to develop pulsations? This would allow the important conclusion that the GW Vir stars have a fundamentally different evolutionary history than the nonpulsators. In this regard, one final culprit however still remained: PG 1144+005. Ever since the detection of strong N V emission lines in its spectrum (Werner & Heber 1991) and the realization that all pulsating PG 1159 stars are N rich (Dreizler & Heber 1998) it was the only known N-rich PG 1159 star that was never discovered to pulsate.

PG 1144+005 ($T_{\text{eff}} = 150,000 \pm 15,000$ K, $\log g = 6.5 \pm 0.5$, Werner & Heber 1991) is a $G = 15.1734$ mag star (Gaia Collaboration 2018) found in the Palomar-Green (PG) Survey by the UV excess (Green et al. 1986). A number of authors observed PG 1144+005 since then, over the last 30 yr. In the pioneering search for extremely hot pulsating stars, Grauer et al. (1987a, 1987b) did not find any variability consistent with pulsations among the program stars, including PG 1144+005, regrettably not providing the detection limit. Over a decade later, Schuh et al. (2000) observed it twice, with a null result. Unfortunately, again, these authors did not note the detection limit of these observations. Finally, Steininger et al. (2003) revisited the object and observed it for four nights on the 1 m telescope at Piszkestető. Data collected over 5.6 hr showed a light curve with no visible variability and a semi-amplitude of about 0.02 mag. The lack of variability was then reflected in the Fourier amplitude spectrum over the range from about 50 day^{-1} to about 700 day^{-1} , where no peak exceeded an amplitude of 4 mmag. No further time-series observations of the star have been reported since.

2. Discovery Observations with GTC

We included PG 1144+005 in a sample of PG 1159 stars selected for a survey for variability (P. Sowicka et al. 2021, in preparation). The observations were carried out on 2018 January 17 with the 10 m Gran Telescopio Canarias (GTC) equipped with OSIRIS in one observing block as a filler target. OSIRIS consists of a mosaic of two CCDs of 2048×4096 pixels each and has an unvignetted field of view (FOV) of $7'8 \times 7'8$. We used a Sloan r' filter with an exposure time of 6 s and standard readout time, resulting in a duty cycle of about 29 s, over the 1.1 hr length of observations. The data were reduced using standard Astropy (Astropy Collaboration et al. 2013, 2018) `ccdproc` (Craig et al. 2017) routines consisting of bias subtraction, flat-field and gain correction.

PG 1144+005 is a challenging object for differential photometry. Because of the lack of suitable nearby comparison stars in the typical small FOV of relatively large telescopes, we used a “master” comparison star created as a sum of flux from three stars after making sure they are photometrically constant: MGC 24209, MGC 24219, and MGC 24226, to improve the signal-to-noise ratio (S/N) in the light curve as all those stars are at least 1 mag fainter than the target in r' .

We performed aperture photometry using our own procedures utilizing scaled adaptive aperture sizes to the seeing

conditions, as described in Sowicka et al. (2018), in this case characterized by a scaling factor of $1.5 \times \text{FWHM}$ for each frame. The differential light curve was then corrected for differential color extinction. Figure 1 shows the final light curve with clear variability, and its Fourier amplitude spectrum up to the Nyquist frequency of 1439 day^{-1} , calculated using `Period04` (Lenz & Breger 2005).

The semi-amplitude is about 5 mmag in the light curve, while the median noise level of the Fourier amplitude spectrum is 0.36 mmag (calculated in the range $400\text{--}1439 \text{ day}^{-1}$). We identified two peaks, $f_1 = 81.60 \pm 0.82 \text{ day}^{-1}$ with amplitude $A_1 = 5.37 \pm 0.37$ mmag (S/N of 14.92) and $f_2 = 124.036 \pm 1.70 \text{ day}^{-1}$ with $A_2 = 2.60 \pm 0.37$ mmag (S/N of 7.22).

This is good evidence that the only remaining N-rich PG 1159 star, PG 1144+005, is a pulsating star and therefore belongs to the GW Vir family. However, the short light curve and the relatively long variability periods called for confirmation.

3. Follow-up SAAO Observations

Follow-up observations were carried out on five nights in 2021 May 6, 8, 9, 10, 11. We observed PG 1144+005 using the 1 m Lesedi telescope located at the South African Astronomical Observatory (SAAO), equipped with the Sutherland High Speed Optical Camera (SHOC; Coppejans et al. 2013) instrument SHA. Thanks to Lesedi’s $5'7 \times 5'7$ FOV, the $G = 12.8$ mag star MGC 24274 (saturated in GTC observations) could be used as the primary comparison star. PG 1144+005 was visible for about 5 hr in the first half of each night and we collected 24.06 hr of data. We varied the exposure time during the nights to adjust to the changing atmospheric conditions and airmass, to avoid saturation of the comparison star, and to mitigate possible Nyquist frequency ambiguities. Table 1 shows the detailed log of observations.

We performed data reduction (including bias, flat-field, and gain correction) and differential aperture photometry using `TEA-Phot` (Bowman & Holdsworth 2019). `TEA-Phot` is a data reduction and photometry package designed especially to work with data cubes from the SHOC instruments. It uses adaptive elliptical apertures to extract photometry, where the optimum major and minor axes of the apertures are calculated for each frame from an initial guess from the user based on examination of the displayed curve of growth for the target and comparison star separately. We then corrected each combined nightly light curve for differential color extinction and removed outlying points (3.5σ clipping) and bad-quality parts of data (observations through thick clouds). Figure 2 shows the final light curves from each night, and binned in 40 s overplotted to show the variability more clearly.

The best quality data (in terms of observing conditions) come from the end of the run. The time base of the whole run is $\Delta T = 5.1554$ days. The frequency resolution needed to resolve the modes and determine the amplitudes and phases correctly is calculated as $\Delta f = 1.5/\Delta T$ (Loumos & Deeming 1978) and equals $\Delta f = 0.29096 \text{ day}^{-1}$. We first calculated Fourier amplitude spectra of each nightly light curve separately. Then we combined the data and calculated the amplitude spectrum of the whole run, together with the spectral window (a single sine wave of arbitrary, constant amplitude—in our case 1—sampled at the times of our time-series data, which shows the aliasing pattern around each frequency in the data). The nightly light

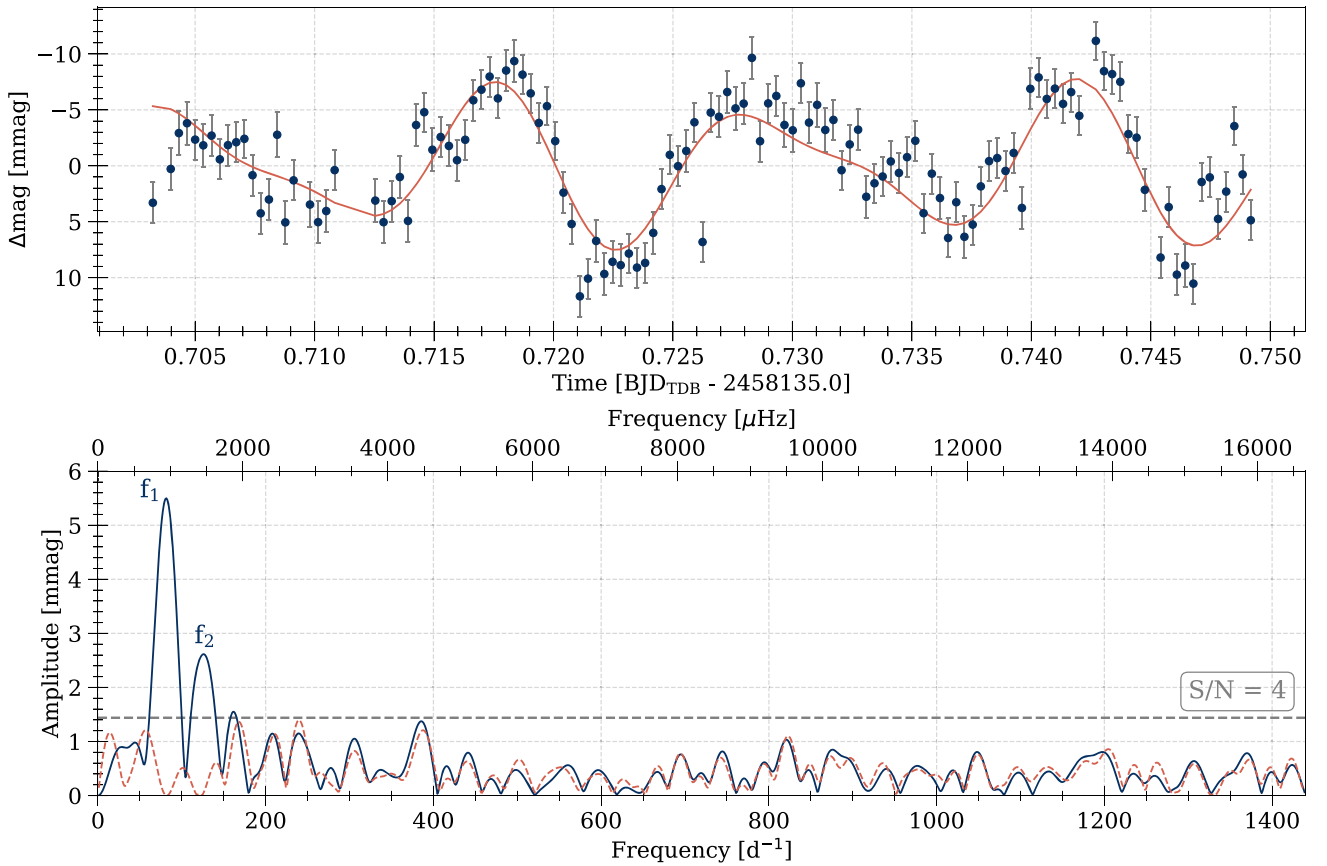


Figure 1. Top: GTC differential light curve of PG 1144+005 (blue circles) with a temporary model fit calculated using f_1 and f_2 shown for clarity. Bottom: Fourier amplitude spectrum (blue solid line) with the significance criterion of $S/N = 4$ (gray dashed line). The two extracted frequencies are labeled, while the residual amplitude spectrum after prewhitening of these two modes is shown as an orange dashed line.

curves, amplitude spectra, and the spectral window are shown in Figure 2. Frequencies, amplitudes, and phases were determined by simultaneously fitting a nonlinear least-squares solution to the data using `Period04` (Lenz & Breger 2005) and the formal solution is presented in Table 2, where we omitted frequencies below 10 day^{-1} that we judged to have originated in the Earth’s atmosphere.

In the new data we detect the presence of peaks at the same frequency ranges as in our exploratory GTC run, with the main pulsation modes grouped around 40, 55, 97, and 112 day^{-1} . With the caveat that the two higher-frequency groups may be combination frequencies of the two lower-frequency ones, the detected frequencies are consistent with g-mode pulsations excited by the κ -mechanism due to partial ionization of carbon and/or oxygen in the envelopes of PG 1159 stars. The frequencies correspond to periods of about 700–3000 s, in agreement with the period ranges of other known variable PG 1159 stars (e.g., Figure 7 in Córscico et al. 2006). We also find that the amplitude spectrum of PG 1144+005 is variable, with amplitudes of the modes changing between consecutive nights, but the frequencies remaining the same within the temporal resolution. It can be most clearly seen in the case of the region around 55 day^{-1} in the insets in Figure 2, where the amplitudes change between less than 4 mmag to over 6 mmag. This kind of temporal variability has been shown for other GW Vir stars, either as highly variable amplitudes and/or frequencies, or even as a complete disappearance of the

pulsations for a period of time. A more conservative interpretation is the beating of closely spaced pulsation frequencies.

Also, according to Córscico et al. (2009), PG 1144+005 lies in the overlapping region in the H-R diagram where both the κ - and ϵ -mechanism can operate. We therefore inspected our nightly amplitude spectra for the presence of high-frequency, ϵ -driven modes. We did not find any peaks above the detection threshold of 1 mmag for frequencies above 150 day^{-1} .

Even though we do not attempt to create an asteroseismic model for PG 1144+005, our most important result is the confirmation of the variability preliminarily detected in our GTC run.

4. Summary and Discussion

We obtained new observations of the N-rich PG 1159 star PG 1144+005 allowing for the discovery of long sought-after pulsations in this star. The first, short, run from the GTC allowed us to estimate the expected frequencies and amplitudes ($80\text{--}130 \text{ day}^{-1}$ and 3–6 mmag). Follow-up observations over 5 nights at SAAO clearly showed low-amplitude multiperiodic pulsations of PG 1144+005. The pulsations mainly appeared in four regions: 40, 55, 97, and 112 day^{-1} , while the amplitudes were variable over the course of observations. The detected variability is consistent with g-mode pulsations excited in PG 1159 stars.

Table 1

Journal of Time-series Photometric Observations of PG 1144+005 in 2021 May

Night	UTC Start	Exp. Time (s)	No. of Frames
2021-05-06	18:41:40.360181	20	120
	19:38:46.344030	10	1206
2021-05-08	17:05:31.746625	10	327
	18:02:09.824185	20	115
	19:29:37.096074	10	364
	20:30:33.424220	9	68
	20:41:05.839185	8	790
	22:26:44.605522	10	152
2021-05-09	17:32:45.588846	10	170
	18:01:49.315274	8	1090
	20:27:54.069439	7	540
	21:31:17.963203	8	190
	21:56:52.790226	10	65
	22:07:57.782761	9	268
2021-05-10	16:53:12.174974	8	300
	17:40:50.857600	8	300
	18:35:59.625951	8	844
	20:28:58.190206	7	600
	21:39:17.597373	8	486
2021-05-11	16:57:30.036797	10	600
	18:37:45.304383	8	1200
	21:19:29.860689	10	330
	22:14:42.561065	12	60

Note. Some parts of the data were removed because of bad quality.

The g-mode pulsations of PG 1159 stars are low amplitude and high frequency in nature. Most PG 1159 stars are faint, making required high-speed and high-quality follow-up observations challenging. To resolve individual modes and rotational splittings, the time base of a few days is needed (depending on the rotation period). The application of multisite campaigns for the study of these stars, as well as other pulsating white dwarfs and subdwarfs, has already been successfully shown, although only for a handful of the brightest targets. Usually many large telescopes are needed, and the observing time is hard to get. Are the future space telescopes for faint blue stars the only way to study the faintest ones (especially the PG 1159 stars discovered in the Sloan Digital Sky Survey)?

Our discovery of the pulsations in PG 1144+005 provides the last missing piece for the current picture of the excitation mechanism and abundance patterns in PG 1159 stars. Is the N problem thus solved, and the whole picture complete? Or will we find more N-rich nonpulsators or N-poor pulsators if we push the detection limit down?

Out of 55 known PG 1159 stars only 14 objects have their nitrogen abundance, or its upper limit, assessed. These are: the N-rich stars PG 1144+005, PG 1159-035, PG 2131+066, PG 1707+427, PG 0122+200, and A43, and N-poor stars PG 1520+525, PG 1424+535, HS 1517+7403, MCT 0130-1937, HS 0704+6153, H 1504+65, RXJ 0439.8-6809, and NGC 7094. Prerequisites for this type of analysis were spectroscopic observations in (far-)ultraviolet and model atmospheres for such high effective temperatures. Therefore the stars with their nitrogen abundance assessed are those having good-quality Hubble Space Telescope spectra available,

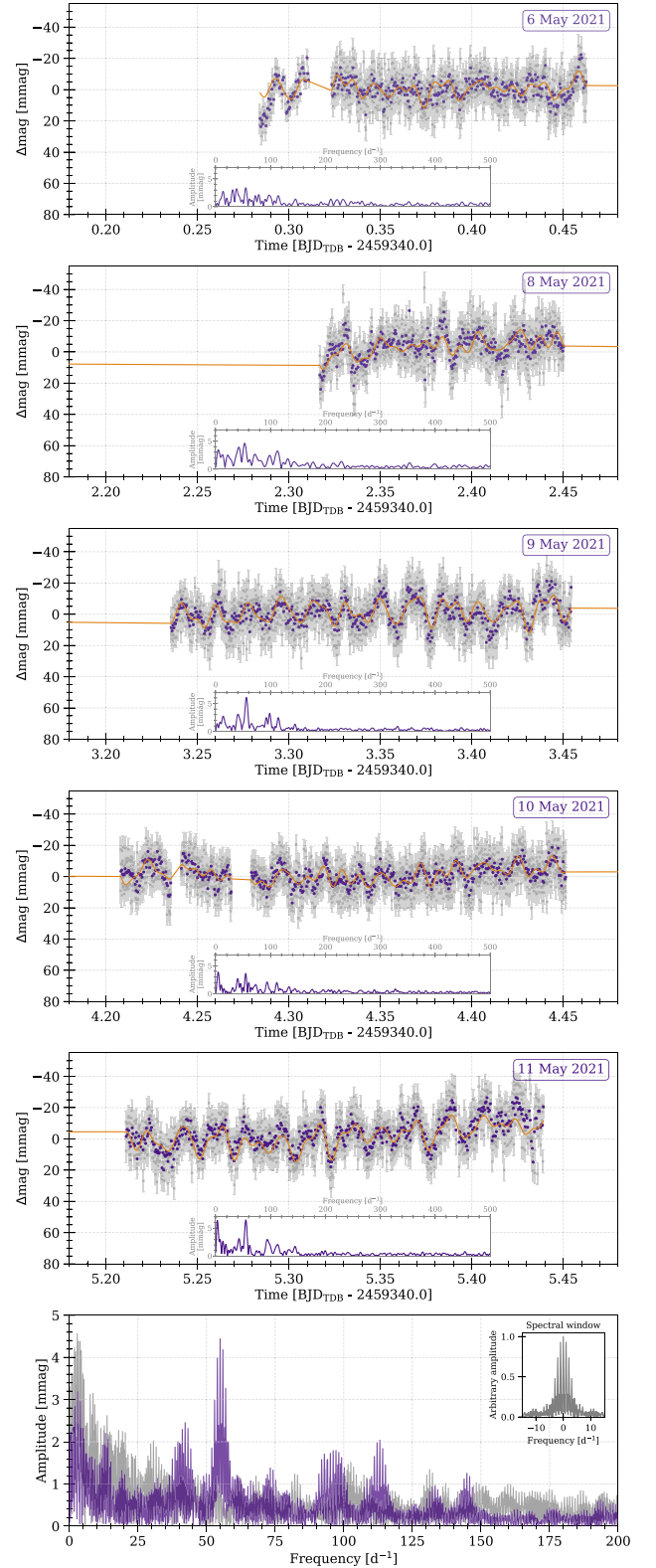


Figure 2. Top five panels: nightly light curves with amplitude spectra as insets. Each gray “x” with error bars is an original data point, filled purple circles are 40 s binned data points. A fit from `Period04` is shown as an orange solid line to indicate variability. Bottom panel: combined amplitude spectra of the run as semitransparent purple and gray solid lines for PG 1144+005 and the comparison star, respectively. The spectral window is shown in the inset.

Table 2

The Formal Frequency Solution Using the Combined SAAO Data Set with Analytical Uncertainties

	Frequency (day ⁻¹)	Frequency (μ Hz)	Amplitude (mmag)
ν_1	54.963(3)	636.15(3)	4.39(12)
ν_2	56.528(6)	654.26(7)	2.00(12)
ν_3	113.163(7)	1309.76(8)	1.98(12)
ν_4	42.219(7)	488.65(8)	1.96(12)
ν_5	39.542(7)	457.66(8)	1.90(12)
ν_6^a	96.147(7)	1112.81(8)	1.88(12)
ν_7	91.945(8)	1064.18(9)	1.61(12)

Notes. Frequencies below 10 day⁻¹ are omitted.^a The +1 day⁻¹ alias of ν_6 would correspond to $\nu_1 + \nu_4$ within the errors.

with nitrogen lines ideally not blended with strong interstellar absorption. In only a few cases could additional optical N lines have been used. Even though the evolutionary link to the nitrogen abundance appears to hold, this is still statistically a small number considering the total number of known PG 1159 stars. A detailed assessment of elemental abundances for a larger sample of stars is needed.

For the time being, however, there is a clear separation: PG 1159 stars with significant amounts of nitrogen in the atmosphere pulsate, the others do not. This is evidence that pulsating and nonpulsating PG 1159 stars have different evolutionary histories. It seems necessary that a star has to undergo a VLTP to become a pulsator, and that nitrogen is a tracer of this history.

We thank Bruno Steininger for discussions and for supplying his observational data. P.S. and G.H. acknowledge financial support by the Polish NCN grant 2015/18/A/ST9/00578. D.J. acknowledges support from the Erasmus+ program of the European Union under grant No. 2020-1-CZ01-KA203-078200. This paper uses observations made at the South African Astronomical Observatory (SAAO). Based on observations made with the Gran Telescopio Canarias (GTC), installed in the Spanish Observatorio del Roque de los Muchachos of the Instituto de Astrofísica de Canarias, in the island of La Palma.

Facilities: GTC (OSIRIS), SAAO: Lesedi (SHOC).

Software: Astropy (Astropy Collaboration et al. 2013, 2018), ccdproc (Craig et al. 2017), Matplotlib (Hunter 2007), Period04 (Lenz & Breger 2005), TEA-Phot (Bowman & Holdsworth 2019).

ORCID iDsPaulina Sowicka  <https://orcid.org/0000-0002-6605-0268>Gerald Handler  <https://orcid.org/0000-0001-7756-1568>David Jones  <https://orcid.org/0000-0003-3947-5946>**References**

- Astropy Collaboration, Price-Whelan, A. M., Sipőcz, B. M., et al. 2018, *AJ*, **156**, 123
- Astropy Collaboration, Robitaille, T. P., Tollerud, E. J., et al. 2013, *A&A*, **558**, A33
- Blöcker, T. 2001, *Ap&SS*, **275**, 1
- Bowman, D. M., & Holdsworth, D. L. 2019, *A&A*, **629**, A21
- Coppejans, R., Gulbis, A. A. S., Kotze, M. M., et al. 2013, *PASP*, **125**, 976
- Córsico, A. H., Althaus, L. G., & Miller Bertolami, M. M. 2006, *A&A*, **458**, 259
- Córsico, A. H., Althaus, L. G., Miller Bertolami, M. M., González Pérez, J. M., & Kepler, S. O. 2009, *ApJ*, **701**, 1008
- Córsico, A. H., Althaus, L. G., Miller Bertolami, M. M., & Kepler, S. O. 2019, *A&ARv*, **27**, 7
- Crowther, P. A., De Marco, O., & Barlow, M. J. 1998, *MNRAS*, **296**, 367
- Craig, M., Crawford, S., Seifert, M., et al. 2017, astropy/ccdproc: v1.3.0.post1, Zenodo, doi:10.5281/zenodo.1069648
- Dreizler, S., & Heber, U. 1998, *A&A*, **334**, 618
- Gaia Collaboration 2018, *A&A*, **616**, A1
- Grauer, A. D., Bond, H. E., Green, R. F., & Liebert, J. 1987a, in IAU Coll. 95: Second Conf. on Faint Blue Stars, ed. A. G. D. Philip, D. S. Hayes, & J. W. Liebert (Schenectady, NY: Davis Press), 231
- Grauer, A. D., Bond, H. E., Liebert, J., Fleming, T. A., & Green, R. F. 1987b, *ApJ*, **323**, 271
- Green, R. F., Schmidt, M., & Liebert, J. 1986, *ApJS*, **61**, 305
- Herwig, F. 2001, *Ap&SS*, **275**, 15
- Hunter, J. D. 2007, *CSE*, **9**, 90
- Iben, I., Jr., Kaler, J. B., Truran, J. W., & Renzini, A. 1983, *ApJ*, **264**, 605
- Lenz, P., & Breger, M. 2005, *CoAst*, **146**, 53
- Loumos, G. L., & Deeming, T. J. 1978, *Ap&SS*, **56**, 285
- Miller Bertolami, M. M., & Althaus, L. G. 2006, *A&A*, **454**, 845
- Quirion, P. O., Fontaine, G., & Brassard, P. 2004, *ApJ*, **610**, 436
- Quirion, P. O., Fontaine, G., & Brassard, P. 2007, *ApJS*, **171**, 219
- Schuh, S., Dreizler, S., Deetjen, J. L., Heber, U., & Geckeler, R. D. 2000, *BaltA*, **9**, 395
- Sowicka, P., Handler, G., & Jones, D. 2018, *MNRAS*, **479**, 2476
- Starrfield, S., Cox, A. N., Kidman, R. B., & Pesnell, W. D. 1984, *ApJ*, **281**, 800
- Starrfield, S. G., Cox, A. N., Hodson, S. W., & Pesnell, W. D. 1983, *ApJL*, **268**, L27
- Steininger, B., Paparo, M., Viraaghalm, G., Zsuffa, D., & Breger, M. 2003, in ASP Conf. Ser. 292, Interplay of Periodic, Cyclic and Stochastic Variability in Selected Areas of the H-R Diagram, ed. C. Sterken (San Francisco, CA: ASP), 237
- Werner, K. 2001, *Ap&SS*, **275**, 27
- Werner, K., & Heber, U. 1991, *A&A*, **247**, 476
- Werner, K., Rauch, T., Reiff, E., & Kruk, J. W. 2008, in ASP Conf. Ser. 391, Hydrogen-Deficient Stars, ed. A. Werner & T. Rauch (San Francisco, CA: ASP), 109
- Winget, D. E., & Kepler, S. O. 2008, *ARA&A*, **46**, 157

THE GW VIR INSTABILITY STRIP IN THE LIGHT OF NEW OBSERVATIONS OF PG 1159 STARS

This chapter has been accepted for publication in the *Astrophysical Journal Supplement Series* on September 19, 2023 as

“The GW Vir instability strip in the light of new observations of PG 1159 stars. Discovery of pulsations in the central star of Abell 72 and variability of RX J0122.9–7521”

Sowicka, P., Handler, G., Jones, D., Caldwell, J. A. R., van Wyk, F., Paunzen, E., Bąkowska, K., Peralta de Arriba, L., Suárez-Andrés, L., Werner, K., Karjalainen, M., Holdsworth, D. L., 2023, arXiv: [2309.16537](https://arxiv.org/abs/2309.16537)

The author was responsible for the preparation of observing proposals and application for parts of observing time, observations of four objects, data reduction of almost all data (with only two exceptions: DLH extracted single FITS files from data cubes of the SA19+SHOC run, and EP reduced DK+DFOSC data), photometry and frequency analysis of all data. The author also compiled literature data for PG 1159 stars, astrometric parameters and bolometric corrections, derived luminosities, placed the sample in the HR diagrams, computed radii and pulsation constants, and prepared all figures. Finally, the author wrote the text with contribution from GH (who in particular proposed Section 10 and wrote part of it) and feedback from co-authors.

WORK IN CONTEXT

The apparent confirmation of the N-dichotomy within PG 1159 stars (Sowicka et al., [2021](#)) highlighted the need to test this hypothesis on a larger sample of PG 1159 stars. For that, complete information for each star is necessary, and consists of the measurement of the N abundance and search for GW Vir pulsations in photometric observations. Detecting pulsations in PG 1159 stars is challenging for a number of reasons – the pulsations are of low amplitude, the stars are faint making reaching appropriate detection thresholds hard, pulsation spectra are variable, and there are periods of time when observed pulsational amplitudes are pushed down below the detection threshold due to, e.g., destructive interference between modes or nonlinear mode coupling. The latter highlight the need to observe each star over different observing seasons before claiming it a nonvariable. More-









over, the GW Vir instability strip is not pure, in contrast to the other domains of WD pulsators (DAVs and DBVs). Previous observations showed that about 50% of stars within the GW Vir instability strip pulsate (see, e.g., Fig. 2 in Uzundag et al., 2022). If this result really reflects the reality, and is not only the effect of observational bias (insufficient detection threshold), then some important consequences follow. It would mean that there are two distinct evolutionary channels producing pulsators and non-pulsators, and that the interiors of pulsators studied with the methods of asteroseismology may not reflect the interiors of non-pulsators. It is therefore very important to put solid observational limits for nonvariability of stars in the GW Vir instability strip.

Since the works by Ciardullo & Bond (1996) and González Pérez et al. (2006), many new PG 1159 stars were discovered, indicating the need for photometric follow-up observations capable of detecting low-amplitude short-period pulsations. We carried out a survey for variability among PG 1159 stars and related objects in the years 2014–2022, using a multitude of telescopes of different aperture sizes located in both Hemispheres.

This work presents the first results for a subset of stars not surrounded by bright PNe. We observed 29 stars and detected pulsations in the N-rich central star of planetary nebula Abell 72, variability in RX J0122.9–7521, that can be attributed to pulsations, binarity, rotation, or spots, and we improved the detection limits for non-pulsators. Our results combined with the literature data place the pulsating PG 1159 stars within the GW Vir instability strip at 36%, lower than previously observed 50%.

Using the *Gaia* data, we placed all PG 1159 stars in the theoretical HR diagram ($\log L_*/L_\odot - \log T_{\text{eff}}$), for the first time in that way. That allowed us to calculate radii and pulsation constants for the pulsators to discuss them as a group, and argue against the misleading usage of the division of GW Vir stars into “DOVs” and “PNNVs”, based on a solid observational ground. We also identify objects that do not fit the relation between N abundance and the presence of pulsations, and further challenge our understanding of the evolution and excitation of pulsations of these objects.

**The GW Vir instability strip in the light of new observations of PG 1159 stars.
Discovery of pulsations in the central star of Abell 72 and variability of RX J0122.9–7521**

PAULINA SOWICKA ¹, GERALD HANDLER ¹, DAVID JONES ^{2, 3, 4}, JOHN A. R. CALDWELL,⁵ FRANCOIS VAN WYK,⁶
ERNST PAUNZEN ⁷, KAROLINA BĄKOWSKA ⁸, LUIS PERALTA DE ARRIBA ^{9, 10}, LUCÍA SUÁREZ-ANDRÉS ¹⁰,
KLAUS WERNER ¹¹, MARIE KARJALAINEN ¹² AND DANIEL L. HOLDSWORTH ¹³

¹*Nicolaus Copernicus Astronomical Center, Polish Academy of Sciences, ul. Bartycka 18, PL-00-716, Warszawa, Poland*

²*Instituto de Astrofísica de Canarias, E-38205 La Laguna, Tenerife, Spain*

³*Departamento de Astrofísica, Universidad de La Laguna, E-38206 La Laguna, Tenerife, Spain*

⁴*Nordic Optical Telescope, Rambla José Ana Fernández Pérez 7, 38711, Breña Baja, Spain*

⁵*McDonald Observatory, 82 Mt. Locke Road, McDonald Observatory, TX 79734, USA*

⁶*South African Astronomical Observatory, PO Box 9, Observatory, 7935 Cape, South Africa*

⁷*Department of Theoretical Physics and Astrophysics, Faculty of Science, Masaryk University, Kotlářská 2, Brno, Czech Republic*

⁸*Institute of Astronomy, Faculty of Physics, Astronomy and Informatics, Nicolaus Copernicus University, ul. Grudziądzka 5, 87-100 Toruń, Poland*

⁹*Centro de Astrobiología (CAB), CSIC-INTA, Camino Bajo del Castillo s/n, 28692 Villanueva de la Cañada, Madrid, Spain*

¹⁰*Isaac Newton Group of Telescopes, E-38700 Santa Cruz de La Palma, La Palma, Spain*

¹¹*Institut für Astronomie und Astrophysik, Kepler Center for Astro and Particle Physics, Eberhard Karls Universität, Sand 1, D-72076 Tübingen, Germany*

¹²*Astronomical Institute, Czech Academy of Sciences, Fričova 298, 25165, Ondřejov, Czech Republic*

¹³*Jeremiah Horrocks Institute, University of Central Lancashire, Preston, PR1 2HE, UK*

(Accepted September 19, 2023)

ABSTRACT

We present the results of new time series photometric observations of 29 pre-white dwarf stars of PG 1159 spectral type, carried out in the years 2014 – 2022. For the majority of stars, a median noise level in Fourier amplitude spectra of 0.5 – 1.0 mmag was achieved. This allowed the detection of pulsations in the central star of planetary nebula Abell 72, consistent with g-modes excited in GW Vir stars, and variability in RX J0122.9–7521 that could be due to pulsations, binarity or rotation. For the remaining stars from the sample that were not observed to vary, we placed upper limits for variability. After combination with literature data, our results place the fraction of pulsating PG 1159 stars within the GW Vir instability strip at 36%. An updated list of all known PG 1159 stars is provided, containing astrometric measurements from the recent *Gaia* DR3 data, as well as information on physical parameters, variability, and nitrogen content. Those data are used to calculate luminosities for all PG 1159 stars to place the whole sample on the theoretical Hertzsprung-Russell diagram for the first time in that way. The pulsating stars are discussed as a group and arguments are given that the traditional separation of GW Vir pulsators in “DOV” and “PNNV” stars is misleading and should not be used.

Keywords: PG 1159 stars (1216), Pulsating variable stars (1307), Stellar pulsations (1625), Non-radial pulsations (1117), Stellar evolution (1599), CCD photometry(208), Hertzsprung Russell diagram(725), Post-asymptotic giant branch(1287)

1. INTRODUCTION

Pre-white dwarf stars of PG 1159 spectral type (named after the prototype, PG 1159–035, Green & Liebert 1979) are important to study in the context of

stellar evolution, as they are supposed main progenitors of H-deficient white dwarfs (WDs). PG 1159 stars populate the GW Vir instability strip, together with central stars of planetary nebulae with C-rich Wolf-Rayet spectra ([WC]-types, exhibiting He, C, and O lines in emission, Crowther et al. 1998), and [WC]-PG1159 stars, so-called transition objects (Leuenhagen et al. 1993; Toalá et al. 2015). PG 1159 stars exhibit a broad absorption “trough” made by He II at 4686 Å and adjacent C IV lines (see, e.g., Fig. 2 from Werner & Rauch 2014), and typically have He-, C- and O-rich atmospheres, but notable variations in He, C, and O abundances were found from star to star (e.g., Dreizler & Heber 1998, Werner 2001). Other groups of (pre-) white dwarf stars also show He II and C IV lines – while the O(He) stars show significantly less carbon than PG 1159 stars (up to 3% in their atmospheres, Reindl et al. 2014), the limit to distinguish between PG 1159 stars and DO white dwarfs is model-dependent – Werner et al. (2014) adopted C/He up to 9% (by mass) for DO stars.

Their formation history involves either a single star evolution scenario – a “born-again” episode (a Very Late Thermal Pulse – VLTP, or a Late Thermal Pulse – LTP; PG 1159-hybrid stars experience an AGB Final Thermal Pulse – AFTP), or binary evolution – binary white dwarf merger (Werner et al. 2022b; Miller Bertolami et al. 2022). Only some stars within the GW Vir instability strip show pulsations, a striking difference from the other two classical white dwarf instability strips (DAV and DBV), which are believed to be pure (e.g., see Fontaine & Brassard 2008). The GW Vir pulsations are due to nonradial g-modes, where the main restoring force is gravity (buoyancy), driven by the $\kappa - \gamma$ mechanism associated with the partial ionization of the K-shell electrons of carbon and/or oxygen in the envelope. The pulsations typically are of short period (between 300 s and about 6000 s) and low amplitude (typically 1 mmag – 0.15 mag, Córscico et al. 2019).

A current hypothesis, based on combined photometric and spectroscopic observations, states that there is a clear separation within PG 1159 stars: all N-rich (about 1% atmospheric N/He abundance) PG 1159 stars are pulsators, while all N-poor ones (below about 0.01% N/He) do not pulsate (Dreizler & Heber 1998; Sowicka et al. 2021). Since N is a tracer of the evolutionary history, an important conclusion follows: the pulsating and non-pulsating PG 1159 stars have different evolutionary histories, and it seems necessary that a star undergoes a VLTP in order to develop pulsations. Recently, considerable progress has been made in the study of PG 1159 stars’ atmospheric structure, composition, and evolution through optical and ultraviolet spectroscopy and

advancement in non-LTE model atmospheres, as well as in probing their interiors through asteroseismology with space-based observations (e.g., the *TESS* mission (Ricker et al. 2015) observed several already known GW Vir stars, Córscico et al. 2021). In the light of these findings, it is important to further test this hypothesis on a larger sample of PG 1159 stars, by obtaining high-quality, high-speed photometric observations aimed at detecting low-amplitude pulsations if present, as well as spectroscopic observations capable of detecting the nitrogen lines.

The number of known PG 1159 stars has increased in recent years, both due to the detection of pulsations typical for GW Vir stars in new photometric surveys (e.g., *TESS*, Uzundag et al. (2021, 2022), confirmed by spectroscopy), and classification of targets of spectroscopic surveys (e.g., the most recent discoveries with HET, Bond et al. 2023). Currently, 67 PG 1159 stars are known¹, including hybrid-PG 1159 stars (whose atmospheres have traces of hydrogen). While these stars lay within the GW Vir instability strip, some of them were either never checked for (or reported) variability, or the quality of previous observations was not sufficient to detect low amplitude pulsations. They also could have been observed when beating between closely spaced modes was destructive and pushed the observed amplitudes below the detection threshold. Moreover, some of these objects have temporally highly variable pulsation spectra (Ciardullo & Bond 1996). Therefore, it is worth re-observing those stars in different observing cycles to look for photometric variability. To date, there was no extensive and systematic photometric survey for variability among those stars since the works of Grauer et al. (1987b), Ciardullo & Bond (1996), and González Pérez et al. (2006).

The aim of the work presented in this paper is to obtain new photometric observations of a selected sample of PG 1159 stars to find new pulsators (or candidates) and put limits on non-variability. We also provide the most up-to-date list of PG 1159 stars and their properties from the *Gaia* mission and follow-up works. Finally, we place the PG 1159 stars on the theoretical Hertzsprung-Russell (HR) diagram ($\log L_*/L_\odot - \log T_{\text{eff}}$) and discuss the implications of our findings.

¹ Based on a list from Werner & Herwig (2006), updated by us.

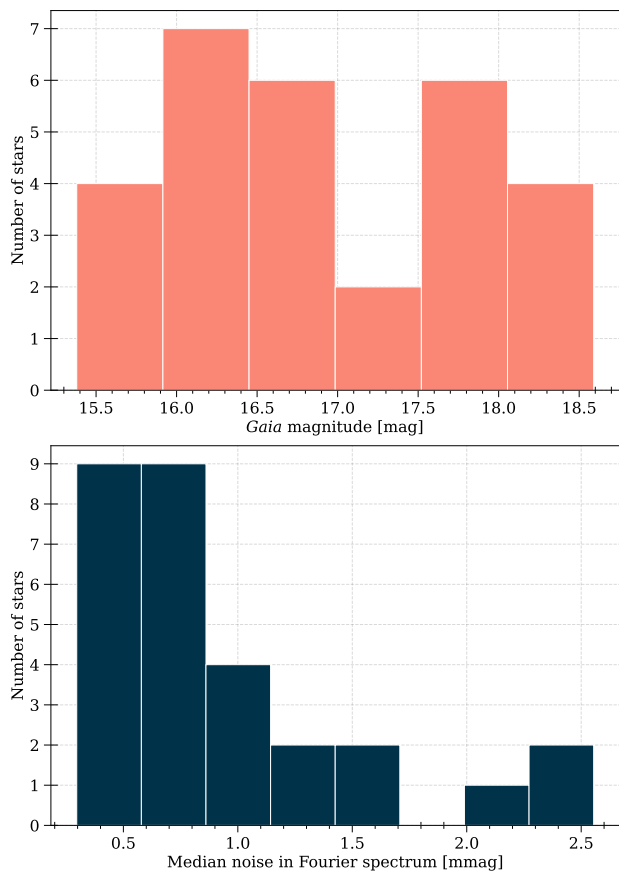


Figure 1. *Top:* *Gaia* magnitude distribution of the observed sample of 29 PG 1159 stars. *Bottom:* Distribution of the median noise level achieved in the survey.

2. PHOTOMETRIC OBSERVATIONS

We selected a sample of PG 1159 stars for a survey of variability carried out in the years 2014 – 2022 with a network of telescopes, covering both hemispheres. The selection was based on only one criterion: a given star was included in our target list if it was never observed photometrically with time resolution sufficient for the detection of GW Vir pulsations, or was classified as non-variable, but either the reported detection limits could have been improved by new observations or were not provided by the previous authors. The top panel in Figure 1 shows the brightness distribution of observed stars. The observing plan assumed the acquisition of observing blocks lasting at least one hour per target. The following telescopes and instruments were used for observations:

- **DFOSC at the 1.54-m Danish Telescope at ESO (DK):**

The 1.54-m Danish Telescope located at La Silla Observatory was equipped with the Danish Faint Object Spectrograph and Camera (DFOSC; An-

dersen et al. 1995). DFOSC uses a $2K \times 2K$ thinned Loral CCD chip with a Field of View (FOV) of 13.7×13.7 arcmin. No filter was used. Six stars were observed with this telescope.

- **OSIRIS at 10.4-m Gran Telescopio Canarias (GTC):**

The 10.4-m Gran Telescopio Canarias (GTC) is located at the Observatorio del Roque de los Muchachos (ORM, La Palma) and is equipped with Optical System for Imaging and low-Intermediate-Resolution Integrated Spectroscopy (OSIRIS; Cepa 1998). OSIRIS consists of a mosaic of two CCDs of 2048×4096 pixels each and has an unvignetted FOV of 7.8×7.8 arcmin. Either no filter or a Sloan r' filter was used. We used 2×2 binning and a standard readout time of about 23 seconds. Eleven stars were observed with this telescope.

- **WFC at 2.54-m Isaac Newton Telescope (INT):**

The 2.54-m Isaac Newton Telescope (INT) is located at the Observatorio del Roque de los Muchachos (ORM, La Palma) and is equipped with the Wide Field Camera (WFC; Walton et al. 2001), an optical mosaic camera mounted in the prime focus. WFC consists of four thinned EEV $2k \times 4k$ CCDs. Because the readout time of the whole CCD mosaic is rather long, we used it in windowing mode – for a FOV of 5×5 arcmin (910×910 pixels) the readout time was 6 seconds in the slow (less noisy) mode. No binning was used. We used a Harris V filter. Five stars were observed with this telescope.

- **ProEM at the 2.1-m Otto Struve Telescope (MD):**

The 2.1-m Otto Struve Telescope is located at McDonald Observatory, and is equipped with ProEM, which is a frame-transfer CCD detector with optional electron-multiplication with high frame-rate, optimized for high-speed time-series photometry (providing effectively zero readout time). The CCD has 1024×1024 pixels and a FOV of 1.6×1.6 arcmin. We used 4×4 binning for an effective plate scale of 0.36 arcsec pixel^{-1} . We used a BG40 filter. Nine stars were observed with this telescope.

- **Andor at the 1.3-m McGraw-Hill Telescope (MDM):**

The 1.3-m McGraw-Hill Telescope is located at the MDM Observatory, on the south-west ridge of Kitt Peak in Arizona. It was equipped with Andor Ikon DU937_BV CCD camera, which was used in

Frame Transfer mode and 4×4 binning. We used a BG38 filter. One star was observed with this telescope.

- **SHOC at the SAAO 1.9-m Telescope and 1.0-m Telescope (SA19, SA10):**

The telescopes are located at the Sutherland station of the South African Astronomical Observatory (SAAO), and are equipped with one of the Sutherland High Speed Optical Cameras (SHOC; Coppejans et al. 2013). SHOC 1 and 2 are high-speed cameras operating in frame-transfer mode for visible wavelength range that have an electron-multiplying (EM) capability². The imaging area of the detectors is 1024×1024 pixels, which corresponds to a FOV of 2.79×2.79 arcmin for the 1.9-m telescope with the focal reducer, and 2.85×2.85 arcmin for the 1.0-m telescope. A selection of amplifiers can be used, each resulting in a different gain setting, as well as binning and readout speed. The slowest readout speed was usually chosen, resulting in the lowest readout noise. Binning was determined by the observer to match the observing conditions and especially avoid undersampling of the Point Spread Function (PSF). Observations were done without a filter. Four stars were observed with these telescopes.

The data were reduced using the following procedures. For data from DK we applied standard IRAF routines for all reduction steps. We extracted bad columns and hot pixels from the night’s bias frames and flat fields, then cleaned the images for bad and hot pixels after the basic reduction steps (bias subtraction, dark and flat correction). As the last step, we checked for intensity gradients in the x and y directions (which sometimes occur in the presence of a bright Moon) and removed them, if necessary. The data from all the other instruments were reduced using standard *Astropy* (Astropy Collaboration et al. 2013, 2018, 2022) *ccdproc* (Craig et al. 2017) routines consisting of bias subtraction, dark correction (only for observations with ProEM), flat-field and gain correction. Then, we performed aperture photometry using our own photometry pipeline with the use of adaptive circular apertures with sizes scaled to the seeing conditions for each frame (Sowicka et al. 2018, 2021) with a scaling factor determined for each star and run. Comparison stars were chosen (wherever possible) such that they were brighter than the target and close to it, isolated and outside any faint nebulae, and

² The EM mode has not been used for observations presented in this work.

when the target was the brightest in the field, an “artificial” comparison star comprising the summed flux from up to three available comparison stars was used. Because our target stars usually are much hotter than the available comparison stars, the differential light curves were corrected for differential color extinction by fitting a straight line to a Bouguer plot (differential magnitude vs. air mass). In the final step, we cleaned the light curves by removing outliers (3.5σ clipping) and parts of data with bad quality (e.g., observations through thick clouds). We also inspected our differential magnitudes plotted against FWHM measurements to make sure that there is no correlation introduced by our photometry procedure. The constancy of the comparison stars was checked by examining differential light curves when more than one comparison star could be used. In case of fields with only a single comparison star, we looked up their *Gaia* $G_{BP} - G_{RP}$ colors, transformed these to $V - I_c$ ³, and those to $B - V$ (Caldwell et al. 1993). In that way, and with a rough correction for interstellar reddening, we inferred that none of the single comparison stars had $(B - V)_0 < 0.7$ and hence none of them lies in a κ -driven instability strip.

In this work, we present the results for a sample of 29 PG 1159 stars that are not surrounded by bright planetary nebulae. The list of targets, observing log and information on the scaling factor used in the photometry procedure is given in Table 1. The light curves are presented in Figure 2.

3. FREQUENCY ANALYSIS

The light curves prepared in the previous step were the subject of frequency analysis. We used *Period04* (Lenz & Breger 2005) to calculate Fourier amplitude spectra for each star and run separately, up to the corresponding Nyquist frequency. The Fourier amplitude spectra are shown in Figure 2. The frequency range for which our survey is sensitive to varies from star to star. The length of observations varied from slightly below an hour to a few hours, resulting in poor frequency resolution for the shortest ones (based on Loumos & Deeming (1978) criterion of $\Delta f = 1.0/\Delta T$ for only the detection of modes⁴). For each Fourier amplitude spectrum, we calculated the median noise level, as well as our detection threshold

³ https://gea.esac.esa.int/archive/documentation/GDR3/Data_processing/chap_cu5pho/cu5pho_sec_photSystem/cu5pho_ssec_photRelations.html

⁴ We note that for a correct determination of amplitudes and phases the criterion is $\Delta f > 1.5/\Delta T$.

Table 1. Log of photometric observations

Name	Equip.	Observer	Date	Filter	t_{exp}	Scale	ΔT	Δf	Med. noise
			+UTC Start		(s)	factor		(d^{-1})	(mmag)
BMP 0739–1418	DK	EP	2014-12-26T05:48:30	no filter	30	1.5	2.39 hr	10.06	0.31
H1504+65	GTC	SA	2016-03-09T02:07:53	Sloan r	6	1.5	48 min	30.00	0.42
HS 0444+0453	DK	EP	2014-12-26T03:44:44	no filter	20	1.2	1.81 hr	13.24	0.52
HS 0704+6153	GTC	SA	2016-03-09T22:30:36	Sloan r	10	1.5	48 min	30.34	0.53
HS 1517+7403	MD	GH	2016-05-24T02:59:58	BG40	10	0.9	1.51 hr	15.88	0.61
MCT 0130–1937	SA19	PS	2014-12-05T19:15:59	no filter	10	0.9	2.30 hr	10.45	0.83
PG 1151–029	INT	NH	2016-03-29T21:44:06	Harris V	10	1.5	1.45 hr	16.61	0.57
PG 1520+525	MD	GH	2016-05-30T02:47:51	BG40	15	1.2	1.15 hr	20.87	0.66
PN A66 (Abell) 21	DK	EP	2015-02-10T02:01:46	no filter	40	1.2	1.16 hr	20.71	2.02
	GTC	SA	2016-03-08T22:26:12	Sloan r	6	1.2	50 min	29.04	0.44
PN A66 (Abell) 72	SA10	FW	2022-10-07T18:35:41	no filter	25	1.8	3.05 hr	7.87	1.29
			2022-10-08T18:01:35	no filter	30-35	1.5	2.04 hr	11.76	1.58
PN IsWe 1	INT	MK+Students	2016-10-19T04:11:53	Harris V	5	0.9	1.94 hr	12.40	0.81
PN Jn 1	INT	LSA, PSh	2016-12-12T20:47:54	Harris V	10	1.2	3.01 hr	7.98	0.81
	MD	JC	2017-08-16T07:54:09	BG40	10	1.2	3.75 hr	6.40	0.30
	MD	JC	2017-08-17T09:37:05	BG40	10	1.2	1.93 hr	12.41	0.35
	INT	DJ	2017-08-28T01:45:39	Harris V	5	1.5	3.71 hr	6.47	0.41
	INT	DJ	2017-08-30T03:03:13	Harris V	10	1.2	2.64 hr	9.09	0.45
PN Lo (Longmore) 3	DK	EP	2015-02-10T00:41:13	no filter	40	1.2	1.16 hr	20.65	2.40
RX J0122.9–7521	SA19	PS	2014-12-04T19:05:30	no filter	10	0.9	1.95 hr	12.32	0.49
			2014-12-09T18:32:43	no filter	10	0.9	2.42 hr	9.92	0.46
SDSS J000945.46+135814.4	GTC	SA	2017-12-06T22:18:56	no filter	10	1.2	58 min	24.63	2.55
SDSS J001651.42–011329.3	SA19	PS	2017-12-06T22:18:55	Sloan r	20	0.9	1.71 hr	14.04	1.58
SDSS J055905.02+633448.4	GTC	SA	2017-09-15T04:09:52	Sloan r	20	1.2	59 min	24.43	0.98
SDSS J075540.94+400918.0	GTC	SA	2016-03-06T23:31:33	Sloan r	15	1.2	57 min	25.21	0.59
	DK	EP	2015-01-02T06:26:02	no filter	30	0.9	1.55 hr	15.45	1.37
	MD	JC	2017-05-06T03:00:17	BG40	30	1.2	2.92 hr	8.23	1.85
SDSS J102327.41+535258.7	GTC	SA	2018-08-14T14:45:58	Sloan r	20	1.2	57 min	25.05	0.86
	INT	LPA	2016-02-03T02:40:54	Harris V	20	1.2	2.52 hr	9.54	1.58
	MD	JC	2017-05-02T03:34:16	BG40	20	0.9	2.27 hr	10.56	0.78
	MD	JC	2017-05-07T03:08:52	BG40	22	0.9	3.04 hr	7.89	1.91
	GTC	SA	2017-12-29T02:27:34	Sloan r	10	1.2	1.05 hr	22.96	0.57
SDSS J105300.24+174932.9	MDM	KB	2019-04-24T04:19:17	BG38	30	1.5	1.99 hr	12.09	0.79
	MDM	KB	2019-04-25T03:36:34	BG38	30	1.2	1.82 hr	13.20	1.55
	MDM	KB	2019-04-26T02:54:19	BG38	30	1.2	4.00 hr	6.01	1.11
SDSS J121523.09+120300.8	DK	EP	2015-04-14T02:32:52	no filter	40	0.9	1.26 hr	19.04	2.97
	GTC	SA	2018-01-17T06:01:53	Sloan r	20	1.2	1.13 hr	21.17	0.95
SDSS J123930.61+244321.7	INT	PS, MT	2016-03-11T00:46:00	Harris V	20	0.9	2.10 hr	11.42	1.24
SDSS J134341.88+670154.5	MD	GH	2016-05-26T02:57:55	BG40	20	1.5	59 min	24.56	1.11
			2016-05-29T02:47:32	BG40	20	1.2	1.50 hr	16.00	0.92
SDSS J141556.26+061822.5	MD	JC	2017-05-05T05:14:23	BG40	30	1.2	5.20 hr	4.62	0.69
SDSS J144734.12+572053.1	MD	GH	2016-05-28T02:46:07	BG40	30	1.2	1.59 hr	15.08	2.25
SDSS J191845.01+624343.7	MD	JC	2017-05-08T07:08:02	BG40	30	0.9	4.15 hr	5.78	1.05
Sh 2–68	GTC	SA	2016-04-23T04:45:44	Sloan r	10	1.5	58 min	24.81	0.58
Sh 2–78	GTC	SA	2016-04-24T04:27:31	Sloan r	15	1.2	1.24 hr	19.30	0.75

NOTE—SA – Support Astronomer; Students – Rosa Clavero, Francisco Galindo, Bartosz Gauza; GTC – GTC+OSIRIS; DK – DK+DFOSC; MD – McDonald 2.1-m+ProEM; MDM – MDM 1.3-m+Andor; SA19 – SAAO 1.9-m+SHOC; SA10 – SAAO 1.0-m+SHOC; INT – INT+WFC. We refer to the central stars using the PN designations throughout the paper.

(dashed line in Fig. 2), adopted as amplitude ratio of $S/N \geq 4$ (Breger et al. 1993). Table 1 includes the length of observations, corresponding frequency resolution, and median noise level in the Fourier spectra for all observed targets.

4. SURVEY RESULTS

The bottom panel of Figure 1 presents a histogram of the number of stars vs. the median noise level in the Fourier spectrum. In cases when the same star was observed multiple times, the lowest achieved level was taken. For the majority of observed stars, we reached a noise level of about 1 mmag or below. Grauer et al. (1987b) and Ciardullo & Bond (1996) reported their threshold for non-variable targets as the maximum amplitude in the Fourier spectra and reached values of 2.4–2.7 and 2.4–5.3 mmag, respectively. Inspection of Figure 2 shows that our results are comparable to theirs, while our sample covered fainter stars (15.4–18.6 mag in *Gaia*, see the top panel of Fig. 1). This allowed us to discover pulsations in the central star of planetary nebula Abell 72, and variability in RX J0122.9–7521. In addition to that, five objects from our sample could also be variable, but need follow-up observations for eventual confirmation. The majority of our sample did not show any variability consistent with GW Vir pulsations, and in those cases we put upper limits on non-variability. Each Fourier spectrum was also inspected for the presence of short-period ϵ -driven modes (Córscico et al. 2009). No sign of such modes with periods shorter than about 200 s (frequencies above 400 d^{-1}) was found in any of the stars.

5. COMMENTS ON SELECTED STARS

Below, we comment on stars that showed peaks of interest in the Fourier spectrum. While most of our observations turned out to be non-detections, we have to mention one caveat. Pulsating PG 1159 stars are known for their variable pulsation spectra, even on a night-to-night basis. This is often caused by the interference between closely spaced modes, which occasionally becomes destructive and pushes the amplitudes of the modes below the detection threshold. Possible nonlinear mode coupling could have the same effect (e.g., Vauclair et al. 2011). Non-detections because of those reasons could be avoided by observing the targets on multiple nights over the visibility period. While this was the case for eight targets, we were not able to acquire multiple runs for the remaining sample, and this has to be kept in mind regarding our non-detections.

5.1. Pulsator – PN Abell 72⁵

The central star of the planetary nebula Abell 72 was observed in October 2022 over two consecutive nights. The light curves and Fourier amplitude spectra are presented in Fig. 3. We detected significant peaks reaching amplitudes on the order of 10 mmag in the nightly Fourier amplitude spectra, on both nights located in the same frequency range, consistent with g-mode pulsations seen in GW Vir stars. We classify Abell 72 as a multiperiodic pulsator and observations on a longer time base are needed to resolve its pulsation modes.

5.2. Candidates

- **HS 0444+0453**

There is an interesting, but statistically insignificant ($S/N = 3.3$) peak around 45.7 d^{-1} (period of about 1890 s). If confirmed, it fits within the observed period range of GW Vir pulsators.

- **HS 1517+7403**

There are two statistically significant peaks: 17.5 and 40.5 d^{-1} ($S/N = 5.8$ for both, periods of 4945 and 2133 s, respectively). Such long periods are usually found in GW Vir central stars of planetary nebulae, but no nebula around HS 1517+7403 has been reported. Given the short duration of the single run available and that only a single comparison star could be used, it is not clear whether these peaks are due to pulsations of the target.

- **PN IsWe 1**

The highest, possibly unresolved peak at 49 d^{-1} has $S/N=4.4$ and corresponds to a period of about 30 min (1764 s). While such pulsation periods are observed in GW Vir stars, observations on a longer time base are necessary for confirmation.

- **PN Jn 1**

Ciardullo & Bond (1996) observed the star twice, obtaining peaks of maximum amplitude of 2.4 and 4.0 mmag in the Fourier amplitude spectra. They did not detect significant peaks (reaching 99% confidence level) but two candidates: 540.5 and $538.5 \mu\text{Hz}$ (46.70 and 46.53 d^{-1} , respectively), and as a result did not claim the detection of pulsations in the central star of planetary nebula Jn 1. González Pérez et al. (2006) observed the star once and did not find the peaks tentatively detected by Ciardullo & Bond (1996), instead they found a barely

⁵ We refer to the central stars using the PN designations throughout the paper.

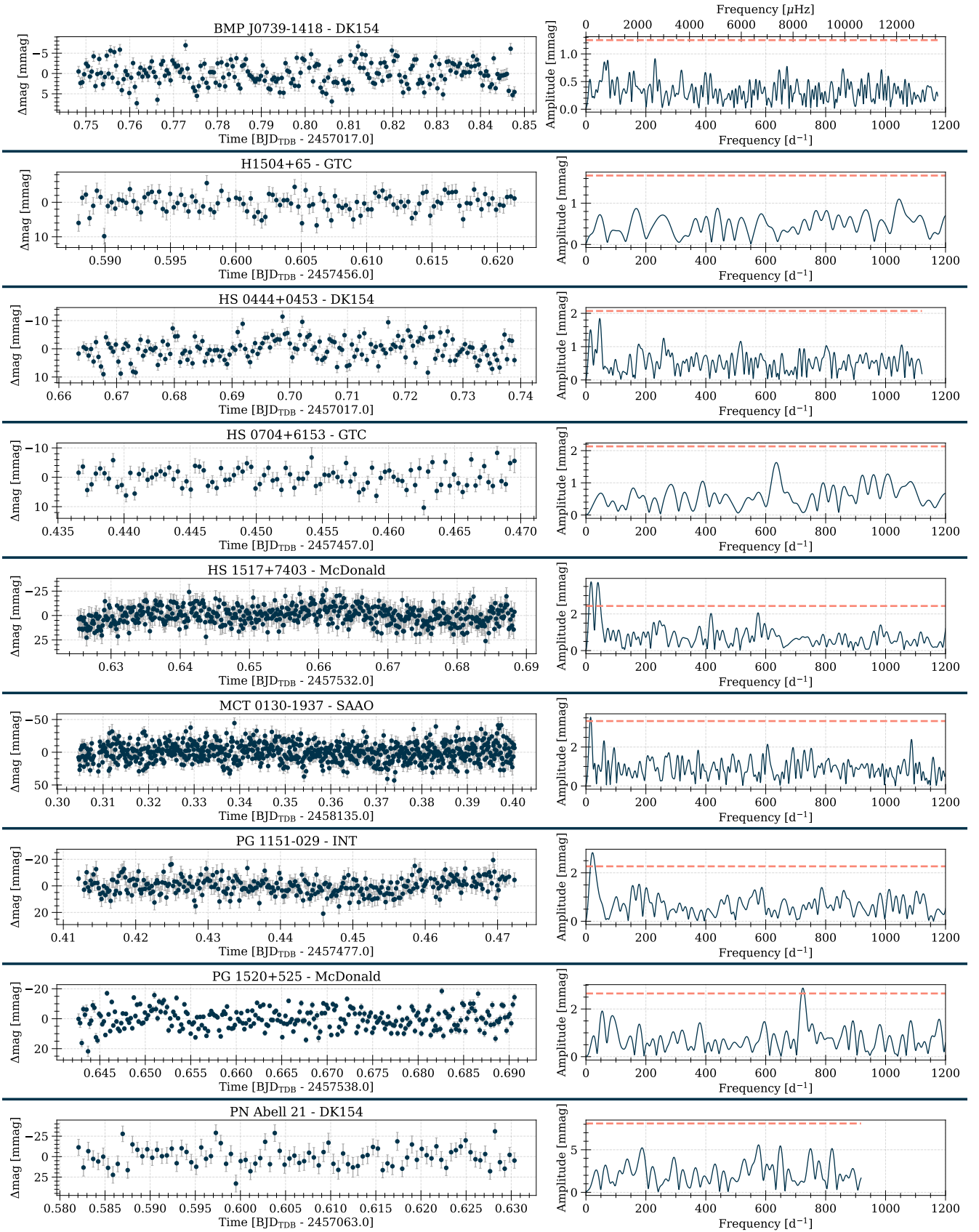


Figure 2. Light curves and their respective Fourier amplitude spectra of the survey targets. Plots for different stars are separated with horizontal lines. *Light curves:* Note different scales. *Fourier spectra:* they were calculated up to their respective Nyquist frequencies, but are plotted until 1200 d⁻¹. Dashed lines show the detection threshold of $S/N \geq 4$. Note different scales.

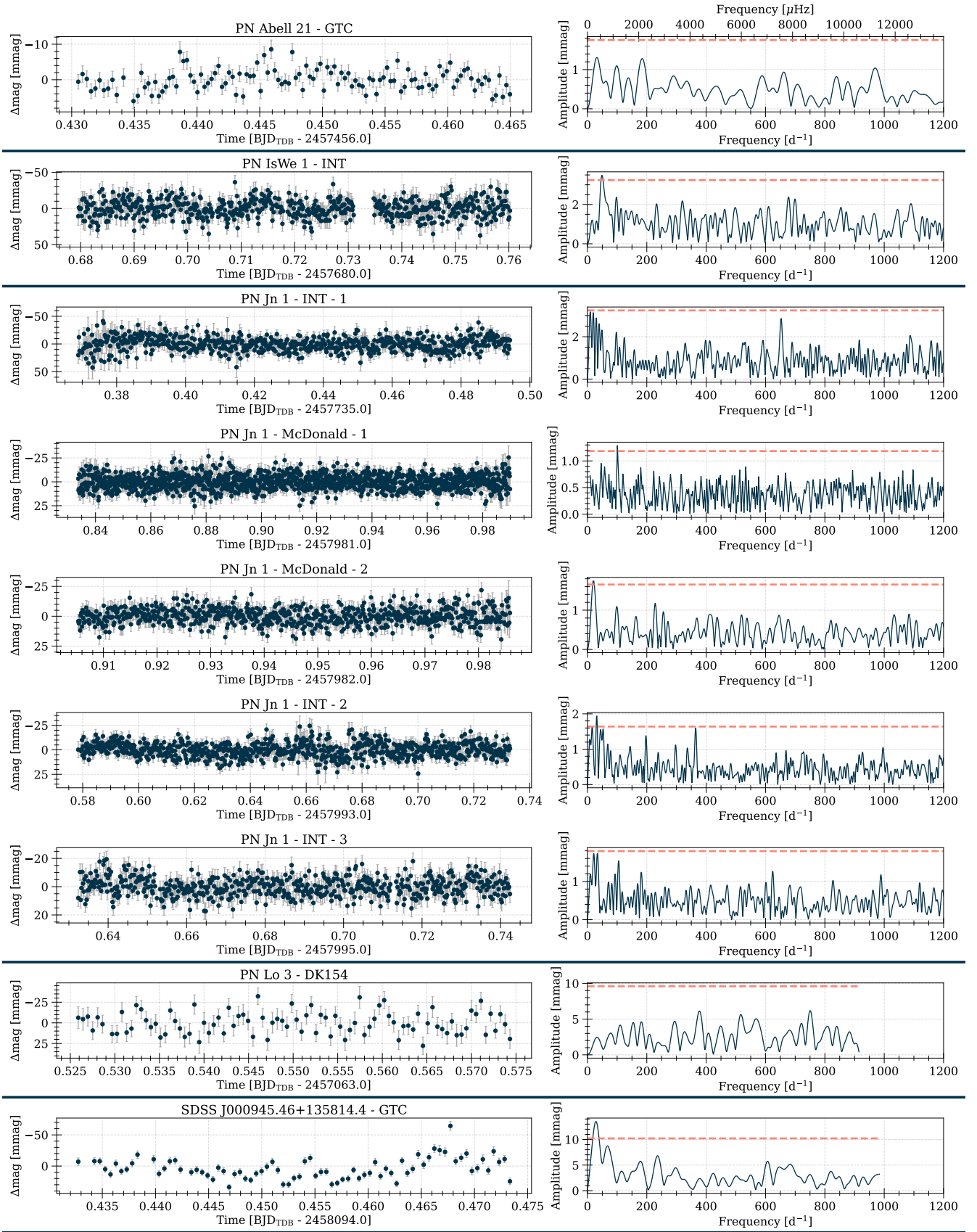


Figure 2. Continued.

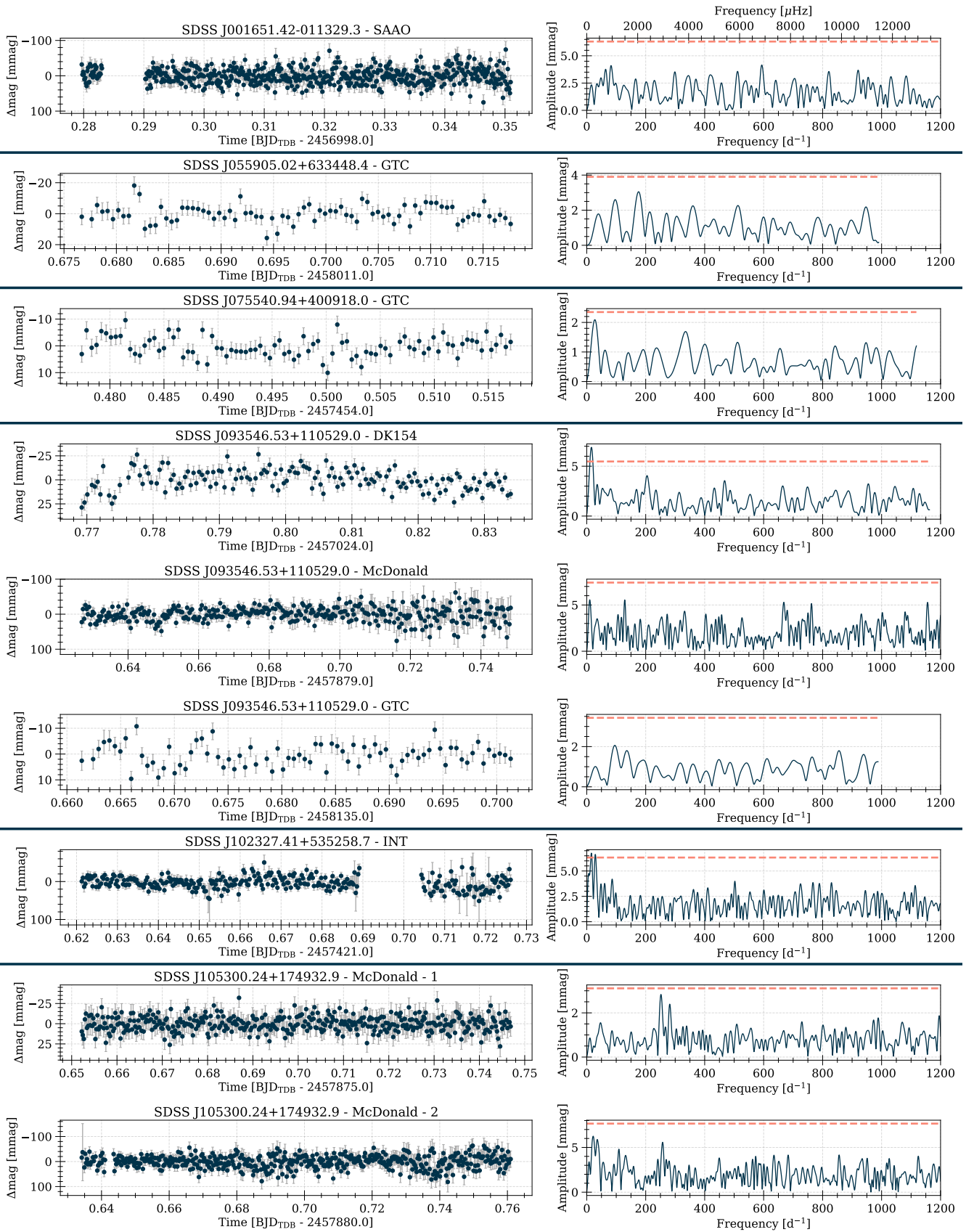


Figure 2. Continued.

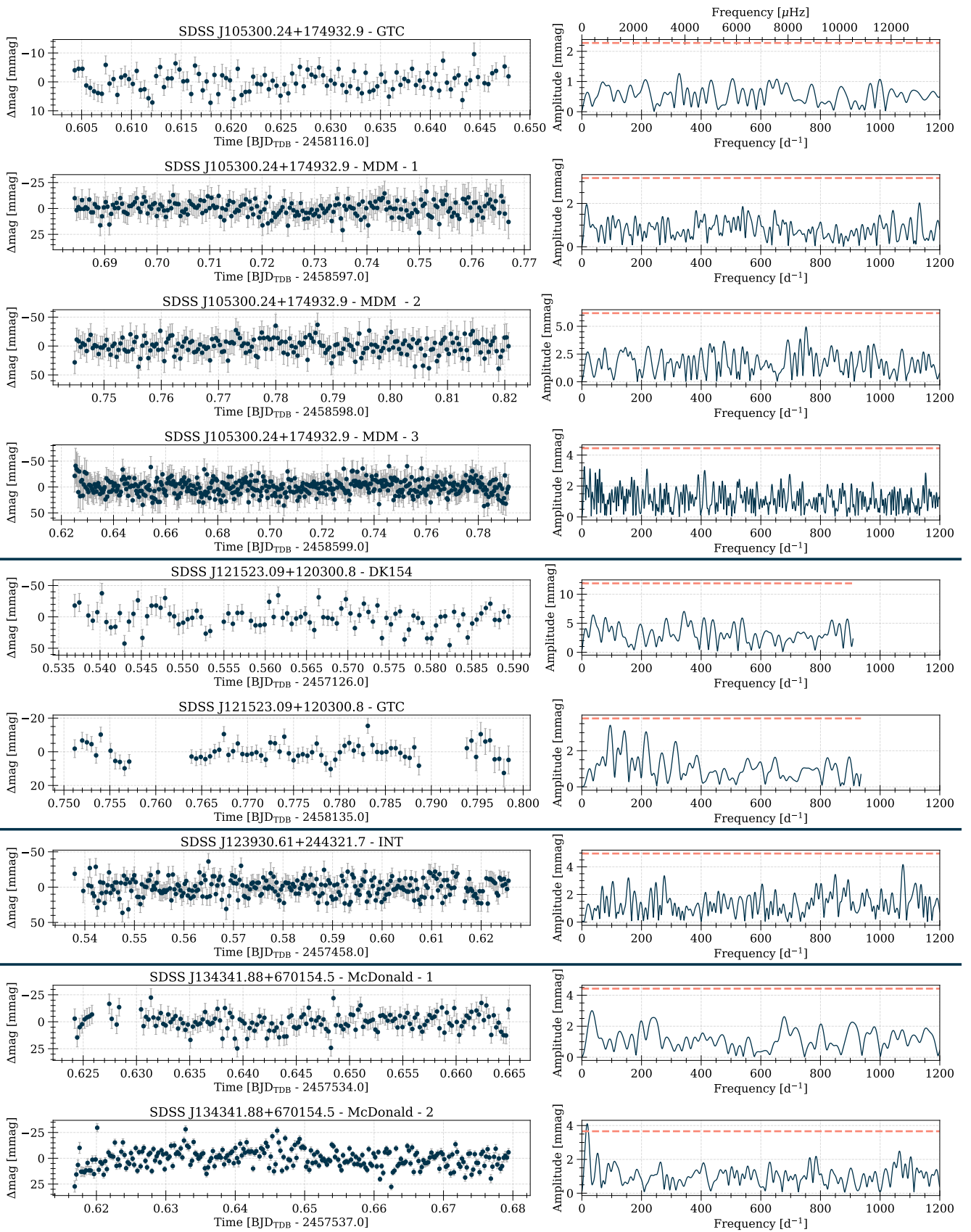


Figure 2. Continued.

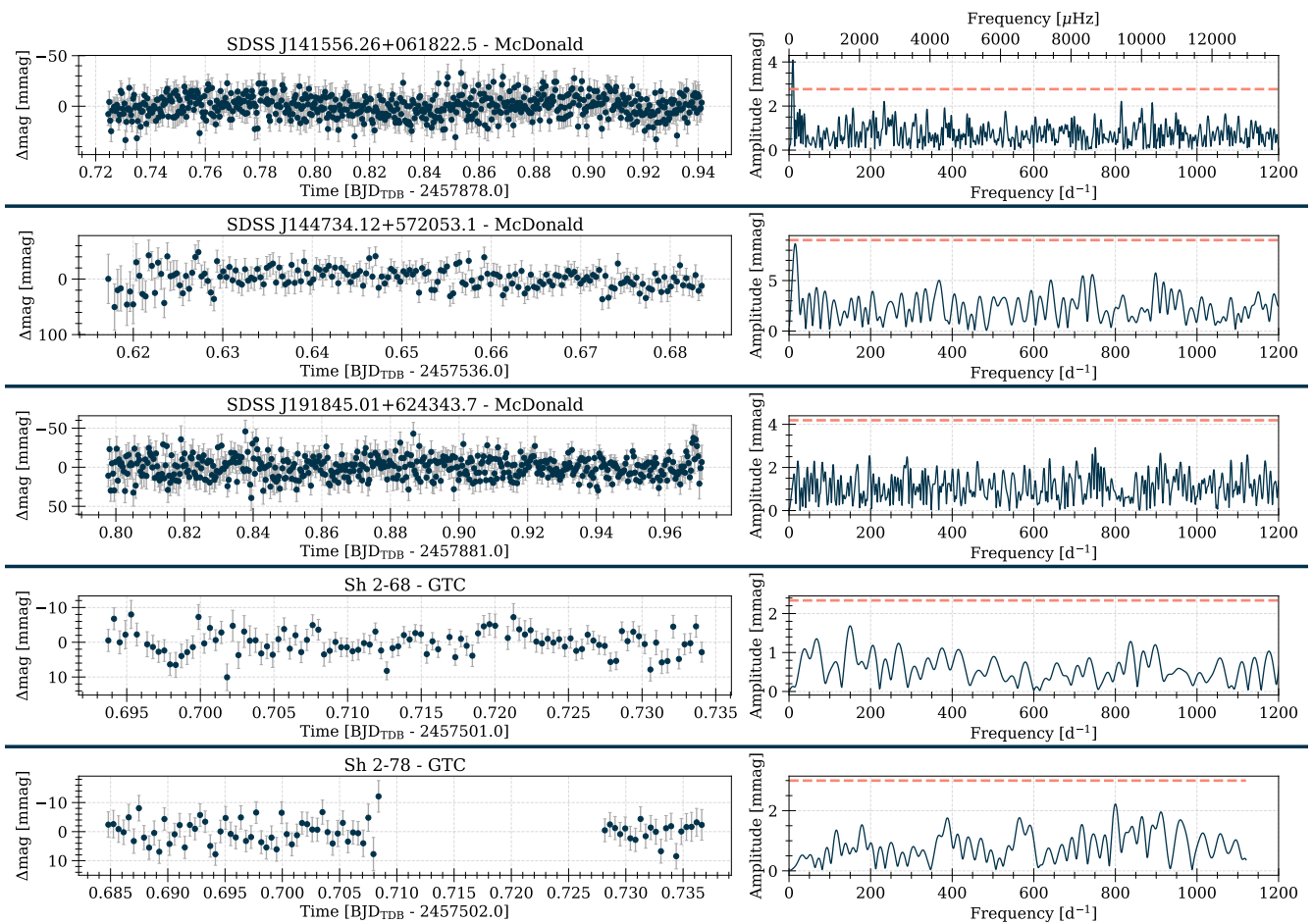


Figure 2. Continued.

significant peak at $2200 \mu\text{Hz}$ (190.1d^{-1}). Nevertheless, they claimed discovery of pulsations on that basis, but called for more observations to confirm their findings. We observed Jn 1 a total of five times in three different runs, and achieved very good median noise levels of $0.30\text{--}0.81$ mmag. In none of the runs we saw signs of peaks previously reported or strong peaks occurring in more than one of our own runs (e.g., a peak at 100d^{-1} with $S/N = 4.3$ only in McDonald-1 run). We thus conclude that there is no convincing evidence that Jn 1 pulsates, and that it requires observations of similar quality to our first McDonald run for eventual confirmation.

- **RX J0122.9–7521**

RX J0122.9–7521 was observed twice in December 2014. The light curves and Fourier amplitude spectra are presented in Fig. 4. We detected a significant peak in the Fourier amplitude spectra of both nights, located at the same frequency of

about 35d^{-1} and reaching an amplitude of $4\text{--}5$ mmag. RX J0122.9–7521 was also observed by *TESS* in Sectors 1, 13, 27, and 28. The same frequency as in our ground-based data is present in the *TESS* observations (34.78d^{-1}). With $T_{\text{eff}} = 18000 \text{K}$ that would make RX J0122.9–7521 the hottest known variable/pulsating PG 1159 star. We further discuss this star in Sect. 10.1.

- **SDSS J102327.41+535258.7**

One suitable comparison star was used. There are two peaks: 15.7 and 30.4d^{-1} with S/N of 4.3 and 4.2 , which correspond to periods of 92 and 47 min (5507 and 2839 s), respectively.

- **SDSS J105300.24+174932.9**

There are two interesting, but insignificant ($S/N = 3.7$ and 3.1) peaks at 251.9 and 281.5d^{-1} , respectively, in the first McDonald run. In the second run, five days later, a peak in the same frequency region is present (at about 257d^{-1}), but due to higher noise the signal (if real) has only

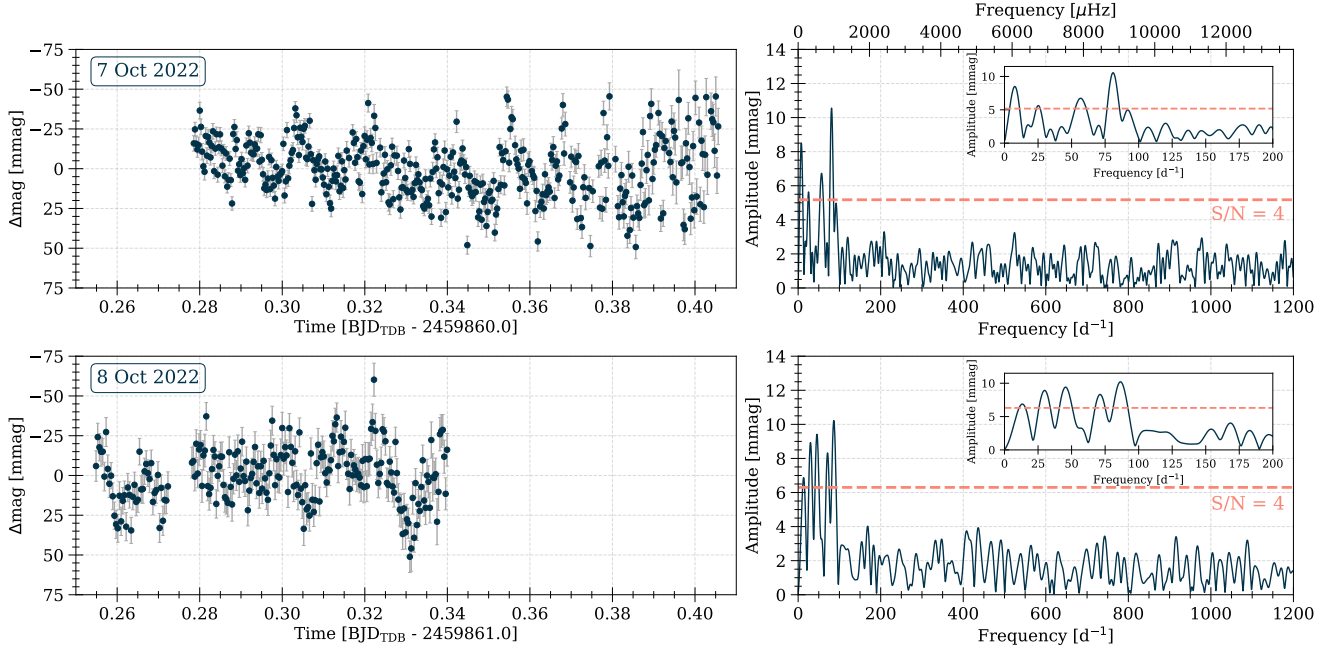


Figure 3. Light curves and Fourier amplitude spectra of two SAAO observing runs on the central star of planetary nebula Abell 72. The Fourier amplitude spectra were calculated up to the Nyquist frequency, but are shown up to 1200 d^{-1} . Insets show a zoomed in view into the frequency range of detected pulsations. Dashed lines show the detection threshold of $S/N \geq 4$. Note the same scales for the light curves and Fourier spectra.

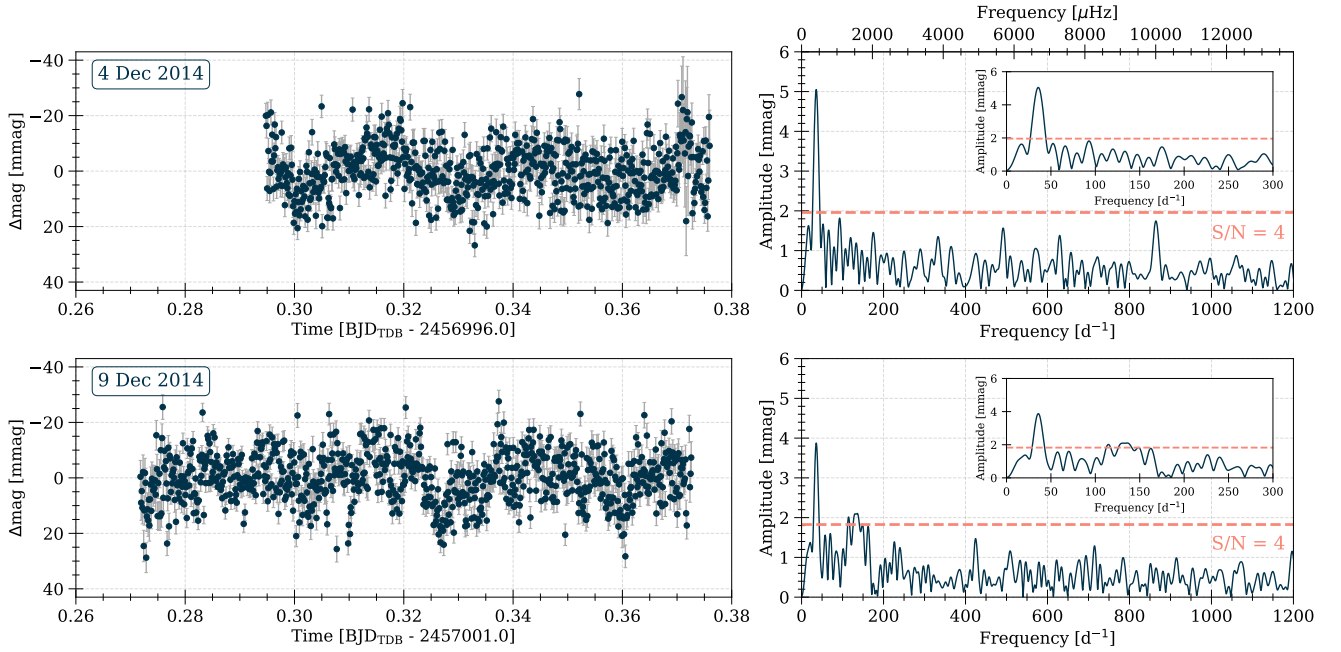


Figure 4. Light curves and Fourier amplitude spectra of two SAAO observing runs on RX J0122.9–7521. The Fourier amplitude spectra were calculated up to the Nyquist frequency, but are shown up to 1200 d^{-1} . Insets show a zoomed in view into the frequency range of the detected variations. Dashed lines show the detection threshold of $S/N \geq 4$. Note the same scales for the light curves and Fourier spectra.

slightly higher amplitude than the highest noise peaks. In the remaining runs we were not able to reach a better noise level than in the first McDonald run, except the GTC run (that was too short).

5.3. *Nonpulsators*

- **MCT 0130–1937**

There is a significant low-frequency trend in the light curve (around 10 d^{-1}) that is likely not intrinsic to the star, particularly because there was only one comparison star available that was fainter than the target.

- **PG 1151–029**

There is a significant low-frequency trend in the light curve, corresponding to a peak around 20 d^{-1} , that is likely caused by sky transparency variations that night.

- **PG 1520+525**

There is a significant peak ($S/N = 4.33$) at 725 d^{-1} . To assess whether this peak is real, we calculated differential light curves between the target and two different comparison stars, as well as between these comparison stars, and then computed the FTs of these light curves. The aforementioned peak showed up only in the difference of (target–comparison star 1), and not, as expected if the target was variable, also in the difference of (target–comparison star 2). We conclude that, even though formally significant in that differential light curve, this peak is not intrinsic to PG 1520+525.

- **SDSS J000945.46+135814.4**

The observing run is too short (hence too low frequency resolution) to decide whether the signals around 50 d^{-1} may be intrinsic to the star.

- **SDSS J093546.53+110529.0**

In the FT from DK there is a peak around 16 d^{-1} that is due to a low-frequency trend in the light curve and not present in the runs from the other two instruments, one of which has a much lower noise level. We therefore conclude that this signal is not due to pulsations from the target.

- **SDSS J134341.88+670154.5**

The second run shows a significant low-frequency trend around 20 d^{-1} that is likely due to variable sky conditions and not intrinsic to the star.

- **SDSS J141556.26+061822.5**

There is a low-frequency peak at 9.46 d^{-1} with $S/N = 5.8$. This peak corresponds to a period

of about 2.5 h (9000 s), which is too long for GW Vir pulsations. This peak is also present in differential light curves between the target and either of the comparison stars. Therefore, the peak might be intrinsic to the target, but of different origin than GW Vir pulsations, e.g., rotation, binarity, or spots.

6. IMPURITY OF GW VIR INSTABILITY STRIP

Previous observations showed that only about 50% of stars within the GW Vir instability strip pulsate (see, e.g., Fig. 2 in Uzundag et al. 2022). A significant number of PG 1159 stars were discovered since then, and with our new results, we can re-determine the current occurrence rate for PG 1159 stars. In Table 2 we listed the physical parameters of all known PG 1159 stars with updated information about their variability.

For a total of 67 PG 1159 stars, 24 stars are confirmed as pulsating, which corresponds to 36%. Still, the majority of PG 1159 stars within the instability strip are found to be non-pulsators. Sowicka et al. (2021) recently showed that there was a clear separation between N-rich ($\approx 1\%$ N/He) pulsators and N-poor ($< 0.01\%$ N/He) non-pulsators. We therefore also listed the N abundance, where available, in Table 2. To date, only 26 PG 1159 stars have published N abundances.

Table 2. Properties of PG 1159 stars

Name	T_{eff} (K)	$\log g$ (cm s^{-2})	PN	Puls.	N	BC (mag)	$\log L_*$ L_{\odot}	Ref.
BMP J0739–1418	120000	6.0	yes	NOP	N-poor	-7.269	$3.48^{+0.11}_{-0.12}$	W+2023
FEGU 248–5	160000	6.5	yes	NVD	N-poor	-8.039	$3.89^{+0.11}_{-0.10}$	W+2023
H1504+65	200000	8.0	no	NOP	N-poor	-8.700	$2.167^{+0.062}_{-0.064}$	W+2004a, WD2005, WR2015, NW2004
HE 1429–1209	160000	6.0	no	yes	no lit. data	-8.039	$3.46^{+0.11}_{-0.12}$	W+2004b
HS 0444+0453	90000	7.0	no	NOP	no lit. data	-6.429	$1.28^{+0.14}_{-0.16}$	D1999
HS 0704+6153	75000	7.0	no	NOP	N-poor	-5.832	$1.03^{+0.17}_{-0.20}$	DH1998
HS 1517+7403	110000	7.0	no	NOP	N-poor	-7.045	$1.84^{+0.10}_{-0.12}$	DH1998
HS 2324+3944	130000	6.2	no	yes	no lit. data	-7.460	$3.390^{+0.092}_{-0.084}$	F+2010, S+1999, C+2021
MCT 0130–1937	90000	7.5	no	NOP	N-poor	-6.429	$1.42^{+0.14}_{-0.16}$	W+2004c, WR2014
NGC 246	150000	5.7	yes	yes	N-poor	-7.855	$3.786^{+0.081}_{-0.084}$	W+2005, CB1996
NGC 650	140000	7.0	yes	NOP	no lit. data	-7.658	$3.27^{+0.67}_{-0.36}$	NS1995
NGC 6852	150000	6.0	yes	yes	no lit. data	-7.855	$2.93^{+0.34}_{-0.26}$	K. Werner, GP+2006
NGC 7094	110000	5.7	yes	yes	N-poor	-7.045	$3.83^{+0.10}_{-0.12}$	F+2010, S+2007
PG 0122+200	80000	7.5	no	yes	N-rich	-6.043	$1.20^{+0.17}_{-0.19}$	WR2014, F+2007
PG 1144+005	150000	6.5	no	yes	N-rich	-7.855	$3.13^{+0.10}_{-0.10}$	W+2005, W+2016, S+2021
PG 1151–029	140000	6.0	no	NOP	no lit. data	-7.658	$2.471^{+0.097}_{-0.091}$	W+2004c
PG 1159–035	140000	7.0	no	yes	N-rich	-7.658	$2.596^{+0.085}_{-0.086}$	W+2005, W+2016, C+2008, O+2022
PG 1424+535	110000	7.0	no	NOP	N-poor	-7.045	$1.838^{+0.092}_{-0.115}$	W+2005, W+2015
PG 1520+525	150000	7.5	yes	NOP	N-poor	-7.866	$2.591^{+0.081}_{-0.087}$	W+2005, W+2016
PG 1707+427	85000	7.5	no	yes	N-rich	-6.243	$1.47^{+0.15}_{-0.17}$	W+2005, W+2015, H+2018, K+2004
PN A66 21	140000	6.5	yes	NOP	no lit. data	-7.658	$2.118^{+0.088}_{-0.086}$	W+2004c
PN A66 43	110000	5.7	yes	yes	N-rich	-7.045	$3.69^{+0.10}_{-0.12}$	F+2010, V+2005
PN A66 72	170000	6.5	yes	yes	N-rich	-8.212	$3.35^{+0.11}_{-0.12}$	B+2023
PN IsWe 1	90000	7.0	yes	NOP	no lit. data	-6.429	$1.34^{+0.14}_{-0.16}$	D1999
PN Jn 1	150000	6.5	yes	NOP	no lit. data	-7.855	$2.687^{+0.097}_{-0.095}$	RW1995
PN K 1–16	160000	5.8	yes	yes	no lit. data	-8.039	$3.601^{+0.083}_{-0.088}$	W+2010, G+1987, C+2021
PN Kn 12	170000	6.5	yes	NVD	no lit. data	-8.212	$3.20^{+0.36}_{-0.28}$	B+2023
PN Kn 61	170000	6.5	yes	yes	N-rich	-8.212	$3.54^{+0.37}_{-0.27}$	DM+2015, B+2023, S+2023
PN Kn 130	170000	6.5	yes	NVD	N-poor	-8.212	$3.40^{+0.13}_{-0.13}$	B+2023
PN Lo 3	140000	6.3	yes	NOP	no lit. data	-7.658	$3.08^{+0.15}_{-0.14}$	W+2004c
PN Lo 4	170000	6.0	yes	yes	N-poor	-8.212	$3.65^{+0.18}_{-0.13}$	W+2010, BM1990
PN Ou 2	170000	6.5	yes	NVD	no lit. data	-8.212	$2.28^{+0.46}_{-0.22}$	B+2023
PN VV 47	130000	7.0	yes	NOP	no lit. data	-7.460	$2.04^{+0.11}_{-0.10}$	RW1995
RL 104	80000	6.0	no	NVD	N-rich	-6.046	$3.17^{+0.15}_{-0.18}$	W+2022
RX J0122.9–7521	180000	7.5	no	NOP	no lit. data	-8.389	$2.958^{+0.067}_{-0.071}$	W+2004c
RX J2117.1+3412	170000	6.0	yes	yes	no lit. data	-8.212	$3.394^{+0.067}_{-0.071}$	W+2005, V+2002, C+2021

Table 2 continued

Table 2 (continued)

Name	T_{eff}	$\log g$	PN	Puls.	N	BC	$\log L_*$	Ref.
	(K)	(cm s^{-2})				(mag)	L_{\odot}	
SALT J172411.7–632147	160000	6.5	no	yes	N-poor	-8.039	$3.01^{+0.11}_{-0.12}$	J+2023
SALT J213742.6–382901	180000	7.0	no	yes	N-rich	-8.376	$3.04^{+0.17}_{-0.13}$	J+2023
SDSS J000945.46+135814.4	120000	7.5	no	NOP	no lit. data	-7.279	$2.49^{+0.44}_{-0.25}$	K+2016
SDSS J001651.42–011329.3	120000	5.5	no	NOP	no lit. data	-7.269	$3.19^{+0.22}_{-0.18}$	H+2006
SDSS J034917.41–005919.3	90000	7.5	no	yes	no lit. data	-6.429	$1.33^{+0.19}_{-0.17}$	H+2006, W+2012
SDSS J055905.02+633448.4	110000	7.5	no	NOP	no lit. data	-7.050	$1.49^{+0.17}_{-0.17}$	W+2014
SDSS J075415.11+085232.1	120000	7.0	no	yes	no lit. data	-7.269	$1.70^{+0.58}_{-0.29}$	W+2014, K+2014
SDSS J075540.94+400918.0	100000	7.6	no	NOP	no lit. data	-6.764	$1.62^{+0.19}_{-0.18}$	H+2006
SDSS J093546.53+110529.0	100000	7.6	no	NOP	no lit. data	-6.764	$1.47^{+0.17}_{-0.17}$	H+2006
SDSS J102327.41+535258.7	110000	7.6	no	NOP	no lit. data	-7.050	$2.15^{+0.23}_{-0.21}$	H+2006
SDSS J105300.24+174932.9	100000	7.0	no	NOP	no lit. data	-6.762	$1.59^{+0.13}_{-0.14}$	W+2014
SDSS J121523.09+120300.8	100000	7.6	no	NOP	no lit. data	-6.764	$1.65^{+0.25}_{-0.21}$	H+2006
SDSS J123930.61+244321.7	100000	7.5	no	NOP	no lit. data	-6.764	$1.64^{+0.25}_{-0.21}$	W+2014
SDSS J134341.88+670154.5	100000	7.6	no	NOP	no lit. data	-6.764	$1.44^{+0.12}_{-0.14}$	H+2006
SDSS J141556.26+061822.5	120000	7.5	no	NOP	no lit. data	-7.279	$1.83^{+0.15}_{-0.13}$	W+2014
SDSS J144734.12+572053.1	100000	7.6	no	NOP	no lit. data	-6.764	$1.58^{+0.19}_{-0.17}$	H+2006
SDSS J152116.00+251437.5	140000	6.0	no	NOP	no lit. data	-7.658	$3.11^{+0.42}_{-0.29}$	W+2014
SDSS J155610.40+254640.3	100000	5.3	no	NVD	no lit. data	-6.762	$3.23^{+0.40}_{-0.37}$	R+2016
SDSS J163727.03+485355.2	100000	7.5	no	NVD	no lit. data	-6.764	$1.86^{+0.39}_{-0.22}$	K+2016
SDSS J191845.01+624343.7	100000	7.2	no	NOP	no lit. data	-6.762	$1.65^{+0.14}_{-0.15}$	W+2014
SDSS J212531.92–010745.8	100000	7.5	no	NOP	no lit. data	-6.764	$2.54^{+0.41}_{-0.25}$	K. Werner
Sh 2–68	84000	7.2	no	NOP	no lit. data	-6.205	$1.70^{+0.17}_{-0.16}$	G+2010
Sh 2–78	120000	7.5	yes	NOP	no lit. data	-7.279	$1.79^{+0.11}_{-0.11}$	D1999
TIC 95332541	100000	7.5	no	yes	N-poor	-6.764	$2.14^{+0.12}_{-0.13}$	U+2021, R+2023
TIC 333432673	120000	7.5	no	yes	no lit. data	-7.279	$1.924^{+0.082}_{-0.095}$	U+2021
TIC 403800675	110000	7.5	no	yes	no lit. data	-7.050	$1.73^{+0.10}_{-0.12}$	U+2022
TIC 1989122424	110000	7.5	no	yes	no lit. data	-7.050	$1.29^{+0.11}_{-0.13}$	U+2022
WD J070204.29+051420.56	100000	7.5	no	NVD	N-poor	-6.764	$1.63^{+0.12}_{-0.14}$	R+2023
NGC 6765	-	-	yes	NVD	no lit. data	-	-	NS1995
PG 2131+066	95000	7.5	no	yes	N-rich	-	-	WR2014, K+1995
RX J0439.8–6809	250000	8.0	no	NOP	N-poor	-	-	WR2015

NOTE—Properties of PG 1159 stars. **Bold**—this work. NOP – Not Observed to Pulsate, NVD – No Variability Data available. The last three stars either lack *Gaia* measurements or T_{eff} and $\log g$ determinations and were excluded from the analysis. References: BM1990 – Bond & Meakes (1990), B+2023 – Bond et al. (2023), CB1996 – Ciardullo & Bond (1996), C+2008 – Costa et al. (2008), C+2021 – Córscico et al. (2021), DH1998 – Dreizler & Heber (1998), D1999 – Dreizler (1999), DM+2015 – De Marco et al. (2015), F+2007 – Fu et al. (2007), F+2010 – Friederich et al. (2010), G+1987 – Grauer et al. (1987a), GP+2006 – González Pérez et al. (2006), G+2010 – Gianninas et al. (2010), H+2006 – Hügelmeier et al. (2006), H+2018 – Hoyer et al. (2018), J+2023 – Jeffery et al. (2023), K+1995 – Kawaler et al. (1995), K+2004 – Kawaler et al. (2004), K+2014 – Kepler et al. (2014), K+2016 – Kepler et al. (2016), NS1995 – Napiwotzki & Schoenberner (1995), NW2004 – Nagel & Werner (2004), O+2022 – Oliveira da Rosa et al. (2022), RW1995 – Rauch & Werner (1995), R+2016 – Reindl et al. (2016), R+2023 – Reindl et al. (2023), S+1999 – Silvotti et al. (1999), S+2007 – Solheim et al. (2007), S+2021 – Sowicka et al. (2021), S+2023 – Sowicka et al. in prep. (2023), U+2021 – Uzundag et al. (2021), U+2022 – Uzundag et al. (2022), V+2002 – Vauclair et al. (2002), V+2005 – Vauclair et al. (2005), W+2004a – Werner et al. (2004a), W+2004b – Werner et al. (2004b), W+2004c – Werner et al. (2004c), W+2005 – Werner et al. (2005), WD2005 – Werner & Drake (2005), W+2010 – Werner et al. (2010), W+2012 – Woudt et al. (2012), W+2014 – Werner et al. (2014), WR2014 – Werner & Rauch (2014), W+2015 – Werner et al. (2015), WR2015 – Werner & Rauch (2015), W+2016 – Werner et al. (2016), W+2022 – Werner et al. (2022a), W+2023 – Weidmann et al. (2023)

7. PROPERTIES OF ALL KNOWN PG 1159 STARS

Thanks to the *Gaia* mission (Gaia Collaboration et al. 2016, 2023) the community received precise measurements of positions and distances of more than 1 billion stars. For the first time, consistent distance mea-

surements became available for almost the entire sample of PG 1159 stars⁶. In Table 3 we compiled available *Gaia* DR3 information for PG 1159 stars: identifiers, positions, *Gaia* G magnitudes and parallaxes with

⁶ With the exception of two stars without sufficient *Gaia* data, which are listed at the bottom of Table 3

geometric distances determined by [Bailer-Jones et al. \(2021\)](#). We also list the corresponding reddening $E(B-V)$ at these distances, determined from the 3D reddening map of [Green et al. \(2018\)](#) (`Bayestar17`) using the Python package `dustmaps`. Even though a newer version of `Bayestar` is available (`Bayestar19`, [Green et al. 2019](#)), it did not cover the distances of all the stars in our sample, hence we used the `Bayestar17` reddening map for all but six stars. Those six stars were not covered because of declination south of -30° . For these cases, we used the 2D dust maps of [Schlafly & Finkbeiner \(2011\)](#) and [Schlegel et al. \(1998\)](#) (SFD), which are equivalent to `Bayestar` in terms of units. We did not take into ac-

count the reddening by the surrounding planetary nebulae in the case of PG 1159 stars being the central stars of planetary nebulae. We also listed the RUWE (Renormalized Unit Weight Error) coefficient for each star, and marked in bold values higher than the canonical 1.4, which might either suggest an unreliable astrometric solution (in a few cases that corresponds with a large parallax error) or be a hint towards binarity. In the final column of [Table 3](#) we put a remark for non-single stars (e.g., known or suspected binaries/triples) and a subclass of so-called “hybrid”-PG 1159 stars (exhibiting traces of hydrogen in the atmosphere).

Table 3. Astrometric properties of PG 1159 stars

Name	<i>Gaia</i> ID	RA (deg)	Dec. (deg)	<i>Gaia</i> G (mag)	ϖ_{Gaia} (mas)	$\sigma_{\varpi_{\text{Gaia}}}/\varpi$ (%)	<i>r</i> _{geo} (kpc)	E(B-V) (mag)	RUWE	Remarks
BMP J0739-1418	303000556082868096	114.96064	-14.30718	15.61	0.458 ± 0.042	9	2.10 ^{+0.18} _{-0.19}	0.258 ± 0.021	1.041	
FEGU 248-5	5594969135329315072	115.59902	-32.79746	17.00	0.528 ± 0.052	10	1.90 ^{+0.19} _{-0.16}	0.944 ^a	0.997	
HI504+65	1645296216119116928	225.54006	+66.20535	16.29	2.156 ± 0.051	2	0.47 ^{+0.12} _{-0.11}	0.0144 ± 0.0028	1.050	
HE 1429-1209	6324298665725984512	218.08641	-12.38006	16.01	0.441 ± 0.054	12	2.16 ^{+0.23} _{-0.22}	0.101575 ± 0.000099	1.012	
HS 0444+0453	3281864642080410112	071.76880	+04.97804	16.23	2.271 ± 0.062	3	0.441 ^{+0.011} _{-0.014}	0.0473 ± 0.0033	0.985	
HS 0704+6153	1099093607199220096	107.38536	+61.80533	16.98	1.643 ± 0.074	5	0.615 ^{+0.033} _{-0.030}	0.0413 ± 0.0050	0.974	
HS 1517+7403	1697669356564165632	229.19327	+73.86865	16.63	1.319 ± 0.061	5	0.781 ^{+0.031} _{-0.037}	0.0278 ± 0.0024	0.963	
HS 2324+3944	1923253820774222272	351.81644	+40.02323	14.77	0.702 ± 0.034	5	1.400 ^{+0.074} _{-0.054}	0.1343 ± 0.0013	1.112	hybrid
MCT 0130-1937	5140121722033618560	023.16399	-19.36138	15.76	2.395 ± 0.066	3	0.414 ^{+0.010} _{-0.011}	0.0297 ± 0.0021	1.283	
NGC 246	2376592910265354368	011.76385	-11.87198	11.80	1.799 ± 0.079	4	0.538 ^{+0.020} _{-0.017}	0.04481 ± 0.00092	1.530	triple
NGC 650	406328443354164480	025.58192	+51.57541	17.42	0.294 ± 0.203	69	3.7 ^{+2.8} _{-1.5}	0.1431 ± 0.0073	1.727	
NGC 6852	4237745794618477440	300.16337	+01.72801	17.91	0.39 ± 0.12	30	3.0 ^{+1.1} _{-0.9}	0.1083 ± 0.0042	1.017	
NGC 7094	1770058865674512896	324.22072	+12.78859	13.52	0.604 ± 0.034	6	1.607 ^{+0.092} _{-0.076}	0.12600 ± 0.00046	0.970	hybrid
PG 0122+200	2786529465445503488	021.34385	+20.29910	16.75	1.641 ± 0.080	5	0.618 ^{+0.042} _{-0.032}	0.0396 ± 0.0018	0.982	
PG 1144+005	3795664157996369024	176.64674	+00.20928	15.16	0.802 ± 0.058	7	1.220 ^{+0.085} _{-0.076}	0.02041 ± 0.00080	1.088	
PG 1151-029	3601781534594624000	178.56280	-03.20143	16.07	1.060 ± 0.063	6	0.938 ^{+0.060} _{-0.046}	0.0382 ± 0.0040	1.044	
PG 1159-035	3600841623951744640	180.44149	-03.76130	14.69	1.691 ± 0.064	4	0.585 ^{+0.020} _{-0.021}	0.0241 ± 0.0031	1.129	
PG 1424+535	1605381435770077312	216.48109	+53.25704	15.88	1.771 ± 0.041	2	0.566 ^{+0.012} _{-0.011}	0.0126 ± 0.0016	1.033	
PG 1520+525	1595941441250636672	230.44399	+52.36779	15.55	1.295 ± 0.041	3	0.783 ^{+0.037} _{-0.030}	0.0256 ± 0.0029	1.045	
PG 1707+427	1355161726346266112	257.19864	+42.68358	16.65	1.402 ± 0.052	4	0.733 ^{+0.032} _{-0.026}	0.0477 ± 0.0012	1.002	
PN A66 21	3163546505053645056	112.26128	+13.24679	15.93	1.689 ± 0.069	4	0.584 ^{+0.024} _{-0.021}	0.0318 ± 0.0013	1.086	
PN A66 43	4488953930631143168	268.38446	+10.62340	14.66	0.458 ± 0.033	7	2.09 ^{+0.12} _{-0.11}	0.1946 ± 0.0087	1.038	hybrid
PN A66 72	1761341417799128320	312.50856	+13.55817	16.01	0.548 ± 0.064	12	1.84 ^{+0.18} _{-0.21}	0.06740 ± 0.00065	1.042	
PN IsWe 1	250358801943821952	057.27473	+50.00410	16.47	2.350 ± 0.057	2	0.424 ^{+0.010} _{-0.009}	0.197 ± 0.045	0.903	
PN Jn 1	2871119705335735552	353.97219	+30.46843	16.00	1.011 ± 0.065	6	0.982 ^{+0.071} _{-0.059}	0.0900 ± 0.0044	1.120	
PN K 1-16	2160562927224840576	275.46708	+64.36482	14.98	0.589 ± 0.035	6	1.737 ^{+0.090} _{-0.092}	0.0388 ± 0.0035	1.102	
PN Kn 12	1823929193070538624	300.84391	+21.59786	18.44	0.33 ± 0.17	49	3.5 ^{+1.5} _{-1.1}	0.2839 ± 0.0071	0.961	
PN Kn 61	2052811676760671872	290.41223	+38.31588	18.25	0.14 ± 0.11	80	5.9 ^{+2.4} _{-1.8}	0.1327 ± 0.0056	0.986	binary?
PN Kn 130	1941078175572093696	348.27200	+45.43838	16.54	0.497 ± 0.054	11	2.115 ^{+0.27} _{-0.27}	0.1826 ± 0.0022	1.051	
PN Lo 3	5509000495257669904	108.70594	-46.96087	16.74	0.467 ± 0.074	16	2.10 ^{+0.30} _{-0.27}	0.172 ^a	1.787	

Table 3 continued

Table 3 (continued)

Name	<i>Gaia</i> ID	RA (deg)	Dec. (deg)	<i>Gaia</i> <i>G</i> (mag)	ϖ_{Gaia} (mas)	$\sigma_{\varpi_{\text{Gaia}}}/\varpi$ (%)	<i>r</i> _{geo} (kpc)	E(B-V) (mag)	RUWE	Remarks
PN Lo 4	5414927915911816704	151.44074	-44.35931	16.59	0.330 ± 0.052	16	3.06 ^{+0.60} _{-0.40}	0.147 ^{<i>d</i>}	1.039	
PN Ou 2	430204780732841600	007.73643	+61.40952	19.27	0.77 ± 0.22	28	1.59 ^{+0.82} _{-0.38}	0.3860 ± 0.0072	1.009	
PN VV 47	936605992140011392	119.46507	+53.42137	17.06	1.065 ± 0.079	7	0.985 ^{+0.076} _{-0.076}	0.0371 ± 0.0050	1.008	
RL 104	180006683580428928	067.56196	+40.40398	13.71	0.947 ± 0.021	2	1.020 ^{+0.025} _{-0.020}	0.3071 ± 0.0035	0.964	
RX J0122.9-7521	4637921057358156416	020.72372	-75.35420	15.38	1.196 ± 0.035	3	0.830 ^{+0.023} _{-0.024}	0.053 ^{<i>d</i>}	1.089	
RX J2117.1+3412	1855295171732158080	319.28448	+34.20766	13.02	1.991 ± 0.035	2	0.4986 ^{+0.0082} _{-0.0094}	0.0600 ± 0.0021	0.948	
SALT J172411.7-632147	5910236846008692352	261.04877	-63.36322	16.59	0.585 ± 0.063	11	1.78 ^{+0.18} _{-0.19}	0.065 ^{<i>d</i>}	0.936	
SALT J213742.6-382901	6585736932806500736	324.42712	-38.48355	16.95	0.538 ± 0.087	16	1.94 ^{+0.36} _{-0.26}	0.036 ^{<i>d</i>}	1.061	
SDSS J000945.46+135814.4	2767982864653184640	002.43941	+13.97065	18.07	0.31 ± 0.17	55	2.6 ^{+1.3} _{-0.7}	0.0829 ± 0.0041	0.989	
SDSS J001651.42-011329.3	2541718902258404736	004.21425	-01.22487	16.75	0.273 ± 0.079	29	3.36 ^{+0.81} _{-0.60}	0.06729 ± 0.00039	0.995	
SDSS J034917.41-005919.3	3251245339191040256	057.32256	-00.98874	17.80	1.15 ± 0.12	10	0.85 ^{+0.12} _{-0.08}	0.1274 ± 0.0061	1.048	
SDSS J055905.02+633448.4	286746241613044096	089.77088	+63.58012	18.59	0.98 ± 0.16	16	1.06 ^{+0.17} _{-0.14}	0.1606 ± 0.0025	1.078	
SDSS J075415.11+085232.1	3145662944130394496	118.56299	+08.87560	19.08	0.57 ± 0.23	39	1.8 ^{+1.2} _{-0.5}	0.0321 ± 0.0065	0.961	
SDSS J075540.94+400918.0	920621124593362816	118.92053	+40.15497	17.80	0.95 ± 0.13	13	1.14 ^{+0.19} _{-0.13}	0.0572 ± 0.0041	0.968	
SDSS J093546.53+110529.0	589674614326779136	143.94384	+11.09133	17.75	1.10 ± 0.14	13	0.96 ^{+0.13} _{-0.10}	0.0411 ± 0.0030	0.985	
SDSS J102327.41+535258.7	851812381256776832	155.86423	+53.88297	17.92	0.50 ± 0.11	23	2.03 ^{+0.47} _{-0.37}	0.0280 ± 0.0028	0.977	
SDSS J105300.24+174932.9	3982986781494206080	163.25103	+17.82578	16.76	1.429 ± 0.076	5	0.714 ^{+0.040} _{-0.034}	0.0190 ± 0.0016	0.987	
SDSS J121523.09+120300.8	3908341899157118080	183.84614	+12.05020	18.14	0.75 ± 0.14	19	1.44 ^{+0.35} _{-0.23}	0.03492 ± 0.00078	0.928	
SDSS J123930.61+244321.7	3959650269965155584	189.87752	+24.72270	18.30	0.69 ± 0.16	23	1.51 ^{+0.37} _{-0.26}	0.0405 ± 0.0090	0.975	
SDSS J134341.88+670154.5	1672427588951276800	205.92436	+67.03180	17.13	1.455 ± 0.055	4	0.707 ^{+0.023} _{-0.026}	0.0284 ± 0.0014	0.937	
SDSS J141556.26+061822.5	3673120627847661184	213.98441	+06.30622	17.44	1.04 ± 0.13	12	1.00 ^{+0.14} _{-0.11}	0.0303 ± 0.0055	1.102	
SDSS J144734.12+572053.1	161373101969686208	221.89206	+57.34807	18.03	0.835 ± 0.092	11	1.23 ^{+0.21} _{-0.13}	0.0342 ± 0.0082	1.028	
SDSS J152116.00+251437.5	1270099761612163328	230.31665	+25.24375	17.87	0.26 ± 0.11	43	4.4 ^{+2.1} _{-1.4}	0.0386 ± 0.0066	1.058	hybrid
SDSS J155610.40+254640.3	1220049614357436544	239.04334	+25.77784	17.91	0.086 ± 0.098	115	7.5 ^{+3.3} _{-3.0}	0.0630 ± 0.0077	0.981	binary?
SDSS J163727.03+485355.2	141069437787399552	249.36262	+48.89866	18.35	0.57 ± 0.11	19	2.01 ^{+0.84} _{-0.36}	0.0261 ± 0.0055	1.018	
SDSS J191845.01+624343.7	2240494910007892608	289.68757	+62.72883	17.58	0.970 ± 0.074	8	1.111 ^{+0.101} _{-0.079}	0.0262 ± 0.0020	1.012	
SDSS J212531.92-010745.8	2686081102494206080	321.38303	-01.12941	17.54	0.35 ± 0.11	32	2.9 ^{+1.3} _{-0.7}	0.03730 ± 0.00084	1.034	binary
Sh 2-68	4276328581046447104	276.24337	+00.85976	16.40	2.446 ± 0.059	2	0.405 ^{+0.010} _{-0.010}	0.622 ± 0.048	1.088	hybrid
Sh 2-78	4506484097383382272	285.79198	+14.11631	17.61	1.43 ± 0.10	7	0.696 ^{+0.059} _{-0.044}	0.3160 ± 0.0085	1.045	
TIC 95332541	2997192526074656640	090.68749	-13.85096	15.32	2.593 ± 0.043	2	0.3845 ^{+0.0055} _{-0.0050}	0.0575 ± 0.0049	1.023	
TIC 333432673	2950907725113997312	100.31517	-13.69000	15.21	2.552 ± 0.043	2	0.3892 ^{+0.0054} _{-0.0054}	0.119 ± 0.018	1.093	
TIC 403800675	3486203758501245440	179.36518	-28.06384	16.16	1.875 ± 0.062	3	0.535 ^{+0.019} _{-0.018}	0.0591 ± 0.0040	1.004	

Table 3 continued

Table 3 (*continued*)

Name	<i>Gaia</i> ID	RA (deg)	Dec. (deg)	<i>Gaia</i> G (mag)	ϖ_{Gaia} (mas)	$\sigma_{\varpi_{\text{Gaia}}}/\varpi$ (%)	r_{geo} (kpc)	E(B-V) (mag)	RUWE	Remarks
TIC 1989122424	6462935326662402944	319.40996	-55.46694	16.75	1.471 ± 0.062	4	$0.688^{+0.022}_{-0.026}$	0.058^a	0.987	
WD J070204.29+051420.56	3128765207057429504	105.51783	+5.23904	14.98	3.089 ± 0.053	2	$0.3228^{+0.0053}_{-0.0057}$	0.0472 ± 0.0015	1.091	
NGC 6765	2039515046435901440	287.77732	+30.54545	17.60	0.276 ± 0.078	28	$4.0^{+1.5}_{-1.0}$	0.1505 ± 0.0023	1.002	
PG 2131+066	-	-	-	-	-	-	-	-	-	binary
RX J0439.8-6809	-	-	-	-	-	-	-	-	-	-

^aReddening from SFD

NOTE—Astrometric properties of PG 1159 stars from *Gaia* DR3 (*Gaia* Collaboration et al. 2023). Geometric distances (r_{geo}) are from Bailer-Jones et al. (2021), E(B-V) from Bayestar17 (Green et al. 2018) except for targets with Dec. south of -30° where SFD maps (Schlafly & Finkbeiner 2011; Schlegel et al. 1998) were used. Uncertainties in E(B-V) are calculated as half of the difference between values at 16th and 84th percentile. The last three objects were excluded from the analysis because of the lack of either *Gaia* measurements, or T_{eff} and $\log g$.

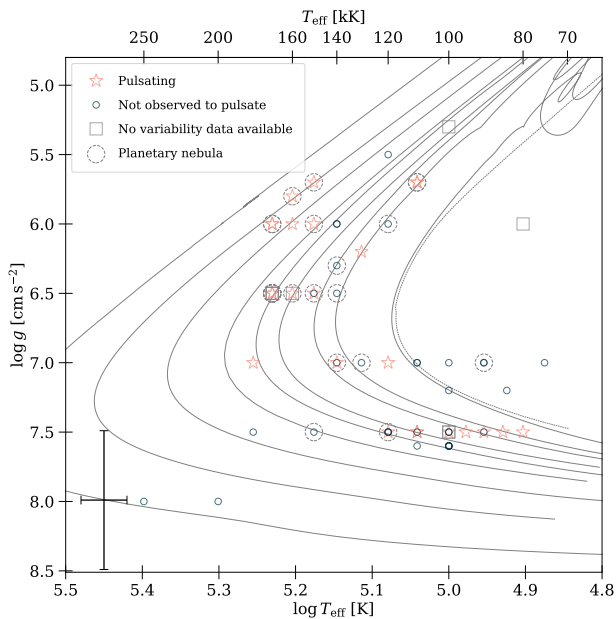


Figure 5. Positions of PG 1159 stars in the surface gravity-effective temperature $\log g - \log T_{\text{eff}}$ diagram. Star symbols represent pulsating PG 1159 stars, circles – non-variable, and squares – with no reported photometric observations. Stars with planetary nebulae are marked with dashed circles. A typical error bar is shown in the bottom left corner. Multiple stars overlap in this diagram, which can be seen as wider and darker borders of symbols. See text for details. Lines represent evolutionary tracks from Miller Bertolami & Althaus (2006): solid – VLTP (from left to right, final masses: 0.870, 0.741, 0.664, 0.609, 0.584, 0.565, 0.542, 0.530, 0.515 M_{\odot}), single dashed line – LTP (0.512 M_{\odot}).

8. PG 1159 STARS ON THE HERTZSPRUNG-RUSSELL DIAGRAM

PG 1159 stars plotted in the surface gravity-effective temperature diagram $\log g - \log T_{\text{eff}}$ (also called the Kiel diagram) cluster horizontally along the lines of constant $\log g$, and vertically along the lines of constant $\log T_{\text{eff}}$ (see Figure 5). The reasons are the current sensitivity of spectroscopic observations (large uncertainties, for some PG 1159 stars even $\pm 0.5 \text{ cm s}^{-2}$ in $\log g$) and availability of advanced model atmospheres for these extremely hot stars, with the latter usually provided in grids with a step of $\log g = 0.5 \text{ cm s}^{-2}$ and $T_{\text{eff}} = 10000 \text{ K}$.

For the discussion in the context of asteroseismology it is useful to place the PG 1159 stars into the theoretical Hertzsprung-Russell diagram ($\log L_{\star}/L_{\odot} - \log T_{\text{eff}}$). However, this requires the knowledge of stellar luminosities and effective temperatures. Derivation of stellar luminosities is especially challenging, because it relies on knowing the total bolometric flux of a given star. There are many ways to tackle this difficult problem.

One solution is based on determining the Spectral Energy Distribution (SED) by fitting model atmospheres to broadband photometric magnitudes (see, e.g., Uzundag et al. 2022). For such hot stars as PG 1159s, the UV photometry and a grid of model atmospheres covering those short wavelengths is essential and, to date, not available for the whole sample of PG 1159 stars.

Another method is to derive the bolometric luminosities, either from mathematical prescriptions, or from apparent magnitudes using bolometric corrections (BCs). In the second case, the observed apparent magnitudes are converted to absolute magnitudes in a given passband b using a distance modulus DM (a logarithmic measure of the distance to the star):

$$m_b = M_b + DM, \quad (1)$$

where m_b is the apparent magnitude and M_b is the absolute magnitude in the passband b . Incorporating the definition of the absolute magnitude gives:

$$DM = m_b - M_b = 5 \log_{10} \frac{d}{(10 \text{ pc})}, \quad (2)$$

where d is distance in parsecs. With the correction for interstellar absorption between the object and observer, the absolute magnitude in a passband b can be derived from:

$$M_b = m_b - DM - A_b, \quad (3)$$

where A_b is the extinction in a passband b . Then the bolometric magnitude is

$$M_{\text{bol}} = M_b + BC_b, \quad (4)$$

where M_{bol} is absolute bolometric magnitude and BC_b is bolometric correction in a given passband, a quantity dependent not only on the photometric passband used in observations, but also the theoretical stellar spectrum used in calculation of the correction (different sets of effective temperature, surface gravity, and metallicity will give different BC values). In the case of extremely hot stars such as pre-white dwarfs of the PG 1159 type, this requires using models including non-local thermodynamic equilibrium (non-LTE) effects. Finally, the absolute bolometric magnitude M_{bol} of a star of a bolometric luminosity L_{\star} , referenced to the Sun, is given by:

$$-2.5 \log_{10} \frac{L_{\star}}{L_{\odot}} = M_{\text{bol}} - M_{\text{bol},\odot}, \quad (5)$$

where $M_{\text{bol},\odot} = 4.74$ is the absolute bolometric magnitude of the Sun, and $L_{\odot} = 3.828 \times 10^{33} \text{ erg s}^{-1}$ is the absolute bolometric luminosity of the Sun⁷.

⁷ IAU Resolution 2015 B2

For white dwarf stars, the first commonly used/tabulated BC values were compiled by [Bergeron et al. \(1995\)](#) for hydrogen- and helium-rich white dwarf model atmospheres, but for a small grid covering surface gravity (only $\log g = 8 \text{ cm s}^{-2}$) and effective temperature (up to 100000 K only for DA white dwarfs). This work was expanded by [Holberg & Bergeron \(2006\)](#), who provided an extensive grid for both DA and DB white dwarfs⁸. The latter work is regularly updated on line⁹. In the most up-to-date version of the tables, models of [Bédard et al. \(2020\)](#), which include non-LTE effects, are used at the highest effective temperatures. Unfortunately, no bolometric corrections have ever been extensively compiled for PG 1159 stars. Some PG 1159 stars had bolometric corrections estimated for the purpose of deriving luminosities for asteroseismic modeling ([Uzundag et al. 2021](#) list three previously used values), but no tabulated prescription has ever been provided.

We calculated the luminosities of PG 1159 stars based on currently available data. We used the distances and interstellar reddening values described in Section 7. The reddening for each star was converted to extinction using the reddening law of [Fitzpatrick \(2004\)](#) with $R_V = 3.1$. *Gaia* magnitudes were converted to V using the following prescription¹⁰:

$$G - V = -0.02704 + 0.01424(G_{\text{BP}} - G_{\text{RP}}) \quad (6) \\ -0.2156(G_{\text{BP}} - G_{\text{RP}})^2 \\ +0.01426(G_{\text{BP}} - G_{\text{RP}})^3.$$

We used tabulated bolometric corrections for pure-helium model atmospheres (DB) provided online on the aforementioned website by the Montreal group. As the bolometric correction primarily depends on the effective temperature and because there are no bolometric corrections computed with proper models for PG 1159 stars, we used those models as the best approach currently available. The tabulated values do not cover surface gravities below $\log g = 7.0 \text{ cm s}^{-2}$, therefore the ones for $\log g = 7.0 \text{ cm s}^{-2}$ were used for matching effective temperatures. The values for effective temperatures over 150000 K were extrapolated to higher effective temperatures for a given $\log g$. The linear extrapolation was done in $\log T_{\text{eff}}$ vs. BC space using `interp1d` class from the `scipy` sub-package `interpolate` and “fill_value=‘extrapolate’”, using the available BC val-

ues for T_{eff} in the range 75000 – 150000 K for a given $\log g$. Table 2 lists the physical properties and chosen BC values for each PG 1159 star in the sample. Then, the luminosities were calculated following equations 1 – 5 and are also listed in Table 2 with uncertainties. The errors were propagated the following way: a) for DM using asymmetric errors from Table 3, b) for $E(B-V)$ using symmetric errors from Table 3, c) for BC_V using asymmetric errors adopted as the BC_V values ± 10000 K for each object, d) for G , G_{BP} , and G_{RP} magnitudes the symmetric errors were calculated as $1.09 \cdot G/\text{SNR}$, where SNR is roughly `phot_g_mean_flux_over_error`¹¹ (example for G).

Figure 6 shows positions of PG 1159 stars in the theoretical Hertzsprung-Russell diagram ($\log L_*/L_\odot - \log T_{\text{eff}}$). For illustration purposes, the blue dotted lines represent theoretical blue edges for $l = 1$ and $l = 2$ modes from [Gautschy et al. \(2005\)](#), but the blue edge is composition dependent – “fuzzy” ([Quirion et al. 2007](#)), and with the red dotted lines we show the presently observed red edges.

9. DISCUSSION

The number of pulsating PG 1159 stars increased to 24 objects with our discovery of pulsations in Abell 72. The main observational challenge in the detection or confirmation of variability in those stars lies in two main areas. Firstly, the amplitudes of the g-mode pulsations are quite low. While Abell 72 showed pulsation amplitudes of up to 10 mmag, PG 1144+005, on the other hand, showed a highly variable (between consecutive nights) Fourier spectrum with amplitudes ranging from 3 to 6 mmag ([Sowicka et al. 2021](#)). This requires reaching a noise level below 1 mmag for a significant detection (assuming $S/N \geq 4$), which is a challenging task for these faint stars. We were not able to reach noise levels below 1.5 mmag for Longmore 3, SDSS J000945.46+135814.4, SDSS J001651.42–011329.3, SDSS J102327.41+535258.7, and SDSS J144734.12+572053.1. Another challenge is the aforementioned change in amplitude spectra for some stars, between observing seasons or even consecutive nights. It is therefore always possible that the star is observed in a temporary state where the pulsations destructively interfere. We aimed at obtaining more than one run for each star in the sample with a sufficient quality, but this was only possible for eight stars.

Our results allowed us to update the fraction of PG 1159 pulsators in the GW Vir instability strip.

⁸ The DA grid covered $T_{\text{eff}} = 2500$ K to 150000 K and $\log g = 7.0$ to 9.0 cm s^{-2} , while the DB grid covered $T_{\text{eff}} = 3250$ K to 150000 K and $\log g = 7.0$ to 9.0 cm s^{-2} .

⁹ <https://www.astro.umontreal.ca/~bergeron/CoolingModels/>

¹⁰ *Gaia* DR3 documentation. We note that a few objects were slightly outside the range of applicability for this relationship.

¹¹ <https://dc.zah.uni-heidelberg.de/gaia/q3/cone/info#note-e>

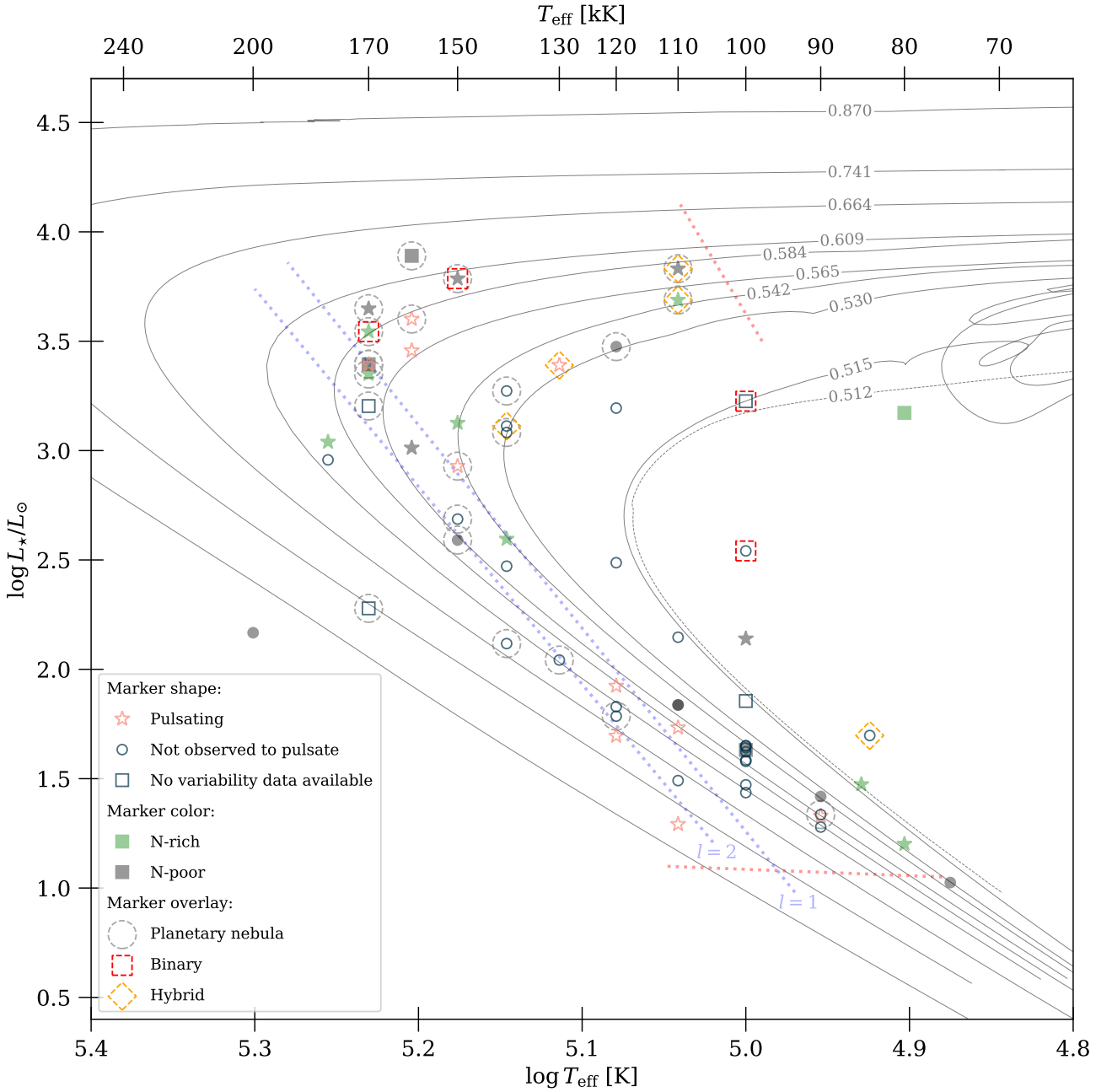


Figure 6. Positions of PG 1159 stars in the theoretical Hertzsprung-Russell diagram ($\log L_*/L_\odot - \log T_{\text{eff}}$). Star symbols represent pulsating PG 1159 stars, circles – non-variable, and squares – with no reported photometric observations. Stars with planetary nebulae are marked with dashed circles. N-rich PG 1159 stars are shown with filled green symbols, while N-poor ones with filled black symbols. Lines represent evolutionary tracks from Miller Bertolami & Althaus (2006): solid – VLTP (from left to right, final masses: 0.870, 0.741, 0.664, 0.609, 0.584, 0.565, 0.542, 0.530, 0.515 M_\odot), single dashed line – LTP (0.512 M_\odot). For illustration purposes, the blue dotted lines represent theoretical blue edges for $l = 1$ and $l = 2$ modes from Gautschy et al. (2005), but the blue edge is composition dependent. The red dotted lines indicate estimated observed red edges, beyond which no GW Vir star has to date been reported.

While previous works quoted values of about 20 – 50%, but including not only PG 1159 stars but also the other stars populating the GW Vir instability strip, we obtain 36% using only stars of PG 1159 spectral type. Our fraction is consistent with previous estimates and shows that only about 1/3 of PG 1159 stars within the GW Vir instability strip are observed to vary.

In this context, it is interesting to see how the variability compares to the nitrogen abundance observed in PG 1159 stars, in the light of the nitrogen dichotomy (N-rich pulsators, N-poor nonpulsators, found by Dreizler & Heber 1998) that appears to hold. While the majority of those stars do not have a determination of their atmospheric nitrogen abundance available in the literature, there are a few stars that may not fit this hypothesis. The most recent analysis of the pulsating central star of NGC 246 by Löbbling (2018) implies sub-solar N abundance. SALT J172411.7–632147 is a N-poor pulsator reported by Jeffery et al. (2023). New spectra of TIC 95332541 analyzed by Reindl et al. (2023) revealed that it is another N-poor pulsator. Longmore 4 is a known pulsator, and does not show N in a number of medium-resolution spectra. It is interesting in the context of the outbursts that it exhibits, temporarily changing its spectral type from PG 1159 to [WCE] (Werner et al. 1992; Bond 2014). RL 104 is also an interesting object, as it is N-rich and claimed to have evolved from a binary merger scenario, but to date was not observed photometrically.

With such a sample tested for variability, we placed the PG 1159 stars in the theoretical Hertzsprung-Russell diagram. We determined luminosities following the procedure described in Sect. 8. We plotted them against available evolutionary tracks for PG 1159 stars. In general, very good agreement between the evolutionary tracks and positions of PG 1159 stars was obtained. The majority of the stars are within the evolutionary tracks for typical PG 1159 masses (0.5–0.6 M_{\odot}). Only one star is found beyond 0.87 M_{\odot} – H1504+65. Nevertheless, a few shortcomings of our attempt need to be noted. The distances from *Gaia* for some stars have large uncertainties due to large relative errors of parallaxes. In Table 3 we marked 14 stars whose relative parallax errors exceed 20%. Four of them are confirmed or suspected binaries, therefore their determined positions might be uncertain. It is worth comparing the distances determined using different (independent) methods, e.g., using planetary nebulae line strengths, but this is out of the scope of this work. Uzundag et al. (2021) quoted available in the literature values of bolometric correction for PG 1159 stars for three objects: PG 1159–035 ($T_{\text{eff}} = 140000$ K, $\log g = 7.0$ cm s^{-2}): $BC = -7.6$,

RX J2117+3142 ($T_{\text{eff}} = 170000$ K, $\log g = 6.0$ cm s^{-2}): $BC = -7.95$, and PG 2131+066 ($T_{\text{eff}} = 95000$ K, $\log g = 7.5$ cm s^{-2}): $BC = -6.0$. They interpolated those values to obtain $BC = -7.05$ for TIC 95332541 and TIC 333432673 ($T_{\text{eff}} = 120000$, $\log g = 7.5$), assuming only the dependence on the effective temperature. We investigated the difference between tabulated BC for DA and DB models. For T_{eff} and $\log g$ of PG 1159–035 (the only exact match with tabulated values), we found BC of -7.964 and -7.658 for DA and DB models, respectively. The value for the DB model atmosphere agrees well with the quoted value of $BC = -7.6$. We also checked how the BC value from DB table changes with $\log g$ for a given temperature. For $T_{\text{eff}} = 140000$ K and $\log g = 7.0, 7.5, 8.0, 8.5$ cm s^{-2} we obtained $BC = -7.658, -7.668, -7.676, -7.681$, respectively. Therefore, we do not expect significant interpolation errors in the parameter space of interest.

10. ONE OR TWO GW VIR INSTABILITY DOMAINS?

The establishment of the PG 1159 spectral class (e.g., see Werner 1992) occurred subsequently to the discovery of pulsations in PG 1159–035 (McGraw et al. 1979) itself. At the time when the pulsating PG 1159 stars emerged as a new group of pulsators (e.g., Bond et al. 1984), they were considered the hottest subgroup of the helium-rich DO white dwarf stars (Wesemael et al. 1985). For that reason, and for the similarity with the designations of the groups of pulsating white dwarfs already known (DAV and DBV) the PG 1159 pulsators were dubbed “the DOVs”.

However, the second pulsating star of the PG 1159 spectral type discovered was located in a planetary nebula (Grauer & Bond 1984) and subsequent searches (e.g., Ciardullo & Bond 1996) revealed several of these “Planetary Nebula Nucleus Variables” (PNNVs). Even though it was realized that the “DOVs” were likely just the same type of pulsating stars, but in a more advanced evolutionary stage than the “PNNVs”, the two groups were historically often separated. The main reason for this separation was that one group of pulsators are surrounded by nebulae whereas the others were not and that one group has significantly longer pulsation periods than the other. Furthermore, theoretical computations (e.g., Córscico et al. 2006, cf. Fig. 6) show that the blue edge of the instability strip intersects with the evolutionary tracks of pre-white dwarf stars in such a way that many of them leave the strip during their evolution and later re-enter it, giving the impression of two separated instability regions.

Quirion et al. (2007) and Fontaine & Brassard (2008) argued, mostly on a theoretical basis, that this separation should be dropped, and that all hot pulsating pre-white dwarf stars should be called “the GW Vir stars”¹². This was motivated by the fact that the pulsational driving mechanism of all GW Vir stars is the same, that stars with a pure DO spectral type are not known to pulsate¹³, and that not all stars classified as “PNNV” even possess a detected planetary nebula. To this it can be added that there are other intrinsically variable central stars of planetary nebulae (e.g., Handler et al. 2013) that do not pulsate at all, which is why a designation “PNNV” is equally misleading as is “DOV”.

Schoenberner & Napiwotzki (1990) showed that some PNNs are spectroscopically indistinguishable from the white dwarfs similar to PG 1159–035, and assigned them all to “PG 1159” type. PG 1159 subclasses introduced by Werner (1992) did not take into account the presence or absence of a nebula, treating the PG 1159 spectral class as a whole. Therefore, not only is the pulsation driving mechanism the same for those stars, but they also share some spectroscopic properties representative of the whole class.

Moreover, the commonly used surface gravity-effective temperature diagram presented in Fig. 5 shows that it is impossible to separate the two groups in the $\log g - \log T_{\text{eff}}$ plane – stars with planetary nebulae are found throughout the whole GW Vir instability strip. This refutes the argument that the PNNVs usually have much lower surface gravities, as no strict boundary can be placed in such a plane.

In the following, we examine the question whether these two groups are distinct, or should be distinguished, from an observational point of view. The top panel in Figure 7 shows the ranges of pulsation periods observed in pulsating pre-white dwarf stars (of PG 1159 spectral type) versus stellar radius (as derived from Fig. 6 and the Stefan-Boltzmann law).

Several things are noteworthy in Fig. 7. First of all, there is a clear overlap between the objects with and without a planetary nebula, already suggesting these two groups are not distinct. Second, an obvious trend as already noticed by others earlier is visible, namely that the larger, less evolved objects have longer pulsation periods.

¹² GW Vir is the variable star designation of PG 1159–035, Kholopov et al. (1985).

¹³ The PG 1159 spectral class had meanwhile been established as a separate group, and we recall that some pulsating pre-white dwarfs are of [WCE] or [WCE/PG 1159] spectral types.

To look into this in some more detail, the bottom panel in Fig. 7 compares the pulsation periods with the pulsation constant $Q = P\sqrt{\rho_*/\rho_\odot}$, a measure of the radial overtone of the excited pulsation modes. There is a slight trend that the longer the pulsation period, the smaller is the pulsation constant. In other words, the more evolved a pulsating pre-white dwarf, the higher radial overtones of the gravity modes are excited. This is consistent with the theoretical expectation that with progressing evolution the pulsational driving region becomes located closer to the stellar surface (see Gautschy et al. 2005).

We therefore conclude that the distinction between “DOVs” and “PNNVs” is, according to current knowledge, artificial and based on selection effects and hence should not be used. All pulsating pre-white dwarf stars oscillating in gravity modes excited by the $\kappa - \gamma$ mechanism due to ionization of carbon and oxygen should henceforth be called “GW Vir stars”.

10.1. The case of RX J0122.9–7521

In Sect. 5.2 we reported the detection of variability of RX J0122.9–7521 and mentioned that it would be the hottest GW Vir pulsator. However, we are reluctant to claim the firm detection of pulsation for this star, for several reasons.

Although its 41-min period fits in the range of pulsation periods observed in GW Vir stars (Althaus et al. 2010), we detected only a single period that could therefore in principle be of a different origin, like rotation, binarity, or spots (Reindl et al. 2021). Furthermore, in Fig. 7, the period of this star is rather long with respect to stars with similar radii.

RX J0122.9–7521 lies outside the theoretical blue edge of GW Vir instability strip, and Quirion et al. (2004) unsurprisingly did not find an asteroseismic model with unstable periods in this star. Werner (1995) reported the detection of nitrogen in its spectrum.

In any case, time-resolved spectroscopy or high signal-to-noise photometry would be needed to establish the cause of the variability of RX J0122.9–7521.

11. SUMMARY AND CONCLUSIONS

We obtained new photometric observations of 29 PG 1159 stars. Over 86 hours of time-series photometry were collected in the years 2014 – 2022 using telescopes of different sizes, ranging from 1.0-m to 10.4-m, and located in both hemispheres. For the majority of stars we achieved a median noise level in Fourier amplitude spectra in the range 0.3 – 1.0 mmag, which allowed us to discover multiperiodic pulsations in the central star of planetary nebula Abell 72, and variability in

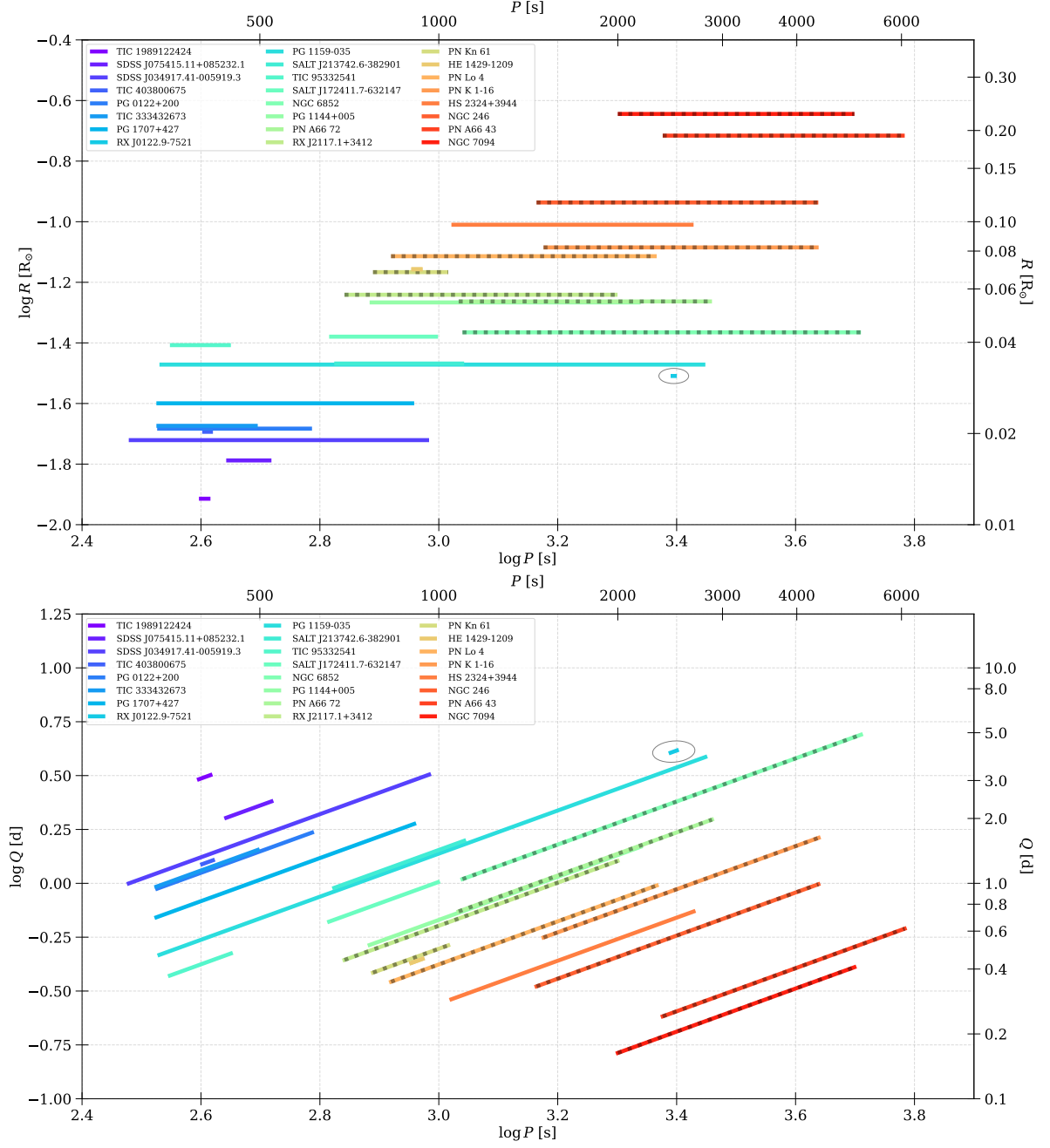


Figure 7. *Top:* The period ranges of pulsating pre-white dwarf stars (only of PG 1159 spectral type) versus stellar radius (horizontal bars). *Bottom:* The period ranges of pulsating pre-white dwarf stars (only of PG 1159 spectral type) versus pulsation constant (horizontal bars). Objects surrounded by a planetary nebula are denoted with grey-dotted bars. The object marked with an ellipse is RX J0122.9–7521 (see Sect. 10.1).

RX J0122.9–7521 that could be due to pulsations, binarity or rotation. Five stars showed interesting peaks but require follow-up observations for confirmation. For the remaining stars our observations put limits on nonvariability. As a result, we derived the fraction of pulsating PG 1159 stars within the GW Vir instability strip – 36%.

In the light of N dichotomy in PG 1159 stars, we compared the new variability results with the literature data on N abundances for those stars and identified objects that could be culprits for this hypothesis: NGC 246, SALT J172411.7–632147 and TIC 95332541 may be N-poor pulsators. Longmore 4 is probably a N-poor pulsator, but temporarily changes its spectral type from PG 1159 to [WCE] during outbursts.

Taking advantage of the currently available data, we used distances derived from *Gaia* parallaxes, interstellar extinction from 3D reddening maps, and bolometric correction values from DB tables, to derive luminosities and place the PG 1159 stars in the theoretical Hertzsprung-Russell diagram. Regardless of the possible caveats of our approach, all stars align well with the PG 1159 evolutionary tracks from Miller Bertolami & Althaus (2006).

Finally, we derived radii and pulsation constants for known pulsators, and plotted them against period ranges observed in those stars to further argue against the distinction between “DOVs” and “PNNVs”, and suggested using only the “GW Vir” designation for all stars belonging to that family of pulsating white dwarfs.

12. AUTHOR CONTRIBUTIONS

PS with GH and DJ applied for observing time. PS, GH, DJ, JC, FvW, EP, KB, LP, LSA, and MK observed the targets. DLH extracted single FITS files from data cubes of the SA19+SHOC run. PS did the data reduction for all targets except those observed with DK+DFOSC (EP reduced those data). PS also did photometry and frequency analysis, as well as compiled astrometric parameters of PG 1159 stars and bolometric corrections, derived luminosities, placed the sample in the HR diagrams, and computed radii and pulsation constants. GH and DJ supervised the work. KW provided parts of the data included in Table 2. PS wrote

the text with contribution from GH and feedback from co-authors.

We thank Philip Short, Nicholas Humphries, and Martha Tabor who contributed to the observations. This research was supported in part by the National Science Foundation under Grant No. NSF PHY-1748958 and by the Polish National Center for Science (NCN) through grants 2015/18/A/ST9/00578 and 2021/43/B/ST9/02972. MK acknowledges the support from ESA-PRODEX PEA4000127913. This paper uses observations made at the South African Astronomical Observatory (SAAO). Based on observations made with the Gran Telescopio Canarias (GTC), installed in the Spanish Observatorio del Roque de los Muchachos of the Instituto de Astrofísica de Canarias, in the island of La Palma. Based on observations with the Isaac Newton Telescope operated by the Isaac Newton Group at the Observatorio del Roque de los Muchachos of the Instituto de Astrofísica de Canarias on the island of La Palma, Spain. This paper includes data taken at The McDonald Observatory of The University of Texas at Austin. Data were obtained (in part) using the 1.3 m McGraw-Hill Telescope of the MDM Observatory. This work has made use of data from the European Space Agency (ESA) mission *Gaia* (<https://www.cosmos.esa.int/gaia>), processed by the *Gaia* Data Processing and Analysis Consortium (DPAC, <https://www.cosmos.esa.int/web/gaia/dpac/consortium>). Funding for the DPAC has been provided by national institutions, in particular the institutions participating in the *Gaia* Multilateral Agreement.

Facilities: GTC (OSIRIS), SAAO: Radcliffe, Elizabeth (SHOC), ING:Newton (WFC), Struve (ProEM), Danish 1.54m Telescope (DFOSC), McGraw-Hill (Andor)

Software: Astropy (Astropy Collaboration et al. 2013, 2018, 2022), ccdproc (Craig et al. 2017), dustmaps (Green 2018), matplotlib (Hunter 2007), numpy (Harris et al. 2020), pandas (Wes McKinney 2010; pandas development team 2020), Period04 (Lenz & Breger 2005), scipy (Virtanen et al. 2020)

REFERENCES

- Althaus, L. G., Córscico, A. H., Isern, J., & García-Berro, E. 2010, *A&A Rv*, 18, 471, doi: [10.1007/s00159-010-0033-1](https://doi.org/10.1007/s00159-010-0033-1)
- Andersen, J., Andersen, M. I., Klougart, J., et al. 1995, *The Messenger*, 79, 12
- Astropy Collaboration, Robitaille, T. P., Tollerud, E. J., et al. 2013, *A&A*, 558, A33, doi: [10.1051/0004-6361/201322068](https://doi.org/10.1051/0004-6361/201322068)
- Astropy Collaboration, Price-Whelan, A. M., Sipőcz, B. M., et al. 2018, *AJ*, 156, 123, doi: [10.3847/1538-3881/aabc4f](https://doi.org/10.3847/1538-3881/aabc4f)

- Astropy Collaboration, Price-Whelan, A. M., Lim, P. L., et al. 2022, *ApJ*, 935, 167, doi: [10.3847/1538-4357/ac7c74](https://doi.org/10.3847/1538-4357/ac7c74)
- Bailer-Jones, C. A. L., Rybizki, J., Fouesneau, M., Demleitner, M., & Andrae, R. 2021, *AJ*, 161, 147, doi: [10.3847/1538-3881/abd806](https://doi.org/10.3847/1538-3881/abd806)
- Bédard, A., Bergeron, P., Brassard, P., & Fontaine, G. 2020, *ApJ*, 901, 93, doi: [10.3847/1538-4357/abafbe](https://doi.org/10.3847/1538-4357/abafbe)
- Bergeron, P., Wesemael, F., & Beauchamp, A. 1995, *PASP*, 107, 1047, doi: [10.1086/133661](https://doi.org/10.1086/133661)
- Bond, H. E. 2014, *AJ*, 148, 44, doi: [10.1088/0004-6256/148/3/44](https://doi.org/10.1088/0004-6256/148/3/44)
- Bond, H. E., Grauer, A. D., Green, R. F., & Liebert, J. W. 1984, *ApJ*, 279, 751, doi: [10.1086/161943](https://doi.org/10.1086/161943)
- Bond, H. E., & Meakes, M. G. 1990, *AJ*, 100, 788, doi: [10.1086/115560](https://doi.org/10.1086/115560)
- Bond, H. E., Werner, K., Jacoby, G. H., & Zeimann, G. R. 2023, *MNRAS*, 521, 668, doi: [10.1093/mnras/stad524](https://doi.org/10.1093/mnras/stad524)
- Breger, M., Stich, J., Garrido, R., et al. 1993, *A&A*, 271, 482
- Caldwell, J. A. R., Cousins, A. W. J., Ahlers, C. C., van Wamelen, P., & Maritz, E. J. 1993, *South African Astronomical Observatory Circular*, 15, 1
- Cepa, J. 1998, *Ap&SS*, 263, 369, doi: [10.1023/A:1002144913887](https://doi.org/10.1023/A:1002144913887)
- Ciardullo, R., & Bond, H. E. 1996, *AJ*, 111, 2332, doi: [10.1086/117967](https://doi.org/10.1086/117967)
- Coppejans, R., Gulbis, A. A. S., Kotze, M. M., et al. 2013, *PASP*, 125, 976, doi: [10.1086/672156](https://doi.org/10.1086/672156)
- Córsico, A. H., Althaus, L. G., & Miller Bertolami, M. M. 2006, *A&A*, 458, 259, doi: [10.1051/0004-6361:20065423](https://doi.org/10.1051/0004-6361:20065423)
- Córsico, A. H., Althaus, L. G., Miller Bertolami, M. M., González Pérez, J. M., & Kepler, S. O. 2009, *ApJ*, 701, 1008, doi: [10.1088/0004-637X/701/2/1008](https://doi.org/10.1088/0004-637X/701/2/1008)
- Córsico, A. H., Althaus, L. G., Miller Bertolami, M. M., & Kepler, S. O. 2019, *A&A Rv*, 27, 7, doi: [10.1007/s00159-019-0118-4](https://doi.org/10.1007/s00159-019-0118-4)
- Córsico, A. H., Uzundag, M., Kepler, S. O., et al. 2021, *A&A*, 645, A117, doi: [10.1051/0004-6361/202039202](https://doi.org/10.1051/0004-6361/202039202)
- Costa, J. E. S., Kepler, S. O., Winget, D. E., et al. 2008, *A&A*, 477, 627, doi: [10.1051/0004-6361:20053470](https://doi.org/10.1051/0004-6361:20053470)
- Craig, M., Crawford, S., Seifert, M., et al. 2017, *astropy/ccdproc: v1.3.0.post1, v1.3.0.post1*, Zenodo, doi: [10.5281/zenodo.1069648](https://doi.org/10.5281/zenodo.1069648)
- Crowther, P. A., De Marco, O., & Barlow, M. J. 1998, *MNRAS*, 296, 367, doi: [10.1046/j.1365-8711.1998.01360.x](https://doi.org/10.1046/j.1365-8711.1998.01360.x)
- De Marco, O., Long, J., Jacoby, G. H., et al. 2015, *MNRAS*, 448, 3587, doi: [10.1093/mnras/stv249](https://doi.org/10.1093/mnras/stv249)
- Dreizler, S. 1999, *Reviews in Modern Astronomy*, 12, 255
- Dreizler, S., & Heber, U. 1998, *A&A*, 334, 618
- Fitzpatrick, E. L. 2004, in *Astronomical Society of the Pacific Conference Series*, Vol. 309, *Astrophysics of Dust*, ed. A. N. Witt, G. C. Clayton, & B. T. Draine, 33, doi: [10.48550/arXiv.astro-ph/0401344](https://doi.org/10.48550/arXiv.astro-ph/0401344)
- Fontaine, G., & Brassard, P. 2008, *PASP*, 120, 1043, doi: [10.1086/592788](https://doi.org/10.1086/592788)
- Friederich, F., Rauch, T., Werner, K., Koesterke, L., & Kruk, J. W. 2010, in *American Institute of Physics Conference Series*, Vol. 1273, *17th European White Dwarf Workshop*, ed. K. Werner & T. Rauch, 231–234, doi: [10.1063/1.3527810](https://doi.org/10.1063/1.3527810)
- Fu, J. N., Vauclair, G., Solheim, J. E., et al. 2007, *A&A*, 467, 237, doi: [10.1051/0004-6361:20066295](https://doi.org/10.1051/0004-6361:20066295)
- Gaia Collaboration, Prusti, T., de Bruijne, J. H. J., et al. 2016, *A&A*, 595, A1, doi: [10.1051/0004-6361/201629272](https://doi.org/10.1051/0004-6361/201629272)
- Gaia Collaboration, Vallenari, A., Brown, A. G. A., et al. 2023, *A&A*, 674, A1, doi: [10.1051/0004-6361/202243940](https://doi.org/10.1051/0004-6361/202243940)
- Gautschy, A., Althaus, L. G., & Saio, H. 2005, *A&A*, 438, 1013, doi: [10.1051/0004-6361:20042486](https://doi.org/10.1051/0004-6361:20042486)
- Gianninas, A., Bergeron, P., Dupuis, J., & Ruiz, M. T. 2010, *ApJ*, 720, 581, doi: [10.1088/0004-637X/720/1/581](https://doi.org/10.1088/0004-637X/720/1/581)
- González Pérez, J. M., Solheim, J. E., & Kamben, R. 2006, *A&A*, 454, 527, doi: [10.1051/0004-6361:20053468](https://doi.org/10.1051/0004-6361:20053468)
- Grauer, A. D., & Bond, H. E. 1984, *ApJ*, 277, 211, doi: [10.1086/161685](https://doi.org/10.1086/161685)
- Grauer, A. D., Bond, H. E., Green, R. F., & Liebert, J. 1987a, in *IAU Colloq. 95: Second Conference on Faint Blue Stars*, ed. A. G. D. Philip, D. S. Hayes, & J. W. Liebert, 231–236
- Grauer, A. D., Bond, H. E., Liebert, J., Fleming, T. A., & Green, R. F. 1987b, *ApJ*, 323, 271, doi: [10.1086/165824](https://doi.org/10.1086/165824)
- Green, G. 2018, *The Journal of Open Source Software*, 3, 695, doi: [10.21105/joss.00695](https://doi.org/10.21105/joss.00695)
- Green, G. M., Schlafly, E., Zucker, C., Speagle, J. S., & Finkbeiner, D. 2019, *ApJ*, 887, 93, doi: [10.3847/1538-4357/ab5362](https://doi.org/10.3847/1538-4357/ab5362)
- Green, G. M., Schlafly, E. F., Finkbeiner, D., et al. 2018, *MNRAS*, 478, 651, doi: [10.1093/mnras/sty1008](https://doi.org/10.1093/mnras/sty1008)
- Green, R. F., & Liebert, J. W. 1979, in *IAU Colloq. 53: White Dwarfs and Variable Degenerate Stars*, ed. H. M. van Horn, V. Weidemann, & M. P. Savedoff, 118
- Handler, G., Prinja, R. K., Urbaneja, M. A., et al. 2013, *MNRAS*, 430, 2923, doi: [10.1093/mnras/stt092](https://doi.org/10.1093/mnras/stt092)
- Harris, C. R., Millman, K. J., van der Walt, S. J., et al. 2020, *Nature*, 585, 357, doi: [10.1038/s41586-020-2649-2](https://doi.org/10.1038/s41586-020-2649-2)
- Holberg, J. B., & Bergeron, P. 2006, *AJ*, 132, 1221, doi: [10.1086/505938](https://doi.org/10.1086/505938)
- Hoyer, D., Rauch, T., Werner, K., & Kruk, J. W. 2018, *A&A*, 612, A62, doi: [10.1051/0004-6361/201732401](https://doi.org/10.1051/0004-6361/201732401)

- Hügelmeier, S. D., Dreizler, S., Homeier, D., et al. 2006, *A&A*, 454, 617, doi: [10.1051/0004-6361:20064869](https://doi.org/10.1051/0004-6361:20064869)
- Hunter, J. D. 2007, *Computing in Science & Engineering*, 9, 90, doi: [10.1109/MCSE.2007.55](https://doi.org/10.1109/MCSE.2007.55)
- Jeffery, C. S., Werner, K., Kilkenny, D., et al. 2023, *MNRAS*, 519, 2321, doi: [10.1093/mnras/stac3531](https://doi.org/10.1093/mnras/stac3531)
- Kawaler, S. D., O'Brien, M. S., Clemens, J. C., et al. 1995, *ApJ*, 450, 350, doi: [10.1086/176145](https://doi.org/10.1086/176145)
- Kawaler, S. D., Potter, E. M., Vučković, M., et al. 2004, *A&A*, 428, 969, doi: [10.1051/0004-6361:20041475](https://doi.org/10.1051/0004-6361:20041475)
- Kepler, S. O., Fraga, L., Winget, D. E., et al. 2014, *MNRAS*, 442, 2278, doi: [10.1093/mnras/stu1019](https://doi.org/10.1093/mnras/stu1019)
- Kepler, S. O., Pelisoli, I., Koester, D., et al. 2016, *MNRAS*, 455, 3413, doi: [10.1093/mnras/stv2526](https://doi.org/10.1093/mnras/stv2526)
- Kholopov, P. N., Samus, N. N., Kazarovets, E. V., & Perova, N. B. 1985, *Information Bulletin on Variable Stars*, 2681, 1
- Lenz, P., & Breger, M. 2005, *Communications in Asteroseismology*, 146, 53, doi: [10.1553/cia146s53](https://doi.org/10.1553/cia146s53)
- Leuenhagen, U., Koesterke, L., & Hamann, W. R. 1993, *AcA*, 43, 329
- Löbbling, L. 2018, *Galaxies*, 6, 65, doi: [10.3390/galaxies6020065](https://doi.org/10.3390/galaxies6020065)
- Loumos, G. L., & Deeming, T. J. 1978, *Ap&SS*, 56, 285, doi: [10.1007/BF01879560](https://doi.org/10.1007/BF01879560)
- McGraw, J. T., Starrfield, S. G., Liebert, J., & Green, R. 1979, in *IAU Colloq. 53: White Dwarfs and Variable Degenerate Stars*, ed. H. M. van Horn, V. Weidemann, & M. P. Savedoff, 377
- Miller Bertolami, M. M., & Althaus, L. G. 2006, *A&A*, 454, 845, doi: [10.1051/0004-6361:20054723](https://doi.org/10.1051/0004-6361:20054723)
- Miller Bertolami, M. M., Battich, T., Córscico, A. H., Althaus, L. G., & Wachlin, F. C. 2022, *MNRAS*, 511, L60, doi: [10.1093/mnras/rlab134](https://doi.org/10.1093/mnras/rlab134)
- Nagel, T., & Werner, K. 2004, *A&A*, 426, L45, doi: [10.1051/0004-6361:200400079](https://doi.org/10.1051/0004-6361:200400079)
- Napiwotzki, R., & Schoenberner, D. 1995, *A&A*, 301, 545
- Oliveira da Rosa, G., Kepler, S. O., Córscico, A. H., et al. 2022, *ApJ*, 936, 187, doi: [10.3847/1538-4357/ac8871](https://doi.org/10.3847/1538-4357/ac8871)
- pandas development team, T. 2020, *pandas-dev/pandas: Pandas, latest*, Zenodo, doi: [10.5281/zenodo.3509134](https://doi.org/10.5281/zenodo.3509134)
- Quirion, P. O., Fontaine, G., & Brassard, P. 2004, *ApJ*, 610, 436, doi: [10.1086/421447](https://doi.org/10.1086/421447)
- . 2007, *ApJS*, 171, 219, doi: [10.1086/513870](https://doi.org/10.1086/513870)
- Rauch, T., & Werner, K. 1995, in *White Dwarfs*, ed. D. Koester & K. Werner, Vol. 443, 186, doi: [10.1007/3-540-59157-5_202](https://doi.org/10.1007/3-540-59157-5_202)
- Reindl, N., Geier, S., Kupfer, T., et al. 2016, *A&A*, 587, A101, doi: [10.1051/0004-6361/201527637](https://doi.org/10.1051/0004-6361/201527637)
- Reindl, N., Rauch, T., Werner, K., Kruk, J. W., & Todt, H. 2014, *A&A*, 566, A116, doi: [10.1051/0004-6361/201423498](https://doi.org/10.1051/0004-6361/201423498)
- Reindl, N., Schaffenroth, V., Filiz, S., et al. 2021, *A&A*, 647, A184, doi: [10.1051/0004-6361/202140289](https://doi.org/10.1051/0004-6361/202140289)
- Reindl, N., Islami, R., Werner, K., et al. 2023, *arXiv e-prints*, arXiv:2307.03721, doi: [10.48550/arXiv.2307.03721](https://doi.org/10.48550/arXiv.2307.03721)
- Ricker, G. R., Winn, J. N., Vanderspek, R., et al. 2015, *Journal of Astronomical Telescopes, Instruments, and Systems*, 1, 014003, doi: [10.1117/1.JATIS.1.1.014003](https://doi.org/10.1117/1.JATIS.1.1.014003)
- Schlafly, E. F., & Finkbeiner, D. P. 2011, *ApJ*, 737, 103, doi: [10.1088/0004-637X/737/2/103](https://doi.org/10.1088/0004-637X/737/2/103)
- Schlegel, D. J., Finkbeiner, D. P., & Davis, M. 1998, *ApJ*, 500, 525, doi: [10.1086/305772](https://doi.org/10.1086/305772)
- Schoenberner, D., & Napiwotzki, R. 1990, *A&A*, 231, L33
- Silvotti, R., Dreizler, S., Handler, G., & Jiang, X. J. 1999, *A&A*, 342, 745, doi: [10.48550/arXiv.astro-ph/9811178](https://doi.org/10.48550/arXiv.astro-ph/9811178)
- Solheim, J. E., Vauclair, G., Mukadam, A. S., Janulis, R., & Dobrovolskas, V. 2007, *A&A*, 468, 1057, doi: [10.1051/0004-6361:20077364](https://doi.org/10.1051/0004-6361:20077364)
- Sowicka, P., Handler, G., & Jones, D. 2018, *MNRAS*, 479, 2476, doi: [10.1093/mnras/sty1660](https://doi.org/10.1093/mnras/sty1660)
- Sowicka, P., Handler, G., Jones, D., & van Wyk, F. 2021, *ApJL*, 918, L1, doi: [10.3847/2041-8213/ac1c08](https://doi.org/10.3847/2041-8213/ac1c08)
- Toalá, J. A., Guerrero, M. A., Todt, H., et al. 2015, *ApJ*, 799, 67, doi: [10.1088/0004-637X/799/1/67](https://doi.org/10.1088/0004-637X/799/1/67)
- Uzundag, M., Córscico, A. H., Kepler, S. O., et al. 2022, *MNRAS*, 513, 2285, doi: [10.1093/mnras/stac1027](https://doi.org/10.1093/mnras/stac1027)
- . 2021, *A&A*, 655, A27, doi: [10.1051/0004-6361/202141253](https://doi.org/10.1051/0004-6361/202141253)
- Vauclair, G., Solheim, J. E., & Østensen, R. H. 2005, *A&A*, 433, 1097, doi: [10.1051/0004-6361:20041999](https://doi.org/10.1051/0004-6361:20041999)
- Vauclair, G., Moskalik, P., Pfeiffer, B., et al. 2002, *A&A*, 381, 122, doi: [10.1051/0004-6361:20011483](https://doi.org/10.1051/0004-6361:20011483)
- Vauclair, G., Fu, J. N., Solheim, J. E., et al. 2011, *A&A*, 528, A5, doi: [10.1051/0004-6361/201014457](https://doi.org/10.1051/0004-6361/201014457)
- Virtanen, P., Gommers, R., Oliphant, T. E., et al. 2020, *Nature Methods*, 17, 261, doi: [10.1038/s41592-019-0686-2](https://doi.org/10.1038/s41592-019-0686-2)
- Walton, N. A., Lennon, D. J., Greimel, R., et al. 2001, *The Newsletter of the Isaac Newton Group of Telescopes*, 4, 7
- Weidmann, W. A., Werner, K., Ahumada, J. A., Pignata, R. A., & Firpo, V. 2023, *A&A*, 676, A1, doi: [10.1051/0004-6361/202346401](https://doi.org/10.1051/0004-6361/202346401)
- Werner, K. 1992, in *The Atmospheres of Early-Type Stars*, ed. U. Heber & C. S. Jeffery, Vol. 401, 273, doi: [10.1007/3-540-55256-1_321](https://doi.org/10.1007/3-540-55256-1_321)
- . 1995, *Baltic Astronomy*, 4, 340, doi: [10.1515/astro-1995-0309](https://doi.org/10.1515/astro-1995-0309)
- . 2001, *Ap&SS*, 275, 27

- Werner, K., & Drake, J. J. 2005, *A&A*, 434, 707, doi: [10.1051/0004-6361:20042057](https://doi.org/10.1051/0004-6361:20042057)
- Werner, K., Hamann, W. R., Heber, U., et al. 1992, *A&A*, 259, L69
- Werner, K., & Herwig, F. 2006, *PASP*, 118, 183, doi: [10.1086/500443](https://doi.org/10.1086/500443)
- Werner, K., & Rauch, T. 2014, *A&A*, 569, A99, doi: [10.1051/0004-6361/201424051](https://doi.org/10.1051/0004-6361/201424051)
- . 2015, *A&A*, 584, A19, doi: [10.1051/0004-6361/201527261](https://doi.org/10.1051/0004-6361/201527261)
- Werner, K., Rauch, T., Barstow, M. A., & Kruk, J. W. 2004a, *A&A*, 421, 1169, doi: [10.1051/0004-6361:20047154](https://doi.org/10.1051/0004-6361:20047154)
- Werner, K., Rauch, T., & Kepler, S. O. 2014, *A&A*, 564, A53, doi: [10.1051/0004-6361/201423441](https://doi.org/10.1051/0004-6361/201423441)
- Werner, K., Rauch, T., & Kruk, J. W. 2005, *A&A*, 433, 641, doi: [10.1051/0004-6361:20042258](https://doi.org/10.1051/0004-6361:20042258)
- . 2010, *ApJL*, 719, L32, doi: [10.1088/2041-8205/719/1/L32](https://doi.org/10.1088/2041-8205/719/1/L32)
- . 2015, *A&A*, 582, A94, doi: [10.1051/0004-6361/201526842](https://doi.org/10.1051/0004-6361/201526842)
- . 2016, *A&A*, 593, A104, doi: [10.1051/0004-6361/201628892](https://doi.org/10.1051/0004-6361/201628892)
- Werner, K., Rauch, T., Napiwotzki, R., et al. 2004b, *A&A*, 424, 657, doi: [10.1051/0004-6361:20041157](https://doi.org/10.1051/0004-6361:20041157)
- Werner, K., Rauch, T., Reiff, E., Kruk, J. W., & Napiwotzki, R. 2004c, *A&A*, 427, 685, doi: [10.1051/0004-6361:20041165](https://doi.org/10.1051/0004-6361:20041165)
- Werner, K., Reindl, N., Dorsch, M., et al. 2022a, *A&A*, 658, A66, doi: [10.1051/0004-6361/202142397](https://doi.org/10.1051/0004-6361/202142397)
- Werner, K., Reindl, N., Geier, S., & Pritzkeleit, M. 2022b, *MNRAS*, 511, L66, doi: [10.1093/mnrasl/slac005](https://doi.org/10.1093/mnrasl/slac005)
- Wes McKinney. 2010, in *Proceedings of the 9th Python in Science Conference*, ed. Stéfan van der Walt & Jarrod Millman, 56 – 61, doi: [10.25080/Majora-92bf1922-00a](https://doi.org/10.25080/Majora-92bf1922-00a)
- Wesemael, F., Green, R. F., & Liebert, J. 1985, *ApJS*, 58, 379, doi: [10.1086/191046](https://doi.org/10.1086/191046)
- Woudt, P. A., Warner, B., & Zietsman, E. 2012, *MNRAS*, 426, 2137, doi: [10.1111/j.1365-2966.2012.21899.x](https://doi.org/10.1111/j.1365-2966.2012.21899.x)

CONCLUSIONS AND FUTURE WORK

This thesis presents new photometric time-series observations of 31 pre-WD stars of PG 1159 spectral type (almost 50% of all known PG 1159 stars), obtained to expand our knowledge of stars within the GW Vir instability strip. These stars are important to study in the context of stellar evolution as supposed main progenitors of H-deficient WDs. However, despite their importance, there were problems in our understanding of those stars that we attempted to solve.

If GW Vir pulsators still had He-burning shells, they should show oscillations driven by the ϵ mechanism, according to theoretical predictions. Almost 100 years ago, this mechanism had been proposed to excite stellar pulsations, but even today, convincing evidence for it operating in any kind of pulsating star is missing. The central star of planetary nebula VV 47 was the most promising candidate left, for which pulsations due to the ϵ mechanism were claimed. We re-observed the star in order to confirm the alleged pulsations using the 4.2-m William Herschel Telescope. In the new data the star appeared constant with an improved detection threshold, and the re-analysis of the discovery data showed that the star was not oscillating even then. We attributed the detection of ϵ -driven modes by the previous authors to confusion with noise peaks due to a particularly relaxed detection criterion. On the basis of this finding, we ruled out the ϵ -driven pulsations in both observing runs. Even though the star lies in the overlapping region in the HR diagram for both κ - and ϵ -destabilized modes, there are a number of possible reasons for the non-detection. First, the ϵ mechanism operating in the remnants of He-shell burning in pre-WDs is not very efficient, therefore the low- k -order g modes excited by it might not develop observable amplitudes. Second, the e -folding time for those modes is so long, that a star may leave the instability strip before the modes can reach observable amplitudes. Third, even our improved detection threshold is too high to detect oscillations in this star. Fourth, it could have been an extremely unfortunate situation that during both observing runs the star was observed in a period of time when the amplitudes of the modes were pushed below the detection threshold due to destructive interference or non-linear mode coupling. Finally, VV 47 might just have a different evolutionary history than the one necessary to produce a GW Vir pulsator.

One of the most important targets studied in this thesis was PG 1144+005 – the only known N-rich PG 1159 star that was not previously shown to pulsate, and the only counterexample to the current view of the excitation theory and abundance patterns of these stars. After a preliminary detection of pulsations in data collected using the 10.4-m Gran Telescopio Canarias, we obtained high-quality observations on a longer time-base and con-

firmed the pulsations in PG 1144+005. This provided the final piece of evidence that there is a clear separation, namely all known N-rich PG 1159 stars pulsate and the N-poor ones do not. An important conclusion followed: the pulsating and non-pulsating PG 1159 stars have different evolutionary history, and it seems necessary that a star undergoes a VLTP to develop pulsations, as nitrogen is a tracer of this evolutionary history. While the confirmation of the N dichotomy is a significant step forward, this hypothesis is based on a small number statistics – the majority of known PG 1159 stars did not have complete information, i.e., both photometric detection of pulsations or limits on non-variability, and measured nitrogen surface abundance, indicating the need for further observational efforts to fully study those stars.

We also planned and executed an extensive survey for variability among PG 1159 stars and related objects with several telescopes located in both Hemispheres. The survey results presented in this thesis covered 29 PG 1159 stars, over 40% of all known PG 1159 stars. We discovered pulsations in the central star of planetary nebula Abell 72, and variability in RX J0122.9–7521 that can be due to pulsations or other sources. For the rest of the sample, we provided significant limits for non-variability. That allowed us to measure the fraction of pulsating PG 1159 stars within the GW Vir instability strip to be 36%, the most robust pulsator fraction to date, conclusively proving that the pulsator to non-pulsator fraction is lower than previously published 50%. The impurity of the GW Vir instability strip is therefore unlikely to be due to observational bias, but rather a true outcome of different evolutionary histories.

Using the data collected from the literature and measurements provided in *Gaia* DR3 (*Gaia* parallaxes allowed the derivation of self-consistent distances for all known PG 1159 stars), we calculated consistent luminosities for the whole sample of PG 1159 stars, which allowed us to place those stars in the theoretical HR diagram for the first time. In general, we obtained a very good agreement with the evolutionary tracks of Miller Bertolami & Althaus (2006), however we identify a number of possible improvements. First, the bolometric corrections that we used were not calculated for PG 1159 model atmospheres, but were the best option currently available. Because of a variety of PG 1159 configurations, i.e., effective temperatures, surface gravities, and different proportions of atmospheric abundances of He, C, and O between individual PG 1159 stars, it is important to calculate bolometric corrections for a grid of different physical parameters and compositions to quantitatively assess how big the influence of the chemical composition on the bolometric corrections is. Second, we did not take into account the reddening from the surrounding PN. Twenty-three PG 1159 stars are surrounded by a PN, and while most of them have low surface brightness around the central star, there are cases with very bright nebulae, like NGC 650. In these cases, both the parallax measurements and derived luminosities can be influenced, and it has to be taken into account before drawing final conclusions about those stars. Third, mass estimations should be done using appropriate post-AGB evolutionary tracks, decided upon the chemical abundances for individual stars. Miller Bertolami & Althaus (2007) already noted possible issues with using VLTP evolutionary tracks for all PG 1159 stars, and while their VLTP and LTP tracks for objects with low H abundance and

surface gravities higher than $\log g = 6$ are similar, those with different H abundances differ, highlighting a possible issue with the use of VLTP tracks for AFTP objects. Moreover, Löblich et al. (2019) computed three AFTP tracks, and while at the location of their objects the AFTP tracks coincide with the VLTP ones, the differences might be more prominent at other locations and therefore should be studied. These estimates were based on the evolutionary tracks in the $\log g - \log T_{\text{eff}}$ plane, therefore affected by associated uncertainties on the spectroscopic parameters, and it will be interesting to explore it in the future in the $\log L_*/L_{\odot} - \log T_{\text{eff}}$ plane.

Our sample contained only PG 1159 stars without bright nebulae, meaning that the sample of PG 1159 stars in the centers of PNe is currently under-observed. Bright nebulae introduce challenges for photometric observations of the central stars, and different methods to remove the nebula influence have been used (e.g., using specific filters, PSF photometry, or adopting nebula subtraction procedures, see, e.g., Ciardullo & Bond 1996). Our survey included also those objects, which will be the subject of subsequent work. A number of objects from our sample require follow-up observations. That concerns the stars that were observed only once, the observations were of insufficient quality, or there were peaks in the FTs that need to be verified (e.g., to distinguish between possible sources of variability). In particular, RX J0122.9–7521 may need extensive photometric and/or spectroscopic follow-up observations to confirm or reject different scenarios (including pulsations, binarity, rotation, or spots). If the observed variability is due to pulsations, a refined mode stability analysis for this star will be necessary, as it currently lies outside the GW Vir instability strip and κ -driven modes were not unstable in theoretical calculations (Quirion et al., 2004). Furthermore, with the analysis of literature data, we were able to identify targets that may not fit the current scenario. That concerns four apparently N-poor pulsators that require a more in-depth study. It indicates the need to examine the N dichotomy with regard to the presence of pulsations with an even larger sample of stars and better spectra (higher S/N and higher resolution). Finally, given that there might be an undetected binary fraction among PG 1159 stars (currently only $\sim 10\%$ of confirmed or suspected binaries within the PG 1159 stars), there remains a question whether that fraction can change our view of the GW Vir stars? In particular, the current value of this binary fraction could be a severe underestimate and thus some systematics (e.g., chemical abundance patterns) related to it may be disguised. A systematic survey for binarity in the whole sample should therefore be carried out in the future, as well as a detailed study of different evolutionary scenarios including binarity.

Discovery of new pulsators within the GW Vir instability strip is very important, as more objects can be studied with the methods of asteroseismology, and allows us to learn more about those stars in aspects that are not available for non-pulsating stars. Therefore, one of our future goals is to make more GW Vir pulsators accessible to asteroseismic study. The amount of information provided in a star's pulsation spectrum strongly depends on the number of resolved pulsation modes, therefore high-quality observations, on a time-base sufficient to resolve closely spaced and rotationally split modes, are necessary. Given the fact that the best targets for asteroseismology have rich pulsation spectra, not only in

a sense of the number of detected modes, but also what part of the stellar interior they probe, photometric observations will need to be even more sensitive to detect more modes. The GW Vir pulsators that have been studied with the methods of asteroseismology are the brightest members of that family. Obtaining ground-based time-series photometric observations of sufficient quality to detect very low-amplitude pulsations of the remaining ones will require the use of large telescopes, and with the lack of dedicated space missions will require observing campaigns such as the Whole Earth Telescope runs (Nather et al., 1990), which will need extensive international collaborations. For such runs, the observing time on larger telescopes will be needed, and is perhaps more available now than a few decades ago, as the leading telescopes are getting larger. However, the caveat is the ever decreasing availability of photometric instrumentation.

The work presented in this thesis is the first step to provide the first statistically significant sample of well-studied PG 1159 stars with information on their evolutionary history and excitation of pulsations. Our sample is the most complete to date and thus is the best in which further study can be carried out. Ultimately, we plan to place constraints on the various post-AGB evolutionary channels and the observational verification of the statistical VLTP/LTP occurrence rates.

To reach that goal, we need both photometric and spectroscopic observations. With a statistically significant sample of PG 1159 stars tested for variability, we are now in place to study the individual chemical surface patterns of the target stars, with a special focus on measuring the N abundance. Only 26 stars (not even $1/3$) have published nitrogen surface abundances, or their upper limits. The available spectra for many stars are not sufficient to detect N lines, either due to too low resolution, or too low S/N. We have already obtained pilot data of a sample of PG 1159 stars to measure the element abundances of the most relevant species, i.e., H, He, C, N, O, and plan to utilize spectral analysis with non-LTE model atmospheres. T_{eff} and $\log g$ will be re-determined for the stars that had only low-resolution spectra available. A re-assessment of the T_{eff} and $\log g$ using high-resolution high-quality spectra is crucial especially for the pulsators, as the methods for determination of asteroseismic masses rely on the spectroscopic parameters and are affected by their uncertainties. The development of non-LTE model atmospheres with atomic data for additional elements serving as, e.g., temperature diagnostics fully supports this need.

We have presented here the most complete picture of the GW Vir stars, and now it is time to work on the whole PG 1159 group. As outlined above, the opportunities for future study of PG 1159 stars are broad, and we are now in position to take advantage of those opportunities.

BIBLIOGRAPHY

- Adam, C., Mugrauer, M., 2014, “HIP 3678: a hierarchical triple stellar system in the centre of the planetary nebula NGC 246”, *MNRAS*, 444, 3459–3465, doi: [10.1093/mnras/stu1677](https://doi.org/10.1093/mnras/stu1677).
- Aerts, C., Christensen-Dalsgaard, J., Kurtz, D. W., 2010, *Asteroseismology*, doi: [10.1007/978-1-4020-5803-5](https://doi.org/10.1007/978-1-4020-5803-5).
- Aerts, C., Mathis, S., Rogers, T. M., 2019, “Angular Momentum Transport in Stellar Interiors”, *ARA&A*, 57, 35–78, doi: [10.1146/annurev-astro-091918-104359](https://doi.org/10.1146/annurev-astro-091918-104359).
- Althaus, L. G., Córscico, A. H., Kepler, S. O., Miller Bertolami, M. M., 2008, “On the systematics of asteroseismological mass determinations of PG 1159 stars”, *A&A*, 478, 1, 175–180, doi: [10.1051/0004-6361:20078524](https://doi.org/10.1051/0004-6361:20078524).
- Althaus, L. G., Miller Bertolami, M. M., Córscico, A. H., García-Berro, E., Gil-Pons, P., 2005a, “The formation of DA white dwarfs with thin hydrogen envelopes”, *A&A*, 440, 1, L1–L4, doi: [10.1051/0004-6361:200500159](https://doi.org/10.1051/0004-6361:200500159).
- Althaus, L. G., Serenelli, A. M., Panei, J. A., Córscico, A. H., García-Berro, E., Scóccola, C. G., 2005b, “The formation and evolution of hydrogen-deficient post-AGB white dwarfs: The emerging chemical profile and the expectations for the PG 1159-DB-DQ evolutionary connection”, *A&A*, 435, 2, 631–648, doi: [10.1051/0004-6361:20041965](https://doi.org/10.1051/0004-6361:20041965).
- Althaus, L. G., Córscico, A. H., Isern, J., García-Berro, E., 2010, “Evolutionary and pulsational properties of white dwarf stars”, *A&A Rev.*, 18, 4, 471–566, doi: [10.1007/s00159-010-0033-1](https://doi.org/10.1007/s00159-010-0033-1).
- Andersen, J. et al., 1995, “New power for the Danish 1.54-m telescope.”, *The Messenger*, 79, 12–14.
- Baker, N., Kippenhahn, R., 1962, “The Pulsations of Models of δ Cephei Stars. With 17 Figures in the Text”, *ZAp*, 54, 114.
- Baran, A. S., Koen, C., 2021, “A Detection Threshold in the Amplitude Spectra Calculated from TESS Time-Series Data”, *Acta Astron.*, 71, 2, 113–121, doi: [10.32023/0001-5237/71.2.3](https://doi.org/10.32023/0001-5237/71.2.3).
- Baran, A. S., Winiarski, M., Krzesiński, J., Fox-Machado, L., Kawaler, S. D., Drózd, M., Faltenbacher, A., Thompson, M. A., Reed, M. D., 2011, “Mt. Suhora Survey - Searching for Pulsating M Dwarfs. I”, *Acta Astron.*, 61, 37–58.
- Battich, T., Miller Bertolami, M. M., Córscico, A. H., Althaus, L. G., 2018, “Pulsational instabilities driven by the ϵ mechanism in hot pre-horizontal branch stars. I. The hot-flasher scenario”, *A&A*, 614, A136, doi: [10.1051/0004-6361/201731463](https://doi.org/10.1051/0004-6361/201731463).
- Bédard, A., Bergeron, P., Brassard, P., 2022, “On the Spectral Evolution of Hot White Dwarf Stars. III. The PG 1159-DO-DB-DQ Evolutionary Channel Revisited”, *ApJ*, 930, 1, 8, doi: [10.3847/1538-4357/ac609d](https://doi.org/10.3847/1538-4357/ac609d).
- Beek, B., Schuh, S., Nagel, T., Traulsen, I., 2009, “Towards a dynamical mass of a PG 1159 star: radial velocities and spectral analysis of SDSS J212531-010745”, *Communications in Asteroseismology*, 159, 111–113, doi: [10.1553/cia159s111](https://doi.org/10.1553/cia159s111).
- Bell, K. J., Hermes, J. J., Vanderbosch, Z., Montgomery, M. H., Winget, D. E., Dennihy, E., Fuchs, J. T., Tremblay, P. E., 2017, “Destroying Aliases from the Ground and Space: Super-Nyquist ZZ Ceti in K2 Long Cadence Data”, *ApJ*, 851, 1, 24, doi: [10.3847/1538-4357/aa9702](https://doi.org/10.3847/1538-4357/aa9702).
- Benn, C., Dee, K., Agócs, T., 2008, “ACAM: a new imager/spectrograph for the William Herschel Telescope”, in: *Ground-based and Airborne Instrumentation for Astronomy II*, ed. by I. S. McLean, M. M. Casali, vol. 7014, Society of Photo-Optical Instrumentation Engineers (SPIE) Conference Series, 70146X, doi: [10.1117/12.788694](https://doi.org/10.1117/12.788694).
- Berry, R., Burnell, J., 2005, *The handbook of astronomical image processing*, vol. 2.
- Blecha, A., Schaller, G., Maeder, A., 1992, “Fast pulsations in a Wolf-Rayet star”, *Nature*, 360, 320, doi: [10.1038/360320a0](https://doi.org/10.1038/360320a0).
- Boffin, H. M. J., Jones, D., 2019, *The Importance of Binaries in the Formation and Evolution of Planetary Nebulae*, doi: [10.1007/978-3-030-25059-1](https://doi.org/10.1007/978-3-030-25059-1).
- Bond, H. E., Grauer, A. D., Green, R. F., Liebert, J. W., 1984, “Two new extremely hot pulsating white dwarfs.”, *ApJ*, 279, 751–757, doi: [10.1086/161943](https://doi.org/10.1086/161943).
- Bowman, D. M., Holdsworth, D. L., 2019, “Adaptive elliptical aperture photometry: A software package for high-cadence ground-based photometry. I. Application to rapid oscillators observed from SAAO”, *A&A*, 629, A21, doi: [10.1051/0004-6361/201935640](https://doi.org/10.1051/0004-6361/201935640).
- Boyle, W. S., Smith, G. E., 1970, “Charge coupled semiconductor devices”, *The Bell System Technical Journal*, 49, 4, 587–593, doi: [10.1002/j.1538-7305.1970.tb01790.x](https://doi.org/10.1002/j.1538-7305.1970.tb01790.x).
- Bradley, P. A., Dziembowski, W. A., 1996, “A Theoretical Analysis of Pulsation Driving in PG 1159 Stars”, *ApJ*, 462, 376, doi: [10.1086/177159](https://doi.org/10.1086/177159).
- Bratschi, P., Blecha, A., 1996, “Pulsations of WR stars: results of a 3 year survey of 6 WR stars.”, *A&A*, 313, 537–544.

- Breger, M., Stich, J., Garrido, R., Martin, B., Jiang, S. Y., Li, Z. P., Hube, D. P., Ostermann, W., Paparo, M., Scheck, M., 1993, “Nonradial Pulsation of the Delta-Scuti Star Bu-Cancri in the Praesepe Cluster”, *A&A*, 271, 482.
- Calcaferro, L. M., Córscico, A. H., Althaus, L. G., 2016, “Asteroseismology of the GW Virginis stars SDSS J0349-0059 and VV 47”, *A&A*, 589, A40, doi: [10.1051/0004-6361/201527996](https://doi.org/10.1051/0004-6361/201527996).
- Carroll, B. W., Ostlie, D. A., 2017, *An Introduction to Modern Astrophysics*, 2nd ed., Cambridge University Press, doi: [10.1017/9781108380980](https://doi.org/10.1017/9781108380980).
- Cepa, J., 1998, “OSIRIS Imaging and Spectroscopy for the GTC”, *Ap&SS*, 263, 369–372, doi: [10.1023/A:1002144913887](https://doi.org/10.1023/A:1002144913887).
- Christensen-Dalsgaard, J., Frandsen, S., 1983, “Stellar 5-MIN Oscillations”, *Sol. Phys.*, 82, 1-2, 469–486, doi: [10.1007/BF00145588](https://doi.org/10.1007/BF00145588).
- Ciardullo, R., Bond, H. E., 1996, “A Survey for Pulsations in OVI Nuclei of Planetary Nebulae”, *AJ*, 111, 2332, doi: [10.1086/117967](https://doi.org/10.1086/117967).
- Coppejans, R., Gulbis, A. A. S., Kotze, M. M., Coppejans, D. L., Worters, H. L., Woudt, P. A., Whittal, H., Cloete, J., Fourie, P., 2013, “Characterizing and Commissioning the Sutherland High-Speed Optical Cameras (SHOC)”, *PASP*, 125, 930, 976, doi: [10.1086/672156](https://doi.org/10.1086/672156).
- Córscico, A. H., Althaus, L. G., Kawaler, S. D., Miller Bertolami, M. M., García-Berro, E., Kepler, S. O., 2011, “Probing the internal rotation of pre-white dwarf stars with asteroseismology: the case of PG 0122+200”, *MNRAS*, 418, 4, 2519–2526, doi: [10.1111/j.1365-2966.2011.19642.x](https://doi.org/10.1111/j.1365-2966.2011.19642.x).
- Córscico, A. H., Althaus, L. G., Miller Bertolami, M. M., 2006, “New nonadiabatic pulsation computations on full PG 1159 evolutionary models: the theoretical GW Virginis instability strip revisited”, *A&A*, 458, 1, 259–267, doi: [10.1051/0004-6361:20065423](https://doi.org/10.1051/0004-6361:20065423).
- Córscico, A. H., Althaus, L. G., Miller Bertolami, M. M., García-Berro, E., 2009a, “Asteroseismology of hot pre-white dwarf stars: the case of the DOV stars PG 2131+066 and PG 1707+427, and the PNNV star NGC 1501”, *A&A*, 499, 1, 257–266, doi: [10.1051/0004-6361/200810727](https://doi.org/10.1051/0004-6361/200810727).
- Córscico, A. H., Althaus, L. G., Miller Bertolami, M. M., González Pérez, J. M., Kepler, S. O., 2009b, “On the Possible Existence of Short-Period g-Mode Instabilities Powered by Nuclear-Burning Shells in Post-Asymptotic Giant Branch H-Deficient (PG1159-Type) Stars”, *ApJ*, 701, 1008–1014, doi: [10.1088/0004-637X/701/2/1008](https://doi.org/10.1088/0004-637X/701/2/1008).
- Córscico, A. H., Miller Bertolami, M. M., Althaus, L. G., Vauclair, G., Werner, K., 2007, “Asteroseismological constraints on the coolest GW Virginis variable star (PG 1159-type) PG 0122+200”, *A&A*, 475, 2, 619–627, doi: [10.1051/0004-6361:20078145](https://doi.org/10.1051/0004-6361:20078145).
- Córscico, A. H., Althaus, L. G., Miller Bertolami, M. M., Kepler, S. O., 2019, “Pulsating white dwarfs: new insights”, *A&A Rev.*, 27, 1, 7, doi: [10.1007/s00159-019-0118-4](https://doi.org/10.1007/s00159-019-0118-4).
- Cox, A. N., 2003, “A Pulsation Mechanism for GW Virginis Variables”, *ApJ*, 585, 2, 975–982, doi: [10.1086/346228](https://doi.org/10.1086/346228).
- Craig, M. et al., 2017, *astropy/ccdproc: v1.3.0.post1*, version v1.3.0.post1, doi: [10.5281/zenodo.1069648](https://doi.org/10.5281/zenodo.1069648), URL: <https://doi.org/10.5281/zenodo.1069648>.
- Crowther, P. A., De Marco, O., Barlow, M. J., 1998, “Quantitative classification of WC and WO stars”, *MNRAS*, 296, 2, 367–378, doi: [10.1046/j.1365-8711.1998.01360.x](https://doi.org/10.1046/j.1365-8711.1998.01360.x).
- De Marco, O., Long, J., Jacoby, G. H., Hillwig, T., Kronberger, M., Howell, S. B., Reindl, N., Margheim, S., 2015, “Identifying close binary central stars of PN with Kepler”, *MNRAS*, 448, 3587–3602, doi: [10.1093/mnras/stv249](https://doi.org/10.1093/mnras/stv249).
- De Marco, O., Bond, H. E., Harmer, D., Fleming, A. J., 2004, “Indications of a Large Fraction of Spectroscopic Binaries among Nuclei of Planetary Nebulae”, *ApJ*, 602, 2, L93–L96, doi: [10.1086/382156](https://doi.org/10.1086/382156).
- Deeming, T. J., 1975, “Fourier Analysis with Unequally-Spaced Data”, *Ap&SS*, 36, 1, 137–158, doi: [10.1007/BF00681947](https://doi.org/10.1007/BF00681947).
- Dreizler, S., Heber, U., 1998, “Spectral analyses of PG 1159 star: constraints on the GW Virginis pulsations from HST observations”, *A&A*, 334, 618–632.
- Dziembowski, W., 1977, “Light and radial velocity variations in a nonradially oscillating star.”, *Acta Astron.*, 27, 203–211.
- Eastman, J., Siverd, R., Gaudi, B. S., 2010, “Achieving Better Than 1 Minute Accuracy in the Heliocentric and Barycentric Julian Dates”, *PASP*, 122, 894, 935, doi: [10.1086/655938](https://doi.org/10.1086/655938).
- Eddington, A. S., 1926, *The Internal Constitution of the Stars*.
- Eyer, L., Bartholdi, P., 1999, “Variable stars: Which Nyquist frequency?”, *A&AS*, 135, 1–3, doi: [10.1051/aas:1999102](https://doi.org/10.1051/aas:1999102).
- Fontaine, G., Brassard, P., 2008, “The Pulsating White Dwarf Stars”, *PASP*, 120, 872, 1043, doi: [10.1086/592788](https://doi.org/10.1086/592788).
- Fontaine, G., Brassard, P., Bergeron, P., 2001, “The Potential of White Dwarf Cosmochronology”, *PASP*, 113, 782, 409–435, doi: [10.1086/319535](https://doi.org/10.1086/319535).
- Fujimoto, M. Y., 1977, “On the Origin of R-Type Carbon Stars: Possibility of Hydrogen Mixing during Helium Flicker”, *PASJ*, 29, 331–350.

- García-Díaz, M. T., González-Buitrago, D., López, J. A., Zharikov, S., Tovmassian, G., Borisov, N., Valyavin, G., 2014, “A Spectroscopic and Photometric Study of the Planetary Nebulae Kn 61 and Pa 5”, *AJ*, 148, 3, 57, doi: [10.1088/0004-6256/148/3/57](https://doi.org/10.1088/0004-6256/148/3/57).
- Gautschy, A., 1997, “A further look into the pulsating PG 1159 stars.”, *A&A*, 320, 811–822, doi: [10.48550/arXiv.astro-ph/9606136](https://doi.org/10.48550/arXiv.astro-ph/9606136).
- Gautschy, A., Althaus, L. G., Saio, H., 2005, “On the excitation of PG 1159-type pulsations”, *A&A*, 438, 3, 1013–1020, doi: [10.1051/0004-6361:20042486](https://doi.org/10.1051/0004-6361:20042486).
- González Pérez, J. M., Solheim, J.-E., Kamben, R., 2006, “A search for photometric variability of hydrogen-deficient planetary-nebula nuclei”, *A&A*, 454, 527–536, doi: [10.1051/0004-6361:20053468](https://doi.org/10.1051/0004-6361:20053468).
- Grauer, A. D., Bond, H. E., 1984, “The pulsating central star of the planetary nebula Kohoutek 1-16.”, *ApJ*, 277, 211–215, doi: [10.1086/161685](https://doi.org/10.1086/161685).
- Grauer, A. D., Bond, H. E., Green, R. F., Liebert, J., 1987a, “Observations of K1-16, the GW Vir stars and related objects.”, in: *IAU Colloq. 95: Second Conference on Faint Blue Stars*, ed. by A. G. D. Philip, D. S. Hayes, J. W. Liebert, 231–236.
- Grauer, A. D., Bond, H. E., Liebert, J., Fleming, T. A., Green, R. F., 1987b, “A Search for Pulsating Stars Similar to PG 1159-035 and K1-16”, *ApJ*, 323, 271, doi: [10.1086/165824](https://doi.org/10.1086/165824).
- Green, R. F., Liebert, J. W., 1979, “Spectrophotometry of Hot White Dwarfs from the Palomar-Green Survey”, in: *IAU Colloq. 53: White Dwarfs and Variable Degenerate Stars*, ed. by H. M. van Horn, V. Weidemann, M. P. Savedoff, 118.
- Greenstein, J. L., 1958, “The Spectra of the White Dwarfs.”, *Handbuch der Physik*, 50, 161, doi: [10.1007/978-3-642-45906-1_5](https://doi.org/10.1007/978-3-642-45906-1_5).
- Guzik, J. A., Kaye, A. B., Bradley, P. A., Cox, A. N., Neuforge, C., 2000, “Driving the Gravity-Mode Pulsations in γ Doradus Variables”, *ApJ*, 542, 1, L57–L60, doi: [10.1086/312908](https://doi.org/10.1086/312908).
- Handler, G., Shobbrook, R. R., 2002, “On the relationship between the δ Scuti and γ Doradus pulsators”, *MNRAS*, 333, 2, 251–262, doi: [10.1046/j.1365-8711.2002.05401.x](https://doi.org/10.1046/j.1365-8711.2002.05401.x).
- Handler, G. et al., 2009, “Asteroseismology of Hybrid Pulsators Made Possible: Simultaneous MOST Space Photometry and Ground-Based Spectroscopy of γ Peg”, *ApJ*, 698, 1, L56–L59, doi: [10.1088/0004-637X/698/1/L56](https://doi.org/10.1088/0004-637X/698/1/L56).
- Handler, G., 2013, “Asteroseismology”, in: *Planets, Stars and Stellar Systems. Volume 4: Stellar Structure and Evolution*, ed. by T. D. Oswalt, M. A. Barstow, vol. 4, 207, doi: [10.1007/978-94-007-5615-1_4](https://doi.org/10.1007/978-94-007-5615-1_4).
- Harris, C. R. et al., 2020, “Array programming with NumPy”, *Nature*, 585, 7825, 357–362, doi: [10.1038/s41586-020-2649-2](https://doi.org/10.1038/s41586-020-2649-2).
- Hayashi, C., Nakano, T., 1963, “Evolution of Stars of Small Masses in the Pre-Main-Sequence Stages”, *Progress of Theoretical Physics*, 30, 4, 460–474, doi: [10.1143/PTP.30.460](https://doi.org/10.1143/PTP.30.460).
- Herwig, F., 2001, “Internal mixing and surface abundance of [WC]-CSPN”, *Ap&SS*, 275, 15–26.
- Howell, S. B., 1989, “Two-Dimensional Aperture Photometry: Signal-to-Noise Ratio of Point-Source Observations and Optimal Data-Extraction Techniques”, *PASP*, 101, 616, doi: [10.1086/132477](https://doi.org/10.1086/132477).
- 1992, “Introduction to Differential Time-Series Astronomical Photometry Using Charged-Coupled Devices”, in: *Astronomical CCD Observing and Reduction Techniques*, ed. by S. B. Howell, vol. 23, Astronomical Society of the Pacific Conference Series, 105.
- Howell, S. B., 2006, *Handbook of CCD Astronomy*, 2nd ed., Cambridge Observing Handbooks for Research Astronomers, Cambridge University Press, doi: [10.1017/CB09780511807909](https://doi.org/10.1017/CB09780511807909).
- Hoyer, D., Rauch, T., Werner, K., Kruk, J. W., 2018, “Search for trans-iron elements in hot, helium-rich white dwarfs with the HST Cosmic Origins Spectrograph”, *A&A*, 612, A62, doi: [10.1051/0004-6361/201732401](https://doi.org/10.1051/0004-6361/201732401).
- Hügelmeier, S. D., Dreizler, S., Homeier, D., Krzesiński, J., Werner, K., Nitta, A., Kleinman, S. J., 2006, “Spectral analyses of eighteen hot H-deficient (pre-) white dwarfs from the Sloan Digital Sky Survey Data Release 4”, *A&A*, 454, 2, 617–624, doi: [10.1051/0004-6361:20064869](https://doi.org/10.1051/0004-6361:20064869).
- Iben I., J., Kaler, J. B., Truran, J. W., Renzini, A., 1983, “On the evolution of those nuclei of planetary nebulae that experience a final helium shell flash.”, *ApJ*, 264, 605–612, doi: [10.1086/160631](https://doi.org/10.1086/160631).
- Jacoby, G. H., Hillwig, T. C., Jones, D., 2020, “Abell 30 - A binary central star among the born-again planetary nebulae”, *MNRAS*, 498, 1, L114–L118, doi: [10.1093/mnrasl/slaa138](https://doi.org/10.1093/mnrasl/slaa138).
- Jones, D., Boffin, H. M. J., Rodríguez-Gil, P., Wesson, R., Corradi, R. L. M., Miszalski, B., Mohamed, S., 2015, “The post-common envelope central stars of the planetary nebulae Henize 2-155 and Henize 2-161”, *A&A*, 580, A19, doi: [10.1051/0004-6361/201425454](https://doi.org/10.1051/0004-6361/201425454).
- Jones, D., Boffin, H. M. J., 2017, “Binary stars as the key to understanding planetary nebulae”, *Nature Astronomy*, 1, 0117, doi: [10.1038/s41550-017-0117](https://doi.org/10.1038/s41550-017-0117).
- Kawaler, S. D., Winget, D. E., Hansen, C. J., Iben Jr., I., 1986, “The helium shell game - Nonradial g-mode instabilities in hydrogen-deficient planetary nebula nuclei”, *ApJ*, 306, L41–L44, doi: [10.1086/184701](https://doi.org/10.1086/184701).
- Kawaler, S. D., Bradley, P. A., 1994, “Precision Asteroseismology of Pulsating PG 1159 Stars”, *ApJ*, 427, 415, doi: [10.1086/174152](https://doi.org/10.1086/174152).
- Kepler, S. O., 1993, “Whole earth telescope data analysis.”, *Baltic Astronomy*, 2, 515–529, doi: [10.1515/astro-1993-3-425](https://doi.org/10.1515/astro-1993-3-425).
- Kippenhahn, R., Weigert, A., Weiss, A., 2013, *Stellar Structure and Evolution*, doi: [10.1007/978-3-642-30304-3](https://doi.org/10.1007/978-3-642-30304-3).

- Koch, D. G. et al., 2010, “Kepler Mission Design, Realized Photometric Performance, and Early Science”, *ApJ*, 713, 2, L79–L86, doi: [10.1088/2041-8205/713/2/L79](https://doi.org/10.1088/2041-8205/713/2/L79).
- Lenz, P., Breger, M., 2005, “Period04 User Guide”, *Communications in Asteroseismology*, 146, 53–136, doi: [10.1553/cia146s53](https://doi.org/10.1553/cia146s53).
- Leuenhagen, U., Koesterke, L., Hamann, W. R., 1993, “Analyses of PNNi with [WC] Spectral Type”, *Acta Astron.*, 43, 329–335.
- Liebert, J., Fleming, T. A., Green, R. F., Grauer, A. D., 1988, “The nucleus of the planetary nebula VV 47 - Similarities with the pulsating PG1159-035/K1-16 variables”, *PASP*, 100, 187–191, doi: [10.1086/132154](https://doi.org/10.1086/132154).
- Löbbling, L., Rauch, T., Miller Bertolami, M. M., Todt, H., Friederich, F., Ziegler, M., Werner, K., Kruk, J. W., 2019, “Spectral analysis of the hybrid PG 1159-type central stars of the planetary nebulae Abell 43 and NGC 7094”, *MNRAS*, 489, 1, 1054–1071, doi: [10.1093/mnras/stz1994](https://doi.org/10.1093/mnras/stz1994).
- Loumos, G. L., Deeming, T. J., 1978, “Spurious Results from Fourier Analysis of Data with Closely Spaced Frequencies”, *Ap&SS*, 56, 2, 285–291, doi: [10.1007/BF01879560](https://doi.org/10.1007/BF01879560).
- Maeder, A., Meynet, G., 2000, “The Evolution of Rotating Stars”, *ARA&A*, 38, 143–190, doi: [10.1146/annurev.astro.38.1.143](https://doi.org/10.1146/annurev.astro.38.1.143).
- McCook, G. P., Sion, E. M., 1999, “A Catalog of Spectroscopically Identified White Dwarfs”, *ApJS*, 121, 1, 1–130, doi: [10.1086/313186](https://doi.org/10.1086/313186).
- McCully, C. et al., 2018, *Astropy/Astroscrappy: V1.0.5 Zenodo Release*, Zenodo, version v1.0.5, doi: [10.5281/zenodo.1482019](https://doi.org/10.5281/zenodo.1482019).
- McGraw, J. T., Starrfield, S. G., Liebert, J., Green, R., 1979, “PG 1159-035: a New, Hot, Non-Da Pulsating Degenerate”, in: *IAU Colloq. 53: White Dwarfs and Variable Degenerate Stars*, ed. by H. M. van Horn, V. Weidemann, M. P. Savedoff, 377.
- Merline, W. J., Howell, S. B., 1995, “A Realistic Model for Point-sources Imaged on Array Detectors: The Model and Initial Results”, *Experimental Astronomy*, 6, 1-2, 163–210, doi: [10.1007/BF00421131](https://doi.org/10.1007/BF00421131).
- Miller Bertolami, M. M., Althaus, L. G., 2006, “Full evolutionary models for PG 1159 stars. Implications for the helium-rich O(He) stars”, *A&A*, 454, 3, 845–854, doi: [10.1051/0004-6361:20054723](https://doi.org/10.1051/0004-6361:20054723).
- 2007, “On the robustness of H-deficient post-AGB tracks”, *A&A*, 470, 2, 675–684, doi: [10.1051/0004-6361:20077256](https://doi.org/10.1051/0004-6361:20077256).
- Miller Bertolami, M. M., Battich, T., Córscico, A. H., Althaus, L. G., Wachlin, F. C., 2022, “An evolutionary channel for CO-rich and pulsating He-rich subdwarfs”, *MNRAS*, 511, 1, L60–L65, doi: [10.1093/mnras/lsab134](https://doi.org/10.1093/mnras/lsab134).
- Miller Bertolami, M. M., Córscico, A. H., Althaus, L. G., 2011, “On the Challenging Variability of LS IV-14°116: Pulsational Instabilities Excited by the ϵ -Mechanism”, *ApJ*, 741, L3, doi: [10.1088/2041-8205/741/1/L3](https://doi.org/10.1088/2041-8205/741/1/L3).
- Murphy, S. J., Shibahashi, H., Kurtz, D. W., 2013, “Super-Nyquist asteroseismology with the Kepler Space Telescope”, *MNRAS*, 430, 4, 2986–2998, doi: [10.1093/mnras/stt105](https://doi.org/10.1093/mnras/stt105).
- Nagel, T., Schuh, S., Kusterer, D. J., Stahn, T., Hügelmeier, S. D., Dreizler, S., Gänsicke, B. T., Schreiber, M. R., 2006, “SDSS J212531.92-010745.9 - the first definite PG 1159 close binary system”, *A&A*, 448, 2, L25–L28, doi: [10.1051/0004-6361:200600009](https://doi.org/10.1051/0004-6361:200600009).
- Napiwotzki, R., Schoenberner, D., 1991, “Spectroscopic investigation of old planetaries. II. Detection of a “hybrid” central star.”, *A&A*, 249, L16.
- Nather, R. E., Winget, D. E., Clemens, J. C., Hansen, C. J., Hine, B. P., 1990, “The Whole Earth Telescope: A New Astronomical Instrument”, *ApJ*, 361, 309, doi: [10.1086/169196](https://doi.org/10.1086/169196).
- Naylor, T., 1998, “An optimal extraction algorithm for imaging photometry”, *MNRAS*, 296, 339–346, doi: [10.1046/j.1365-8711.1998.01314.x](https://doi.org/10.1046/j.1365-8711.1998.01314.x).
- Oliveira da Rosa, G. et al., 2022, “Kepler and TESS Observations of PG 1159-035”, *ApJ*, 936, 2, 187, doi: [10.3847/1538-4357/ac8871](https://doi.org/10.3847/1538-4357/ac8871).
- Papaloizou, J., Pringle, J. E., 1978, “Non-radial oscillations of rotating stars and their relevance to the short-period oscillations of cataclysmic variables.”, *MNRAS*, 182, 423–442, doi: [10.1093/mnras/182.3.423](https://doi.org/10.1093/mnras/182.3.423).
- Quirion, P. O., Fontaine, G., Brassard, P., 2004, “On the Driving Mechanism and the Coexistence of Variable and Nonvariable Stars in the Domain of the Pulsating PG 1159 Stars”, *ApJ*, 610, 1, 436–442, doi: [10.1086/421447](https://doi.org/10.1086/421447).
- 2007, “Mapping the Instability Domains of GW Vir Stars in the Effective Temperature-Surface Gravity Diagram”, *ApJS*, 171, 1, 219–248, doi: [10.1086/513870](https://doi.org/10.1086/513870).
- 2012, “Wind Competing Against Settling: A Coherent Model of the GW Virginis Instability Domain”, *ApJ*, 755, 2, 128, doi: [10.1088/0004-637X/755/2/128](https://doi.org/10.1088/0004-637X/755/2/128).
- Raghavan, D., McAlister, H. A., Henry, T. J., Latham, D. W., Marcy, G. W., Mason, B. D., Gies, D. R., White, R. J., ten Brummelaar, T. A., 2010, “A Survey of Stellar Families: Multiplicity of Solar-type Stars”, *ApJS*, 190, 1, 1–42, doi: [10.1088/0067-0049/190/1/1](https://doi.org/10.1088/0067-0049/190/1/1).
- Randall, S. K., Bagnulo, S., Ziegerer, E., Geier, S., Fontaine, G., 2015, “The enigmatic He-sdB pulsator LS IV-14°116: new insights from the VLT”, *A&A*, 576, A65, doi: [10.1051/0004-6361/201425251](https://doi.org/10.1051/0004-6361/201425251).
- Reed, M. D., Kawaler, S. D., O’Brien, M. S., 2000, “PG 2131+066: A Test of Pre-White Dwarf Asteroseismology”, *ApJ*, 545, 1, 429–434, doi: [10.1086/317781](https://doi.org/10.1086/317781).

- Reindl, N., Geier, S., Kupfer, T., Bloemen, S., Schaffenroth, V., Heber, U., Barlow, B. N., Østensen, R. H., 2016, “Radial velocity variable, hot post-AGB stars from the MUCHFUSS project. Classification, atmospheric parameters, formation scenarios”, *A&A*, 587, A101, doi: [10.1051/0004-6361/201527637](https://doi.org/10.1051/0004-6361/201527637).
- Reindl, N., Rauch, T., Werner, K., Kruk, J. W., Todt, H., 2014, “On helium-dominated stellar evolution: the mysterious role of the O(He)-type stars”, *A&A*, 566, A116, doi: [10.1051/0004-6361/201423498](https://doi.org/10.1051/0004-6361/201423498).
- Reindl, N., Schaffenroth, V., Filiz, S., Geier, S., Pelisoli, I., Kepler, S. O., 2021, “Mysterious, variable, and extremely hot: White dwarfs showing ultra-high excitation lines. I. Photometric variability”, *A&A*, 647, A184, doi: [10.1051/0004-6361/202140289](https://doi.org/10.1051/0004-6361/202140289).
- Ricker, G. R. et al., 2015, “Transiting Exoplanet Survey Satellite (TESS)”, *Journal of Astronomical Telescopes, Instruments, and Systems*, 1, 014003, doi: [10.1117/1.JATIS.1.1.014003](https://doi.org/10.1117/1.JATIS.1.1.014003).
- Saio, H., 1996, “Linear models for hydrogen-deficient star pulsations”, in: *Hydrogen Deficient Stars*, ed. by C. S. Jeffery, U. Heber, vol. 96, Astronomical Society of the Pacific Conference Series, 361.
- Saio, H., Kurtz, D. W., Murphy, S. J., Antoci, V. L., Lee, U., 2018, “Theory and evidence of global Rossby waves in upper main-sequence stars: r-mode oscillations in many Kepler stars”, *MNRAS*, 474, 2, 2774–2786, doi: [10.1093/mnras/stx2962](https://doi.org/10.1093/mnras/stx2962).
- Sana, H., de Mink, S. E., de Koter, A., Langer, N., Evans, C. J., Gieles, M., Gosset, E., Izzard, R. G., Le Bouquin, J. B., Schneider, F. R. N., 2012, “Binary Interaction Dominates the Evolution of Massive Stars”, *Science*, 337, 6093, 444, doi: [10.1126/science.1223344](https://doi.org/10.1126/science.1223344).
- Schoenberner, D., 1979, “Asymptotic giant branch evolution with steady mass loss.”, *A&A*, 79, 108–114.
- Schoenberner, D., Napiwotzki, R., 1990, “Spectroscopic investigation of old planetaries. I. Detection of two new “PG 1159” central stars.”, *A&A*, 231, L33–L35.
- Schönberg, M., Chandrasekhar, S., 1942, “On the Evolution of the Main-Sequence Stars.”, *ApJ*, 96, 161, doi: [10.1086/144444](https://doi.org/10.1086/144444).
- Schuh, S., Beeck, B., Nagel, T., 2009, “Dynamic masses for the close PG1159 binary SDSSJ212531.92-010745.9”, in: *Journal of Physics Conference Series*, vol. 172, Journal of Physics Conference Series, 012065, doi: [10.1088/1742-6596/172/1/012065](https://doi.org/10.1088/1742-6596/172/1/012065).
- Schuh, S., Traulsen, I., Nagel, T., Reiff, E., Homeier, D., Schwager, H., Kusterer, D. J., Lutz, R., Schreiber, M. R., 2008, “A new period determination for the close PG1159 binary SDSS J212531.92-010745.9”, *Astronomische Nachrichten*, 329, 4, 376, doi: [10.1002/asna.200710920](https://doi.org/10.1002/asna.200710920).
- Schuh, S., Dreizler, S., Deetjen, J. L., Heber, U., Geckeler, R. D., 2000, “CCD Photometry of Variable Subdwarfs and White Dwarfs at Calar Alto Observatory”, *Baltic Astronomy*, 9, 395–402, doi: [10.1515/astro-2000-0306](https://doi.org/10.1515/astro-2000-0306).
- Schwarzschild, M., Härm, R., 1965, “Thermal Instability in Non-Degenerate Stars.”, *ApJ*, 142, 855, doi: [10.1086/148358](https://doi.org/10.1086/148358).
- Shimansky, V. V., Borisov, N. V., Nurtdinova, D. N., Solovyeva, Y. N., Sakhbullin, N. A., Spiridonova, O. I., 2015, “Modeling the optical radiation of the precataclysmic variable SDSS J212531-010745”, *Astronomy Reports*, 59, 3, 199–212, doi: [10.1134/S1063772915030063](https://doi.org/10.1134/S1063772915030063).
- Smith, B. A., 1976, “Astronomical imaging applications for CCDs”, in: *Charge-Coupled Device Technology and Applications*, 135–138.
- Sowicka, P., Handler, G., Jones, D., 2018, “On ϵ -mechanism-driven pulsations in VV 47”, *MNRAS*, 479, 2, 2476–2480, doi: [10.1093/mnras/sty1660](https://doi.org/10.1093/mnras/sty1660).
- Sowicka, P., Handler, G., Jones, D., van Wyk, F., 2021, “The Missing Link? Discovery of Pulsations in the Nitrogen-rich PG 1159 Star PG 1144+005”, *ApJ*, 918, 1, L1, doi: [10.3847/2041-8213/ac1c08](https://doi.org/10.3847/2041-8213/ac1c08).
- Sowicka, P. et al., 2023, *The GW Vir instability strip in the light of new observations of PG 1159 stars. Discovery of pulsations in the central star of Abell 72 and variability of RX J0122.9-7521*, arXiv: [2309.16537](https://arxiv.org/abs/2309.16537).
- Sperl, M., 1998, “Manual for Period98: V1.0.4; A period search-program for Windows and Unix”, *Communications in Asteroseismology*, 111, 1–100.
- Stanghellini, L., Cox, A. N., Starrfield, S., 1991, “Post-Asymptotic Giant Branch Nonradial Instability Strips”, *ApJ*, 383, 766, doi: [10.1086/170835](https://doi.org/10.1086/170835).
- Starrfield, S., Cox, A. N., Kidman, R. B., Pensnell, W. D., 1985, “An analysis of nonradial pulsations of the central star of the planetary nebula K1-16.”, *ApJ*, 293, L23–L27, doi: [10.1086/184484](https://doi.org/10.1086/184484).
- Starrfield, S., Cox, A. N., Kidman, R. B., Pensnell, W. D., 1984, “Nonradial instability strips based on carbon and oxygen partial ionization in hot, evolved stars.”, *ApJ*, 281, 800–810, doi: [10.1086/162158](https://doi.org/10.1086/162158).
- Starrfield, S. G., Cox, A. N., Hodson, S. W., Pensnell, W. D., 1983, “The discovery of nonradial instability strips for hot, evolved stars.”, *ApJ*, 268, L27–L32, doi: [10.1086/184023](https://doi.org/10.1086/184023).
- Steininger, B., Paparo, M., Viraaghalmy, G., Zsuffa, D., Breger, M., 2003, “The White Dwarfs PG1144+005 and G117-B15A”, in: *Interplay of Periodic, Cyclic and Stochastic Variability in Selected Areas of the H-R Diagram*, ed. by C. Sterken, vol. 292, Astronomical Society of the Pacific Conference Series, 237.
- Tassoul, M., 1980, “Asymptotic approximations for stellar nonradial pulsations.”, *ApJS*, 43, 469–490, doi: [10.1086/190678](https://doi.org/10.1086/190678).
- Toalá, J. A. et al., 2015, “The Born-again Planetary Nebula A78: An X-Ray Twin of A30”, *ApJ*, 799, 1, 67, doi: [10.1088/0004-637X/799/1/67](https://doi.org/10.1088/0004-637X/799/1/67).

- Unglaub, K., Bues, I., 2000, “The chemical evolution of hot white dwarfs in the presence of diffusion and mass loss”, *A&A*, 359, 1042–1058.
- Unno, W., Osaki, Y., Ando, H., Saio, H., Shibahashi, H., 1989, *Nonradial oscillations of stars*.
- Uzundag, M. et al., 2021, “Pulsating hydrogen-deficient white dwarfs and pre-white dwarfs observed with TESS. II. Discovery of two new GW Vir stars: TIC 333432673 and TIC 095332541”, *A&A*, 655, A27, doi: [10.1051/0004-6361/202141253](https://doi.org/10.1051/0004-6361/202141253).
- Uzundag, M., Córscico, A. H., Kepler, S. O., Althaus, L. G., Werner, K., Reindl, N., Vučković, M., 2022, “Pulsating hydrogen-deficient white dwarfs and pre-white dwarfs observed with TESS - IV. Discovery of two new GW Vir stars: TIC 0403800675 and TIC 1989122424”, *MNRAS*, 513, 2, 2285–2291, doi: [10.1093/mnras/stac1027](https://doi.org/10.1093/mnras/stac1027).
- Van Der Walt, S., Colbert, S. C., Varoquaux, G., 2011, “The NumPy array: a structure for efficient numerical computation”, *Computing in Science and Engineering*, 13, 2.
- van Dokkum, P. G., 2001, “Cosmic-Ray Rejection by Laplacian Edge Detection”, *PASP*, 113, 789, 1420–1427, doi: [10.1086/323894](https://doi.org/10.1086/323894).
- Vauclair, G. et al., 2002, “Asteroseismology of RXJ 2117+3412, the hottest pulsating PG 1159 star”, *A&A*, 381, 122–150, doi: [10.1051/0004-6361:20011483](https://doi.org/10.1051/0004-6361:20011483).
- Virtanen, P. et al., 2020, “SciPy 1.0: Fundamental Algorithms for Scientific Computing in Python”, *Nature Methods*, 17, 261–272, doi: [10.1038/s41592-019-0686-2](https://doi.org/10.1038/s41592-019-0686-2).
- Walton, N. A., Lennon, D. J., Greimel, R., Irwin, M. J., Lewis, J. R., Rixon, G. T., 2001, “The Wide Field Camera and Infrastructure”, *The Newsletter of the Isaac Newton Group of Telescopes*, 4, 7–8.
- Weidmann, W. A., Mari, M. B., Schmidt, E. O., Gaspar, G., Miller Bertolami, M. M., Oio, G. A., Gutiérrez-Soto, L. A., Volpe, M. G., Gamen, R., Mast, D., 2020, “Catalogue of the central stars of planetary nebulae. Expanded edition”, *A&A*, 640, A10, doi: [10.1051/0004-6361/202037998](https://doi.org/10.1051/0004-6361/202037998).
- Werner, K., 1992, “Analysis of PG 1159 stars”, in: *The Atmospheres of Early-Type Stars*, ed. by U. Heber, C. S. Jeffery, vol. 401, 273, doi: [10.1007/3-540-55256-1_321](https://doi.org/10.1007/3-540-55256-1_321).
- Werner, K., Rauch, T., 2014, “Weak metal lines in optical high-resolution Very Large Telescope and Keck spectra of “cool” PG 1159 stars”, *A&A*, 569, A99, doi: [10.1051/0004-6361/201424051](https://doi.org/10.1051/0004-6361/201424051).
- 2015, “Analysis of HST/COS spectra of the bare C-O stellar core H1504+65 and a high-velocity twin in the Galactic halo”, *A&A*, 584, A19, doi: [10.1051/0004-6361/201527261](https://doi.org/10.1051/0004-6361/201527261).
- Werner, K., Rauch, T., Kepler, S. O., 2014, “New hydrogen-deficient (pre-) white dwarfs in the Sloan Digital Sky Survey Data Release 10”, *A&A*, 564, A53, doi: [10.1051/0004-6361/201423441](https://doi.org/10.1051/0004-6361/201423441).
- Werner, K., Rauch, T., Kruk, J. W., 2015, “The far-ultraviolet spectra of “cool” PG 1159 stars”, *A&A*, 582, A94, doi: [10.1051/0004-6361/201526842](https://doi.org/10.1051/0004-6361/201526842).
- 2016, “The far-ultraviolet spectra of two hot PG 1159 stars”, *A&A*, 593, A104, doi: [10.1051/0004-6361/201628892](https://doi.org/10.1051/0004-6361/201628892).
- Werner, K., Herwig, F., 2006, “The Elemental Abundances in Bare Planetary Nebula Central Stars and the Shell Burning in AGB Stars”, *PASP*, 118, 840, 183–204, doi: [10.1086/500443](https://doi.org/10.1086/500443).
- Werner, K., Reindl, N., Dorsch, M., Geier, S., Munari, U., Raddi, R., 2022a, “Non-local thermodynamic equilibrium spectral analysis of five hot, hydrogen-deficient pre-white dwarfs”, *A&A*, 658, A66, doi: [10.1051/0004-6361/202142397](https://doi.org/10.1051/0004-6361/202142397).
- Werner, K., Reindl, N., Geier, S., Pritzkeleit, M., 2022b, “Discovery of hot subdwarfs covered with helium-burning ash”, *MNRAS*, 511, 1, L66–L71, doi: [10.1093/mnrasl/slac005](https://doi.org/10.1093/mnrasl/slac005).
- Wesemael, F., Green, R. F., Liebert, J., 1985, “Spectrophotometric and model-atmosphere analyses of the hot DO and DAO white dwarfs from the Palomar-Green survey”, *ApJS*, 58, 379–411, doi: [10.1086/191046](https://doi.org/10.1086/191046).
- Winget, D. E., Kepler, S. O., 2008, “Pulsating white dwarf stars and precision asteroseismology”, *ARA&A*, 46, 157–199, doi: [10.1146/annurev.astro.46.060407.145250](https://doi.org/10.1146/annurev.astro.46.060407.145250).
- Zhevakin, S. A., 1953, *Russ. Astr. J.*, 30, 161.